



HAL
open science

Hydro-mechanical behavior of claystone-based backfill materials under geo-environmental conditions

Marvin Middelhoff

► **To cite this version:**

Marvin Middelhoff. Hydro-mechanical behavior of claystone-based backfill materials under geo-environmental conditions. Géotechnique. Université de Lorraine, 2020. English. NNT: 2020LORR0239 . tel-03202708

HAL Id: tel-03202708

<https://hal.univ-lorraine.fr/tel-03202708>

Submitted on 20 Apr 2021

HAL is a multi-disciplinary open access archive for the deposit and dissemination of scientific research documents, whether they are published or not. The documents may come from teaching and research institutions in France or abroad, or from public or private research centers.

L'archive ouverte pluridisciplinaire **HAL**, est destinée au dépôt et à la diffusion de documents scientifiques de niveau recherche, publiés ou non, émanant des établissements d'enseignement et de recherche français ou étrangers, des laboratoires publics ou privés.



AVERTISSEMENT

Ce document est le fruit d'un long travail approuvé par le jury de soutenance et mis à disposition de l'ensemble de la communauté universitaire élargie.

Il est soumis à la propriété intellectuelle de l'auteur. Ceci implique une obligation de citation et de référencement lors de l'utilisation de ce document.

D'autre part, toute contrefaçon, plagiat, reproduction illicite encourt une poursuite pénale.

Contact : ddoc-theses-contact@univ-lorraine.fr

LIENS

Code de la Propriété Intellectuelle. articles L 122. 4

Code de la Propriété Intellectuelle. articles L 335.2- L 335.10

http://www.cfcopies.com/V2/leg/leg_droi.php

<http://www.culture.gouv.fr/culture/infos-pratiques/droits/protection.htm>



UNIVERSITÉ DE LORRAINE

École doctorale Science et Ingénierie des Molécules, des Produits, des Procédés
et de l'Énergie (SIMPPÉ)

Laboratoire d'Énergétique et de Mécanique Théorique et Appliquée (LEMMA)

THÈSE

Présentée en vue de l'obtention du grade de

Docteur de l'Université de Lorraine

Spécialité : Énergie et Mécanique

Par

Marvin MIDDELHOFF

Hydro-mechanical behavior of claystone-based backfill materials under geo-environmental conditions

Soutenance prévue le 18 décembre 2020 devant la commission d'examen :

M. Yu Jun CUI	Professeur – ENPC ParisTech	Rapporteur
M. Enrique ROMERO MORALES	Directeur de recherche – UPC BarcelonaTech	Rapporteur
Mme Cristina JOMMI	Professeur – TU Delft	Examinatrice
M. Jean TALANDIER	Ingénieur de recherché – ANDRA	Examineur
Mme Nathalie CONIL	Ingénieur de recherché – INERIS	Examinatrice
M. Chun-Liang ZHANG	Ingénieur de recherché – GRS	Examineur
Mme Farimah MASROURI	Professeur – ENSG UL	Directrice de Thèse
M. Olivier CUISINIER	Professeur – ENSG UL	Co-Directeur de Thèse
M. Stéphane GABOREAU	Ingénieur de recherché – BRGM	Invité

To my parents,

To my grandparents,

To Michèle

Acknowledgements

First of all, I would like to thank the French agency for radioactive waste management (Andra) as it has funded my PhD-position for more than three years. Its financial support allowed me to realize and advance my research. I would like to express my gratitude to its solid and fluid mechanics research group, in particular to Dr. Gilles Armand, Dr. Jean Talandier and Dr. Nathalie Conil, who supported me throughout my thesis. The frequent group meetings helped me to orientate the scientific objectives of my thesis towards the issues faced by Andra as the Cigèò-project enters its industrial phase. In this regard, I would like to thank Dr. Talandier, who accepted to be my supervisor at Andra and whose support helped me to keep the link between the scientific aspects and industrial issues.

Although they are affiliated to a different research groups, I would like to thank Dr. Nicolas Michau of Andra and Dr. Stéphane Gaboreau of BRGM as they gave me an understanding of physico-chemical interaction processes in clays and clay-solution-systems.

I would also like to express my gratitude to the laboratory for energy and theoretical and applied mechanics (LEMTA) at the University of Lorraine (UL) in Nancy, in particular to its soil mechanics and geotechnics research group. The group members received me cordially despite my initial lack of the French language. Here, I would like to thank Professor Farimah Masrouri and Professor Olivier Cuisinier, who proposed me for the PhD-position. Professor Masrouri gave me an understanding of coherence and consistency, whereas Professor Cuisinier made me aware of the importance of curiosity, creativity and fun in science from the very first day. In Germany, the director and co-director are commonly referred to as the parents of the thesis, and I am grateful to refer Professor Masrouri and Professor Cuisinier to as the mother and father of my thesis, respectively. I would also like to thank Dr. Adel Abdallah and Dr. Sandrine Rosin Paumier for fruitful discussions related to professional and personal questions. I am grateful for the support of Mrs. Sarah Feuillatre and Mr. Jacques Tisot as they introduced me to the French language, society and culture. Eventually, I would like to express my gratitude to the other PhD-students in the research group, namely Ahmed, Alice, Jaime, Moïse, Mojdeh, Nicolas, Soheib and Zayed (alphabetically listed to not imply any preference). We shared our worst and best experiences, which brought us together and resulted in great friendships.

I would like to thank Prof. Yu-Jun Cui, Prof. Enrique Romero, Prof. Cristina Jommi, Dr. Jean Talandier, Dr. Nathalie Conil, Dr. Chun-Liang Zhang and Dr. Stéphane Gaboreau for accepting their roles as reporters or examiners in my thesis committee and for discussing fruitfully different aspects during my thesis defense.

I would like to eventually express my gratitude to my friends and family. When I felt desperate and doubted my abilities, they encouraged and support me, regardless of their personal or professional situations. Apart from my friends, I would like to thank my parents and grandparents as their continuous love and support allowed me to achieve all my aims. Finally, I would like to express my greatest gratitude to my star, whose light let me always find my way. Thank you!

Abstract

In the context of the Cigéo-project, the French agency in charge of radioactive waste management (Andra) studies claystone-based materials as to whether they can be potentially used to backfill shafts and drifts of the future repository for intermediate - and high-level radioactive waste located in the clay-rich Callovo-Oxfordian (COX) sedimentary rock formation at a depth of around 500 m. The installation of backfill in shafts and drifts generally aims to ensure the integrity of the repository system upon its closure. In particular, it is installed to stabilize the geological formation and to limit the propagation of the damaged/ disturbed zone evolving around the excavations. Potential backfill materials must thus sustain the overburden pressure and exhibit swelling pressure when they saturate under constant-volume conditions. In addition, the closure of hydraulic conductive voids ensues through the swelling under constant-volume conditions. Crushed and sieved COX-claystone spoil and its mixtures with MX80-bentonite are potential backfill materials as they contain smectite, which typically exhibits such a hydro-mechanical behavior. On account of the fraction of smectite, potential backfill materials and their hydro-mechanical behavior are affected by different geo-environmental conditions.

In this laboratory experimental study, it is of general interest to analyze how variations in geo-environmental conditions affect the performance of potential claystone-based backfill materials, in particular their volume change and hydraulic conductivity behavior. Relevant geo-environmental conditions are the fraction of smectite in the materials, the maximum grain diameter of the bentonite fraction in the mixture, the as-compacted/ initial dry density, the degree of saturation, the saturating solution chemistry, in particular its pH, and their combinations. Variations in the as-compacted/ initial dry density are expected to be of greatest relevance as conventional compaction techniques might be employed to compact the backfill material in-situ.

The hydro-mechanical behavior of processed COX-claystone spoil and its mixture with MX80-bentonite are analyzed by means of constant-volume swelling pressure, free-swell potential, one-dimensional compression/ oedometer and constant-head hydraulic conductivity experiments. Initially, it is evaluated how the fraction of smectite in the materials, the maximum grain diameter of the bentonite fraction, the initial dry density and the saturating solution chemistry affect individually and combined the evolution of the swelling pressure of claystone-based backfill materials. The individual and combined impact of the fraction of smectite in the materials as well as of the saturating solution chemistry on the evolution of the hydraulic conductivity are subsequently assessed. In order to analyze the impact of the pH of solutions, the hydraulic conductivity experiments are complemented by microstructural and textural analysis. The volume change behavior of the processed COX-claystone/ MX80-bentonite-mixture are evaluated not only in the saturated but also in the unsaturated state allowing to identify possible hydro-mechanical path dependencies. By considering samples compacted to different initial dry densities, it is assessed whether the initial dry density affects possible dependencies of the volume-change behavior on the hydro-mechanical path. Based on the performed investigations,

conclusions regarding the hydro-mechanical behavior of claystone-based backfill materials are drawn, and suggestions for future studies are made.

Résumé

Dans le cadre du projet Cigéo, l'agence française chargée de la gestion des déchets radioactifs (Andra) étudie des matériaux à base d'argile qui pourraient être utilisés pour remblayer les puits et les galeries du futur stockage de déchets radioactifs de moyenne et haute activité, situé dans la roche sédimentaire Callovo-Oxfordienne (COX) riche en argile, à une profondeur d'environ 500 m. L'installation de remblai dans les puits et les galeries vise généralement à assurer l'intégrité du système de stockage dès sa fermeture. Il sert à stabiliser la formation géologique et à limiter la propagation de la zone endommagée/perturbée autour des excavations. Les matériaux de remblai potentiels doivent donc supporter la contrainte verticale in situ et montrer une pression de gonflement lorsqu'ils saturent dans des conditions de volume constant, celle-ci provoque la fermeture des vides conducteurs hydrauliques. Les déblais d'argile COX broyés et tamisés et leurs mélanges avec de la bentonite MX80 sont des matériaux de remblai potentiels, car ils contiennent de la smectite qui présente un tel comportement hydromécanique. En raison de la présence de smectite, les matériaux de remblai potentiels et leur comportement hydromécanique sont impactés par différentes conditions géo-environnementales.

Dans cette étude expérimentale en laboratoire, il est judicieux d'analyser comment les variations des conditions géo-environnementales adéquates affectent la performance des matériaux de remblai potentiels à base d'argile, et plus spécifiquement leur changement de volume et leur comportement de conductivité hydraulique. Les conditions géo-environnementales pertinentes qui affectent les différents paramètres du remblai, sont la fraction de smectite dans les matériaux, le diamètre de grain maximum de la fraction de bentonite dans le mélange, la densité sèche initiale, le degré de saturation, la chimie de la solution saturante, en particulier son pH, et leurs combinaisons. Les variations de la densité sèche initiale devraient être les plus importantes car les techniques de compactage conventionnelles pourraient être utilisées pour compacter le matériau de remblai in situ.

Le comportement hydromécanique des déblais d'argile COX traités et de leur mélange avec la bentonite MX80 est analysé par le biais des méthodes de pression de gonflement à volume constant, de potentiel de gonflement libre, de compression/ oedomètre unidimensionnel et de conductivité hydraulique à charge hydraulique constante. Dans un premier temps, on évalue comment la fraction de smectite dans les matériaux, le diamètre de grain maximum de la fraction de bentonite, la densité sèche initiale et la chimie de la solution saturante affectent individuellement et conjointement l'évolution de la pression de gonflement des matériaux de remblai à base d'argile. L'impact individuel et combiné de la fraction de smectite, ainsi que celui de la chimie de la solution saturante sur l'évolution de la conductivité hydraulique sont ensuite évalués. Afin d'affiner l'impact du pH des solutions, des analyses microstructurales et de texture viennent compléter les essais de conductivité hydraulique. Puis le comportement des changements de volume du mélange COX-argile/ MX80-bentonite traité est évalué, non seulement à l'état saturé mais aussi à l'état non saturé, ce qui permet d'identifier les éventuelles dépendances des schémas hydromécaniques. Enfin, en considérant des échantillons compactés à différentes

densités sèches initiales, il est déterminé si la densité sèche initiale affecte les éventuelles dépendances du comportement de changement de volume sur le chemin hydromécanique. Sur la base des recherches effectuées, des conclusions concernant le comportement hydromécanique des matériaux de remblai à base d'argile sont présentées et des suggestions sont faites pour de futures études.

Zusammenfassung

Im Rahmen des Cigéo-Projekts untersucht die französische Agentur für die Entsorgung radioaktiver Abfälle (Andra), ob tonsteinbasierte Materialien für den Versatz von Schächten und Strecken des zukünftigen Endlagers für mittel- und hochradioaktive Abfälle im tonreichen Callovo-Oxfordian (COX)-Sedimentgestein in ca. 500 m Tiefe verwendet werden können. Das Versetzen von Schächten und Strecken zielt im Allgemeinen darauf ab, die Integrität des Endlagersystems nach dessen Verschluss zu gewährleisten. Insbesondere wird er eingebracht, um die geologische Formation zu stabilisieren und die Ausbreitung der sich um die Schächte entwickelnden Schadens-/Störungszone zu begrenzen. Potenzielle Versatzmaterialien müssen daher den Gebirgsdruck entgegenwirken und einen Quelldruck aufweisen, wenn sie sich unter konstanten Volumenbedingungen sättigen. Zusätzlich erfolgt durch das Quellen unter konstanten Volumenbedingungen der Verschluss von hydraulisch-leitfähigen Hohlräumen. Gebrochener und gesiebter COX-Tonsteinausbruch und dessen Mischungen mit MX80-Bentonit sind potentielle Versatzmaterialien, da sie Smektiten enthalten, die typischerweise ein solches hydromechanisches Verhalten aufweisen. Aufgrund der Smektitfraktion werden die potentiellen Versatzmaterialien und ihr hydromechanisches Verhalten durch unterschiedliche Geo-Umweltbedingungen beeinflusst.

In dieser experimentellen Laborstudie ist es von allgemeinem Interesse zu analysieren, wie sich Variationen der Geo-Umweltbedingungen auf das Verhalten potenzieller tonsteinbasierter Versatzmaterialien auswirken, insbesondere auf die Volumenänderung und die hydraulische Leitfähigkeit. Relevante Geo-Umweltbedingungen sind die Smektitfraktion in den Materialien, der maximale Korndurchmesser der Bentonitfraktion in der Mischung, die Trockendichte, der Sättigungsgrad, die Sättigungslösung, insbesondere der pH-Wert, und deren Kombinationen. Es wird erwartet, dass Variationen der Trockendichte von größter Relevanz sind, da in-situ konventionelle Techniken zur Verdichtung des Versatzmaterials eingesetzt werden können.

Das hydromechanische Verhalten von aufbereitetem COX-Tonsteinausbruch und dessen Mischung mit MX80-Bentonit wird mittels Quelldruckversuchen unter konstanten Volumenbedingungen, Quellverformungsversuchen unter freien Volumenbedingungen, eindimensionalen Kompressions-/ Ödometerversuchen und Constant-Head-Versuchen analysiert. Zunächst wird ausgewertet, wie sich die Smektitfraktion in den Materialien, der maximale Korndurchmesser der Bentonitfraktion, die Anfangstrockendichte und die Eigenschaften der Sättigungslösung einzeln und kombiniert auf die Entwicklung des Quelldrucks von tonsteinbasierten Versatzmaterialien auswirken. Anschließend wird der individuelle und kombinierte Einfluss der Smektitfraktion in den Materialien sowie der Eigenschaften der Sättigungslösung auf die Entwicklung der hydraulischen Leitfähigkeit untersucht. Um den Einfluss des pH-Wertes der Lösungen zu analysieren, werden die hydraulischen Leitfähigkeitsversuche durch mikrostrukturelle und textuelle Analysen ergänzt. Das Volumenänderungsverhalten des aufbereiteten Gemisches aus COX-Tonsteinausbruch und MX80-Bentonit wird nicht nur im gesättigten, sondern auch im

ungesättigten Zustand ausgewertet, um mögliche hydro-mechanische Belastungspfadabhängigkeiten zu identifizieren. Durch die Berücksichtigung von Proben, die sich durch unterschiedliche Anfangstrockenrohdichten auszeichnen, wird beurteilt, ob die Anfangstrockenrohddichte mögliche Abhängigkeiten des Volumenänderungsverhaltens vom hydromechanischen Belastungspfad beeinflusst. Basierend auf den durchgeführten Untersuchungen werden Schlussfolgerungen hinsichtlich des hydromechanischen Verhaltens von tonsteinbasierten Versatzmaterialien gezogen und Vorschläge für zukünftige Untersuchungen gemacht.

Publications

This is a list of all the work published, submitted or to be submitted, related to this PhD.

Peer reviewed journals:

1. **Middelhoff M**, Cuisinier O, Masrouri F, Talandier J and Conil N (2020) Combined impact of selected material properties and environmental conditions on the swelling pressure compacted claystone/bentonite mixtures. *Applied Clay Science* **184**: 105389, 10.1016/j.clay.2019.105389.
2. **Middelhoff M**, Cuisinier O, Gaboreau S, Masrouri F, Talandier J and Michau N (2020) Hydraulic conductivity, microstructure and texture of compacted claystone/ bentonite-mixtures saturated with different solutions. *Engineering Geology*, (Submitted July 2020, under review)
3. **Middelhoff M**, Cuisinier O, Masrouri F and Talandier J (2020) Hydro-mechanical path dependency of claystone/ bentonite mixture samples characterized by different initial dry densities. *Acta Geotechnica*, (Submitted October 2020, under review)

Conference proceedings:

1. **Middelhoff M**, Cuisinier O, Masrouri F, Talandier J and Conil N (2020) Swelling behavior of unsaturated claystone/ bentonite mixtures. In *4th European Conference on Unsaturated Soils*, Lisbon.
2. **Middelhoff M**, Cuisinier O, Masrouri F and Talandier J (2021) Impact of saturating solution chemistry on the swelling pressure evolution of processed claystone and its mixture with MX80-bentonite. In *3rd International Symposium on Coupled Phenomena in Environmental Geotechnics*, Kyoto.

Abstracts and Posters:

1. **Middelhoff M**, Cuisinier O, Masrouri F and Talandier J (2021) Impact of variations in the initial dry density induced by conventional compaction techniques on the swelling behavior of claystone based backfill materials. In *Clays in Natural and Engineered Barriers for Radioactive Waste Confinement*, Nancy (Abstract and Poster)

2. **Middelhoff M**, Cuisinier O, Gaboreau S, Masrouri F, Talandier J and Michau N (2021) Impact of saturating solution chemistry on the hydraulic conductivity of claystone based backfill materials. *In Clays in Natural and Engineered Barriers for Radioactive Waste Confinement*, Nancy (Abstract and Oral presentation)

Table of Content

Table of Content.....	i
List of Figures	vii
List of Tables.....	xi
1 Introduction	1
1.1 Reference backfill and seal concept	3
1.2 Motivation and objectives	6
1.3 Thesis layout.....	8
2 Literature review	11
2.1 Scale dependence in expansive soil testing.....	12
2.2 Nature of expansive soils	12
2.2.1 Mineralogy of expansive soils.....	13
2.2.2 Structure of expansive soils.....	16
2.2.3 Experimental determination	17
2.2.4 Conclusion.....	18
2.3 Interactions in clay particle – solution systems.....	19
2.3.1 Effect of pH in clay particle – solution systems.....	19
2.3.2 Hydration mechanisms	20
2.3.3 Crystalline swelling mechanism.....	20
2.3.4 Osmotic swelling mechanism.....	22
2.3.5 Cation exchange processes	27
2.3.6 Conclusion.....	28
2.4 Solution retention behavior of expansive soils.....	28
2.4.1 Concept of suction in expansive soils	28

2.4.2	Solution retention in expansive soils.....	30
2.4.3	Experimental determination	31
2.4.4	Impact of physical and physico-chemical parameters.....	33
2.4.5	Impact of compaction conditions	34
2.4.6	Conclusion.....	34
2.5	Compaction behavior of expansive soils.....	35
2.5.1	Experimental determination	36
2.5.2	Impact of physical and physico-chemical conditions.....	36
2.5.3	Relations of the compaction conditions to the structure	37
2.5.4	Conclusion.....	39
2.6	Swelling behavior of expansive soils	39
2.6.1	Experimental determination	39
2.6.2	Swelling pressure evolution at experimental different scales	41
2.6.3	Impact of physical and physico-chemical parameters.....	42
2.6.4	Impact of compaction conditions	43
2.6.5	Impact of environmental conditions and stress history	46
2.6.6	Conclusion.....	49
2.7	Compression behavior of expansive soils	49
2.7.1	Experimental determination	49
2.7.2	Impact of physical and physico-chemical parameters.....	51
2.7.3	Impact of compaction conditions	52
2.7.4	Impact of environmental conditions and stress history	52
2.7.5	Conclusion.....	54
2.8	Hydraulic conductivity behaviour of expansive soils	55
2.8.1	Experimental determination	56
2.8.2	Impact of the hydraulic gradient	57
2.8.3	Impact of physical and physico-chemical parameters.....	58
2.8.4	Impact of compaction conditions	59

2.8.5	Impact of environmental conditions and stress history	61
2.8.6	Conclusion.....	62
2.9	Constitutive modelling of expansive soil behavior	63
2.9.1	Elastic behavior	64
2.9.2	Loading-collapse (LC) and suction increase (SI) yield curves	64
2.9.3	Plastic behavior	65
2.9.4	Comments.....	66
2.10	Extended constitutive modelling of expansive soils	66
2.10.1	Basic preliminary assumptions.....	67
2.10.2	Elastic behaviour	68
2.10.3	Suction increase (SI) and suction decrease (SD) yield curves	69
2.10.4	Interaction between micro- and macrostructural levels	70
2.10.5	Plastic behavior	72
2.10.6	Comments.....	72
2.11	Conclusions and anticipated contributions.....	73
3	Combined impact of selected material properties and environmental conditions on the swelling pressure of compacted claystone/ bentonite mixtures	75
<i>Abstract</i>		75
3.1	Introduction	77
3.2	Theoretical background.....	80
3.3	Materials.....	82
3.4	Methods.....	86
3.5	Results	87
3.6	Discussion	91
3.6.1	Introduction of expansive mineral dry density (EDD).....	91
3.6.2	Impact of expansive mineral content and grain size distribution.....	93
3.6.3	Individual impact of EDD and solution chemistry.....	94

3.6.4	Combined impact of solution chemistry and EDD	96
3.7	Conclusions	98
4	Hydraulic conductivity, microstructure and texture of compacted claystone/ bentonite mixtures saturated with different solutions	101
<i>Abstract</i>		101
4.1	Introduction and background.....	103
4.2	Materials	106
4.3	Experiments.....	109
4.3.1	Sample preparation.....	109
4.3.2	Hydraulic conductivity	110
4.3.3	Microstructural analysis	111
4.3.4	Textural analysis.....	112
4.3.5	Experimental program.....	112
4.4	Results	113
4.4.1	Hydraulic conductivity experiments	113
4.4.2	Microstructural analysis	115
4.4.3	Textural analysis.....	119
4.5	Discussion	120
4.5.1	Textural analysis.....	120
4.5.2	Microstructural analysis	121
4.5.3	Hydraulic conductivity experiments	123
4.6	Conclusions	126
5	Hydro-mechanical path dependency of claystone/ bentonite mixture samples characterized by different initial dry densities	129
<i>Abstract</i>		129
5.1	Introduction	131

5.2	Material	134
5.2.1	General characteristics	134
5.2.2	Microstructural characteristics	135
5.2.3	Water retention characteristics	137
5.3	Oedometer and constant-volume swelling pressure experiments	139
5.3.1	Approach	139
5.3.2	Sample preparation.....	140
5.3.3	Suction-controlled oedometer experiments.....	141
5.3.4	Suction-controlled constant-volume swelling pressure experiments	141
5.3.5	Hydro-mechanical paths and experimental program.....	141
5.4	Results	143
5.4.1	Suction-controlled oedometer experiments.....	143
5.4.2	Suction-controlled constant-volume swelling pressure experiments	145
5.5	Discussion	146
5.5.1	Compression behavior	146
5.5.2	Swelling behavior.....	149
5.5.3	Comparison of yield behavior	151
5.6	Conclusions	152
6	Conclusions and perspectives.....	157
6.1	Approaches	158
6.2	Synthesizes and conclusions	159
6.3	Perspectives	161
A	Supplementary material.....	165
	References	169
	Résumé détaillé	191

List of Figures

Figure 1.1: Layout of Cigéo underground facilities (Leverd et al., 2017)	2
Figure 1.2: Side view at a drift backfilled and sealed according to the French reference concept (modified after ANDRA (2005))	3
Figure 1.3: Impact of geo-environmental conditions (a. Simplified variations in the initial dry density, b. Evolution of a wetting front & percolation with hyperalkaline solutions) on the in-situ compacted backfill material (1. Backfill, 2. Concrete lining, 3. Excavation damaged/ disturbed zone, 4. Rock formation).....	7
Figure 2.1: Sketch of the structure of a smectite	15
Figure 2.2: Sketch of the multiscale structure of expansive soils comprising particles, aggregates, assemblies of aggregates and the corresponding interlayer, interparticle and interaggregate pores (modified after Wang and Wei (2015))	17
Figure 2.3: Evolution of discrete layers of water molecules in a) Na-montmorillonite and b) Ca- montmorillonite as a function of imposed relative humidity (Black-framed symbols indicate compacted and confined samples; Black-framed and colored symbols indicate compacted samples under free swell conditions; Colored symbols indicate powdered samples under free swell conditions)	22
Figure 2.4: a) Schematic sketch of the distribution of ions adjacent to a clay particle face according to the concept of the diffuse double layer, b) Corresponding exponential decrease of the electrostatic potential of clay particle faces with distance, c) Corresponding exponential decrease and increase of cations and anions, respectively, with distance (modified after van Olphen (1980) and Sposito (1992)).....	24
Figure 2.5: Two negatively charged clay layers with diffuse double layers.....	25
Figure 2.6: Net energy of interactions (assuming a low ion concentration in the adjacent solution (modified after van Olphen (1980))	27
Figure 2.7: Variations of a) the maximum dry density and b) the optimum water content of sand and/ or clayey soils/ bentonite-mixtures as a function of the bentonite content	37
Figure 2.8: Pore-size distribution functions of compacted clayey soils under a) saturation (Monroy et al., 2010) and b) loading (Sivakumar et al., 2006).....	38
Figure 2.9: Swelling pressure evolution determined under constant-volume conditions at REV-scale (C_1 : Pusch (1980); C_2 : Sridharan et al. (1986b)) and at full scale (C_3 : Goudarzi (2019)).....	41

Figure 2.10: Exponential relation between initial dry density and maximum swelling pressure in the cases of a) Na-bentonites and b) Ca-bentonites (taken from various references)	44
Figure 2.11: a) Impact of alkaline solution circulation over 18 months on the pore size distribution function of compacted material b) Detail of a secondary electron picture of a polished section of the leached material, showing the opening of microporosity (Cuisinier et al., 2014).....	48
Figure 2.12: Variation of apparent preconsolidation stress of FEBEX-bentonite as a function of imposed suction (Lloret et al., 2003)	53
Figure 2.13: Verification of the hydration path dependency of the unsaturated compressibility behaviour of FEBEX-bentonite (Lloret et al., 2003)	54
Figure 2.14: Relation between flow rate and hydraulic gradient for Darcian and non-Darcian flow (modified after Mitchell and Soga (2005))	57
Figure 2.15: Exponential relation between initial dry density and maximum swelling pressure in the cases of a) Na-bentonites and b) Ca-bentonites (taken from various references)	60
Figure 2.16: Barcelona Basic Model yield loci in (p, q, s) – planes (Alonso et al., 1999)	66
Figure 2.17: Definition of microstructural swelling and contraction directions (Sánchez et al., 2005).....	68
Figure 2.18: Barcelona Expansive Model yield loci in the (p, s) – plane (Alonso et al., 1999)	69
Figure 2.19: Summary of interaction mechanisms between the micro- and macrostructure as a function of the ratio of the current mean net stress p to the preconsolidation stress p_0 (Alonso et al., 1999).....	71
Figure 2.20: Shift of the loading-collapse yield curve due to microstructural effects (Sánchez et al., 2005).....	71
Figure 2.21: Compilation of conditions affecting the hydro-mechanical behavior of expansive soils.....	73
Figure 3.2: Results of the standard and modified Proctor tests performed on a) COXc and b) the grain- and powder-mixtures	85
Figure 3.3: Evolution of swelling pressure of COX _c , the grain- and powder-mixture compacted to their individual maximum dry densities at optimum water contents and saturated with demineralized/ deaired water (DW).....	88
Figure 3.4: Evolution of swelling pressure of COXc, the grain- and powder-mixtures compacted to their individual maximum dry densities at optimum water contents and saturated with demineralized/ deaired water (DW), artificial Bure site solution (ABSS) and artificial Portland cement solution (APCS).....	89

Figure 3.5: Evolution of swelling pressure of the grain-mixture compacted to 1) maximum dry density, 2) maximum dry density reduced by 3.5%, 3) maximum dry density reduced by 7.5%, and 4) maximum dry density reduced by 17.5% at optimum water content and saturated with deaired/ demineralized water (DW)	89
Figure 3.6: Depiction of the exponential relation between the reduction of initial dry density and the maximum swelling pressure, including the impact of the saturated solution chemistry: a) Relation of grain-mixture, b) Relation of powder-mixture	90
Figure 3.7: Defined four phases of a mixture composed of different expansive soils	92
Figure 3.8: Exponential relationship between EDD and the maximum swelling pressure including results of various expansive clays and their mixtures with varying amounts of non-expansive materials taken from literature	95
Figure 3.9: Exponential relation of EDD and maximum swelling pressure in the case of the a) grain-mixture and b) the powder-mixture (saturated with deaired/demineralised water (DW), artificial Bure site solution (ABSS) and artificial Portland cement solution (APCS))	97
Figure 4.1: Grain size distribution of COX _c and the mixture obtained by dry sieving and laser diffractometry	108
Figure 4.2: Evolution of the hydraulic conductivity of a) COX _c ($\rho_{d, ini} = 1.95 \text{ Mg/m}^3$) and b) the mixture ($\rho_{d, ini} = 1.72 \text{ Mg/m}^3$) as a function of the normalized outflow (saturated with water (-W), site solution (-SS) and alkaline solution(-AS)).....	115
Figure 4.3: Results of mercury intrusion porosimetry (MIP) experiments conducted on the top (T) and bottom (B) parts of C-I and M-I.....	116
Figure 4.4: Results of mercury intrusion porosimetry (MIP) experiments preformed on the top (T) and bottom (B) parts of M-SS and M-AS	118
Figure 4.5: Normalized cumulative void ratio curves of the top (T) and bottom (B) parts of C-I ($\rho_{d, ini} = 1.95 \text{ Mg/m}^3$) and M-I ($\rho_{d, ini} = 1.72 \text{ Mg/m}^3$)	122
Figure 4.6: Swelling pressure evolution in COX _c and mixture-samples under constant-volume conditions taken from Middelhoff et al. (2020) (Initial characteristics of solutions and materials employed coincided the values given in <i>Table 4.2</i> and <i>Table 4.3</i> , respectively) ...	125
Figure 5.1: Possible combinations of hydraulic and mechanical paths subjected to the backfill upon terminating the installation phase.....	131
Figure 5.2: Results of mercury intrusion porosimetry (MIP) experiments conducted on samples characterized by initial dry densities of $\rho_{d, ini} = 1.72 \text{ Mg/m}^3$ and $\rho_{d, ini} = 1.44 \text{ Mg/m}^3$	136
Figure 5.3: Water retention characteristics of mixture samples characterized by initial dry densities of $\rho_{d, ini} = 1.72 \text{ Mg/m}^3$ and $\rho_{d, ini} = 1.44 \text{ Mg/m}^3$	138

Figure 5.4: Hydro-mechanical paths followed in suction-controlled oedometer experiments	142
Figure 5.5: Hydration paths followed in suction-controlled constant-volume swelling pressure experiments	142
Figure 5.6: Results of oedometer experiments conducted on samples characterized by different initial dry densities upon imposing different hydro-mechanical paths	144
Figure 5.7: Swelling pressure evolution of a) samples characterized by different initial dry densities upon imposing hydration path E and b) samples characterized by the same initial dry density upon imposing hydration paths E, F, and G	145
Figure 5.8: Loading-collapse (LC) curves derived from suction-controlled oedometer experiments	148
Figure 5.9: Comparison between the swelling pressure evolution of a) samples characterized by the same initial dry density upon saturating directly and imposing hydration paths E and b) samples upon saturating directly and imposing hydration paths E, F, and G	150
Figure 5.10: Comparison between LC-curves derived from suction-controlled oedometer experiments and swelling pressure evolution under constant-volume conditions	152

List of Tables

Table 1.1: Compilation of geotechnical barriers	4
Table 1.2: Compilation of frequently studied backfill and sealing material installation methods	5
Table 2.1: Name, range and purpose of performance at different experiment scales	12
Table 2.2: Mineralogical composition of natural and artificially activated bentonites investigated in terms of their hydro-mechanical behavior	13
Table 2.3: SSA of natural and artificially activated bentonites investigated in terms of their hydro-mechanical behavior	16
Table 2.4: Principles, derived properties and covered ranges of techniques for microstructure analysis	18
Table 2.5: CEC of natural and artificially activated bentonites investigated in terms of their hydro-mechanical behavior	28
Table 2.6: Characteristics of the different states of saturation (Aitchison, 1965).....	31
Table 2.7: Characteristics of different techniques frequently employed to control suction	32
Table 2.8: Principle of standard and modified Proctor experiments and derived parameters .	36
Table 2.9: Principles and derived parameters of free-swell potential and different swelling pressure experiments	40
Table 2.10: σ_{min} - and β -parameters corresponding to the individual regression lines depicted in <i>Figure 2.10</i>	45
Table 2.11: Experimental methods, their principles and major derived parameters to analyze the one-dimensional compression behavior	50
Table 2.12: Experimental methods, their principles and major derived parameters to analyze the (un-) saturated hydraulic conductivity behavior	56
Table 2.13: $k_{w, max}$ - and β - parameters corresponding to the individual regression lines depicted in <i>Figure 2.15</i>	61
Table 3.1: Mineralogical composition of MX80-bentonite taken from different references...	80
Table 3.2: Determined physical properties of COX _c , MX80-bentonite, the grain- and powder mixture	83
Figure 3.1: Grain size distribution curves of COX _c , the grain- and powder-mixtures obtained by means of dry sieving and laser diffractometry	84

Table 3.3: Compounds and characteristics of solutions being employed	85
Table 3.4: Material parameters obtained by correlation of experiment and literature data	96
Table 4.1: Physical and physico-chemical characteristics of COX _c and its mixtures with MX80-bentonite	107
Table 4.2: Composition of the site and the alkaline solution (Middelhoff et al., 2020)	109
Table 4.3: Initial characteristics of employed samples	110
Table 4.4: Experimental program including hydraulic conductivity experiments, microstructural and textural analysis.....	113
Table 4.5: Microstructural characteristics of C-I, M-I, M-SS and M-AS obtained by means of MIP-experiments	117
Table 4.6: SSA-values of different samples obtained by means of BET and t-plot	119
Table 4.7: Macro-, micro-, and unaccounted void ratios normalized to the total void ratio..	122
Table 5.1: Initial characteristics of samples	140
Table 5.2: Experiment program including microstructural and water retention analysis, suction-controlled constant-volume swelling pressure and oedometer experiments	143
Table A.1: Details of COX _c , grain- and mixture samples employed in swelling pressure experiments	165
Table A.2: Compilation of results obtained in swelling pressure experiments (comprising COX _c , grain- and powder mixture).....	166

1 Introduction

Radioactive waste arises not only from electricity production in nuclear power plants, but also from different other activities, e.g. medical treatments in hospitals, research, national defense, and mineral processing. It is classified into different groups as it differs in level of radioactivity and period of radioactive decay. Characterized by the highest level of radioactivity, high-level waste (HLW) exclusively arises from electricity production, whereas intermediate-level waste (ILW) or low-level waste (LLW) mainly arise from the other activities previously mentioned. Despite the differences in the level of radioactivity, the common characteristic of all types of radioactive waste is its potential to represent a hazard to people and to the environment (International Atomic Energy Agency, 2009).

International Atomic Energy Agency (2011) formulated safety requirements regarding the construction, operation, closure, and post-closure phases of disposal facilities for radioactive waste. In general, it aimed to ensure the long-term safety of people and the environment against the hazard of ionizing radiation. In this regard, disposal refers to the emplacement of radioactive waste into a facility exclusively designed to contain the waste by means of a system of multiple engineered and natural barriers. The barriers complement each other without maintenance for a defined period of time in order to isolate the waste from the accessible biosphere. In general, such a facility is referred to as repository system.

The safety requirements suggest the disposal of ILW and HLW in facilities, which are constructed in geological formations at least some hundred meters below ground level. Main se-

lection criteria are the long-term stability and hydrogeological properties of the geological formation, henceforth referred to as host rock formation. The safety requirements are formulated irrespectively of the host rock formation, so the radioactive waste might be disposed in either sediment, or sedimentary rock, or crystalline rock, or rock salt formations. Since a complete isolation is less practicable and the hazard associated with the radioactive waste declines with time, it is envisaged to inhibit, reduce and delay the migration of radionuclides from the waste to the accessible biosphere at any time (International Atomic Energy Agency, 2011).

The French agency in charge of radioactive waste management (ANDRA) bases its reference concept for long-term ILW- and HLW-disposal in geological formations (Cigéo project – Industrial Centre for Geological Disposal) on those safety requirements (ANDRA, 2005). The design of the underground facilities of the future repository is sketched in *Figure 1.1*. The future disposal site is constructed in the Meuse/ Haute-Marne-region (North-East France) and is situated in the clay-rich Callovo-Oxfordian sedimentary rock formation, henceforth referred to as Callovo-Oxfordian (COX) claystone. Its depth of occurrence, geological stability, hydrogeological situation, and low permeability account for the consideration. The natural barrier represents the major barrier for radionuclides. The backfill, seals, and canisters represent engineered barriers and complement the natural barrier. In combination, they constitute a system of multiple barriers.

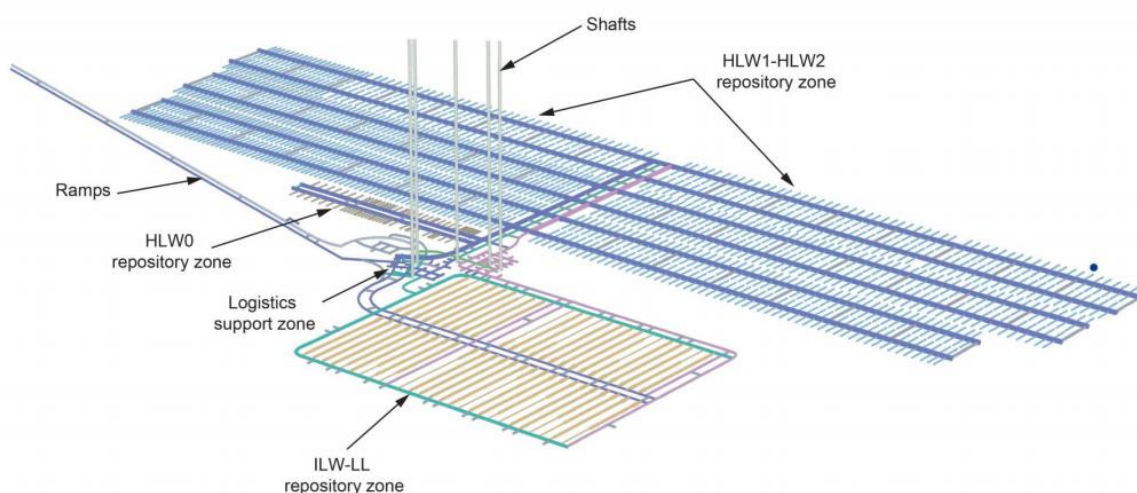


Figure 1.1: Layout of Cigéo underground facilities (Leverd et al., 2017)

1.1 Reference backfill and seal concept

Constructed in the middle of the COX-claystone formation on a single level, the future underground disposal site comprises independent disposal zones for the respective types of radioactive waste. In this regard, independent disposal zone refers to the fact that those zones are constructed, operated and closed independently of each other (ANDRA, 2005). As highlighted in *Figure 1.1*, the accumulated length of the underground structure comprising the shafts, ramps, drifts and disposal cells exceeds one hundred kilometers.

During the operational phase, the canisters containing the radioactive waste are transported from the surface facilities via access shafts and drifts to the emplacement level, at which they are emplaced in the disposal cells. The disposal cells are sealed once they reach their capacity. During the closure phase, backfill and seals are installed in the drifts and shafts, whose concrete lining is partially left in place. The reference backfill and seal concept is sketched in *Figure 1.2*.

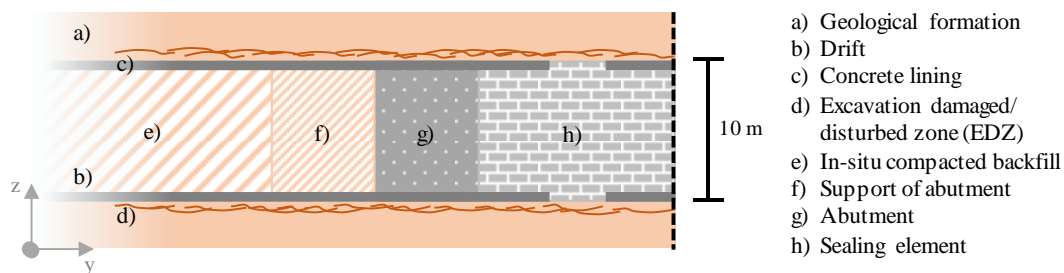


Figure 1.2: Side view at a drift backfilled and sealed according to the French reference concept (modified after ANDRA (2005))

Their installation generally aims to re-establish the integrity of the repository system upon terminating the closure phase. The integrity is reduced not only through the excavation of shafts and drifts, but also through the disturbance and damage of the COX-claystone formation surrounding them. This phenomenon is referred to as excavation disturbed/ damaged zone (EDZ) (e.g. Emsley et al., 1997). The major purposes of geotechnical barrier installation are related to the limitation of the propagation of the excavated damaged/ disturbed zone, as highlighted in *Table 1.1*.

Table 1.1: Compilation of geotechnical barriers

Geotechnical barrier	Specifications/ Purpose of installation	Potential materials	Selected reference
Backfill	<ul style="list-style-type: none"> ○ Stabilization of the host rock formation ○ Limitation of the propagation of the EDZ ○ Solution retention ● through the evolution of free swell potential under unconfined conditions and of swelling pressure under confined conditions upon saturation 	<ul style="list-style-type: none"> ○ Bentonite-based materials, whose mineralogical composition is dominated by the non-bentonite fraction 	<ul style="list-style-type: none"> ○ Pusch (1995) ○ Gunnarsson et al. (2001) ○ Villar (2006) ○ Komine (2010) ○ Rawat et al. (2019)
Seals	<ul style="list-style-type: none"> ○ Stabilization of the host rock formation ○ Compression of the EDZ ○ Closure of hydraulic conductive voids/ Limitation of advective fluid transport from the accessible biosphere to the radioactive waste and vice versa ○ Solution retention ● through the evolution of enhanced free swell potential under unconfined conditions and of enhanced swelling pressure under confined conditions upon saturation 	<ul style="list-style-type: none"> ○ Bentonite ○ Bentonite-based materials, whose mineralogical composition is dominated by the bentonite 	<ul style="list-style-type: none"> ○ Cho et al. (1999) ○ Alonso et al. (2005b) ○ Karnland et al. (2008) ○ Wang et al. (2014) ○ Lang et al. (2019)

Bentonites are particular expansive soils and are considered as potential backfill and sealing materials. Indeed, they exhibit favorable swelling, hydraulic conductivity, and retention characteristics, which are attributed to the elevated expansive mineral fraction dominating their mineralogical composition (e.g. Pusch, 1992). However, the expansive mineral fraction also accounts for the sensitivity of their hydro-mechanical behavior to variations in the material properties (e.g. physico-chemical characteristics, initial dry density), the environmental conditions (e.g. degree of saturation, solution chemistry) and stress history (e.g. preconsolidation stress) (e.g. Alonso et al., 1987; Chen, 1988). The ambient temperature is of less relevance in the context of backfill. Henceforth, those initial and boundary conditions are referred to as geo-environmental conditions. Bentonites are alternatively mixed with sand or materials, which are obtained while excavating shafts and drifts. Henceforth, those mixtures are referred to as bentonite-based materials. The reemployment aims to reduce the risk of mineralogical and physico-chemical incompatibilities of materials and the geological formation, and requires the pre-processing of excavated material, including its crushing and sieving to pre-defined grain sizes. Despite its relevance, information about the multi-scale hydro-mechanical behavior of mixtures composed of bentonite and processed materials are scarcely available (Pusch, 1995).

There are different methods that can be employed to install backfill and sealing materials. Those methods are assessed regarding their applicability, manageability, and costs. As being of major importance, the performance of potential materials is evaluated after preparing them to initial conditions (e.g. initial dry density, initial water content) that are believed to portray the initial conditions likely induced through the different installation methods. The installation methods most frequently studied are the pre-fabricated block method, the pre-fabricated pellet method, the in-situ compaction method, and their combinations. Their procedures, as well as their major advantages and disadvantages are compiled in *Table 1.2*.

Table 1.2: Compilation of frequently studied backfill and sealing material installation methods

Installation method	Procedure	Major advantages/ disadvantages	Selected reference
Pre-fabricated block method	<ul style="list-style-type: none"> ○ Compaction of materials off-side by means of a hydraulic press ○ Installation by means of a special lift truck ○ Option to adjust the compaction energy 	<ul style="list-style-type: none"> ○ Option to apply high compaction energies ○ Adjustment of the material performance to the individual requirements ○ Complex installation onsite ○ Complex supply chain management 	<ul style="list-style-type: none"> ○ Pusch (1992) ○ Lloret et al. (2003) ○ Baille et al. (2010) ○ Zhang and Kröhn (2019)
Pre-fabricated pellet method	<ul style="list-style-type: none"> ○ Compaction of materials off-side by means of a hydraulic press ○ Installation by means of special feeding device ○ Option to adjust the compaction energy ○ Option to mix the pellets with different materials 	<ul style="list-style-type: none"> ○ Option to apply high compaction energies ○ Adjustment of the material performance to the individual requirements ○ Option of further compaction ○ Less complex installation onsite ○ Complex supply chain management 	<ul style="list-style-type: none"> ○ Hoffmann et al. (2007) ○ Karnland et al. (2008) ○ Gens et al. (2013) ○ Darde et al. (2018)
In-situ compaction method	<ul style="list-style-type: none"> ○ Compaction of materials inside the drifts and shafts ○ Installation of previously moistened materials by conventional techniques (e.g. vibration, tamping or rolling) 	<ul style="list-style-type: none"> ○ Less complex material pretreatment ○ Application of a limited compaction energy ○ Limited material performance ○ Considered only for the installation of backfill ○ High demands on quality control 	<ul style="list-style-type: none"> ○ Komine and Ogata (1999) ○ Mata and Ledesma (2003) ○ Komine (2010) ○ Cuisinier et al. (2014)

There is a wealth of information about the behavior of bentonite-based materials, whose initial conditions portrayed those conditions likely induced by the pre-fabricated block or by the pre-fabricated pellet method. It appears that it is well understood how the multi-scale performance of bentonite-based materials can be adjusted by these means. Due to this confidence, those

techniques are preferentially employed to install seals. In contrast, the in-situ method involves great uncertainties, so it is of major importance to determine and to quantify the impact of this installation technique on the performance of bentonite-based materials, also as it might be employed to install backfill material.

1.2 Motivation and objectives

The French reference concept for backfill installation considers the re-employment of COX-claystone, which is obtained while excavating shafts and drifts of the future disposal site and processed to pre-defined maximum grain sizes afterwards. Henceforth, the processed excavated material is referred to as COX_c. In addition, a mixture composed of 70 % COX_c and 30 % MX80-bentonite in weight is considered to be a potential backfill material. Its elevated expansive mineral fraction is expected to enhance the performance of the backfill material. The decision to limit the bentonite fraction principally bases upon the requirement to re-employ as much excavated material as high as technically possible. Apart from that, the specifications related to the performance of backfill materials are limited, as indicated in *Table 1.1*. The reference concept envisages installing the backfill material by means of the in-situ compaction method. Not only might its employment affect the performance, but also might the geo-environmental conditions encountered in the shafts and drifts cause a significant discrepancy between the actual and the expected performance of backfill materials. It is thus of paramount importance to take those factors into consideration.

Following, the major questions are described, claiming to be answered in order to improve the confidence in the potential backfill materials and the potential installation method:

- Most valuable information about how the hydro-mechanical behavior of bentonite-based backfill materials varies as a consequence of the in-situ installation method are provided by the full-scale in-situ *Backfill and Plug Test (BPT)* that was conducted in the Swedish underground research laboratory (URL) in Äspö (Gunnarsson et al., 2001). It principally aimed to assess whether conventional compaction techniques are applicable to install backfill materials in-situ, and to evaluate whether the subsequent performance of materials conforms the safety requirements. The experiment setup allowed to monitor the spatial evolu-

tion of different parameters, such as total stresses, pore pressures, and displacements. Evidently, the maximum swelling pressure close to the drift top was up to 20 % less than that in the centre of the drift. Those observations were attributed to reduced initial dry densities of backfill material. Reductions ensued as the compactor handling became difficult close to the drift top and drift wall, which impeded the application of its full compaction energy, in turn (*Figure 1.3*). Numerous studies emphasized that the initial dry density is one of the key parameters controlling the hydro-mechanical behaviour of bentonite-based materials (e.g. Pusch, 1992; Sridharan and Choudhury, 2002; Schanz and Tripathy, 2009; Gao et al., 2019). In view of the reference concept, it is thus of major importance to study how possible variations in the initial dry density affect the performance of COX_c-based backfill materials.

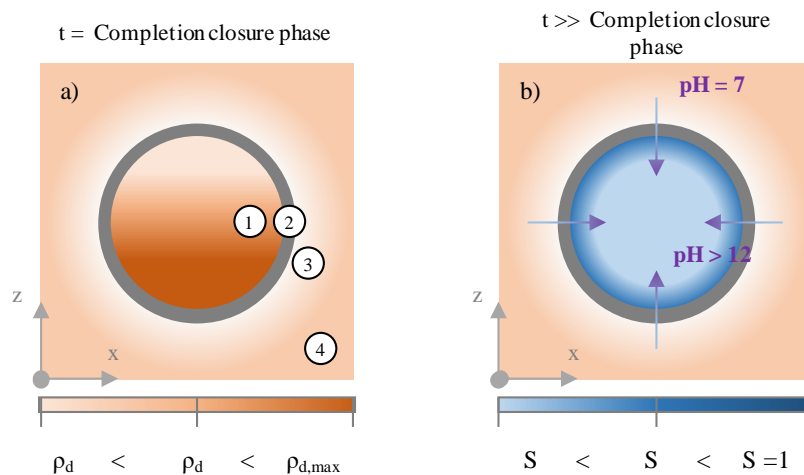


Figure 1.3: Impact of geo-environmental conditions (a. Simplified variations in the initial dry density, b. Evolution of a wetting front & percolation with hyperalkaline solutions) on the in-situ compacted backfill material (1. Backfill, 2. Concrete lining, 3. Excavation damaged/ disturbed zone, 4. Rock formation)

- As sketched in *Figure 1.3b*, the backfill material is installed under unsaturated conditions and saturates completely over time. Thus, their hydro-mechanical behavior is principally controlled by the degree of saturation and/ or the suction that varies with the progressive hydration. The impact of great variations in suction on the hydro-mechanical behavior of bentonite-based materials was highlighted in numerous studies (e.g. Al-Mukhtar et al., 1999; Cui et al., 2008; Romero, 2013; Lang et al., 2019). As the backfill material is characterized by a comparably low initial suction and is subjected to wetting only, it is of major

importance to study the hydro-mechanical behavior of COX_c-based backfill materials under different hydro-mechanical paths, in general.

- Once the closure phase of the repository is terminated, the backfill is saturated with solutions, which originate in the surrounding geological formation and percolate through the concrete lining left in place (*Figure 1.3b*). The initial leachate is characterized by a pH above 13.5. This elevated pH is attributable to the release of potassium and sodium hydroxides from the concrete. After their leachate, the solution chemistry is controlled by the dissolution of portlandite at a pH of 12.5 and later by the dissolution of cement phases at a pH ranging from 10.5 to 12.5. The phenomenon is referred to as hyperalkaline plume and might trigger cation exchange processes, the dissolution and precipitation of clay minerals, and the formation of secondary minerals, while saturating the backfill (e.g. Huertas et al., 2000; Michau, 2005). Since the reaction kinetics are low in-situ, the impact of the saturating solution chemistry on the performance of COX_c-based backfill must be expected to be highly time-dependent.

There is a wealth of information about how the individual geo-environmental conditions affect the multi-scale hydro-mechanical behavior of bentonite-based materials. It is still of major importance to improve the understanding of how the individual geo-environmental conditions affect the performance of potential COX_c-based backfill materials, in particular over time.

1.3 Thesis layout

The thesis layout orientates itself towards the major objectives that are generally described in the section above. The thesis comprises six chapters in total, arranged and presented as follows:

- The first chapter generally introduces into the French reference concept for backfill installation and the issues probably ensuing as COX_c-based backfill materials might be installed by means of conventional compaction techniques upon the operational phase of the future ILW and HLW disposal site terminates.
- The second chapter presents the literature being relevant to understand the origins of the characteristic hydro-mechanical behavior of expansive soils, in particular, the exhibition of swelling pressure and free swell potential under confined and unconfined conditions,

respectively, upon saturation. The chapter then outlines how the different geo-environmental conditions affect the hydro-mechanical behavior. Eventually, it describes constitutive models frequently used to reproduce the hydro-mechanical behavior of expansive soils.

- The third chapter focuses on the combined impact of variations in the initial dry density and the solution chemistry on the swelling pressure evolution of COX_c and its mixtures with MX80-bentonite. It also gives information about the physical and compaction characteristics of materials. Eventually, results obtained are compared to those of previous studies in order to assess the individual and combined impact of the initial dry density and solution chemistry.
- In the fourth chapter, it is evaluated how the saturation with solutions of different chemistry changes the texture and microstructure of COX_c and its mixtures with MX80-bentonite over time, and how the monitored evolution of their hydraulic conductivity can be related to those changes at the nano- and microscale. Further, this chapter gives information about the physico-chemical and microstructural characteristics of materials tested.
- The fifth chapter evaluates whether the compression and swelling behavior of COX_c-based materials depend on the imposed hydro-mechanical path, and how variations in the initial dry density affect those possible path dependencies. It is of particular interest to analyze the impact of variations in the initial dry density on the yield behavior under different hydro-mechanical paths. Further, this chapter gives information about the microstructure and solution retention characteristics of materials tested.
- The sixth chapter synthesizes the major results and gives further approaches in order to interpret globally the impact of the geo-environmental conditions on the hydro-mechanical behavior of COX_c-based materials. Eventually, it outlines questions which are left open and whose answers are claimed.

2 Literature review

After emphasizing the importance of the experiment scale, the literature review presents the major characteristics of expansive soils, in particular their mineralogy and structure, since those microstructural features determine the macrostructural behavior. The subsequent section emphasizes how clay particles interact with water molecules and solutes, including the mechanisms of hydration, swelling and cation exchange. After presenting the clay particle – solution interactions, the concept of suction is introduced, generally adopted to describe the mechanical behavior of materials in partially saturated state. A brief description of solution retention behavior in expansive soils complements the section. As it is of major relevance in the context of backfill materials compacted in situ, the subsequent section highlights the particular compaction behavior and its relation to the microstructural properties of expansive soils. Also, it indicates the impact of physical and physico-chemical parameters on the compaction behavior. The three major sections of the literature review then briefly describe the swelling, compression and hydraulic conductivity behavior of expansive soils and emphasize how they are possibly affected by the physical and physico-chemical material parameters, compaction conditions, environmental conditions and stress history. Then, two constitutive models are briefly presented, frequently employed to reproduce the complex behavior of expansive soils. The finally drawn conclusions aim to provide the basis for formulating the objectives of this study and for highlighting its scientific and technical contributions.

2.1 Scale dependence in expansive soil testing

The (thermo-chemo-) hydro-mechanical behaviour of expansive soils is investigated at various scales (e.g. Alonso et al., 2005a; Armand et al., 2017). Information obtained at the scales serve different purposes, such as the description of the individual/ combined impact of boundary conditions on the material behaviour. Scales, their range and purposes are compiled in *Table 2.1*:

Table 2.1: Different experiment scales considered in expansive soil testing

Name/ Range	Characteristics/ Objectives	Selected references
Nano/ Microscale (10^{-9} m – 10^{-3} m)	<ul style="list-style-type: none"> ○ Description of the basic physical mechanisms determining the macrostructural material behavior ○ Determination of elementary particle arrangement ○ Determination of pores and their distribution 	<ul style="list-style-type: none"> ○ Sposito (1992) ○ Romero (1999) ○ Saiyouri et al. (2004) ○ Massat et al. (2016)
Representative Elementary Volume (<i>REV</i>) (10^{-3} m – 10^{-1} m)	<ul style="list-style-type: none"> ○ Description of the individual impact of different initial and boundary conditions on the material behavior ○ Control of reaction kinetics ○ Material parameter derivation (e.g. for constitutive modelling)/ Intrinsic soil properties 	<ul style="list-style-type: none"> ○ Bolt (1956) ○ Madsen and Müller-Vonmoos (1989) ○ Priyanto et al. (2011) ○ Yuan et al. (2019)
Boundary Value Problem (<i>BVP</i>) (10^{-1} m – 10^0 m)	<ul style="list-style-type: none"> ○ Description of the individual or combined impact of different boundary conditions on the material behavior ○ Adjustable reaction kinetics ○ Calibration (and validation) of constitutive models 	<ul style="list-style-type: none"> ○ Saba et al. (2014) ○ Villar et al. (2016) ○ Rawat et al. (2019)
Full-scale (10^0 m – 10^1 m)	<ul style="list-style-type: none"> ○ Investigation of the material as an entity affected by the interacting initial and evolving boundary conditions ○ No option of reaction kinetics adjustment ○ (Calibration and) Validation of constitutive models (Full system behavior) 	<ul style="list-style-type: none"> ○ Gunnarsson et al. (2001) ○ Martín and Barcala (2005) ○ Gens et al. (2013)

The experiment scale is of major importance when interpreting the impact of the geo-environmental conditions on the evolution of (thermo-chemo-) hydro-mechanical behavior of expansive soils. Following sections mainly analyze experiments performed at the nano-/ microscale and REV-scale. Findings obtained at BVP- and full-scale are considered, in particular when spatial variations in conditions are expected to significantly affect the material performance.

2.2 Nature of expansive soils

Sections 2.2.1 and 2.2.2 cover the mineralogical composition and structure of expansive soils, respectively. The former emphasizes the characteristic features of expansive clay minerals, such

as the surface charge and the interlayer bonding by means of exchangeable cations. The latter describes how the size and shape of clay particles affect the hydro-mechanical behavior. In addition, the different pore populations encountered in expansive soils are explained.

2.2.1 Mineralogy of expansive soils

Natural expansive soils are generally products of volcanic rock alteration and are composed of clay minerals and associated minerals. Clay minerals are classified into expansive clay minerals, like montmorillonite and beidellite, and non-expansive clay minerals, like kaolinite and illite (e.g. Bergaya and Lagaly, 2013). Associated minerals refer to those minerals, whose properties have no impact on the behavior of the individual expansive soil. Common associated minerals are quartz, feldspar(s), carbonate(s), mica(s), sulfate(s) and sulfide(s). Bentonites are particular expansive soils, since the fraction of expansive clay minerals dominates their mineralogical composition (Grim, 1962). The main deposit, mineralogical composition, and dominant exchangeable cation species of four bentonites are listed in *Table 2.2*.

Table 2.2: Mineralogical composition of bentonites frequently investigated in terms of their hydro-mechanical behavior

		MX80 ¹	GMZ01 ²	FEBEX ³	Bavaria Ben. ⁴
Main deposit		Wyoming, USA	Gu Xing region, China	Almería region, Spain	Bavaria, Germany
Expansive clay minerals	[%]	83	76	92	78
Non-expansive clay minerals	[%]	-	-	-	10
Carbonates	[%]	1	-	-	8
Cristobalite	[%]	3	8	1	-
Feldspars	[%]	-	4	-	-
Mica	[%]	1	-	-	-
Quartz	[%]	5	12	2	4
Plagioclases	[%]	7	-	2	-
Sulfides	[%]	-	-	3	-
Dominant exchangeable cation species	-	Na ⁺	Na ⁺	Ca ²⁺	Ca ²⁺

¹: Karnland et al. (2006); ²: Ye et al. (2014a); ³: Lloret and Villar (2007); ⁴: Baille (2014)

By definition, clay minerals are classified as phyllosilicates (e.g. Meunier, 2010). The major characteristic is their layered structure at nanoscale. Tetrahedra and octahedra refer to as the basic structural units of those individual layers (Grim, 1962):

- A single tetrahedra (T) consists of a cation, which is coordinated to four oxygen-anions due to the orbital geometry and ionic size. It links to other tetrahedra by sharing its three basal oxygen-anions forming a continuous hexagonal mesh in the crystallographic a- and b-directions. The apical oxygen-anions typically point to the same side of the sheet. Common tetrahedral cations are Si^{4+} , Al^{3+} and Fe^{3+} . Generally, oxygen sharing is one type of covalent bonding, whose bonding energy is high compared to that of other types.
- A single octahedra (O) consists of a cation coordinated to six oxygen-anions. It lays on one of its triangular faces and links to other octahedra by sharing its edges. By this means, octahedra form a continuous mesh in the crystallographic a- and b-directions characterized by its hexagonal symmetry. Common octahedral cations are Al^{3+} , Fe^{3+} , Mg^{2+} and Fe^{2+} . The oxygen-anions, which are situated at the broken edges and not involved in oxygen-sharing, form hydroxyl groups as a function of the pH of the ambient solution.

Layers arise from the linkage of the apical oxygen-anions of the tetrahedral sheet with most of the oxygen-anions of the octahedral sheet. They thus expand in the crystallographic c-direction. Layers of the TO-type clay minerals, like kaolinite, are composed of one tetrahedral and one octahedral sheet, whereas layers of the TOT-type clay minerals, like montmorillonite and illite, are formed by sandwiching one octahedral sheet between two tetrahedral sheets. Most phyllosilicates can be correspondingly characterized by their periodically arranged stack of layers of either the TO-type clay mineral or the TOT-type clay mineral, as depicted in *Figure 2.1*

The unit cell of the TOT-type clay mineral includes eight tetrahedral and six octahedral sites. A trioctahedral sheet is defined as one octahedral sheet, whose six sites are occupied by three divalent cations, whereas a dioctahedral sheet refers to the case of the occupation of four sites by two trivalent cations. Both the substitution of Al^{3+} - for Mg^{2+} -cations and the presence of vacancies in the octahedral sites are the major source of a constant negative (interlayer) surface charge ζ . The negative (interlayer) surface charge is henceforth referred to as surface charge. In turn, this surface charge causes an electrostatic surface potential ψ (e.g. Meunier, 2010).

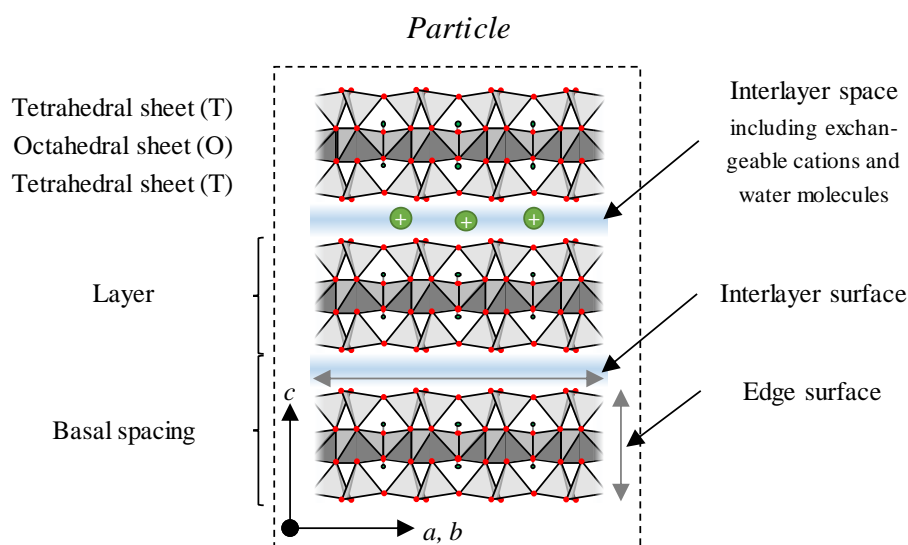


Figure 2.1: Sketch of the structure of a smectite

Although both illite and smectite(s) are classified as TOT-type clay minerals, they differ considerably in their surface charge. The surface charges of illite and smectite(s) ranges between 0.2 to 0.6 per half unit cell and 0.6 to 1.0 per half unit cell, respectively. As both systems claim electro-neutrality, the surface charges must be balanced. Therefore, illite incorporates K^+ -cations in the hexagonal holes of its tetrahedral sheets, whereas the interlayer space of smectite(s) is occupied by positively charged cation species, such as Na^+ , K^+ , Ca^{2+} and Mg^{2+} . They are referred to as exchangeable cations since they are exchangeable when polar molecules solvate them. The basal spacing of smectite(s) varies as a function of their nature and properties. For instance, the basal spacing of an anhydrous MX80-bentonite is 9.6 \AA under ambient conditions (Grim, 1962).

As indicated in *Table 2.2*, the dominant exchangeable cation species determine the type of smectite(s). For instance, bentonites, whose mineralogical compositions are dominated by Na^+ -montmorillonite, can be classified as Na-bentonite. Most frequently studied Na- and Ca-bentonites are MX80- and FEBEX-bentonites, respectively.

Interstratifications of illite and smectite(s) can occur due to their similarity. However, the evolution of interstratified illite-smectite requires the presence of K^+ -cations as well as high temperatures and pressures over a long time (e.g. Brigatti et al., 2013).

By comparing the magnitude of bonding energy through the incorporation of monovalent cations and exchangeable cations, it becomes evident that the interlayer bonding is significantly weaker in the case of exchangeable cations. This weak interlayer bonding is one characteristic feature of expansive clay minerals.

For the purpose of consistency, expansive clay minerals are henceforth referred to as smectite, since only smectite(s), like montmorillonite and beidellite, are characterized by such a mode of interlayer bonding.

2.2.2 Structure of expansive soils

Particles of smectite can be usually characterized by the small ratio of their height to their length and width. A stack of layers forming an individual particle is exemplified in *Figure 2.1*. The mostly platy-like appearance is attributed to the strong covalent bonding interlinking the individual tetrahedra and octahedra in the crystallographic a- and b-directions, and to the weak interlayer bonding by means of exchangeable cations that hold the individual layers in the crystallographic c-direction together (Grim, 1962). As a consequence of their appearance, smectite has a significantly elevated specific surface area (SSA), compared to other clay minerals or associated minerals (e.g. Pusch, 2001b). SSA is defined as the ratio of the total surface area of a porous material to a unit of mass and is usually expressed in m^2/g . Michot and Villiéras (2013) emphasized that SSA has a major impact on the hydro-mechanical behavior of expansive soils as it controls surface phenomena, in particular the sorption and retention of molecular and ionic species. SSA of four selected bentonites are listed in *Table 2.3*.

Table 2.3: SSA of bentonites frequently investigated in terms of their hydro-mechanical behavior

	MX80 ¹	GMZ01 ²	FEBEX ³	Bavaria Ben. ⁴
Specific Surface Area (SSA) ^a [m ² /g]	562	570	725	525

¹: Madsen (1998); ²: Ye et al. (2014a); ³: Lloret and Villar (2007); ⁴: Baille (2014)

^a: determined by means of Keeling hygroscopticity method

In contrast to non-expansive soils, expansive soils are characterized by different structural units at micro- as well as macroscale, whose size, shape, and arrangement determine the material behavior. As described above, an individual particle is composed of multiple periodically

stacked layers linked by the exchangeable cation population. Multiple particles positioned closely to each other are referred to as an aggregate, whereas multiple aggregates are referred to as an assembly of aggregates (*Figure 2.2*). The size of the individual structure increases from tenth of nanometers in the case of the layers to hundreds of thousands of nanometers in the case of assemblies of aggregates (e.g. Massat et al., 2016).

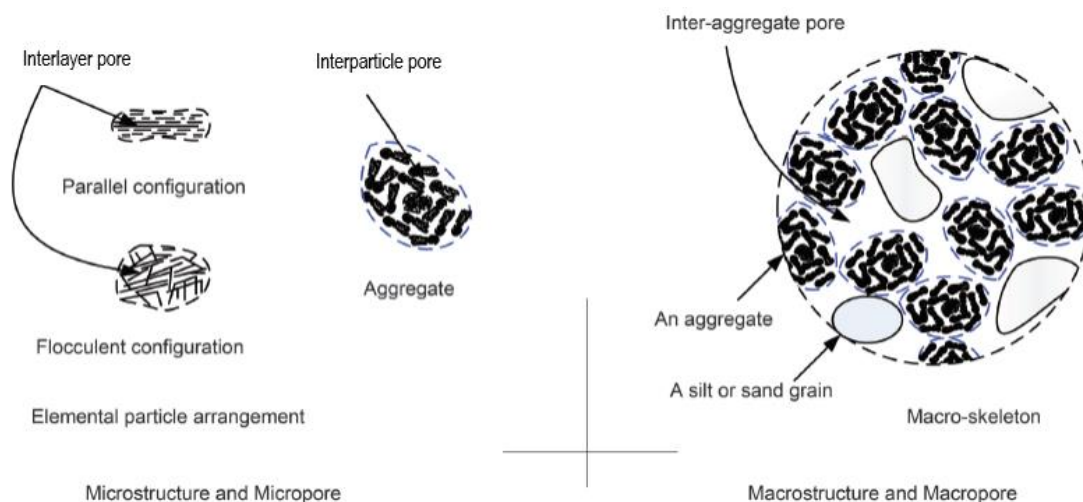


Figure 2.2: Sketch of the multiscale structure of expansive soils comprising particles, aggregates, assemblies of aggregates and the corresponding interlayer, interparticle and interaggregate pores (modified after Wang and Wei (2015))

The pore space of expansive soils can be generally classified in interlayer pores, interparticle pores and interaggregate pores. Interlayer pores are planar void spaces between the layers, and interparticle pores are present between the particles as well as inside the aggregates. Randomly arranged aggregates account for interaggregate pores (*Figure 2.2*). The latter two pore populations are referred to as micropores and macropores, respectively (e.g. Alonso et al., 1987; Romero et al., 1999; Delage et al., 2006; Romero, 2013).

2.2.3 Experimental determination

The structure of expansive soils can be studied by means of different quantitative and qualitative methods. The former comprises gas sorption isotherms and mercury intrusion porosimetry (MIP), for instance. The latter refers to image-producing techniques, such as (high-resolution) X-ray/ μ -focus computed tomography and scanning electron microscopy (SEM). There is a

variety of techniques available for structure analysis in expansive soils. The techniques most frequently employed are compiled below. Their principles, derived properties and ranges are compiled in *Table 2.4*.

Table 2.4: Principles, derived properties and covered ranges of techniques for microstructure analysis

Name	Principle/ Derived properties	Range/ Comments	Selected references
Nitrogen/ Argon gas adsorption/ desorption isotherms	<ul style="list-style-type: none"> ○ Physical adsorption/ desorption of non-reactive nitrogen/ argon gas molecules on solid surfaces ○ Determination of the (external) specific surface area (SSA) ○ Determination of the pore size distribution ○ Information about the pore shape 	<ul style="list-style-type: none"> ○ Micropores: $d_p < 2\text{nm}$ ○ Mesopores: $2\text{nm} < d_p < 50\text{ nm}$ ○ Macropores: $d_p > 50\text{ nm}$ 	<ul style="list-style-type: none"> ○ Gregg and Sing (1969) ○ Cases et al. (1997) ○ Fernández et al. (2014)
Mercury intrusion porosimetry (MIP)	<ul style="list-style-type: none"> ○ Forced penetration of a non-wetting fluid, such as mercury, into a porous medium by increasing the fluid injection pressure step-wise ○ Determination of the pore size distribution 	<ul style="list-style-type: none"> ○ Few nanometers (nm) – tens of micrometers (μm) ○ Limitations, such as non-detected or constricted porosity, isolated pores etc. 	<ul style="list-style-type: none"> ○ Garcia-Ben-gochea et al. (1979) ○ Romero et al. (1999) ○ Romero and Simms (2008) ○ Yuan et al. (2016)
High-resolution X-ray/ μ -focus computed tomography	<ul style="list-style-type: none"> ○ Measurement of the attenuation coefficient to X-rays ○ Record of a set of two-dimensional X-ray radiographs of an object at several angles ○ Reconstruction of 3D slices from the radiographs by means of a mathematical algorithm ○ Information about the pore shape 	<ul style="list-style-type: none"> ○ Hundreds of nanometers (nm) – tens of millimeters (mm) 	<ul style="list-style-type: none"> ○ van Geet et al. (2005) ○ Gens et al. (2011) ○ Massat et al. (2016) ○ Molinero Guerra et al. (2018)
Scanning electron microscope/ Environmental scanning electron microscope	<ul style="list-style-type: none"> ○ (under vacuum conditions) ○ Scan of samples by means of a focused electron beam ○ Detection of electrons emitted by atoms after their stimulation ○ Information about the pore shape 	<ul style="list-style-type: none"> ○ Few nanometers (nm) – tens of millimeters (mm) ○ Limitations, such as the exclusive observation of the material surface 	<ul style="list-style-type: none"> ○ Graham et al. (1989) ○ Pusch (2001b) ○ Romero and Simms (2008) ○ Musso et al. (2013)

2.2.4 Conclusion

It can be finally concluded that non-expansive and expansive clay minerals differ in their surface charge, mode and magnitude of interlayer bonding, specific surface area and structure. The

weak interlayer bonding in conjunction with the nature and properties of the exchangeable cation species account for the variations in the basal spacing affecting the material behavior of expansive soils. Particular material properties of expansive soils, such as the sorption and retention, can be attributed to the elevated specific surface area in conjunction with the surface charge of the individual particles. Moreover, it was highlighted that expansive soils comprise different micro- and macrostructural units, whose arrangement also affect the material behavior.

2.3 Interactions in clay particle – solution systems

Smectites are characterized by an elevated SSA, a weak interlayer bonding and a negative surface charge. Interactions between the individual clay particles and solutions at nano- and microscale determine the (thermo-chemo-) hydro-mechanical behavior of expansive soils at macroscale. Sections 2.3.2 describes impact of the pH of the solution on clay particles and their orientation towards each other. Sections 2.3.3, 2.3.4 and 2.3.4 then emphasize the interactions between clay particles and solutions at and near the particle – solution interface as they account for the swelling mechanisms. The cation exchange capacity is briefly described in section 2.3.5.

For consistency, soil samples characterized by a low and high ratio of liquid to solid phase are henceforth referred to as compacted and slurried samples, respectively.

2.3.1 Effect of pH in clay particle – solution systems

The negative charge at face sides of clay particles is permanent, whereas the charge at edge sides varies as a function of the pH of the ambient solution. The conditional variation in charge is due to the formation of hydroxyl groups. Those groups are characterized by either a positive charge, when pH-values are low, or a negative charge, if pH-values are high (e.g. van Olphen, 1980). The point of zero charge defines the pH-value, at which the charge at the edge sides is zero (Sposito, 1992). In slurried samples, a reorientation of layers can ensue as the pH varies. They can position themselves face-to-face, edge-to-edge or edge-to-face, which leads to a significant alteration of the rheological properties of the slurry (e.g. van Olphen, 1980).

In addition, the pH of the ambient solution also determines the stability of clay particles. The layers start dissolving once the pH-value goes below 4 or exceeds 11 (Krauskopf, 1956). In the context of backfill materials, this aspect is of particular relevance.

2.3.2 Hydration mechanisms

By definition, a solution is composed of a liquid solvent, in which solutes are dissolved. Accordingly, groundwater is a solution. Water is the liquid solvent, whereas different ions are the solutes. In this regard, water refers to water molecules in the liquid- and gas phase. Inorganic salts are the dominant electrolytes in groundwater. Once dissociated, their ions are hydrated by the polar water molecules. The preference to be hydrated depends mainly on the nature of the ions, such as the ion charge and the ion radius (Adamson and Gast, 1997).

According to Sposito (1992), the higher hydration potential accounts for the migration of water molecules from the ambient solution into the interlayer space of smectites, where they either hydrate the exchangeable cations or interact with the interlayer surface. The system approaches electroneutrality by these means. He indicated that those interactions are mainly governed by the activity of water molecules in the clay particle – solution system, the hydration potential of the exchangeable cations and the polarization of water molecules by the exchangeable cations. In general, cation hydration involves the adsorption of water molecules on the exchangeable cations and the formation of hydration complexes. Cations are preferentially hydrated due to their positive charge and their smaller ion radius. Hydration complexes differ in their mode of interaction with the interlayer surface (e.g. Sposito, 1992):

- Inner sphere complexes are characterized by the direct connection of the cation to the interlayer surface on the one side and to a number of water molecules on the other side.
- The cation of outer sphere complexes interacts with the interlayer surface through its water ligands as it is completely surrounded by water molecules. A discrete layer of water ligands is generally referred to as hydration shell. The formation of outer sphere complexes is a key process accounting for the mobilization of cations.

Water molecules somehow interacting with the interlayer surface are henceforth referred to as interlayer water (e.g. Bradbury and Baeyens, 2003).

2.3.3 Crystalline swelling mechanism

As described above, water molecules hydrate the exchangeable cations and interact with the interlayer surface once they enter the interlayer space. The major interaction is the adsorption

of water molecules on the interlayer surface, where they can constitute a discrete layer. Upon saturation, discrete layers intercalate, which leads to a stepwise increase in the basal spacing of particles. The increase in the basal spacing due to the intercalation of discrete layers of water molecules is referred to as crystalline swelling (Norrish, 1954). The mechanism contributes to soil expansion, predominantly when soils are characterized by a low water content.

Several studies aimed to quantify the discrete layers of water molecules in Na- and Ca-montmorillonites under different compaction and confining conditions upon increasing the relative humidity (*RH*) (e.g. Chipera et al., 1998; Caballero et al., 2004; Saiyouri et al., 2004; Ferrage et al., 2005; Devineau et al., 2006; Villar, 2007). The number of layers was deduced from the basal spacing, which was measured by means of X-ray diffractometry once samples were in equilibrium with the imposed *RH*. The results are compiled in *Figure 2.3a* and *Figure 2.3b*.

In general, different numbers of discrete layers of water molecules can coexist as differences in the layer charge location cause spatial variations in the surface potential on particle face sides. Following, values correspond to average values of basal spacing. In the case of Na-montmorillonite, basal spacing of about 10 Å, 12.5 Å, 15.5 Å and 18.5 Å indicated no, one, two and three discrete layer(s) of water molecules, respectively, regardless of confinement and initial dry density. One, two and three discrete layer(s) of water molecules were adsorbed upon imposing *RH* greater than 30 %, 80 % and 95 %, respectively (Devineau et al., 2006). Saiyouri et al. (2004) reported that the basal spacing even expanded to about 21.5 Å corresponding to a four discrete layers of water molecules. The value was obtained by imposing a relative humidity higher than 99 %. In the case of Ca-montmorillonite, the adsorption of no, one and two discrete layer(s) of water molecules induced basal spacing of about 11 Å, 15.5 Å and 18 Å, respectively. One and two distinct layers evolved upon imposing *RH* greater than 20 % and 95 %, respectively. According to Michot et al. (2013), the maximum basal spacing of Ca-montmorillonite might be limited to 18 Å due to ion correlation forces.

Villar et al. (2012) emphasized that the expansion of the basal spacing is time-dependent and the probability of coexisting hydration states reduces over time as water molecules redistribute from micro- and macropores into the interlayer space. Further, redistribution processes appeared to be accelerated through confined conditions.

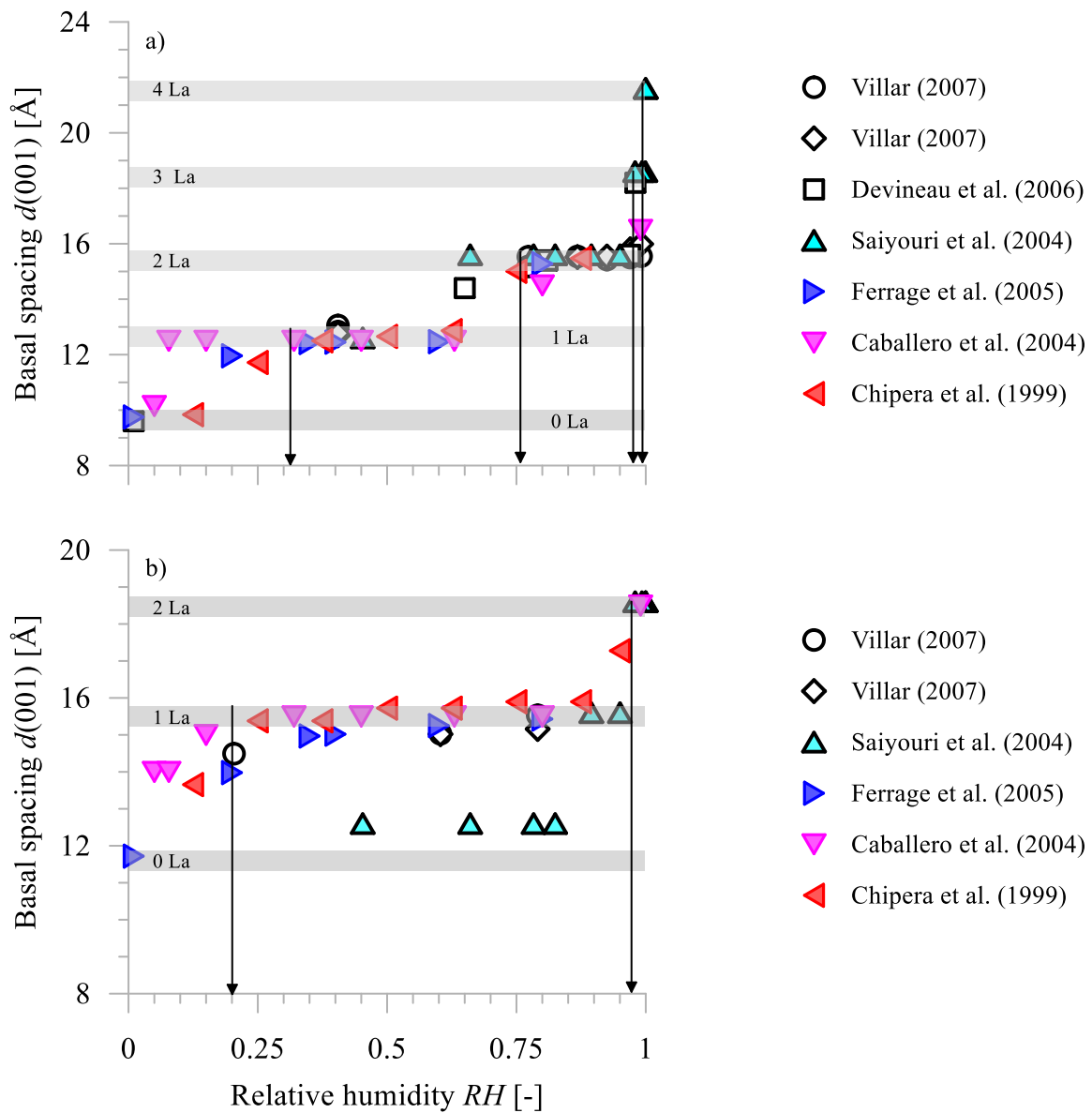


Figure 2.3: Evolution of discrete layers of water molecules in a) Na-montmorillonite and b) Ca-montmorillonite as a function of imposed relative humidity (Black-framed symbols indicate compacted and confined samples; Black-framed and colored symbols indicate compacted samples under free swell conditions; Colored symbols indicate powdered samples under free swell conditions)

2.3.4 Osmotic swelling mechanism

Apart from inner- and outer sphere complexation, electrostatic attraction ensures the electro-neutrality of clay particle – solution systems. The surface charge accounts for the diffusion of cations from the ambient solution towards the particle face sides, where bare cations and inner

sphere complexes are immobilized through adsorption (*Figure 2.4a* and *Figure 2.4b*). A concentration gradient develops as the concentration of cations is higher near the particle face sides than in the ambient solution. Indeed, the cations tend to diffuse away from the particle face sides in order to reduce the concentration gradient and to ensure electroneutrality (n_0) (*Figure 2.4c*). However, their motion is restricted by the surface charge. The simultaneous attraction and repulsion cause a characteristic distribution of ions adjacent to the particle face sides. This phenomenon of the charged particle surface and the distributed charge in the adjacent solution is referred to as diffuse double layer (DDL) (van Olphen, 1980; Sposito, 1992; Mitchell and Soga, 2005).

Water molecules interacting with the diffuse double layers are generally referred to as double layer water. Conversely, water molecules not interacting with the charged surfaces are defined as free water (e.g. Bradbury and Baeyens, 2003).

Mitchell and Soga (2005) referred to the Gouy-Chapman-theory (Gouy, 1910; Chapman, 1913) and the DLVO-theory (Derjaguin and Landau, 1941; Verwey and Overbeek, 1948) as the theories which are most frequently adopted to describe the repulsive and attractive forces generated by those interactions. In both theories, the electrostatic potential decreases exponentially as the distance from the charged particle surface increases (*Figure 2.4b*). The exponential decrease accordingly depends on the ambient temperature as well as the concentration and nature of solutes. Several idealizations accompany the employment of both theories. For instance, ions are considered as point charges. There are no interactions between the ions and no variations in the surface charge. Moreover, the ratio of the double layer thickness and the particle surface is small. The exponential decrease of the electrostatic potential with distance can be mathematically described by a partial differential equation:

$$\frac{d^2\psi}{dx^2} = -\frac{e}{\varepsilon} \sum v_i n_i \exp\left(\frac{-v_i e \psi}{kT}\right) \quad (2.1)$$

Where ψ is the electrostatic potential, x is the distance from the particle surface, e is the electronic charge ($e = 1.602 \times 10^{-19}$ C), ε is the permittivity, v_i is the valence of the ions of the types i , n_i is the concentration of the ions of the types i , k is Boltzmann's constant ($k = 1.381 \times 10^{-23}$ J/K) and T is the temperature.

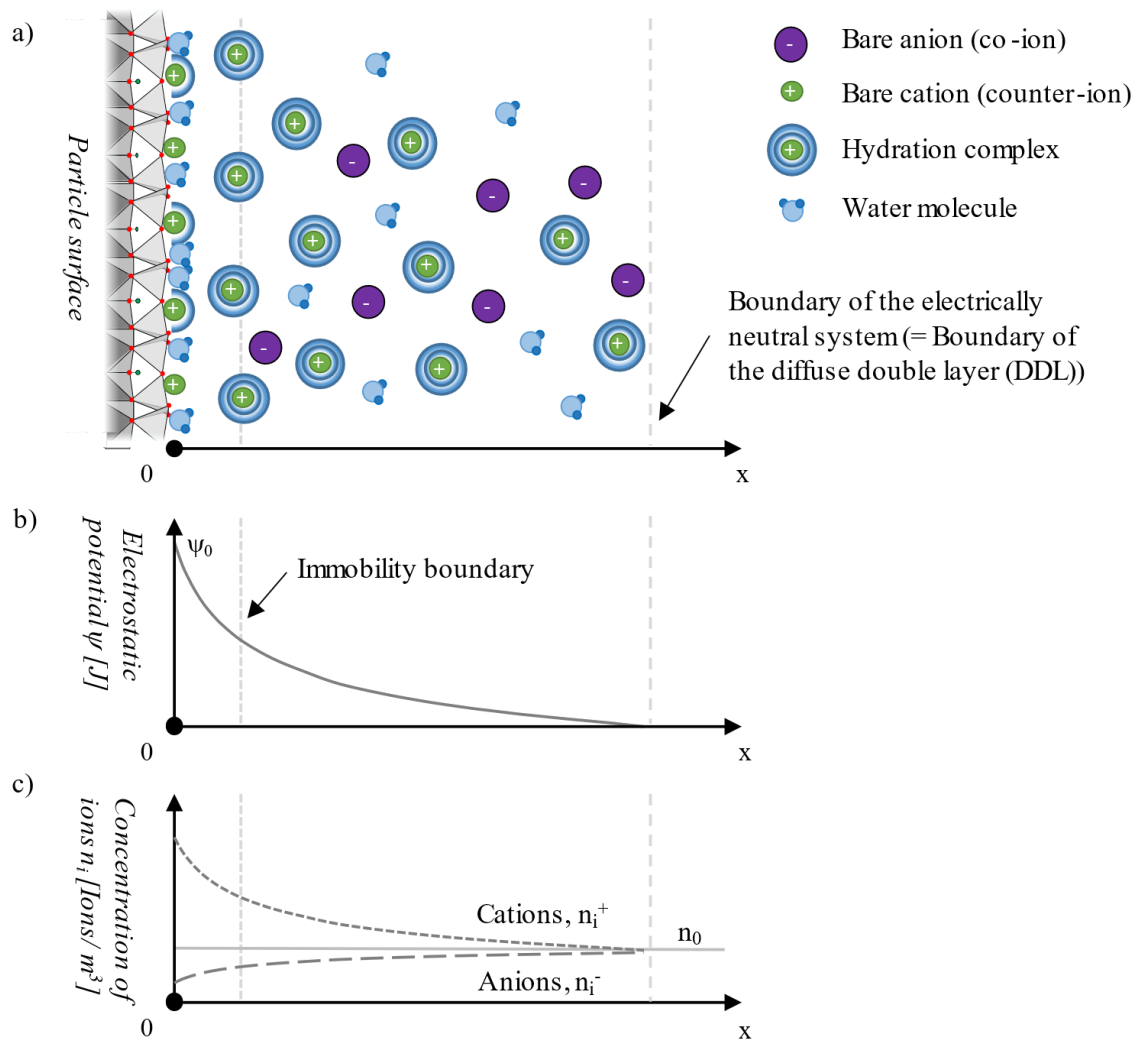


Figure 2.4: a) Schematic sketch of the distribution of ions adjacent to a clay particle face according to the concept of the diffuse double layer, b) Corresponding exponential decrease of the electrostatic potential of clay particle faces with distance, c) Corresponding exponential decrease and increase of cations and anions, respectively, with distance (modified after van Olphen (1980) and Sposito (1992))

The case described above assumes a single clay particle, which interacts with the solutes in the adjacent solution. However, such an idealized case might be encountered in suspensions rather than in compacted expansive soils. A more representative case is depicted in *Figure 2.5*. The two particles are so close to each other that their diffuse double layers of the same sign overlap and repel each other. As a consequence, the distance between the particles increases. The increase in distance between particles due to the repulsion of their diffuse double layers is referred to as osmotic swelling. The mechanism contributes to soil expansion, predominantly when soils are characterized by higher water contents (e.g. Madsen and Müller-Vonmoos, 1989).

The osmotic pressure can be adopted to quantify the energy of the repulsive force (V_R). It develops as the concentration of solutes in the interparticle space (n_i) is higher than in the ambient solution (n_o). In order to reduce the concentration of solutes therein, water molecules enter the interparticle space. According to Yong and Warkentin (1975), the energy of the corresponding repulsive force per unit area can be defined as the difference in osmotic pressure midway between two particles (B) relative to that in the ambient solution (A):

$$\pi = RT \sum (n_{iB} - n_{iA}) \quad (2.2)$$

Where π is the osmotic pressure, R is the universal gas constant ($R = 8.314 \text{ J/ K mol}$), T is the temperature, n_{iB} is the concentration of the individual ion type midway between the particles and n_{iA} is the concentration of the individual ion type beyond the boundary of the electrically neutral system.

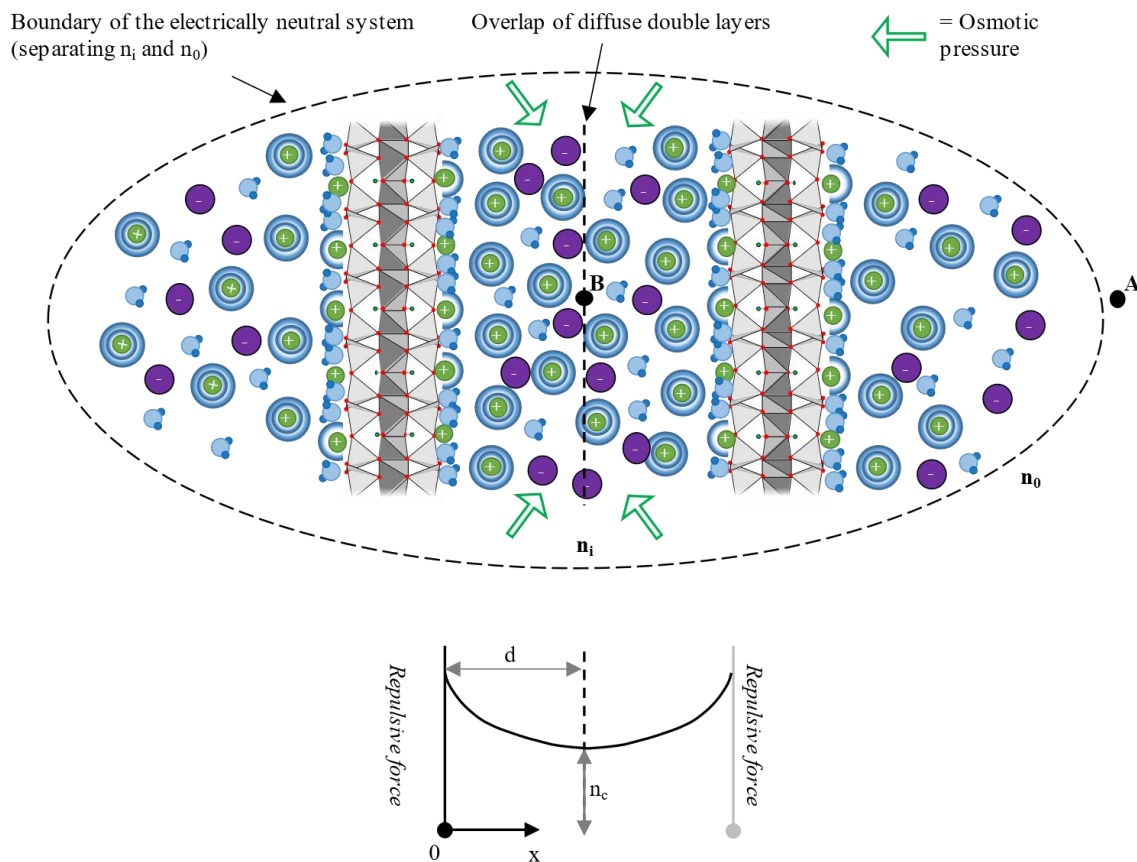


Figure 2.5: Two negatively charged clay layers with diffuse double layers

In contrast to crystalline swelling, whose range is limited by the discrete number of water layers, the repulsion of diffuse double layers can trigger the defoliation or even exfoliation of single layers in slurried samples. The tendency to do so depends on the nature of the exchangeable cations, such as ionic radius and valence (e.g. Brigatti et al., 2013). For instance, Na-montmorillonite exfoliate easily, whereas ion correlation forces prevent Ca-montmorillonite particles from the complete exfoliation (e.g. Kjellander et al., 1988).

The case presented above considers discrete layers of water molecules as well as inner sphere and outer sphere complexes, which surround two clay particles orientated parallel to each other. It might be assumed that material densification leads to a decrease in the halfway distance between the particles and to an increase in the probability of repulsion. This assumption accordingly implies a threshold of the initial dry density, above which no diffuse double layers can evolve due to the limitation of space (e.g. Bolt, 1956; Mitchell and Soga, 2005).

In addition, the DLVO-theory assumes the development of attractive forces between the parallel particle face sides (*Figure 2.5*). Their origin is the fluctuation of dipole bonds commonly referred to as van der Waals bonds. Those bonds are caused by the fact that there are more electrons on one side of the atomic nucleus than on the other side at any time. They are non-directional and act between all units of matter. Mathematically, the energy of attractive forces (V_A) between two parallel plates can be described as follows:

$$V_A = - \frac{A}{48\pi} \left[\frac{1}{d^2} + \frac{1}{(d + \delta)^2} + \frac{2}{\left(d + \frac{\delta}{2}\right)^2} \right] \quad (2.4)$$

Where A is the Hamaker constant, d is the half distance between plates measured from the plane of the surface layer atoms and δ is the thickness of the plate measured between the same planes. The addition of the double layer repulsion energy to the van der Waals attraction energy results in the net energy. Its development as a function of the distance x is depicted in *Figure 2.6*. The major characteristic is the peak commonly referred to as repulsive energy barrier.

In general, particles are not able to approach each other in the case of a high repulsive energy barrier, whereas the particles can easily get close to each other in the case of a low repulsive

energy barrier. Considering *equation 2.1*, it becomes evident that the repulsive energy barrier is mainly affected by the solution chemistry.

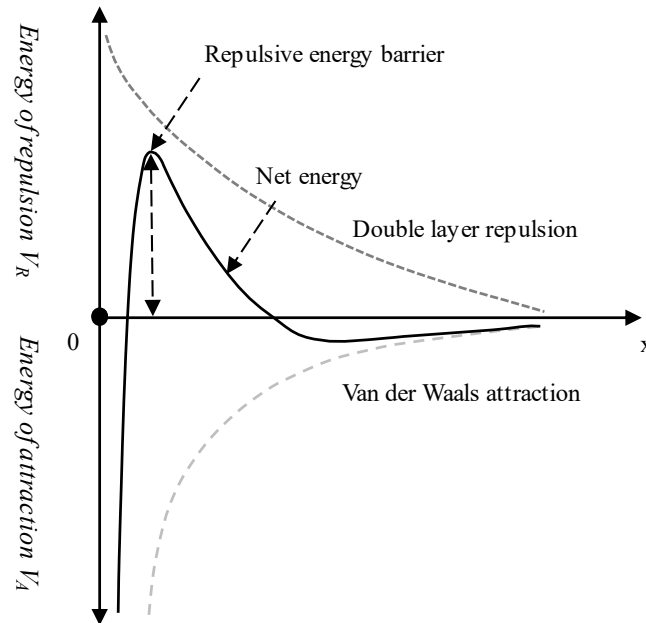


Figure 2.6: Net energy of interactions (assuming a low ion concentration in the adjacent solution (modified after van Olphen (1980))

2.3.5 Cation exchange processes

Different cations from the ambient solution also enter the zone, which is affected by the surface charge of particles. The driving force of their migration is the preference of adsorbing one cation species over another. This preference depends predominantly on the nature of the exchangeable cations and provokes the replacement of cations balancing the surface charge by cations from the ambient solution (e.g. Brigatti et al., 2013). A typical replaceability series is presented in Mitchell and Soga (2005): $\text{Na}^+ < \text{Li}^+ < \text{K}^+ < \text{Mg}^{2+} < \text{Ca}^{2+} < \text{Al}^{3+} < \text{Fe}^{3+}$. The ability of smectites in absorbing cations from the ambient solution is referred to as cation exchange capacity (CEC). In addition to the selectivity of one cation species over another, CEC is characterized by its reversibility and its control by diffusion. Its magnitude depends on the surface charge of particles and SSA. Generally, CEC gives information about the adsorption capacity with regard to individual cation species. CEC of four selected bentonites are listed in *Table 2.5*.

Table 2.5: CEC of natural and artificially activated bentonites investigated in terms of their hydro-mechanical behavior

	MX80 ¹	GMZ01 ²	FEBEX ³	Bavaria Ben. ⁴
Cation Exchange Capacity (CEC) [meq/100 g]	76	77	102	74

¹: Madsen (1998); ²: Ye et al. (2014a); ³: Lloret and Villar (2007); ⁴: Baille (2014)

2.3.6 Conclusion

It can be concluded that solutes and water molecules interact with each other and with the clay particle surface through adsorption at particle face sides, inner and outer sphere hydration complexation, electrostatic attraction, and ion exchange. Crystalline swelling is the result of the intercalation of discrete layers of water molecules upon saturation. It causes the increase of the basal spacing and, in turn, contributes to material expansion. Diffuse double layers comprise the charged particle face sides and the distributed solutes in the adjacent solution. The repulsion of diffuse double layers account for osmotic swelling, which also contributes to material expansion. As highlighted above, those mechanisms are mainly affected by the repulsive energy barrier that depends on the saturating solution chemistry, CEC and SSA. Further, it was emphasized that the solution chemistry, in particular the pH-value, governs the chemical stability of clay minerals.

2.4 Solution retention behavior of expansive soils

According to the reference concept, backfill materials are compacted directly inside the drifts in unsaturated state and saturate through the long-term percolation of solutions originating in the surrounding geological formation. This section covers a brief description of the basic principles of solution retention in expansive soils. It aims to emphasize the difference of the hydro-mechanical behaviour in expansive soil under saturated and unsaturated conditions.

2.4.1 Concept of suction in expansive soils

Partially saturated soils are characterized by a negative pore solution pressure being equal to the total free energy of the pore solution. In this regard, pore solution comprises the interlayer water, the double layer water, the free water, and the solutes, whereas pore air refers to the gas

phase in the different pores. The energy of the pore solution is related to soil-solution potential which portrays the mechanisms triggered by the different thermodynamic forces in soils (Yong and Warkertin, 1975; Yong, 1999). The soil-solution potential comprises five components:

$$\psi_{tot} = \psi_m + \psi_\pi + \psi_g + \psi_a + \psi_p \quad (2.5)$$

Where ψ_{tot} is the total soil-solution potential, ψ_m is the matric soil-solution potential, ψ_π is the osmotic soil-solution potential, ψ_g is the gravimetric soil-solution potential, ψ_a is the pneumatic soil-solution potential and ψ_p is the external pressure soil-solution potential. Matric potential is caused by capillarity in conjunction with adsorption forces, whereas osmotic potential is attributable to differences in the chemical potential of solutes and solvent. In expansive soils, hydration potentials in the interlayer pores, adsorption of ionic and molecular species on clay particles and the formation of diffuse double layers particularly promote capillarity. Matric and osmotic potentials are often considered to be sufficiently precise to portray the total energy of the pore solution. The other components are the gravitational potential being related to the position of the soil in the gravitational field, the pneumatic potential being attributable the pressure in the pore air, and the pressure potential induced by externally applied pressures. Although the latter three potentials exhibit a minor impact compared to the matric and osmotic potential, they still contribute to the total free energy of the pore solution.

The conclusions of Yong and Warkertin (1975) are in accordance with the definition of Aitchison (1965). By his definition, which bases on the principles of capillary condensation in porous media, the total free energy of the pore solution is characterized by its total suction s_{tot} . It is defined as the ratio of the partial vapor pressure of the solution in capillary-like pores p_v to the saturation vapor pressure of the solvent in unconfined conditions p_v^0 . The ratio of the partial vapor pressure to the saturation vapor pressure is commonly referred to as relative humidity RH and can be related to the total suction by Kelvin's law:

$$s_{tot} = -\frac{RT}{Mg} \ln\left(\frac{p_v}{p_v^0}\right) \Rightarrow s_{tot} = -\frac{RT}{Mg} \ln(RH) \quad (2.6)$$

Where s_{tot} is the total suction, R is the universal gas constant, T is the absolute temperature, M is the molar mass of water and g is the gravity acceleration. The components of total suction are matric suction s_m and osmotic suction s_π . Matric suction is mainly caused by capillarity

promoted by other physico-chemical interactions. Since the partial vapor pressure is smaller than the saturation vapor pressure, vapor condenses in the capillaries. The pressure difference is equilibrated by the formation of menisci at the interface of the pore air and pore solution, whose shape changes as a function of the surface tension T of the solvent and the radius r of the capillary. This functional relation can be defined by Young-Laplace's equation for completely wettable solvents:

$$u_a - u_w = \frac{2T}{r} \quad (2.7)$$

Where u_a is the air pressure and u_w is the water pressure. Henceforth, the interface of pore air and pore solution is referred to as contractile skin. Since the contractile skin exhibits a tensile strength, it can rearrange the structure of soils by changing its curvature as a reaction to variations in relative humidity. Osmotic suction can be attributed to the concentration of solutes in the pore solution. The partial vapor pressure of a solution decreases progressively as the solute concentration increases, regardless of the confining conditions.

In the context of crystalline swelling, the stepwise evolution of discrete layers of water molecules was described in section 2.3.3. The results presented can be interpreted as a function of the imposed total suction instead of the imposed relative humidity. According to Saiyouri et al. (2004), one, two, and three discrete layers of water molecules can be expected by imposing suctions smaller than 60 MPa, 4 MPa and 0.05 MPa, respectively.

2.4.2 Solution retention in expansive soils

A gradual increase of total suction causes a progressive removal of pore solution from pores of decreasing sizes. The increasing total suction can thus be related to the decreasing degree of saturation. This relation is represented by the solution retention curve (Aitchison, 1965). The water retention curve can be characterized by four states. The characteristics of each state are described in *Table 2.6*.

- In saturated state, the pore solution pressure is theoretically bigger or equal to zero.
- Total suction as well as the curvature of the contractile skin start increasing by the initialization of evaporation. The progressive removal of pore solution generates the increase in

air volume in the larger pores which are still not in direct contact with the surrounding air. This state is referred to as quasi-saturated.

- Once exceeding their limit curvature, the menisci recede into the soil and air enters the soil. As a consequence, the pore solution becomes discontinuous in the pore space. This state is referred to as partially saturated state. It can be subdivided into further sub-states defining more precisely the connection of pore solution and pore gas phase.
- The last state referred to as residual state is characterized by the isolated presence of pore solution in the pore space. Equilibrium conditions are established through the vapor phase.

Table 2.6: Characteristics of the different states of saturation (Aitchison, 1965)

State	Degree of saturation (S_r)	Pore solution pressure (u_w)	Pore air pressure (u_a)	Rel. compressibility of the pore fluid (N_f)*	Difference in water content (Δw)
	[%]	[kPa]	[kPa]	[-]	[%]
Saturated	100	≥ 0	-	1	0
Quasi-saturated	100	≥ 0	-	1	0
Partially saturated	< 100	< 0	> 0	> 1	> 0
Unsaturated	< 100	< 0	≥ 0	> 1	> 0

*: defined as the ratio of the compressibility of the fluid (C_f) to the compressibility of deaired water (C_w)

^: difference of present water content to the water content at which capillary forces are zero

Soils exhibit a different solution retention behavior when comparing the results which are obtained by drying completely saturated soils and by wetting completely desaturated soils. The solution retention is thus considered as hysteretic. The curve described by a soil dried from saturated state is termed as main drying curve, whereas the reverse curve is termed as main wetting curve. Both curves mark out the domain of possible reachable saturation states. Wetting of soils which were dried to an intermediate degree of saturation before causes a scan of the hysteresis domain from the main drying to the main wetting curve. The corresponding path is referred to as scanning curve.

2.4.3 Experimental determination

There are different techniques to measure and control suction. In *Table 2.7*, only those techniques are described, whose application allows to control suction, such as the suction plate

technique, the pressure plate technique, the osmotic technique and the vapor equilibrium technique. A detailed review of the techniques is given in Delage et al. (2008), for instance.

Table 2.7: Characteristics of different techniques frequently employed to control suction

Name	Principle/ Imposed suction	Range/ Comments	Selected references
Suction plate technique (Water subpressure)	<ul style="list-style-type: none"> ○ Initiation of solution exchange between the pore solution being in contact with a solution characterized by a negative pressure ○ Driven by a pressure gradient ○ Correspondence between imposed negative pressure and suction ○ Imposition of matric suction ○ Predominant liquid phase transport 	<ul style="list-style-type: none"> ○ 0 – 0.08 MPa 	<ul style="list-style-type: none"> ○ Richards (1941) ○ Romero (1999) ○ Iyer et al. (2018)
Pressure plate technique (Air overpressure)	<ul style="list-style-type: none"> ○ Increase in the pressure head of pore solution by increasing the atmospheric pressure in the measuring chamber ○ Driven by a pressure gradient ○ Equilibration through capillarity ○ Imposition of matric suction ○ Predominant liquid phase transport 	<ul style="list-style-type: none"> ○ 0 – 1.5 MPa 	<ul style="list-style-type: none"> ○ Bishop and Donald (1961) ○ Romero et al. (2003) ○ Agus et al. (2013)
Osmotic technique	<ul style="list-style-type: none"> ○ Initiation of water molecule and solute exchange between the pore solution and a solution containing macromolecules ○ Employment of polyethylene glycol (PEG) as macromolecule in solution ○ Separation of pore solution and macromolecular solution by means of semi-permeable membrane being impermeable for macromolecules ○ Empirical relation of suction (s) and concentration of PEG in solution (c): $s = 11c^2$ ○ Imposition of matric suction ○ Predominant liquid phase transport 	<ul style="list-style-type: none"> ○ 0 – 10 MPa ○ Limited experiment duration due to the degradation of the membrane ○ Frequent application of the technique to impose suctions up to 8 MPa 	<ul style="list-style-type: none"> ○ Kassiff and Ben Shalom (1971) ○ Cui and Delage (1996) ○ Delage et al. (1998) ○ Cuisinier and Masrouri (2005) ○ Yigzaw et al. (2016)
Vapor equilibrium technique (with (non)-volatile solutes))	<ul style="list-style-type: none"> ○ Evolution of a stable relative humidity over a reservoir of saline solution in a closed system ○ Equilibrium through the gas phase ○ Relation between imposed relative humidity and suction by means of Kelvin's law ○ Imposition of suctions of different magnitudes by means of different saline solutions ○ Imposition of total suction ○ Vapor phase transport 	<ul style="list-style-type: none"> ○ 10 – 1000 MPa ○ Limitation to more than 10 MPa due to increasing sensitivity of the relative humidity to the ambient temperature 	<ul style="list-style-type: none"> ○ Delage et al. (1998) ○ Alonso et al. (2005) ○ Hoffmann et al. (2007) ○ Wang et al. (2012) ○ Gao et al. (2019)

2.4.4 Impact of physical and physico-chemical parameters

Among others, Villar (2007) investigated MX80- and FEBEX-bentonites with regard to their solution retention behavior. Her major aim was to assess the impact of the dominant exchangeable cation species and confinement on the solution retention behavior. She compacted the samples to target dry densities at hygroscopic water contents and inserted them into special constant volume test cells. Placed in desiccators, samples were subjected to different values of RH by means of the vapor equilibrium method. In addition, materials were prepared to different water contents before compacting them to the target dry densities. The suction of those blocks was determined later by means of a humidity sensor. Her results indicated that the water content of FEBEX-bentonite was higher than that of MX80-bentonite for any given suction in the measured range. She attributed her observations to the higher hydration potential of Ca^{2+} -ions in the interlayer pores (e.g. Caballero et al., 2004).

Among other aspects, Marcial et al. (2002) and Saiyouri et al. (2004) determined the solution retention properties of MX80-, Kunigel-V1- and FoCa-bentonites under free conditions. Kunigel-V1- and FoCa-bentonites are Na- and Ca-bentonites, respectively. Final values of water content and void ratio indicated that Na-bentonites absorbed considerably more water than Ca-bentonites when suctions went below a certain value. These findings were in accordance with section 2.3.3 since the expansion of Na-montmorillonite in its crystallographic c -direction was not limited by ion correlation forces. In addition, Saiyouri et al. (2004) put emphasis on the different textures. FoCa-bentonite is typically characterized by bulky particles, so its specific surface area is smaller.

Al-Mukhtar et al. (1999) investigated the impact of different parameters, in particular the specific surface area (SSA), on the solution retention behavior of two artificially activated Na-bentonites under free and confined conditions by means of the vapor equilibrium technique. Bentonites mainly differed in their SSA. According to their results, bentonites reacted similarly to RH lower than 40 %. Upon imposing higher RH , their retention behavior diverged considerably from each other since the one characterized by the higher SSA adsorbed more water. This result might support the results presented in the paragraph above.

2.4.5 Impact of compaction conditions

Romero et al. (1999) aimed to determine the main wetting and drying paths of Boom-clay, whose smectite-content ranges between 10 % and 20 %. Samples were compacted to two different dry densities at an initial water content of 15 % prior testing. They reported that the initial void ratio affected the main wetting and drying paths once water contents exceeded 15 %. As water contents ranged between 5 % and 15 %, the impact started vanishing and, as water contents went below 5 %, the main wetting and drying paths converged. Thus, densification affected the solution retention behavior, only if macropores controlled the capillary condensation, and became less pronounced when micropores kept the solution bound. The impact of the initial dry density on the distribution of micro- and macropores in expansive soils is emphasized in section 2.5.3.

Gatabin et al. (2016) confirmed the observations of Villar (2007) and Villar et al. (2012) by reporting that samples of MX80-bentonite/ sand-mixtures stored more water under free swell conditions than under confined conditions. However, this effect was less pronounced upon exceeding suctions greater than 10 MPa. Elevated water contents were attributed to the facilitated development of interlayer and diffuse double layer water under free conditions. As highlighted in section 2.3.2, the confinement modified the redistribution of water molecules between the interlayer and the micro- and macropores.

2.4.6 Conclusion

It can be finally concluded that the concept of suction as well as the principles of solution retention apply to expansive soils. In contrast to non-expansive soils, their solution retention behavior is predominantly determined by physico-chemical parameters and the structural characteristics. The initial dry density and confinement have an impact on the solution retention behavior once the soil approaches the quasi-saturated state. This aspect is of importance in the context of in-situ compacted backfill materials and their hydro-mechanical behavior.

2.5 Compaction behavior of expansive soils

Soil compaction aims to expulse pore air from the pore space by applying mechanical energy to the soil mass. It can be applied by means of rolling, tamping or vibration. The degree of compaction is expressed as the dry unit weight γ_d or as the dry density ρ_d of a soil sample, whose magnitude is a function of the water content of the soil mass and the applied compaction energy (Proctor, 1933).

If the compaction energy is limited, the compaction of soils, whose initial water content is low, is difficult due to the high interparticle shear strength. Water might be used as a liquefaction agent to reduce the interparticle shear strength. Progressive addition of water facilitates the rearrangement of particles and leads eventually to their densest packing. The maximum dry density $\rho_{d, max}$ occurs at the optimum water content w_{opt} . Further addition of water has a reverse effect and provokes the reduction of particle density. Water then occupies the accessible pores and prevents the particles from rearranging. For a given water content, samples can thus be compacted at the dry or wet side of optimum water content, depending on the compaction energy (e.g. Daniel and Benson, 1990). Higher compaction energies commonly decrease the optimum water content and increases the maximum dry density due to the smaller fraction of accessible pores. The interpretation approaches base on microstructural analysis described in section 2.5.3.

Likewise, expansive soils exhibit a reduction of the dry density after passing the optimum water content, whereas they show an insensitivity to variations in the water content at the dry side of optimum water content (e.g. Pusch, 1983; Dixon et al., 1985). For instance, Dixon et al. (1985) performed standard Proctor experiments on MX80-bentonite and observed such an insensitivity. They attributed this behavior to diffuse double layers emerging from the addition of water. Particles align parallel to each other upon applying the compaction energy. The parallel alignment is then determined by the diffuse double layers and their repulsion energy. As the compaction energy is less than the repulsive energy, the dry density remains constant. An elevated compaction energy might exceed the repulsive energy, so a maximum dry density and its corresponding optimum water content can be determined.

2.5.1 Experimental determination

The compaction behavior of soils is commonly investigated by means of standard and modified Proctor experiments that differ in the magnitude of applied compaction energy (Association Francaise de Normalisation, 2014b). As described above, the experiment protocol envisages to prepare the materials to different initial water contents and to compact them subsequently by using a constant compaction energy. The principle of Proctor experiments and derived parameters are described in *Table 2.8*.

Table 2.8: Principle of standard and modified Proctor experiments and derived parameters

Name	Principle	Derived parameters/ comments	Reference
Standard/ Modified Proctor experiment	<ul style="list-style-type: none"> ○ Application of a constant compaction energy to soil samples characterized by different initial water contents ○ Difference between standard and modified Proctor experiment through applied compaction energy 	<ul style="list-style-type: none"> ○ Optimum water content w_{opt} ○ Maximum dry density $\rho_{d,max}$ 	<ul style="list-style-type: none"> ○ Association Francaise de Normalisation (2014b)

2.5.2 Impact of physical and physico-chemical conditions

Masrouri et al. (2005) studied Manois-Argillite (MA) and its mixtures with MX80-bentonite with regard to their compaction behavior by means of standard Proctor experiments. The bentonite content in mixtures ranged from 5 % to 20 % in weight. Their results are compiled and depicted in *Figure 2.7*. As a consequence of elevated fraction of associated minerals, optimum water contents were shifted to lower values, whereas maximum dry densities were increased. They attributed the findings to the reduced amount of diffuse double layers and, in turn, to their limited repulsion.

Komine and Ogata (1999) and Srikanth and Mishra (2016) conducted standard Proctor experiments on various sand/ bentonite-mixtures and showed that there was an optimum bentonite content (20% - 30%). It likely ensued when the void space between the sand grains was completely occupied by bentonite particles.

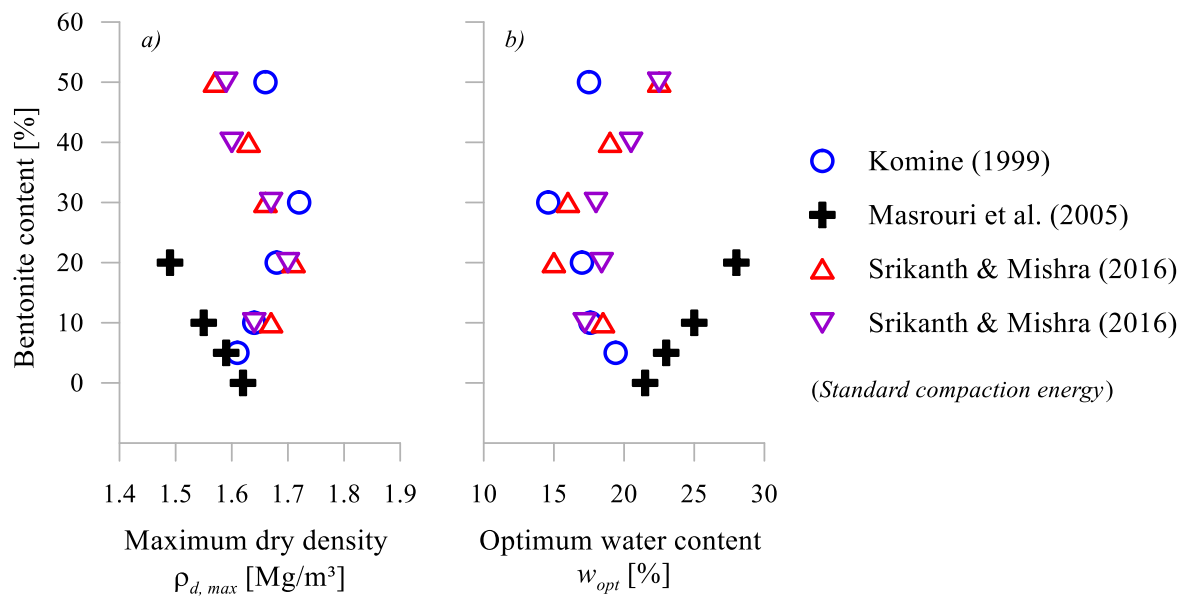


Figure 2.7: Variations of a) the maximum dry density and b) the optimum water content of sand and/ or clayey soils/ bentonite-mixtures as a function of the bentonite content

Likewise, Keto et al. (2006) performed modified Proctor experiments on mixtures of crushed granite rock with MX80-bentonite. The mixtures differed in their bentonite content, maximum grain size and grain size distribution to investigate the impact of those material parameters on the compaction behaviour. They reported with regard on the impact of the grain size distribution that values of maximum dry density were increased by widening the distribution curve and increasing the amount of fines. According to their interpretation approach, a wider grain distribution provokes denser particle packing as fine particles fill the macropores during compaction.

2.5.3 Relations of the compaction conditions to the structure

Diamond (1971) studied kaolinite- and illite-dominated soils with special regard to the impact of the initial water content on their pore size distribution. His experimental protocol comprised the compaction of the samples to their individual maximum dry density at the optimum water content as well as at dry and wet side of optimum before analyzing them by means of mercury intrusion porosimetry (MIP) experiments. The pore size distribution function was bi-modal when the soil was compacted at the dry side and indicated the existence of cardhouse-like aggregations incorporating micro- and macropores. When the water content approached the optimum value, the pore size distribution became mono-modal as the macropores vanished. Their

disappearance was due to the evolution of the cardhouse-like aggregations into bulkier structures. Therein, the clay particles were in face-to-face contact. The further increase of the water content caused a shift of the single peak to greater pore diameter values. Similar results were reported by Tang et al. (2011b) for COX_c, for instance. Some studies reported that soils might exhibit a bi-modal pore size distribution even when they are compacted at the wet side of optimum (e.g. Tarantino and Col, 2008; Monroy et al., 2010). The results of Monroy et al. (2010) are depicted in *Figure 2.8a*.

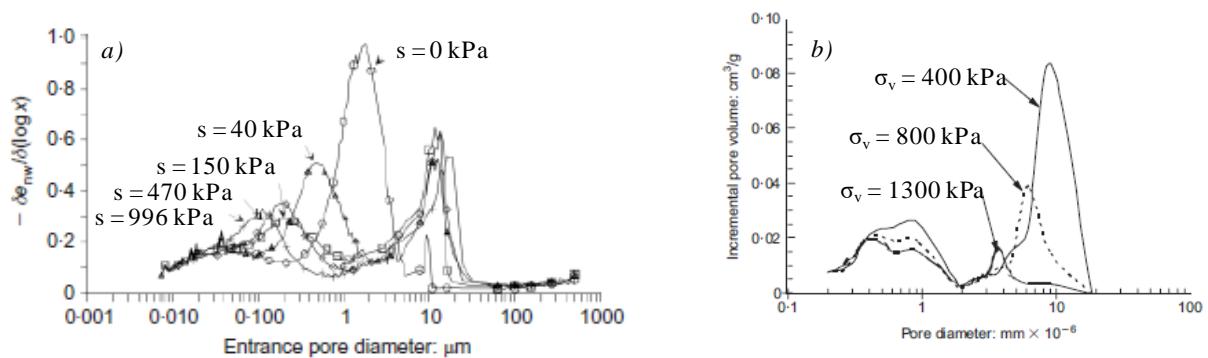


Figure 2.8: Pore-size distribution functions of compacted clayey soils under a) saturation (Monroy et al., 2010) and b) loading (Sivakumar et al., 2006)

As already mentioned in section 2.4.5, densification reduces the amount of macropores, whereas the amount of micropores remains stable (e.g. Sivakumar et al., 2006; Gao et al., 2019). This finding is depicted in *Figure 2.8b*. For instance, Lloret et al. (2003) compacted FEBEX-bentonite to target dry densities of 1.55 Mg/m³ and 1.79 Mg/m³ at hygroscopic water contents before they studied the impact of densification on the microstructure by means of MIP-experiments. Their results showed that the compaction reduced the amount of macropores by about 20 %.

Delage et al. (2006) aimed to investigate whether the microstructure of MX80-bentonite alters over time. They compacted the samples to target dry densities at target water contents and maintained those samples under constant volume and constant water content for different periods of time ranging from 1 to 90 days. Eventually, their microstructure was studied by means of MIP-experiments and ESEM-microscopy. Analysis revealed that the amount of macropores

decreased, whereas the amount of interlayer pores increased. The results were attributed to the redistribution of water molecules and clay particle separation over time.

2.5.4 Conclusion

It can be finally concluded that the compaction characteristics of expansive soils, such as the maximum dry density and the optimum water content, become identifiable, only if the applied compaction energy is higher than the repulsive energy of diffuse double layers, or the amount of associated minerals is increased. In general, higher degrees of compaction can be achieved by widening the grain size distribution curve of materials. Also, it can be concluded that the initial water content and the initial dry density determine the structure of expansive soils. In turn, the structure affects the hydro-mechanical properties and their evolution.

2.6 Swelling behavior of expansive soils

Interactions of clay particles with molecular and ionic species in the pore solution account for the mechanisms of crystalline as well as osmotic swelling. The former is related to the increase in basal spacing triggered by the intercalation of discrete layers of water molecules on particle face sides, whereas the latter is caused by the repulsion of diffuse double layers. Both mechanisms lead to an increase in the distance between layers and particles. As basic mechanisms were elaborately described in section 2.3, this chapter predominantly focusses on the experimental determination and the evolution of the swelling behavior at different scales. Apart from those aspects, the impact of different geo-environmental conditions on the free-swell potential and swelling pressure are evaluated.

2.6.1 Experimental determination

Expansive soils exhibit swelling by either increasing their volume in unconfined conditions or by generating a pressure in confined conditions upon hydration. The former is defined as free swell potential, whereas the latter is defined as swelling pressure. Sridharan et al. (1986b) compared different experiment protocols commonly performed to measure the free swell potential and swelling pressure at REV-scale. Their principles and derived parameters are described in *Table 2.9*:

Sridharan et al. (1986b) concluded that free swell-compression experiments tend to overestimate the swelling pressure, whereas loading swell-compression experiments tend to underestimate the swelling pressure in comparison to constant volume experiments. Thus, constant volume experiments are of major advantage as they require only one sample and allow to monitor the evolution of the swelling pressure in time (e.g. Sridharan et al., 1986b; Nagaraj et al., 2009).

Table 2.9: Principles and derived parameters of free-swell potential and different swelling pressure experiments

Name	Principle	Derived parameters	Selected references
Free swell-potential experiment	<ul style="list-style-type: none"> ○ Imposition of a constant vertical stress on the sample upon saturation ○ Measurement of sample height variation ○ Indication of equilibrium conditions by a constant sample height 	<ul style="list-style-type: none"> ○ Free swell-potential ($\Delta H/H_0$) ○ Free swell strain (ϵ_s) 	<ul style="list-style-type: none"> ○ Association Francaise de Normalisation (1995) ○ Castellanos et al. (2008) ○ Chen et al. (2015)
Constant-volume experiment	<ul style="list-style-type: none"> ○ Maintenance of the initial sample height upon saturation by screwing the lid including the load sensor to the casing ○ Correspondence of measured stresses and swelling pressure ○ Indication of equilibrium conditions by a constant swelling pressure 	<ul style="list-style-type: none"> ○ Swelling pressure (σ_s) 	<ul style="list-style-type: none"> ○ Pusch (1980) ○ Sridharan et al. (1986b) ○ Karnland et al. (2007) ○ Yuan et al. (2019)
Zero-swell experiment	<ul style="list-style-type: none"> ○ Maintenance of the initial sample height upon saturation by increasing stepwise the vertical stress ○ Correspondence of eventually imposed vertical stress and swelling pressure ○ Indication of equilibrium conditions by a constant swelling pressure 	<ul style="list-style-type: none"> ○ Swelling pressure (σ_s) 	<ul style="list-style-type: none"> ○ Sridharan et al. (1986b) ○ Tang et al. (2011a) ○ Wang et al. (2012)
Free swell-potential-compression experiment	<ul style="list-style-type: none"> ○ Performance of a free swell-potential experiment on the sample, followed by the compression to its initial sample height ○ Correspondence of eventually imposed vertical stress and swelling pressure 	<ul style="list-style-type: none"> ○ Free swell-potential ($\Delta H/H_0$) ○ Swelling pressure (σ_s) 	<ul style="list-style-type: none"> ○ Sridharan et al. (1986b) ○ Rao and Thyagaraj (2007) ○ Nagaraj et al. (2009)
Loading swell-compression experiment	<ul style="list-style-type: none"> ○ Requirement of at least three identical samples ○ Imposition of a constant vertical stress to all samples, followed by subjecting each sample to another individual vertical stress upon saturation ○ Detection of either swelling or compression ○ Determination of swelling pressure by plotting the final void ratio against the common logarithm of imposed vertical stress, followed by localizing the intersected vertical stress 	<ul style="list-style-type: none"> ○ Swelling pressure (σ_s) 	<ul style="list-style-type: none"> ○ Association Francaise de Normalisation (1995) ○ Villar and Lloret (2008)

2.6.2 Swelling pressure evolution at experimental different scales

There are three types of curves most frequently representing the evolution of swelling pressure under constant-volume conditions at different scales. They are sketched in *Figure 2.9*.

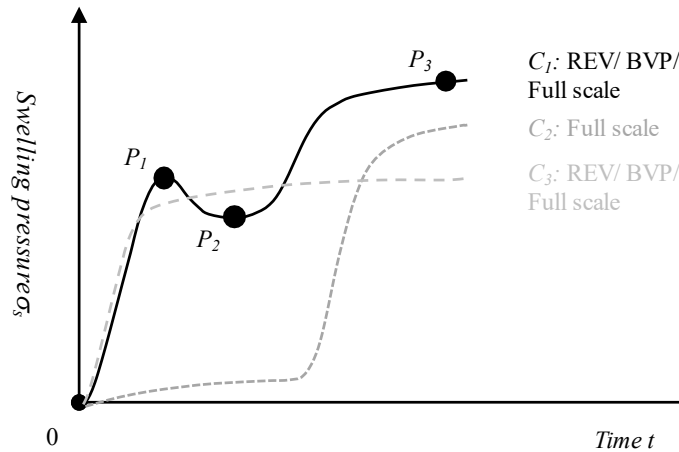


Figure 2.9: Swelling pressure evolution determined under constant-volume conditions at REV-scale (C_1 : Pusch (1980); C_2 : Sridharan et al. (1986b)) and at full scale (C_3 : Goudarzi (2019))

- Pusch (1980) was one of the first, who studied the evolution of swelling pressure of compacted MX80-bentonite samples under constant volume conditions at REV-scale. His observations correspond to curve C_1 in *Figure 2.9*. He described an increase of the swelling pressure to a first peak value (P_1) which was followed by a decrease to a minimum value (P_2). Thereafter, the swelling pressure increased again and attained its maximum value (P_3). Subsequent studies confirmed his findings and their transferability, even though they performed experiments on different expansive soils (e.g. Imbert and Villar, 2006; Schanz and Tripathy, 2009; Massat et al., 2016). Massat et al. (2016) provided substantial information applicable to relate the double peak behavior to micro- and macrostructural changes. They performed swelling pressure experiments under constant volume conditions by means of an X-ray transparent oedometer test cells. In addition, their experiment protocol envisaged to saturate the materials with polar and nonpolar solutions in order to quantify the contribution of the crystalline and osmotic swelling to the total swelling pressure. They attributed the initial increase and subsequent decrease to an increase of osmotic pressure upon hydration in conjunction with the eventual breakdown of macropores. The final

increase of swelling pressure is provoked by the microstructural expansion being greater than the macrostructural breakdown. Samples saturated with the nonpolar solution exhibited an evolution of swelling pressure, whose pattern was characterized by a rapid increase of swelling pressures to a peak value followed by their stabilization at the comparable values. As the nonpolar solution was expected to induce crystalline swelling only, it was concluded that osmotic swelling accounts for the second peak.

- Among other aspects, the swelling behavior of expansive soils and its evolution were studied by Börgesson et al. (2002), Martín and Barcala (2005) and Gens et al. (2011) by means of full scale experiments. Materials investigated were characterized by either a lower initial dry density or a lower smectite content or both compared to those studied by Pusch (1980). Their observation corresponds to curve C_2 in *Figure 2.9*. Indeed, no swelling pressure ensued when hydration started. However, it escalated after a certain time and attained its maximum value. Gens et al. (2011) attributed the delayed increase of swelling pressure to the elevated macroporosity in conjunction with the decelerated saturation of smectite particles through the vapor phase.
- Other studies described an initial increase of the swelling pressure to a maximum value remaining stable in the course of the experiment, regardless of the scale (e.g. Komine and Ogata, 1999, 2004; Saba et al., 2014). The observation corresponds to curve C_3 in *Figure 2.9*. Accordingly, the evolution of the double peak might be attributable the smectite content and its initial dry density, since those studies involved samples which were characterized by both lower smectite contents and lower initial dry densities. For instance, Saba et al. (2014) interpreted the stabilized swelling pressure as the equilibration of microstructural expansion and macrostructural rearrangement under the hydration front.

2.6.3 Impact of physical and physico-chemical parameters

The smectite content controls predominantly the swelling behaviour of expansive soils. An increase in swelling pressure and/ or free swell potential ensues as the smectite content increases. This assumption holds true only under comparable conditions. For instance, Cui et al. (2012) studied the swelling behaviour of GMZ01-bentonite/ sand-mixtures, whose sand content ranged from 0 % to 50 % in weight, by means of constant-volume swelling pressure and free swell

potential experiments. In order to ensure the compatibility of conditions among samples, they were compacted to the same dry density at the same initial water content being far at the dry side of their optimum. Maximum values of swelling pressure and free swell potential dropped by about 80 % and 40 %, respectively, as a consequence of replacing 50 % bentonite by sand. The significant drop was attributed to the lower smectite content in the mixtures. Similar observations were reported by Xu et al. (2016) and Chen et al. (2017), for instance.

The study of Karnland et al. (2006) is of general interest as it comprised fifteen different bentonites and aimed to analyze their swelling behavior, among other aspects. Tested bentonites mainly differed in their diagenesis, type, and purity of exchangeable cation species. Samples were compacted to different initial dry densities at the hygroscopic water content and tested by means of constant volume swelling pressure experiments. Initial dry densities ranged from 0.5 Mg/m³ to 1.8 Mg/m³. Their results indicated that the maximum swelling pressures of purified Na- and Ca-bentonites converged with increasing dry densities. The remarkable differences at low initial dry densities were attributed to evolving diffuse double layers and their thickness. Similar results were reported by Komine and Ogata (2004) and Komine et al. (2009) who studied the swelling behavior of natural Na- and Ca-bentonites. In addition to the constant volume swelling pressure experiments, their laboratory experimental program comprised free swell potential experiments and revealed a significantly higher free swell potential of Na-bentonite, regardless of the initial dry density. The observations were attributed to the complete exfoliation of Na-montmorillonite particles in solution.

2.6.4 Impact of compaction conditions

According to Villar and Lloret (2008), who studied the swelling behavior of FEBEX-bentonite by means of loading swell-compression and constant volume swelling pressure experiments, the initial water content affects the swelling potential to some extent, whereas it has no apparent impact on the maximum swelling pressure. The free swell potential of a sample, which was compacted to a particular target dry density prior to testing, decreased with increasing initial water content at a constant vertical stress. However, if the applied vertical stress approached the maximum swelling pressure measured under constant volume conditions, the impact van-

ished. Thus, they attributed the negligible impact of the initial water content to less deformations in the micro- and macrostructure upon saturation as applied vertical stresses approached preconsolidation stresses. Importantly, the initial water contents considered were still at the dry side of optimum, despite the great range from 10 % to 24 %.

The initial dry density has a major impact on the swelling behaviour of expansive soils. Among many, Karnland et al. (2008), Baille et al. (2010) and Schanz and Al-Badran (2014) studied the impact of variations in the initial dry density on the evolution of swelling pressure of different bentonites upon hydration. Results of various laboratory experimental studies are compiled in *Figure 2.10*. Na- and Ca-bentonites are depicted separately.

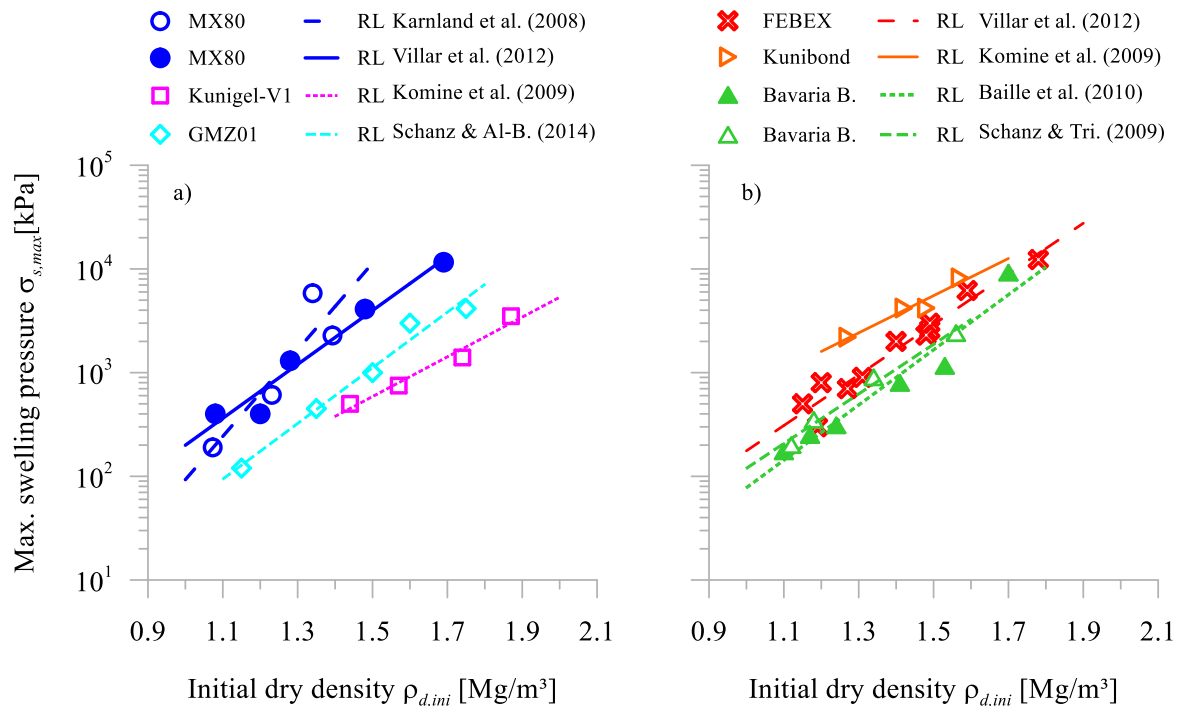


Figure 2.10: Exponential relation between initial dry density and maximum swelling pressure in the cases of a) Na-bentonites and b) Ca-bentonites (taken from various references)

Accordingly, the relation between initial dry density and maximum swelling pressure can be described by an exponential function in the form:

$$\sigma_{max} = \sigma_{min} \exp(\beta \rho_{d,ini}) \quad (2.8)$$

Where σ_{min} is a theoretical swelling pressure evolving from loosest compaction state and β is the slope of the regression line. Values of σ_{min} - and β -parameters for the different bentonites are presented in *Table 2.10*. Both parameters seemed to be material specific and to scatter only to some extent. The figure also indicates a general validity of the exponential relation, regardless of the smectite type. In conjunction with *Figure 2.10*, it is confirmed that the impact of the smectite type vanishes with increasing initial dry densities.

Table 2.10: σ_{min} - and β -parameters corresponding to the individual regression lines depicted in *Figure 2.10*

Bentonite type	Reference	Material	$\sigma_{s, min}$ [kPa]	β [m ³ /Mg]	SC*
Na-bentonite	Karnland et al. (2008)	MX80-bentonite	0.006	9.614	0.83
	Villar et al. (2012)	MX80-bentonite	0.503	5.983	0.83
	Komine et al. (2009)	Kunigel-V1-bento.	0.788	4.410	0.57
	Schanz and Al-Badran (2014)	GMZ01-bentonite	0.105	6.177	0.75
Ca-bentonite	Villar et al. (2012)	FEBEX-bentonite	0.642	5.615	0.92
	Komine et al. (2009)	Kunibond-bentonite	11.262	4.130	0.84
	Baille et al. (2010)	Bavaria-bentonite	0.170	6.124	0.76
	Schanz and Tripathy (2009)	Bavaria-bentonite	0.484	5.510	0.76

*: Smectite content

Sridharan et al. (1986b) attributed the exponential relation between initial dry density and maximum swelling pressure to the higher probability of diffuse double layer repulsion triggered by the clay particles being closer to each other in denser materials. Counterarguments are that the approach neglects the contribution of crystalline swelling and the validity of the exponential relation in ranges of high initial dry densities. Referring to section 2.3.4, diffuse double layers form, only if the porosity is sufficiently high.

The exponential relation between initial dry density and maximum swelling pressure was determined at REV-scale as well. The objectives and approach of the *Backfill and Plug Test (BPT)* were described in section 1.2 (Gunnarsson et al., 2001). The backfill material tested was a mixture composed of 70 % crushed granite rock and 30 % MX80-bentonite in weight. The experiment envisaged its layer-wise compaction directly inside the drift. The experiment setup al-

lowed to analyse the spatial evolution of swelling pressure upon saturation, among other aspects. It became evident that the maximum swelling pressure close to the drift top was up to 20 % less than that in the centre of the drift. Those observations were attributed to reduced initial dry densities of backfill material. Reductions ensued as the compactor handling became difficult close to the drift top and drift wall, which impeded the application of its compaction full energy, in turn. The subsequent full-scale in-situ experiment *Prototype repository* indicated to the same issues (Börgesson et al., 2002; Goudarzi, 2019).

Most of previously mentioned laboratory experimental programs also comprised the performance of free swell potential experiments on different expansive soils (e.g. Villar and Lloret, 2008; Komine et al., 2009) They revealed a similar exponential relation between the initial dry density and the maximum swelling pressure. Likewise, there are no generally applicable interpretation approaches.

2.6.5 Impact of environmental conditions and stress history

Cation exchange processes are likely to impair the swelling behaviour of expansive soils. For instance, Xiang et al. (2019) studied GMZ01-bentonite with special regard to the evolution of its free swell potential upon saturation with different CaCl_2 -solutions. They observed that a reduction of free swell potential ensued as the concentration of Ca^{2+} -ions in solutions increased and attributed the observation to the exchange of Na^+ -ions for Ca^{2+} -ions and, in turn, to a restricted expansion in interlayer pores and diminishing diffuse double layers. Those results were in good agreement with the results of Komine et al. (2009), Zhu et al. (2013) and Wang et al. (2014), who adopted the approach to explain a reduction in maximum swelling pressure.

The study of Wang et al. (2014) is of particular interest. It considered compacted MX80-bentonite/ crushed Callovo-Oxfordian (COX) claystone mixtures and aimed to analyse the variation in the evolution of their swelling pressure. The exchange of Na^+ -ions for Ca^{2+} -ions appeared to account for the progressive decrease of maximum swelling pressures over time.

Elevated concentrations of solutes and consequently increasing osmotic suctions likely impair the swelling pressure and/ or free swelling potential, apart from cation exchange processes (e.g. Rao et al., 2013; Ye et al., 2014b; Chen et al., 2015; Chen et al., 2016). Indeed, high solute

concentrations trigger the screening of particle face sides, which leads to reduced ranges of repulsive forces and, in turn, to a reduced repulsive energy barrier. However, its impact on the swelling behaviour vanishes as their initial dry density increases. For instance, Dixon (2000), Komine et al. (2009) and Lang et al. (2019) reported on this behaviour and attributed it to the restricted space for diffuse double layer evolution.

There are only some studies, like those of Karnland et al. (2007), Cuisinier et al. (2009), Cuisinier et al. (2014) and Chen et al. (2019), whose objectives were related to the phenomenon of the hyperalkaline plume and its impact on the swelling behaviour of expansive soils. Karnland et al. (2007) reported on the dissolution of montmorillonite phases in compacted MX80-bentonite samples after exposing them to a portlandite-saturated solution for more than 40 days. Eventually, their physico-chemical and mineralogical analysis allowed to relate measured reductions in the swelling pressure of MX80-bentonite to the continuous dissolution of montmorillonite and the progressive weakening of the bentonite structure. Similar results were reported by Cuisinier et al. (2014). Their study aimed to attribute variations of the hydro-mechanical behaviour of Callovo-Oxfordian (COX) claystone to structural alterations at nano-/ microscale. Structural alterations ensue after the saturation with alkaline solutions over a long time. Compacted samples were thus aged artificially by saturating them with a portlandite-saturated solution under constant volume and elevated temperature conditions ($> 70^{\circ}\text{C}$). The aging processes lasted longer than 18 months. Subsequent free swell potential experiments revealed that the free swell potential reduced considerably due to the dissolution of smectite and the neo-formation of illite. In addition, the dissolution of smectite led to an opening of the microporosity and, in turn, to a weakening of the soil structure, as highlighted in the pore size distribution function and SEM-image in *Figure 2.11a* and *Figure 2.11b*, respectively.

The impact of suction on crystalline swelling in expansive soils was described in sections 2.3.3 and 2.4.1. The progressive decrease in suction leads to the intercalation of discrete layers of water molecules in the interlayer space of particles, and to their subsequent break-up. Also, the increased availability of water molecules triggers osmotic swelling. For instance, Lloret et al. (2003), Agus et al. (2013) and Yigzaw et al. (2016) aimed to study the evolution of swelling pressure of different bentonites under constant-volume conditions upon stepwise suction decrease.

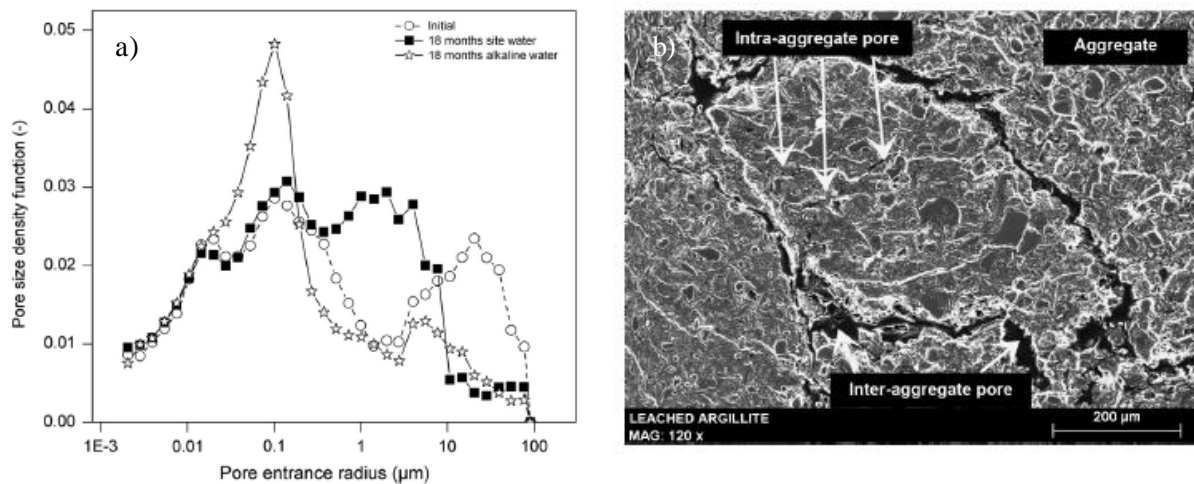


Figure 2.11: a) Impact of alkaline solution circulation over 18 months on the pore size distribution function of compacted material b) Detail of a secondary electron picture of a polished section of the leached material, showing the opening of microporosity (Cuisinier et al., 2014)

Their interpretation approaches were confirmed by the results presented by Massat et al. (2016) as the hydration through the liquid- and the gas-phase proceeded comparably. The first stage of suction decrease resulted crystalline swelling. The consequent expansion of particles in conjunction with the preservation of macropores initiated the evolution of the swelling pressure in constant volume conditions. The first maximum can be related to the maximum expansion of particles during suction decrease, and the load limit of the assembly of aggregates at that stage. The decrease of the swelling pressure ensued when macropores partially collapsed, and particles rearranged in denser particle packing. The second maximum might then indicate to the eventual dominance of microstructural expansion over macrostructural rearrangement.

Tang et al. (2011b) conducted suction-controlled constant-volume swelling pressure experiments on COX_c and observed that swelling pressures increased when suctions were reduced stepwise and reached their peak value upon directly saturating samples with deionized/ distilled water. In the further course of the experiment, swelling pressures stabilized at their peak value. As already described in section 2.6.2, the lack of the second maximum was attributed to the equilibrium of microstructural expansion and macrostructural collapse.

2.6.6 Conclusion

It can be finally concluded that the swelling of expansive soils upon hydration is the result of crystalline and osmotic swelling. Indeed, there are numerous studies about the impact of time-dependent geo-environmental conditions on the swelling pressure of expansive soils. However, those expansive soils were initially characterized by elevated target dry densities and low water contents with respect to their optimum water content. It is thus questionable whether the findings are applicable to predict the performance of backfill materials, which are installed in situ by means of conventional compaction techniques. Also, more investigations are required to assess how the hyperalkaline plume might alter the hydro-mechanical of potential backfill materials. In the regard of in-situ installed backfill materials, it is thus of major relevance to evaluate the impact of compaction conditions in combination with the evolving environmental conditions on the swelling behavior of potential backfill materials.

2.7 Compression behavior of expansive soils

In saturated conditions, soil compressibility is defined as the change in void ratio under loads. The immediate reaction of soils to loading comprises the elastic deformation of soil particles and the compression of pore solution in the pore space. A time-dependent decrease in void ratio ensues as pore solution is expelled from the pore space. By this means, a transfer of pore solution pressure to effective stresses proceeds, whose duration is a function of soil permeability. This stage is referred to as primary consolidation. After fully expelling the pore solution and imposing a constant effective stress, the soil structure might exhibit plastic deformations which are manifested by a constantly decreasing void ratio (Schofield and Wroth, 1968). This stage is referred to as secondary consolidation. Deformations evolving while applying constant effective stress are referred to as creep deformations. The creep phenomenon is explained below.

2.7.1 Experimental determination

At REV-scale, soil compressibility is determined by means of one-dimensional compression experiments, which are commonly referred to as oedometer experiments. Their standardized protocol is described in Association Francaise de Normalisation (2017). Its principles and major derived parameters are given in *Table 2.11*.

Table 2.11: Experimental methods, their principles and major derived parameters to analyze the one-dimensional compression behavior

Name	Principle	Major derived parameters	Selected references
One-dimensional compression/ Oedometer experiment	<ul style="list-style-type: none"> ○ Performance of a free swell-potential experiment on the sample, followed by loading in vertical direction (including the doubling of load in the beginning of each stage) to the maximum load, followed by unloading in vertical direction (including the halving of load in the beginning of each stage) to the initial load ○ Restriction of lateral expansion through a rigid steel ring ○ Drainage of expelled pore solution 	<p>(<i>Classic soil mechanics</i>)</p> <ul style="list-style-type: none"> ○ Compression index (C_c)¹ ○ Decompression index (C_s)¹ ○ Preconsolidation stress (p_{0^*})² ○ Permeability (k) (in combination with the coefficient of consolidation c_v³ and coefficient of volume compressibility m_v) <p>(<i>Critical state soil mechanics</i>)</p> <ul style="list-style-type: none"> ○ Elastic stiffness parameter for changes in the effective mean stress (κ)¹ ○ Stiffness parameter for changes in the effective mean stress for virgin states of the soil (λ)¹ ○ Preconsolidation stress (p_{0^*})² 	<ul style="list-style-type: none"> ○ Association Française de Normalisation (2017)

¹: obtained by means of the corresponding parts of the $e - \log(\sigma_v')$ curves (in classic soil mechanics) or of the $v - \ln(p')$ curves (in critical state soil mechanics)

²: adopting Cassagrande's method, for instance

³: adopting Taylor's method, for instance

In this regard, the study of Marcial et al. (2002) is worth mentioning. It investigated the one-dimensional compression behavior of initially slurried Na- and Ca-bentonites at stresses larger than 20 MPa. Their results revealed that the compression indices of Na-bentonites were by about 300 % larger than that of Ca-bentonite when subjecting them to loads smaller than 1 MPa. However, when loads increased, the compression indices approximated, and the final void ratio of Ca-bentonite exceeded those of Na-bentonites. The transition zone of compression indices ranged between 0.8 MPa and 2 MPa. A similar behavior was reported by Baille et al. (2010), for instance. The bilinear shape of the compression curves was related to the expulsion of solution from macro-pores in the case of smaller stresses, and to physico-chemical interactions of particles and solutions in the case of higher stresses. Particular approaches for behavior interpretation based upon the formation of hydration complexes around different cation species. The impact of the exchangeable cation species on the compression behavior is one of the objects of the following sections.

2.7.2 Impact of physical and physico-chemical parameters

Among other soils, different bentonite – kaolinite mixtures were investigated by Di Maio et al. (2004) by means of standard oedometer experiments, for instance. The smectite content of their mixtures ranged from 10 % to 100 %. According to their results, the compression indices decreased with increasing smectite contents. However, they converged when vertical stresses exceeded values greater than 1 MPa. Their final interpretation based on the assumption that smectite particles in the mixtures reduced the interparticle shear strength and trigger the arrangement of particles in denser packing. Chen et al. (2017) drew similar conclusions after they performed standard oedometer experiments on mixtures composed Na-bentonite and different fractions of either crushed granite rock or sand.

The impact of the smectite type on the one-dimensional compression behavior of expansive soils was investigated by Sridharan et al. (1986a), for instance. Their purified bentonites differed in the type of exchangeable cation species. Evidently, bentonites characterized by polyvalent exchangeable cations were less compressible, compared to those characterized by monovalent exchangeable cations. Other studies followed a similar methodology and confirmed their observations (e.g. Marcial et al., 2002; Tripathy and Schanz, 2007). Interpretation approaches attributed the smaller compressibility to the larger diameters of hydration shells of polyvalent cations, which inhibit the clay particles from approaching closely.

There are only a few studies, whose objective was to analyze the impact of the grain size distribution on the compression behavior of expansive soils. For instance, Tang et al. (2011a) investigated COX_c with special regard to its one-dimensional compression behavior. Materials were crushed and sieved to two different maximum grain sizes of 0.25 mm and 8 mm before they were compacted stepwise to target dry densities. At a given initial water content, materials characterized by smaller maximum grain sizes exhibited larger compression indices. This observation was attributed to increased number of contact points in the finer material and, in turn, to the elevated interparticle friction. In addition, the courser material was characterized by a higher amount of macropores, which tended to be more affected by the densification process.

2.7.3 Impact of compaction conditions

Also, Tang et al. (2011a) also aimed to analyze the impact of the initial water content on the compression behavior. For this reason, they prepared the material to initial water contents of 2.4 % and 7.2 %. According to their results, compaction loads as well as compression indices decreased with increasing initial water contents. Most probably, a reduction in the shear resistance between particles accounted for the reduction of compression indices since the particles in the wetter material can rearrange themselves more easily in denser packing. Similar trends were reported by Baille et al. (2010) on Ca-bentonite. Further, they emphasized the impact of the initial state of samples since slurried samples exhibited considerably lower compression indices than initial compacted samples.

2.7.4 Impact of environmental conditions and stress history

Like the swelling behavior, the one-dimensional compression behavior of compacted expansive soils is sensitive to variations in the solution chemistry (e.g. Di Maio, 1996; Di Maio et al., 2004; Rao and Thyagaraj, 2007; Siddiqua et al., 2011). For instance, Siddiqua et al. (2011) studied the impact of the composition and ionic strength of solutions on the one-dimensional compression behavior of compacted Na-bentonite/ sand-mixtures and Na-bentonite/ crushed granite rock-mixtures by means of standard oedometer experiments. Apart from their composition, mixtures also differed in the initial dry density. In general, they observed a decrease in the compression indices and an increase in the consolidation indices as the ionic strength was increased. The results agreed with those of previous studies and were attributed to the reduced probability of overlapping and repelling diffuse double layers between the clay particles.

In contrast to the ionic strength, there are only a few studies focusing on the pH and its impact on the one-dimensional compression behavior of expansive soils (Cuisinier et al., 2009; Cuisinier et al., 2014). Tested materials and the experimental approach adopted were described above. They reported on a minor impact of the pH-value on the compression indices and attributed the observation to a competing effect of an increase in the surface roughness and an opening of the micro-porosity.

The one-dimensional compression behavior of unsaturated expansive soils was investigated by Lloret et al. (2003), Cuisinier and Masrouri (2005) and Nowamooz and Masrouri (2009), for instance. Suctions were imposed by means of either the vapor equilibrium technique or the osmotic technique. In general, studies revealed that a shift of the preconsolidation pressure p^* to lower values ensued as suction decreased. The variation of the preconsolidation p^* as a function of imposed suction is depicted in *Figure 2.12b*. As described in section 2.6.5, the stepwise suction decrease triggered material swelling and initiated the rearrangement of smectite particles and aggregates at the microscale. Their rearrangement, in turn, induced irreversible deformations at the macroscale. The fact, that material swelling also involved the softening of the assembly of aggregates and the reduction of their load limit, might account for the observed shift. In contrast to the parameter κ , whose magnitude appeared to be stable, the parameter λ was sensitive to variations in the imposed suctions. The sensitivity might be attributed to the reduced load limit of the assembly of aggregates in the case of low suctions. An increase in the parameter λ might ensue as more macropores collapse while loading. This interpretation might also explain the decrease in soil stiffness upon stepwise suction decrease.

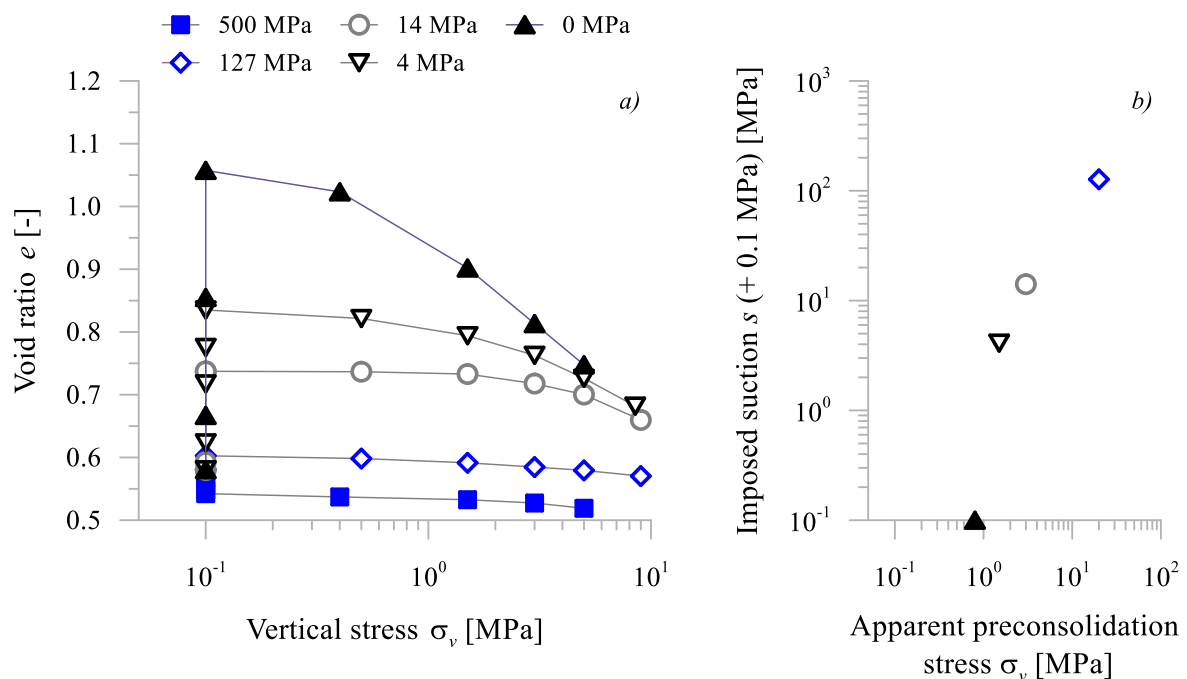


Figure 2.12: Variation of apparent preconsolidation stress of FEBEX-bentonite as a function of imposed suction (Lloret et al., 2003)

In addition, Lloret et al. (2003) studied whether samples exposed to inverse mechanical and hydraulic stress paths are characterized by the same final void ratio. Interestingly, their results indicated a stress path dependency, which is depicted in *Figure 2.13*. The differences were attributed to the different impact of mechanical and hydraulic loads on the microstructure of materials.

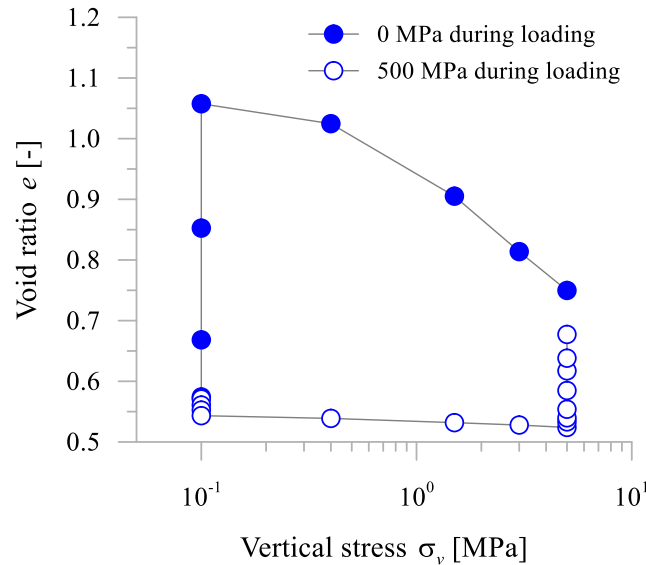


Figure 2.13: Verification of the hydration path dependency of the unsaturated compressibility behaviour of FEBEX-bentonite (Lloret et al., 2003)

2.7.5 Conclusion

It can be finally concluded that numerous studies aimed to evaluate the one-dimensional compression behavior of expansive soils under geo-environmental conditions. In contrast to its relevance in the context of block or pellet fabrication, the one-dimensional compression behavior can be considered to be less relevant in the context of backfill installation by means of conventional compaction techniques as the maximum dry density depends on the initial water content of materials and limited compaction energy. Oedometer experiments might still be of interest. It can be assumed that the overburden pressure affects the backfill material upon the partial degradation of the concrete lining. The backfill material must still sustain the overburden pressure and stabilize the surrounding geological formation. It is thus of relevance to evaluate the yield behavior of differently dense potential backfill materials under different hydro-mechanical paths, regardless of the saturation state.

2.8 Hydraulic conductivity behaviour of expansive soils

The advective flow of fluid phases through the interconnected pore space of soils is driven by a potential gradient ∇h . In particular, in expansive soils, the size and interconnection of the macropores control the flow behavior. The potential gradient arises from the difference in either the pressure head or the elevation head or their combination with respect to the spatial position. It can be formulated as follows:

$$i = -\nabla h \Rightarrow \nabla h = \nabla z + \frac{1}{\rho_\alpha \mathbf{g}} \nabla P_\alpha \quad (2.9)$$

Where i is the hydraulic gradient, ρ is the density of the individual fluid phase, α characterizes the fluid phases (liquid or gaseous phase), \mathbf{g} is the gravity vector, P_α is the pressure head of the individual fluid phase and z is the elevation head. Assuming laminar flow of fluid phases through granular soils, the relationship between the flow rate vector \mathbf{q}_α , and the hydraulic gradient i can be considered as linear. The proportionality commonly termed as Darcy's law can be formulated as follows (Darcy, 1856):

$$\mathbf{q}_\alpha = -\mathbf{k} \nabla h \quad (2.10)$$

Where \mathbf{q}_α is the vector of the velocity of the individual fluid phase with respect to the solid phase, and \mathbf{k} is the tensor of permeability with respect to the fluid phase. The unsaturated hydraulic conductivity depends on the amount of fluid phase and its connectivity within the void space. It varies as a function of different factors, like the degree of saturation, water content, matric suction, and others. According to Mitchell and Soga (2005), the hydraulic conductivity of unsaturated soils can be defined as:

$$\mathbf{k} = k_r \mathbf{K} \frac{\rho_\alpha \mathbf{g}}{\mu_\alpha} \quad (2.11)$$

Where k_r is the relative permeability ranging from zero to one, \mathbf{K} is the tensor of intrinsic permeability and μ_α is the viscosity of the individual fluid. Substitution of \mathbf{k} in equation 2.10 yields the generalized equation of the Darcy's law applicable in saturated and unsaturated state:

$$\mathbf{q}_\alpha = -\frac{k_r \mathbf{K}}{\mu_\alpha} [\nabla P_\alpha + \rho_\alpha \mathbf{g} \nabla z] \quad (2.12)$$

2.8.1 Experimental determination

At REV-scale, the saturated hydraulic conductivity of soils is determined by means of either the constant-head or the falling-head method (Association Francaise de Normalisation, 2019). The instant profile or Wind method are mainly adopted to determine the unsaturated hydraulic conductivity of soils. Their principles and major derived parameters are given in *Table 2.12*.

Table 2.12: Experimental methods, their principles and major derived parameters to analyze the (un-) saturated hydraulic conductivity behavior

Name	Principle	Major derived parameters	Selected references
One-dimensional compression/ Oedometer experiment	<ul style="list-style-type: none"> ○ <i>explained above</i> 	<ul style="list-style-type: none"> ○ Permeability (k) (in combination with the coefficient of consolidation c_v and coefficient of volume compressibility m_v) 	<ul style="list-style-type: none"> ○ Association Francaise de Normalisation (2017)
Constant head method	<ul style="list-style-type: none"> ○ Maintenance of the difference in head between inlet and outlet by permanently adjusting the water supply at the inlet of the test cell 	<ul style="list-style-type: none"> ○ Hydraulic conductivity (k_w) (in steady state conditions basing on Darcy's law) 	<ul style="list-style-type: none"> ○ Association Francaise de Normalisation (2019)
Falling head method	<ul style="list-style-type: none"> ○ Imposition of the difference in head between inlet and outlet ○ Measurement of difference in head over time 	<ul style="list-style-type: none"> ○ Hydraulic conductivity (k_w) (in steady state conditions basing on Darcy's law) 	<ul style="list-style-type: none"> ○ Association Francaise de Normalisation (2019)
Instant profile method	<ul style="list-style-type: none"> ○ Employment of a closed column-shaped hydration cell, whose lateral sides are equipped with relative humidity sensors ○ Monitoring of spatial variations of the relative humidity inside the sample upon saturation ○ Relation of the volumetric water content to the relative humidity by means of the water retention curve 	<ul style="list-style-type: none"> ○ Unsaturated hydraulic conductivity ($k_{w \text{ uns.}}$) (as a function of the imposed relative humidity/suction) 	<ul style="list-style-type: none"> ○ Daniel (1982) ○ Meerdink et al. (1996) ○ Cui et al. (2008) ○ Wang et al. (2013a)
Wind-method	<ul style="list-style-type: none"> ○ Employment of an opened column-shaped hydration cell, whose lateral sides are equipped with relative humidity sensors ○ Monitoring of spatial variations of the relative humidity inside the sample upon desiccation ○ Relation of the volumetric water content to the relative humidity by means of the water retention curve 	<ul style="list-style-type: none"> ○ Unsaturated hydraulic conductivity ($k_{w \text{ uns.}}$) (as a function of the imposed relative humidity/suction) 	<ul style="list-style-type: none"> ○ Wind (1966) ○ Masrouri et al. (2005) ○ Cuisinier et al. (2014)

2.8.2 Impact of the hydraulic gradient

Indeed, the linear relation between flow rate vector \mathbf{q}_α and the hydraulic gradient i applies to clean sands and coarse-grained soils. In the case of clayey soils, the validity of Darcy's law is still questionable, in particular in low hydraulic gradient regimes (Mitchell and Soga, 2005). The issue is depicted in *Figure 2.14*.

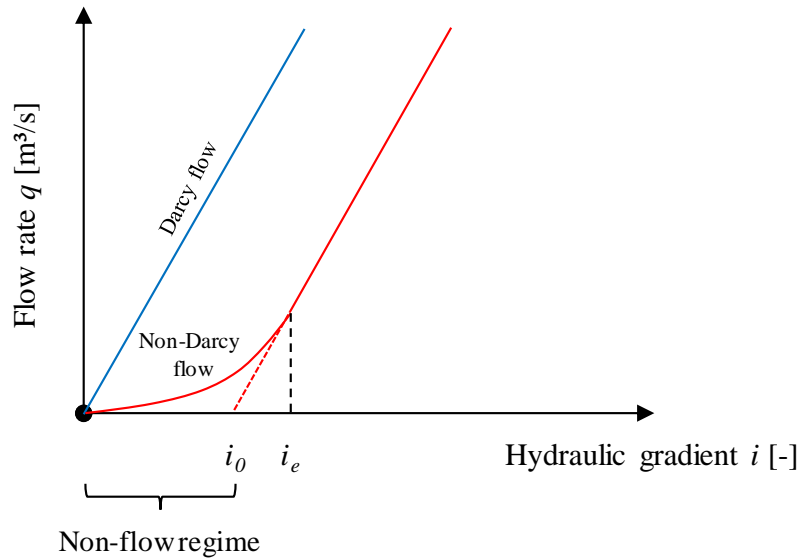


Figure 2.14: Relation between flow rate and hydraulic gradient for Darcian and non-Darcian flow (modified after Mitchell and Soga (2005))

The threshold gradient i_0 and the critical gradient i_e are different approaches to account for the deviations from the linear Darcy flow behavior. Accordingly, the former simply separates the non- from the Darcian flow regime. There is no detectable flow when hydraulic gradients are lower. Conversely, the latter postulates that the flow is exponentially related to the hydraulic gradient in the non-Darcian flow regime. Once the imposed gradient exceeds the critical gradient, a Darcian flow regime might be determined. Phenomenologically, the existence of the non-Darcian flow regime might be attributed to developing diffuse double layers. Villar (2006) highlighted that the viscosity of double layer water is higher than that of free water and its participation in the flow process is possible only when the hydraulic gradient increases more than proportionally.

Still, in most cases, differences in the flow behavior in clayey soils are attributed to experimental uncertainties. Statistical deviations might be of magnitude equal to the values measured and possibly above. Therefore, the non-flow regime likely evolves from evaporation losses, threshold gradients in the measuring capillary and preferential flow paths between the sample and cell wall. Differences in the flow behavior are alternatively caused by high hydraulic gradients since they possibly set free particles and aggregates, which can be transported by means of the flowing solution and progressively clog the hydraulic conductive macropores.

2.8.3 Impact of physical and physico-chemical parameters

The fraction of smectite has a significant impact on the hydraulic conductivity of expansive soils, comparable to that on the volume change behavior. For instance, Xu et al. (2016) determined the hydraulic conductivity of different GMZ01-bentonite/ sand-mixtures, among other hydro-mechanical parameters, by combining constant-volume swelling pressure experiments with constant-head hydraulic conductivity experiments. They reported that, at any given initial dry density and water content, the hydraulic conductivity decreases with an increasing fraction of smectite. They confirmed the findings of previous studies, like those of Komine (2004), Lee and Shackelford (2005) and Karnland et al. (2006) highlighted that the hydraulic conductivity is controlled by the closure of hydraulic conductive macropores through the swelling of smectite particles upon saturation. However, values of hydraulic conductivity remain high when the ratio of smectite to other minerals is low and only some hydraulic conductive voids are affected by material swelling. Another consequence of increasing the fraction of smectite is the more pronounced impact of tortuosity.

The study of Rao and Mathew (1995) is noteworthy in order to assess the impact of the smectite type on the hydraulic conductivity of expansive soils. They tested various natural bentonites differing in valence by means of standard oedometer experiments and determined that the hydraulic conductivity of bentonites increased as the valence of exchangeable cation species increased. Their interpretation related the increase in hydraulic conductivity to the greater hydration radius of polyvalent cations. These findings were confirmed by Ahn and Jo (2009), who determined and evaluated the hydraulic conductivity of purified Na- and Ca-bentonites.

There is a wealth of studies, whose objective was to evaluate the impact of the grain size distribution on the hydraulic conductivity of expansive soils (e.g. Benson et al., 1994; Benson and Trast, 1995; Börgesson et al., 2003). The relative proportion of small and large particles in the material generally affects the size of hydraulic conductive pores. Therefore, well-graded soils exhibit low values of hydraulic conductivity since their fraction of fines likely clogs the hydraulic conductive macropores (Benson and Trast, 1995). As outlined above, the pore space might be additionally clogged by swelling smectite particles. Indeed, the grain size distribution has a considerable impact on the hydraulic conductivity of expansive soils. However, the smectite content is of greater importance in this regard.

2.8.4 Impact of compaction conditions

As outlined in section 2.5.3, the structure of expansive soils is significantly affected by the initial water content in conjunction with the initial dry density. Due to the fact, that the size and interconnection of macropores determine the flow rate, expansive soils might be expected to exhibit lowest values when they are compacted to the optimum water content or slightly above (e.g. Daniel and Benson, 1990; Benson and Trast, 1995). The average pore diameter and the amount of diffuse double layer water aim to lowest and highest values, respectively.

Among many, Cho et al. (1999) evaluated the impact of the initial dry density on the hydraulic conductivity of compacted Ca-bentonite by means of the constant-head method under constant volume conditions. Prior testing, samples were compacted to target dry densities at water contents being far at the dry side of optimum water content. They reported on an exponential relation between the initial dry density and hydraulic conductivity depicted in *Figure 2.15*. They attributed this finding to the facts that the macropores in the samples of higher dry density were initially smaller and were clogged more effectively upon saturation. In addition, they assumed an increase in the impact of tortuosity as the clay particles align perpendicularly to the direction of compaction stress. The approximately exponential relation between initial dry density and hydraulic conductivity was also observed by Karnland et al. (2006) and Karnland et al. (2007). They conducted combined constant-volume swelling pressure and constant-head hydraulic con-

ductivity experiments conducted on different bentonites. Baille et al. (2010) observed an exponential relation between void ratio and hydraulic conductivity after conducting standard oedometer experiments on Ca-bentonite.

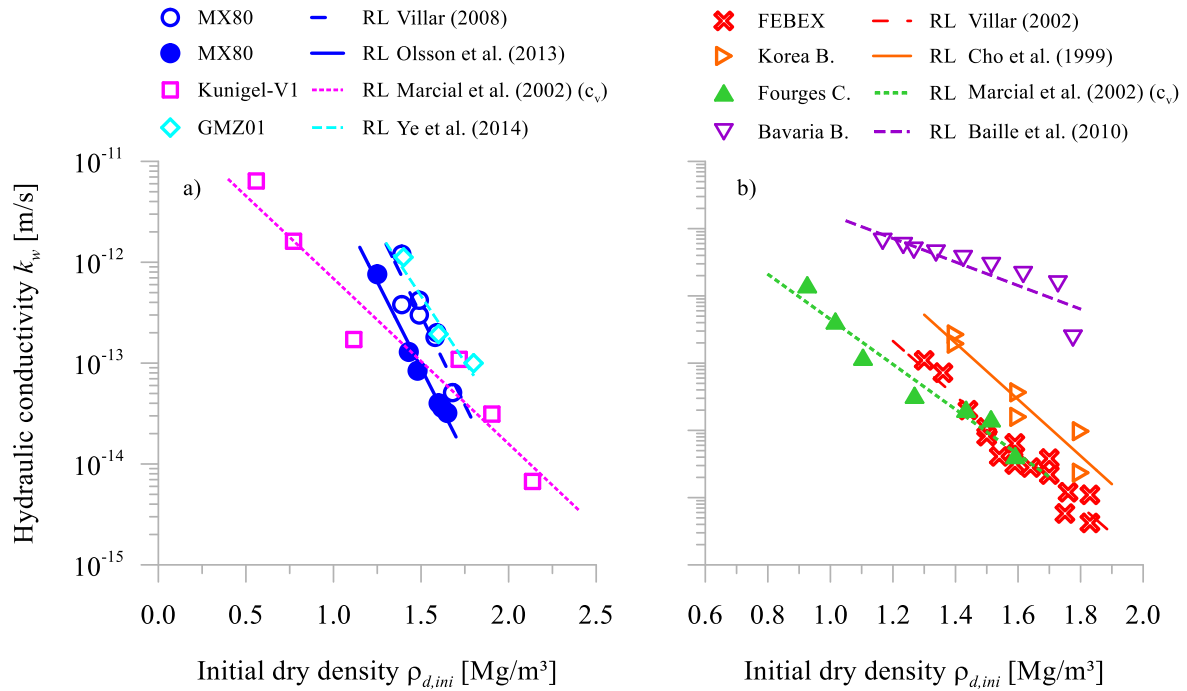


Figure 2.15: Exponential relation between initial dry density and maximum swelling pressure in the cases of a) Na-bentonites and b) Ca-bentonites (taken from various references)

Accordingly, the relation between initial dry density and saturated hydraulic conductivity can be described by an exponential function in the form:

$$k_{w,min} = k_{w,max} \exp(-\beta \rho_{d,ini}) \quad (2.13)$$

Where $k_{w,max}$ is a theoretical hydraulic conductivity reflecting the loosest compaction state and β is the slope of the regression line. Values of $k_{w,max}$ and β -parameters for the different bentonites are presented in *Table 2.13*.

Table 2.13: $k_{w, max}$ - and β - parameters corresponding to the individual regression lines depicted in *Figure 2.15*

Bentonite type	Reference	Material	$k_{w, max}$ [m/s]	β [m ³ /Mg]	SC*
Na-bentonite	Villar (2004)	MX80-bentonite	6.0×10^{-8}	8.15	0.83
	Olsson et al. (2013)	MX80-bentonite	1.2×10^{-8}	7.87	0.83
	Marcial et al. (2002)	Kunigel-V1-bento. ¹	3.0×10^{-11}	3.77	0.57
	Ye et al. (2014a)	GMZ01-bentonite	4.0×10^{-9}	6.04	0.75
Ca-bentonite	Villar (2002)	FEBEX-bentonite	1.7×10^{-7}	9.41	0.92
	Cho et al. (1999)	Korean bentonite	1.5×10^{-6}	9.66	0.84
	Marcial et al. (2002)	Fourges clay ¹	1.0×10^{-8}	7.71	0.80 ²
	Baille et al. (2010)	Bavaria-bentonite ¹	9.0×10^{-9}	4.03	0.76

*: Smectite content

¹: Determined by means of oedometer experiments²: composed of 80 % mixed layer smectite-kaolinite

2.8.5 Impact of environmental conditions and stress history

Numerous studies, such as Dixon (2000), Castellanos et al. (2008) and Chen et al. (2015), showed that the impact of the ionic strength of solutions on the hydraulic conductivity of expansive soils vanishes upon the ionic strength decreases or the dry density increases. For instance, Mata (2003) investigated the hydraulic conductivity of crushed granite rock/ bentonite-mixtures by means of the falling head method. The adopted protocol envisaged the compaction of samples to their maximum dry density at optimum water content and the employment of solutions of different ionic strength. Results indicated to an increase of hydraulic conductivity in the case of the solution being characterized by a higher ionic strength. The experiments of Villar (2006) confirmed those results. She attributed her observations to the modification of the pore size distribution and to the mobility of the water molecules within the pores. As already mentioned above, water molecules are less mobile, if they are affected by diffuse double layers. The increase of ionic strength causes the decrease of the range of diffuse double layers and, in turn, the release of water molecules into the free water. The effective porosity increases by this means. Moreover, the cation exchange impairs the clay particle swelling increasing the size of potential flow path. The combination of both processes results in the significant increase of the hydraulic conductivity. However, this interpretation is only valid, if the initial porosity of the backfill material is so high that diffuse double layers can evolve.

There are only few studies, whose objective was to evaluate the impact of the pH on the hydraulic conductivity behavior of expansive soils (Pusch et al., 2003; Ye et al., 2014b). In the former study, Ca-bentonite was initially saturated with a portlandite-saturated solution by means of diffusion. After the presumable saturation, the hydraulic conductivity was determined by means of the constant-head method. There were no changes in the hydraulic conductivity behavior. The negligible impact was reflected in subsequent mineralogical analysis. They attributed it to the low reaction kinetics of ion exchange and mineral dissolution processes under imposed conditions. Similar results were reported by Ye et al. (2014b), whose laboratory experimental program comprised the saturation of Na-bentonite with a NaOH-solution.

Similarly, only few studies focused on the hydraulic conductivity behavior of expansive soils in unsaturated conditions. For instance, Cui et al. (2008) and Wang et al. (2013a) studied the unsaturated hydraulic conductivity of MX80-bentonite/ sand mixtures by means of the instantaneous profile method. The setup also allowed to perform the experiment under constant volume conditions. Samples were characterized by an initial dry density of about 1.7 Mg/m^3 and an initial suction of about 65 MPa. According to their results, the hydraulic conductivity decreased with increasing suction. However, once the imposed suction goes below a certain threshold, the hydraulic conductivity increases again. The decrease of unsaturated hydraulic conductivity was due to the rearrangement and closure of hydraulic conductive macropores, whereas the final increase was related to the opening of interlayer and micropores triggered by smectite particle breakup. Eventually, hydration leads to a uniform pore size distribution inside the sample (Wang et al., 2013a).

2.8.6 Conclusion

It can be finally concluded that the hydraulic conductivity behavior of expansive soils is governed by the hydraulic conductive macropores, whose size decreases through material swelling upon saturation. In turn, material swelling is significantly affected by the geo-environmental conditions. Although the hydraulic conductivity behavior of expansive soils appears to be well understood, there are still aspects, which are hardly investigated. The impact of the pH-value of solutions is such an aspect, particularly with regard to the hyperalkaline plume. It likely

triggers geochemical reactions inside the backfill, which might impair the hydraulic conductivity behavior over time. However, it is difficult to portray the impact of solution chemistry adequately as the reaction kinetics of geochemical processes are low.

2.9 Constitutive modelling of expansive soil behavior

As partially outlined above, unsaturated soils exhibit an increase of shear strength and preconsolidation pressure with suction, development of reversible swelling strains when suction decreases at low confining stress, an occurrence of irreversible collapse strains when suction decreases at high confining stress, and a development of irreversible shrinkage when suction increases above a threshold value (Alonso et al., 1987). There was the motivation of reproducing those features of unsaturated soil behavior by means of an elasto-plastic constitutive model embedded in the critical state framework, such as the Modified Cam Clay (MCC) model for saturated soils. Alonso et al. (1987) described qualitatively an elasto-plastic constitutive model that considers two independent stress variables, namely net stress σ_{net} and suction s (e.g. Matyas and Radhakrishna, 1968; Fredlund and Morgenstern, 1977) and allows the reproduction of the soil behavior under loading and hydraulic paths. Upon suction reaches zero, it merges to the MCC model. Suction s is considered as follows:

$$s = u_a - u_w \quad (2.14)$$

Where s is the total suction, u_a is the pore air pressure and u_w is the pore solution pressure. In this context, suction refers to the matric component, only. Net stress σ_{net} is defined as follows:

$$\sigma_{net} = \sigma - u_a \mathbf{I} \quad (2.15)$$

Where σ_{net} is the excess of total stress tensor over air pressure (Net stress tensor), σ is the total stress tensor, and \mathbf{I} is the identity tensor.

Alonso et al. (1990) then proposed the mathematical formulation of the elasto-plastic constitutive model, widely known as the *Barcelona Basic Model (BBM)*. Under isotropic stress conditions, the *BBM* uses suction s , void ratio e and/ or specific volume $v (= 1 + e)$, and mean net stress $p (= tr(\sigma_{net})/3)$ as state variables, and displays the behavior in the (p, s) – plane in conjunction with the (v, p) – plane. Its employment allows to reproduce the behavior of fine-grained

soils of low and moderate plasticity. Following sections present the formulation of elastic behavior reproduction, the loading-collapse (LC) and suction increase (SI) yield curves, and plastic behavior reproduction.

2.9.1 Elastic behavior

In the *BBM*-framework, the volumetric strain within the elastic domain is calculated by the following incremental expression:

$$d\varepsilon_v^{el} = - \frac{\kappa}{(1+e)} \frac{dp}{p} - \frac{\kappa_s}{(1+e)} \frac{ds}{(s + p_{atm})} \quad (2.16)$$

Where $d\varepsilon_v^{el}$ ($= de / (1 + e)$) is the elastic volumetric strain increment, κ and κ_s are soil constants related to the elastic soil stiffness with respect to changes in p and s , respectively, and p_{atm} is the atmospheric pressure. The latter was introduced to avoid the prediction of infinite elastic volumetric strains as suctions approach zero.

2.9.2 Loading-collapse (LC) and suction increase (SI) yield curves

Under isotropic stress conditions, the loading-collapse (LC) yield curve represents the first yield function separating the elastic domain from the plastic domain in the (p, s) – plane. In the (v, p) – plane, it is defined by the series of yield points beyond which isotropic virgin compression lines at different values of suction occur and plastic deformations evolve. The corresponding void ratio e and/ or specific volume v on the different isotropic virgin compression lines is calculated by the following expression:

$$v = N(s) - \lambda(s) \ln\left(\frac{p}{p_c}\right) \quad (2.17)$$

Where p_c is a reference value, $N(s)$ is the specific volume v on the virgin compression line at suction s when p is equal to p_c , and $\lambda(s)$ is the slope of the virgin compression line at suction s . The latter variable corresponds to the soil stiffness varying as a function of imposed suction. It is calculated by the following expression:

$$\lambda(s) = \lambda(0)[r + (1 - r) e^{(-\beta s)}] \quad (2.18)$$

Where r is a parameter related to the minimum stiffness at maximum suction, β is a parameter controlling the rate of increase in soil stiffness with suction, and $\lambda(0)$ is the slope of the virgin compression line for saturated conditions. The equation predicts a decreasing soil stiffness with increasing suctions, provided that r ranges between zero and one. In the (p, s) – plane, the shape of the LC yield curve and its evolution during yield curve expansion are derived by combining equations 2.16 and 2.17. It is calculated by the following expression:

$$\left(\frac{p_0}{p^c}\right) = \left(\frac{p_0^*}{p^c}\right)^{\frac{\lambda(0)-\kappa}{\lambda(s)-\kappa}} \quad (2.19)$$

Where p_0 is the mean net stress on the LC yield curve under isotropic stress state at a given suction, and p_0^* is the saturated preconsolidation stress. In addition, it is assumed that the LC yield curve becomes a straight when p_0 approaches p_c in the (p, s) – plane.

The suction increase (SI) yield surface represents the second yield curve in the (p, s) – plane. It provides the increase in tensile strength with suction and is calculated by the following expression:

$$p_s = -ks \quad (2.20)$$

Where k is a constant. In this regard, s equals s_0 referring to the maximum past suction ever experienced by the soil and bounding the transition from the elastic domain to the plastic domain when suction is increased.

2.9.3 Plastic behavior

The change of the void ratio e and/ or specific volume v within the plastic domain is calculated by the following incremental expression:

$$d\varepsilon_v^{pl} = \frac{\lambda(0) - \kappa}{(1 + e)} \frac{dp_0^*}{p_0^*} - \frac{\lambda_s - \kappa_s}{(1 + e)} \frac{ds_0}{(s_0 + p_{atm})} \quad (2.21)$$

Where $d\varepsilon_v^{pl}$ is the plastic volumetric strain increment. In general, the model can be extended to the triaxial stress state described in the (p, q, s) – plane. The parameter q refers to the deviatoric stress state ($q = [(tr(\boldsymbol{\sigma}_{net}))^2 - (tr(\boldsymbol{\sigma}_{net}^2))]/ 2$). The yield surface defined in the (p, q, s) – plane is sketched in *Figure 2.16*.

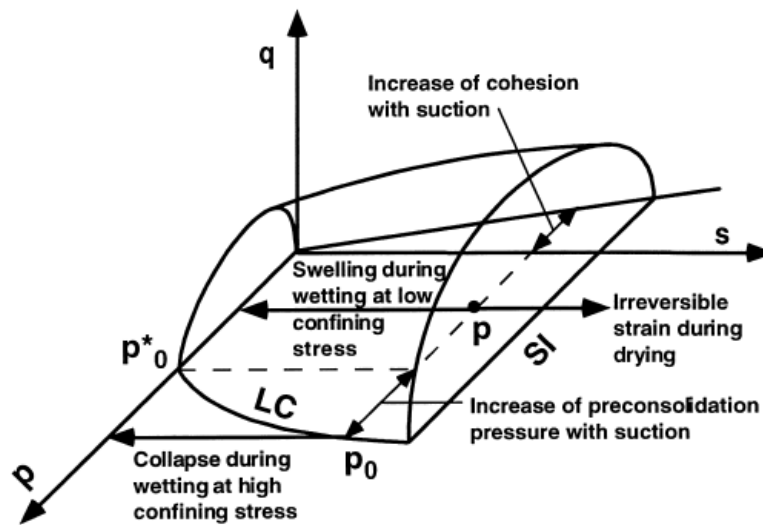


Figure 2.16: Barcelona Basic Model yield loci in (p, q, s) – planes (Alonso et al., 1999)

2.9.4 Comments

The *Barcelona Basic Model (BBM)* proved its applicability to reproduce the major features of the behavior of unsaturated fine-grained soils of low and moderate plasticity, despite there is no experimental evidence of the assumption that the LC yield curve becomes a straight when p_0 approaches p_c in the (p, s) – plane. Also, problems during numerical analysis likely arise as certain combinations of r and (p_0^*/p_c) result in a LC yield curve, whose shape is characterized by its non-convex lower section. In general, the *BBM* is not capable of reproducing the typical features of expansive soils, such as the strain accumulation during suction cycles.

2.10 Extended constitutive modelling of expansive soils

Typical features of unsaturated expansive soils are the dependency of free swell potential and swelling pressure on the initial state, the dependency of free swell potential and swelling pressure on the stress path and the accumulation of strains during suction cycles. However, the *BBM* is not capable to reproduce those features of expansive soils satisfactorily. There was thus the motivation of enhancing the *BBM* by acknowledging the bimodal pore size distribution in expansive soils and incorporating the impact of microstructural phenomena on the global material behavior. Gens and Alonso (1992) presented a conceptual extension of the *BBM*. Its prelimi-

nary mathematical formulation was presented by Alonso et al. (1999), who referred to the extended model as *Barcelona Expansive Model (BExM)*. Sánchez et al. (2005) enhanced the preliminary mathematical formulation and extended it to a double structure generalized plasticity model for expansive soils.

As outlined above, the *BExM* bases on the *BBM* including the concept of two independent stress variables and the utilization of suction s , void ratio e and/ or specific volume v and mean net stress p as state variables under isotropic stress conditions. Also, the soil behavior is displayed in the (p, s) – plane in conjunction with the (v, p) –plane. Following sections present the basic preliminary assumptions, the formulation of elastic behavior reproduction, the suction increase (SI) and suction decrease (SD) yield curves, the coupling between micro- and macrostructural levels, and the formulation of plastic behavior reproduction.

2.10.1 Basic preliminary assumptions

The *BExM* bases on different preliminary assumptions described as follows:

- As highlighted in *Figure 2.8*, the structure of expansive soils comprises two pore populations, namely micro- and macropores. The corresponding void ratios are the microstructural void ratio (e_m) and macrostructural void ratio (e_M), respectively. Their sum is the total void ratio (e). Micropores are assumed to remain saturated, thus the effective stress concept applies therein.
- The microstructural deformations are assumed to be reversible, thus the microstructure reacts purely elastically to changes in mean net stress and/ or suction. This implies that changes in mean net stress and/ or suction affect the microstructure comparably.
- The microstructural deformations presumably affect the macrostructure, whereas variations at the macrostructural scale have no impact on the microstructure. This assumption implies that there are interactions between the micro- and macrostructure.
- Micro- and macrostructure are at mechanical, hydraulic and chemical equilibrium
- In the model, suction s refers to the matric component, only.

2.10.2 Elastic behaviour

In the framework of *BExM*, the elastic microstructural volumetric strain as response to changes in mean net stress and/ or suction is calculated by the following incremental expression:

$$d\varepsilon_{vm}^{el} = \frac{\kappa_m}{(1 + e_m)} \frac{dp_m}{p_m} \quad (2.22)$$

Where $d\varepsilon_{vm}^{el}$ ($= de / (1 + e_m)$) is the elastic microstructural volumetric strain increment, κ_m is the compressibility index of the microstructure and p_m ($= p + s_m$) is a generalized microstructural effective stress, in which the parameter s_m refers to the suction in the micropores.

By definition, the microstructure might exhibit three types of recoverable volumetric strains, depending on the generalized microstructural effective stress p_m :

- No elastic microstructural volumetric strains, if p_m is constant (the stress state, in which p_m is constant, is referred to as neutral loading (NL))
- Elastic microstructural swelling strains, if p_m is smaller than zero
- Elastic microstructural shrinkage strains, if p_m is greater than zero

The microstructural deformations ensuing as the current state moves away from the neutral loading line is depicted in *Figure 2.17*.

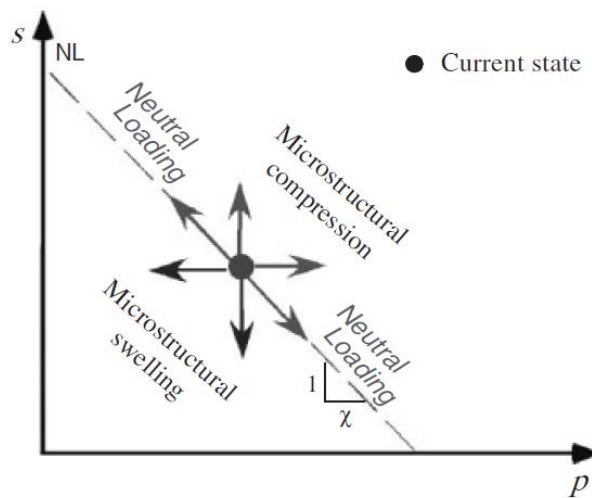


Figure 2.17: Definition of microstructural swelling and contraction directions (Sánchez et al., 2005)

Elastic macrostructural volumetric strains $d\varepsilon_{vM}^{el}$ as a response to changes in the mean net stress state and/ or suction imply changes in the size of the macropores and are reflected by a measurable change in the total void ratio e . They can be described by adopting equation (2.19), which is incorporated in the *BBM*. However, the total void ratio e in the formulation is substituted by the macrostructural void ratio e_M . The total elastic strain $d\varepsilon_v^{el}$ is defined as follows:

$$d\varepsilon_v^{el} = d\varepsilon_{vm}^{el} + d\varepsilon_{vM}^{el} \quad (2.23)$$

Where $d\varepsilon_{vM}^{el}$ is the elastic macrostructural volumetric strain increment.

2.10.3 Suction increase (SI) and suction decrease (SD) yield curves

The *BExM* uses three yield curves, namely the loading-collapse (LC), suction increase (SI) and suction decrease (SD) yield curve in the (p, s) – plane. Indeed, the approach and formulation of the LC yield curve are the same for the *BBM* and the *BExM*, and plastic macrostructural strains evolve once the stress state touches the LC yield curve. However, the formulation of the SI yield curve varies, and the formulation of the SD yield curve is introduced.

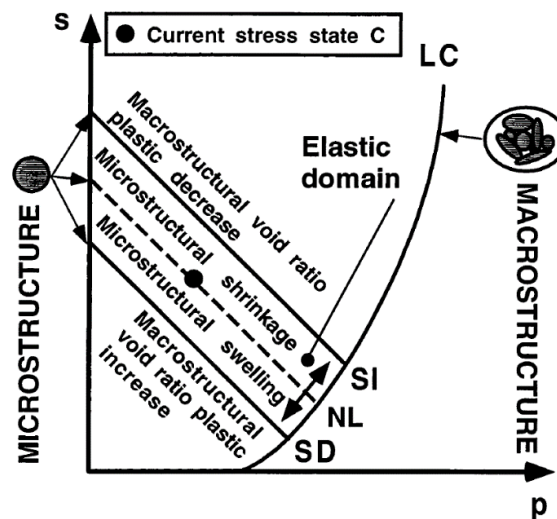


Figure 2.18: Barcelona Expansive Model yield loci in the (p, s) – plane (Alonso et al., 1999)

Their purpose is the consideration of plastic macrostructural strain evolution and accumulation exclusively ensuing as suction increases and/ or decreases. Plastic macrostructural swelling or shrinkage strains evolve in conjunction with a shift of the LC yield curve once the stress state

touches the SI or SD yield curves, respectively. LC, SI and SD yield curves and the predicted deformations at the micro- and macroscale are depicted in *Figure 2.18*. The SI and SD yield curves incline by 45° and are parallel to the NL line. They are defined as follows:

$$p_m - s_I = 0 \quad (2.24)$$

$$p_m - s_D = 0 \quad (2.25)$$

Where s_I and s_D are hardening parameters. Alonso et al. (2005b) hypothesized that the hardening parameters s_I and s_D might be controlled by the applied confining stress and the initial dry density of the material. For a reason of simplicity, it is generally assumed that the SI and SD yield curves are always activated.

2.10.4 Interaction between micro- and macrostructural levels

By postulation, phenomena at the macroscale have no impact on the microstructure of expansive soils. Only by changing the mean net stress state and/ or the suction, microstructural volumetric strains might be induced. Conversely, elastic microstructural volumetric strains might induce plastic macrostructural volumetric strains, so it must be assumed that the micro- and macrostructure are coupled.

The coupling depends on the ratio of the current mean net stress p to the preconsolidation stress p_0 (p/p_0). The preconsolidation stress p_0 is indicated by a specific mean net stress p at the LC yield curve at the corresponding suction s , and determines the position of the LC yield curve in the (p, s) – plane. The interaction mechanisms between the micro- and macrostructure as a function of the ratio of the current mean net stress p to the preconsolidation stress p_0 is depicted in *Figure 2.19*.

Assuming that two samples compacted to different initial dry densities at the same initial water content are subjected to the same mean net stress p , the (p/p_0) – ratio of the denser sample is lower than that of the looser sample as the preconsolidation stress p_0 of the denser sample is higher. The lower (p/p_0) – ratio indicates a denser sample and indicates a considerable modification of the microstructure and, in turn, the evolution of larger plastic volumetric macrostructural strains. Further, the macrostructure softens. Conversely, if the current mean net stress p approaches the preconsolidation stress p_0 , the elastic microstructural volumetric strains have

hardly no impact on the plastic macrostructural strains. This shift of the LC yield curve due to microstructural effects is depicted in *Figure 2.20*.

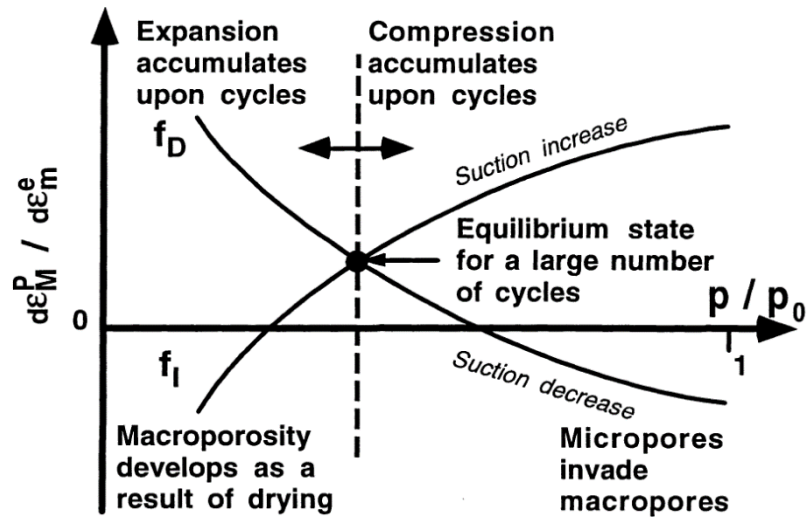


Figure 2.19: Summary of interaction mechanisms between the micro- and macrostructure as a function of the ratio of the current mean net stress p to the preconsolidation stress p_0 (Alonso et al., 1999)

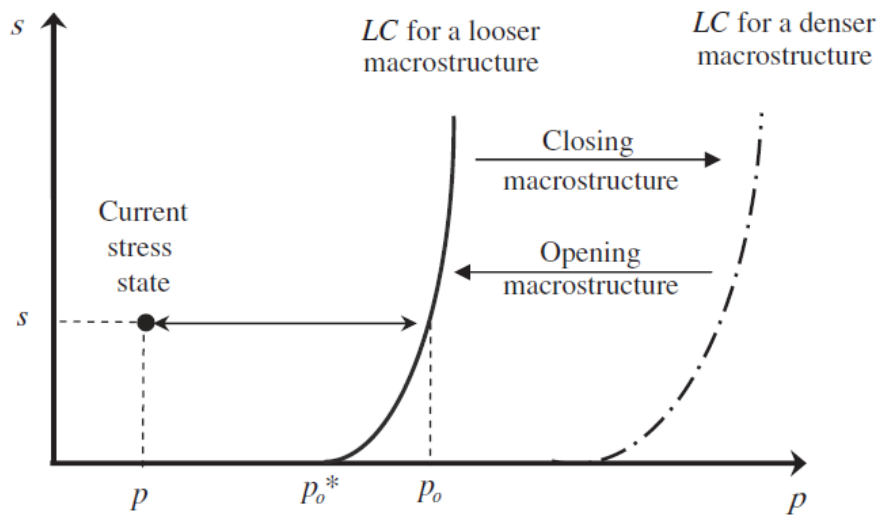


Figure 2.20: Shift of the loading-collapse yield curve due to microstructural effects (Sánchez et al., 2005)

The functions coupling the elastic microstructural volumetric strains and the plastic macrostructural volumetric strains, which are induced by the activation of the SI and SD yield curve, are defined as follows:

$$d\varepsilon_{vMSI}^{pl} = f_I d\varepsilon_{vm}^{el} \quad (2.26)$$

$$d\varepsilon_{vMSD}^{pl} = f_D d\varepsilon_{vm}^{el} \quad (2.27)$$

Where $d\varepsilon_{vMSI}^{pl}$ are the plastic macrostructural volumetric strains induced by the activation of the SI and $d\varepsilon_{vMSD}^{pl}$ are the plastic macrostructural volumetric strains induced by the activation of the SD. Following equations were suggested for f_I and f_D by Gens and Alonso (1992):

$$f_I = f_{I0} + f_{I1} \left(1 - \frac{p}{p_0}\right)^{n_I} \quad (2.28)$$

$$f_D = f_{D0} + f_{D1} \left(1 - \frac{p}{p_0}\right)^{n_D} \quad (2.29)$$

Where $f_{I0}, f_{D0}, f_{I1}, f_{D1}, n_I,$ and n_D are material parameter.

2.10.5 Plastic behavior

In the *BExM*-framework, it is assumed that the sum of plastic macrostructural volumetric strains induced by the activation of SI and SD yield curves ($d\alpha_1 = d\varepsilon_{vMSI}^{pl} + d\varepsilon_{vMSD}^{pl}$) control SI and SD hardening, whereas LC hardening is triggered by the activation of SI, SD and LC yield curves ($d\alpha_2 = d\varepsilon_{vMSI}^{pl} + d\varepsilon_{vMSD}^{pl} + d\varepsilon_{vMLC}^{pl}$). The latter term is given in equation 2.18. Hardening equations are defined as follows:

$$d\alpha_1 = \frac{\kappa_m}{(1 + e_m) p_m} f_I s_I \quad (2.30)$$

$$d\alpha_1 = \frac{\kappa_m}{(1 + e_m) p_m} f_D s_D \quad (2.31)$$

$$d\alpha_2 = \frac{\lambda(0) - \kappa}{(1 + e_M)} \frac{dp_0^*}{p_0^*} \quad (2.32)$$

2.10.6 Comments

The *Barcelona Expansive Model (BExM)* has been widely employed in order to reproduce satisfactorily the hydro-mechanical behavior of expansive soils (e.g. Alonso et al., 2005b; Gens et al., 2009; Wang et al., 2013b). For the purpose of complexity reduction, the model considers

multiple basic assumptions, and thus lacks precision in some cases. Wang et al. (2013b) indicated that the model does not reproduce satisfactorily the water retention characteristics of bentonite-based materials in ranges of high suctions which was attributed to the fact that the microstructure is postulated to be permanently saturated. In general, the mathematical formulation of the coupling functions f_I and f_D might lack complexity being necessary to reproduce the rearrangement processes at the microscale during wetting and/ or drying. Another aspect of special interest in the context of in-situ compacted backfill materials is how variations in the initial dry density changes the shape and position of the LC, SI and SD yield curves including the hardening parameters s_I and s_D .

2.11 Conclusions and anticipated contributions

The literature review highlighted how the physical and physico-chemical material parameters, compaction conditions, environmental conditions and stress history determine the hydro-mechanical behavior of expansive soils upon hydration, as outlined by Alonso et al. (1987) and Chen (1988). Their individual and combined impact is sketched in *Figure 2.21*.

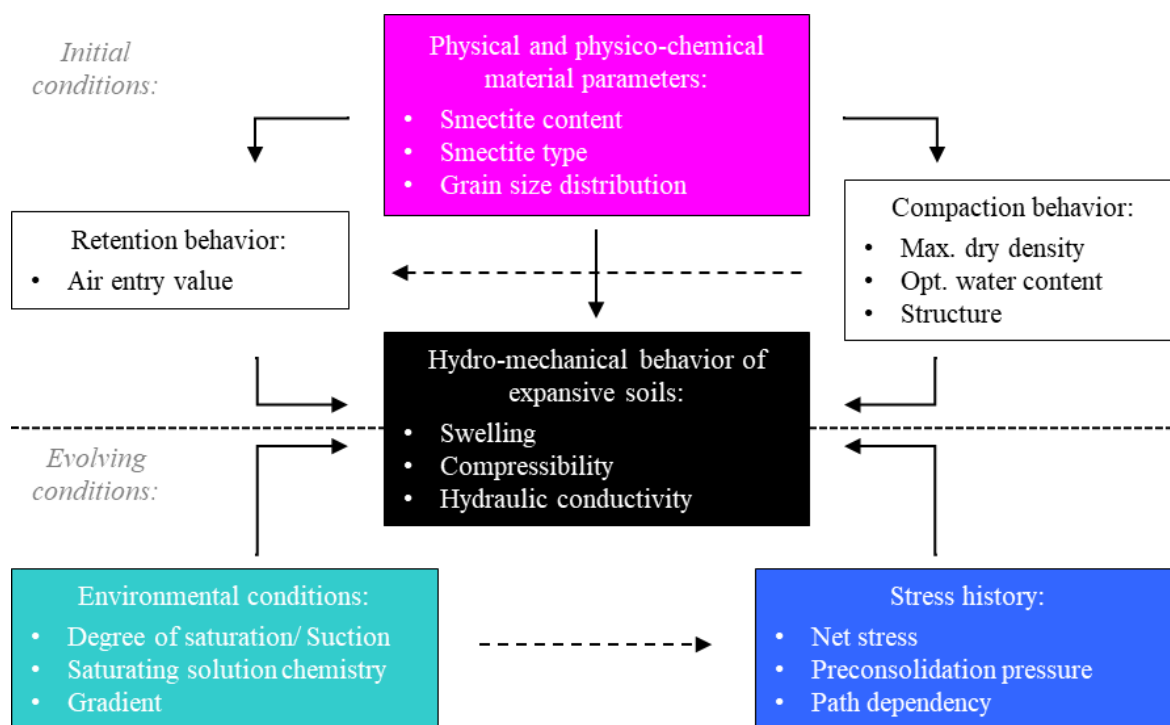


Figure 2.21: Compilation of conditions affecting the hydro-mechanical behavior of expansive soils

Also, the literature review evidenced that the geo-environmental conditions are classifiable as imposed and evolving conditions in order to emphasize possible variations of the hydro-mechanical behavior over time. The physical and physico-chemical material parameters and the compaction conditions determine the hydro-mechanical behavior initially, whereas the environmental conditions and stress history display their impact in conjunction with the imposed conditions over time.

Following questions were revealed by reviewing the literature being relevant to understand how the individual and combined geo-environmental conditions possibly affect the multi-scale hydro-mechanical behaviour of COX_c-based backfill materials:

- Numerous studies aimed to evaluate the impact of variations in the initial dry density on the hydro-mechanical behaviour of expansive soils. Some of them combined the consideration of different initial dry densities with the saturation of samples with solutions of different properties. However, in most cases, only the composition or ionic strength of solutions were varied. Referring to the hyperalkaline plume, it is of interest to evaluate the combined impact of variations in the initial dry density and of the pH of solutions on the hydro-mechanical behaviour, in particular the swelling behaviour. Further, it is of interest to assess to which extent the replacement of COX_c by MX80-bentonite enhances the swelling behaviour of potential backfill materials.
- Also, there are only a few studies evaluating how the pH of solutions affects the hydraulic conductivity of COX_c-based materials. As alkaline solutions likely trigger different geochemical reactions in the samples over time, it is of interest to study the impact of those reactions on the texture and microstructure of materials and to relate the results to variations in the hydraulic conductivity.
- Indeed, there are some studies, whose objective was the analysis of the hydro-mechanical behavior of COX_c-based materials, in particular in unsaturated conditions. However, they hardly evaluated whether the response of those materials depends on the imposed hydro-mechanical path. Particularly with regard to the employment of conventional compaction techniques, it is also of relevance to evaluate whether variations in the initial dry density affect possible path dependencies.

3 Combined impact of selected material properties and environmental conditions on the swelling pressure of compacted claystone/ bentonite mixtures

Based on the published manuscript of the following article:

Middelhoff M, Cuisinier O, Masrouri F, Talandier J and Conil N (2020) Combined impact of selected material properties and environmental conditions on the swelling pressure of compacted claystone/bentonite mixtures. *Applied Clay Science* **184**: 105389, 10.1016/j.clay.2019.105389.

Abstract

Mixtures composed of 70% crushed Callovo-Oxfordian claystone and 30% MX80-bentonite are considered as materials, that could be used for backfilling a future radioactive waste repository in deep sedimentary rock formations. Their characterization is of interest, as the replacement of fractions of crushed claystone by bentonite enhances the chemo-hydro-mechanical performance of backfill. The materials are envisaged to be installed directly in the drifts and shafts by means of conventional compaction techniques. The hydro-mechanical behavior of materials containing expansive mineral phases, and especially their swelling behavior, is known to be significantly affected by the initial material properties and environmental and stress conditions. The present study aimed to assess the combined impact of variations in the material properties and environmental conditions, particularly the grain size distribution, dry density and saturating

solution chemistry, on the swelling pressure of the mixtures, by conducting a comprehensive laboratory experimental program. The results revealed that the adjustment of the grain size distribution of employed bentonite enhanced the compaction behavior and, in turn, the swelling behavior of the mixtures. Generally, swelling pressures of mixtures were less affected by the employed saline and alkaline solutions than those of crushed claystone. The measured swelling pressures were exponentially related to the initial dry density of the expansive mineral phase, regardless of the grain size distribution. Based upon the finding that the expansive mineral phase being present in crushed claystone contributed to measured swelling pressures, a new approach was introduced to calculate the dry density of the expansive mineral phase in bentonites and their mixtures with non-expansive or less-expansive materials.

3.1 Introduction

The long-term integrity of geological repository systems for nuclear waste is envisaged to be ensured by means of installing a multiple barrier system, which is generally composed of waste canisters, backfill, seals and the surrounding geological formation. The major containment might be either the geological formation or the canister, depending on the disposal concept.

According to ANDRA (2005), the French concept favors the former. It plans to install the future repository for disposing intermediate and high-level waste (ILW/ HLW) in the clay-rich Callovo-Oxfordian (COX) sedimentary rock formation, henceforth referred to as COX-claystone. Since the construction of drifts and shafts reduces the integrity of the geological formation, backfill and seals serve the general purpose of recovering the integrity upon terminating the closure-phase. Both are envisaged to fill hydraulic conductive voids and to limit the propagation of the excavation-damaged zone (EDZ) by stabilizing the surrounding rock mass. In addition, seals compress the EDZ, and fluxes of fluid phases from the repository to the biosphere and vice versa are inhibited by these means. Based on the mentioned purposes, the potential seal and backfill materials must exhibit a swelling potential, as well as strength. Specifically, the seal material must possess hydraulic conductivity, which ensures the inhibition of fluid fluxes. ANDRA (2005) proposed the employment of bentonite as a pure material or as a dominant fraction of a mixture with non- or less-expansive material, such as sand or crushed COX-claystone (COX_c), to seal the drifts and shafts. Conversely, backfill material consists of COX_c, which can be alternatively mixed with minor fractions of bentonite. The re-employment pursues the objectives of reducing the negative impact of backfill on the surrounding geological formation, avoiding mineralogical and physico-chemical incompatibilities, and lowering the costs by replacing commercial bentonite with COX_c. Determined in a manifold fashion, the hydro-mechanical behavior of materials containing expansive mineral phases is significantly affected by the material properties, the stress history and the environmental conditions (Chen, 1988; Gens and Alonso, 1992).

Different techniques have been considered to install backfill and seals. Seals are constructed by emplacing either industrially fabricated blocks or pellets into the drifts and shafts. Their industrial fabrication offside is advantageous, since the initial dry density can be adapted to the target values by using, for instance, the required compaction energy. Conversely, the employment of

conventional techniques, such as vibrating plates, is envisaged to compact backfill layer wise in situ. As the applicable compaction energy is limited in the case of in situ compaction, the initial dry density varies as a function of the initial water content. Generally, the maximum dry density is attained at the optimum water content by using constant compaction energy. The backfill is characterized by a lower initial dry density and a significantly higher water content, compared to blocks and pellets (ANDRA, 2005).

The feasibility of in situ compaction as a potential technique for backfill installation was evaluated by Gunnarsson et al. (2001) and Johannesson and Hagman (2013). They aimed to compact the backfill to the maximum dry density at the optimum water content, since the highest swelling pressure and low hydraulic conductivity are likely to be attained by this means Mitchell and Soga (2005). It was hardly realizable to homogeneously compact the material in the cross-section of the drift, especially close to the drift top and walls. They referred to the issues of the position of the compactor, which caused a loss of compaction energy and, in turn, a reduction in the initial dry density up to 20% with respect to the maximum dry density. Great differences in the swelling pressures were thus attributed to variations in these material properties.

In addition to varying material properties, evolving environmental conditions, such as saturating solution chemistry, are likely to have a negative impact on the performance of backfill materials containing expansive mineral phases. The phenomenon known as alkaline plume triggers the dissolution and modification of clay minerals in the backfill material, altering its structure and, in turn, its performance (Bradbury and Baeyens, 2003; Pusch et al., 2003; Karnland et al., 2007; Cuisinier et al., 2009; Cuisinier et al., 2014). These combined variations in the material properties and environmental conditions can impair the performance of backfill materials in such a way that formulated safety requirements are not met.

As information about COX_c was limited, most studies performed within the last few years were focused on characterizing the volume change and hydraulic conductivity behavior, rather than considering additional variations in material properties and environmental conditions. Tang et al. (2010), Tang et al. (2011a) and Tang et al. (2011b) compacted COX_c to initial dry densities of $\approx 2 \text{ Mg/m}^3$ at water contents of $\approx 3 \%$. These densities were in accordance with the envisaged densities of blocks being employed for seal construction. The obtained results indicated that the

swelling pressures ranged from several hundreds of kPa to some MPa. The measured hydraulic conductivities were equal to those of intact drill cores of COX. Wang et al. (2012) and Wang et al. (2014) performed swelling pressure and free swell experiments on compacted MX80-bentonite/ COX_c-mixtures, which were predominantly composed of MX80-bentonite ($\approx 70\%$). Their experiments considered not only a variety of soil properties and environmental conditions but also time effects. Just like in the sand-bentonite mixtures, the magnitude of material swelling was exponentially related to the initial dry density and was hardly affected by the saturation with a solution of low ionic strength. It can be concluded that few studies have examined mixtures of materials that each contains expansive mineral phases. Moreover, the performed experimental programs have hardly considered the variations in the initial material properties, as well as environmental conditions and their impact on the hydro-mechanical behavior of these mixtures.

This experimental program assessed the impact of replacing 30% of COX_c with MX80-bentonite on the structure, as well as the impacts on the compaction characteristics and on the swelling pressure. In particular, the consideration of the total amount of expansive mineral phases in these mixtures was of major interest, as the expansive mineral phases in COX_c were expected to contribute to the evolution of the swelling pressure. Bentonite was processed to maximum grain sizes of 0.25 mm and 2.00 mm before being mixed with COX_c. Henceforth, the mixtures of COX_c with bentonite with maximum grain sizes of 0.25 mm and 2.00 mm are referred to as the powder mixture and the grain mixture, respectively. The short-term development of the swelling pressure was tested by adopting the constant-volume method. Based on the findings of Gunnarsson et al. (2001), the impact of varying the dry densities on the short-term evolution of the swelling pressure was investigated by compacting the mixtures to their maximum and reduced dry densities at the optimum water content. The complementing experiments aimed to assess the impact of solutions with different pH values and ionic strengths on samples that were compacted to their maximum dry density at the optimum water content. Eventually, their combined impact on the performance of claystone/ bentonite-mixtures was analyzed in terms of the swelling pressure.

3.2 Theoretical background

The impact of variations in the saturating solution chemistry and dry density on the swelling behavior of claystone/ bentonite-mixtures is predominantly related to the physico-chemical forces at the molecular scale, namely, attractive and repulsive forces, that occur when saturating expansive clay minerals. These forces, in turn, are affected by the structure of the mixtures (Mitchell and Soga, 2005).

The mineralogical composition of MX80-bentonite is dominated by montmorillonite (Müller-Vonmoos and Kahr, 1983; Herbert et al., 2004; Karnland et al., 2007). *Table 3.1* compiles information about the mineralogical composition of MX80-bentonite taken from the literature. Single montmorillonite particles are characterized by both their platy form and their variable thickness. Their unit layers are composed of one alumina sheet that is sandwiched between two silica sheets. The permanently negative surface charge at their basal planes is attributable to isomorphous substitution, which is usually compensated by exchangeable cations, while the surface charges at their edge faces vary as a function of the proton concentration in the solution. Positively charged species are thus attracted by basal planes and either attracted or repelled by the edge faces (van Olphen, 1980; Tombácz and Szekeres, 2004, 2006). Regardless of the surface charge, dissolution and modification processes alter the clay minerals and their structures, in cases where they are exposed to solutions of different pH (Bradbury and Baeyens, 2003). These processes account for the sensitivity of expansive clays to varying pH values.

Table 3.1: Mineralogical composition of MX80-bentonite taken from different references

Mineral		Müller-Vonmoos and Kahr (1983)	Herbert et al. (2004)	Karnland et al. (2007)
Carbonate	[%]	1	< 2	1
Cristobalite	[%]	-	< 2	3
Feldspar	[%]	7	2	7
Kaolinite	[%]	< 1	-	-
Mica	[%]	< 1	-	1
Montmorillonite	[%]	75	90	83
Quartz	[%]	15	4	5
Pyrite	[%]	> 1	> 1	-

Apart from the pH, the swelling behavior of expansive clays is also affected by the ionic strength of the solution. Once montmorillonite particles are saturated with aqueous solution, the cations and water molecules are adsorbed by attractive forces on particle surfaces, forming diffuse double layers. Water molecules additionally permeate the interlayer space due to the higher hydration potential (Yong, 1999; Pusch and Yong, 2003). The concentration of the cations is high close to the particle surface and declines exponentially, as the distance from the particle surface increases. Repulsive forces occur once the diffuse double layers of the neighboring particles overlap (Bolt, 1956; Sridharan et al., 1986b; Mitchell and Soga, 2005). Among other factors, the thickness of the diffuse double layers varies as a function of the ion concentration and ionic strength (Mitchell and Soga, 2005).

Swelling itself is comprised of two processes, namely, crystalline and osmotic swelling, occurring upon hydration of expansive clay particles (Madsen and Müller-Vonmoos, 1989). Among other factors, such as the interlayer cation nature, their magnitude is related to the pH and ionic strength of the solution. Crystalline swelling is the result of the progressive hydration of exchangeable cations in the interlayer space, while osmotic swelling is caused by the interaction of overlapping diffuse double layers formed on neighboring clay particles. More detailed information about clay swelling is given in Madsen and Müller-Vonmoos (1989), Sridharan and Choudhury (2002) and Schanz and Tripathy (2009). Swelling pressure can be considered as the sum of hydration and repulsion forces, that accumulate upon saturation of expansive clays under confined conditions. Conversely, free swell strains develop under free conditions Madsen and Müller-Vonmoos (1989).

Attractive and repulsive forces account for the structure of the compacted expansive clays at the micro- and macro-scales. However, their structure is hardly affected by the ionic strength and pH of the adjacent solution. Generally, multiple clay particles form aggregates at the micro-scale, in which the single particles are orientated predominantly parallel due to the repulsion of equally charged particle faces. The random assembly of multiple aggregates constitutes macro-scale structures. Several studies, such as those of Alonso et al. (1987), Lloret et al. (2003) and Delage et al. (2006), analyzed the pore size distribution in expansive clays compacted by following the approach of block fabrication. Their results showed, that the total pore space is comprised of different kinds of pore populations at different scales, being characterized by a bi-

modal-shaped pore size distribution curve. Interlayer spaces are planar void spaces between the unit layers, while the inter-particle pores are present between particles and inside aggregates. Randomly arranged aggregates account for the inter-aggregate pores. The latter two pore populations are referred to as micro-pores and macro-pores. Increasing dry densities cause a significant reduction in the macro-porosity, while the micro-porosity remains stable. Overlapping repulsive forces contribute to the conservation of micro-porosity (Lloret et al., 2003).

The exponential relation of the initial dry density and the maximum values of the swelling pressure and free swell strains were determined in several studies (Komine et al., 2009; Schanz and Tripathy, 2009; Baille et al., 2010). The mentioned literature elaborately informs about the approaches adopted to explain this exponential relation.

This experimental program quantified the enhancement of the swelling behavior attainable by mixing COX_c with bentonite. The obtained results were complemented by information regarding the contribution of expansive mineral phases in COX_c to the maximum swelling pressure of mixtures. Moreover, the experiments aimed to determine, whether the swelling behavior of COX_c and its mixtures is more susceptible to variations in initial dry density or saturating solution chemistry, since information about their impact is scarcely available. A comprehensive platform was provided by these means, permitting to assign the observations to the single and combined impacts.

3.3 Materials

COX-claystone was obtained by excavating drifts of ANDRA URL in Bure at a depth of – 490 m. A few weeks afterwards, the excavated material was industrially crushed to maximum grain sizes of 2.00 mm and filled into sealed barrels. According to Robinet et al. (2012) and Conil et al. (2018), the mineralogical composition, initial water content and initial porosity of COX-claystone vary depending on the location in the sedimentary layer. COX-claystone is composed of 20 – 60% clay minerals being dominated by illite and interstratified illite/ smectite, 10 – 40% quartz and feldspars, 15 – 80% carbonates, and low amounts of pyrites. In contrast to intact drill cores of COX-claystone, whose initial water content are approximately 8.0% (Conil et al., 2018), the water content of COX_c was 5.4%. This decrease was attributed to the

crushing process and the duration of the storage. MX80-bentonite (Wyoming, USA) was selected to be mixed with COX_c, since it exhibits beneficial material properties, especially regarding its high volume change, low conductivity and high retention behavior (Pusch, 1992). Like COX_c, it was industrially crushed to maximum grain diameters of 0.28 mm and 2.00 mm, and filled by the supplier (Laviosa-MPC SAS, Limay, France) into sealed buckets. Information regarding the approximated mineralogical composition of the employed MX80-bentonite is given in *Table 3.1*. The water content, liquid limit, plastic limit and specific gravity of COX_c and the mixtures were determined following the French standard (Association Francaise de Normalisation, 1991, 1993). The determined physical properties of COX_c and the mixtures are compiled in *Table 3.2*. The corresponding values of MX80-bentonite are provided for the purpose of comparison.

Table 3.2: Determined physical properties of COX_c, MX80-bentonite, the grain- and powder mixture

Material	Physical properties					
	Natural water content	Specific gravity	Liquid limit	Plastic limit	10 %-Passing	60 %-Passing
	w	G_s	LL	PL	D_{10}	D_{60}
	[%]	[-]	[%]	[%]	[mm]	[mm]
COX _c	5.4	2.68	37.3	24.9	0.01	0.8
MX80 ^{a, b}	-	2.65 - 2.88	420.0 - 520.0	38.0 - 65.0	-	-
Grain mix.	6.4	2.64	112.5	34.7	0.008	0.8
Powd. mix.	6.4	2.64	112.5	34.7	0.004	0.2

^a : Delage et al. (2006)

^b : Komine et al. (2009)

The grain size distribution curves were obtained in two steps. First, grains larger than 0.80 mm in diameter were separated from the finer fractions via dry sieving. Since the bentonite fraction in the mixtures was expected to clog the finer meshes when coming into contact with water, the method of dry sieving was favored over wet sieving. The grain size distribution of the finer fractions was measured via laser diffractometry, following ISO (2009). The obtained distribution curves are depicted in *Figure 3.1*. The replacement of COX_c by bentonite with a maximum grain size of 0.28 mm caused a shift in the distribution curve to higher values, corresponding to a general increase in the amount of fines in the powder mixture.

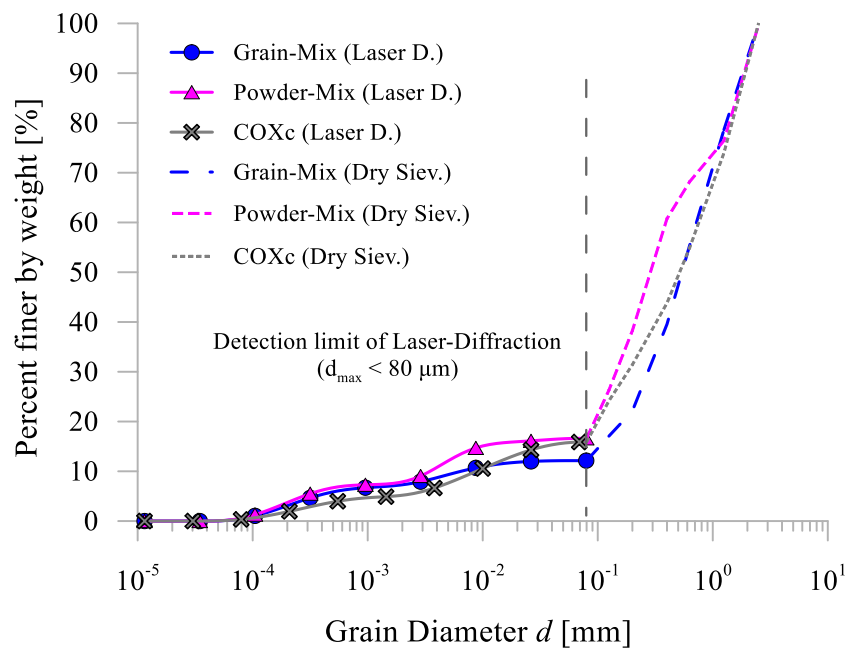


Figure 3.1: Grain size distribution curves of COXc, the grain- and powder-mixtures obtained by means of dry sieving and laser diffractometry

Sample preparation, as well as standard and modified Proctor tests, were conducted according to the French standard (Association Francaise de Normalisation, 2014a). The materials were prepared in a mechanical mixer at various molding water contents and filled in plastic bags after termination of the mixing process. Various molding water contents were established by adding deaired/ demineralized water to the original materials. The bags were then stored under ambient room conditions ($T = 20 \pm 2^\circ\text{C}$). During a period of one week, the plastic bags were frequently revolved to guarantee a homogeneous water content distribution. The results of the standard and modified Proctors tests performed on COX_c and the mixtures are depicted in *Figure 3.2a* and *Figure 3.2b*. The replacement of COX_c reduced the maximum dry density considerably and shifted the optimum water contents to higher values, regardless of the applied compaction energy. In the case of compacting the mixtures by using standard compaction energy, the impact of an increasing water content on the dry density at the dry side of the optimum water content was negligible.

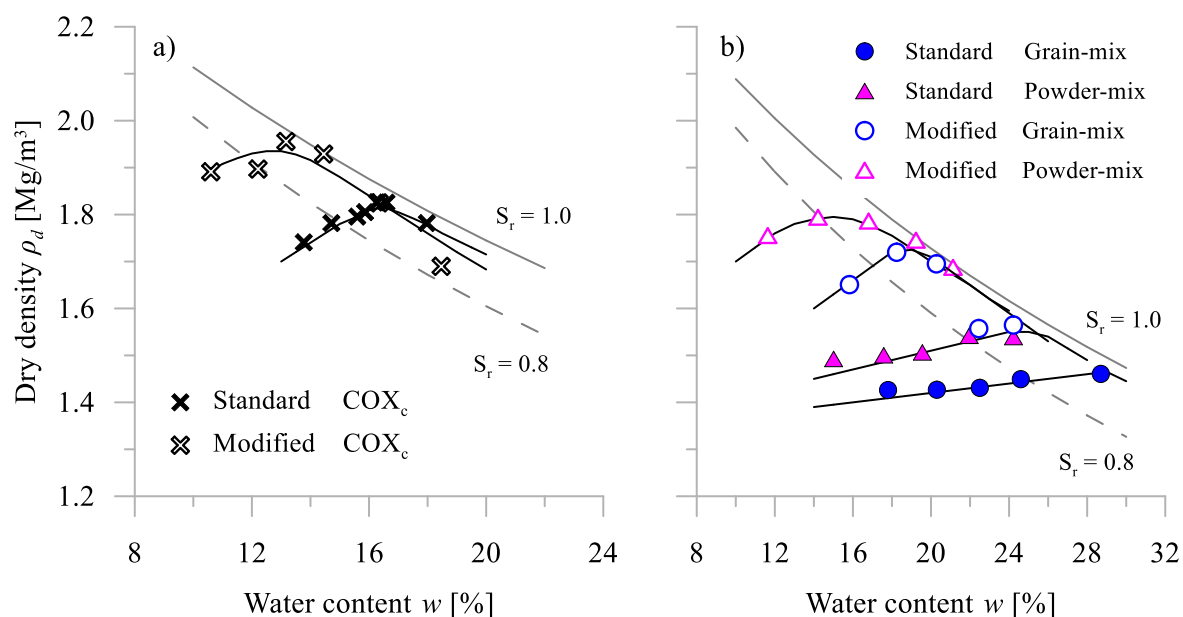


Figure 3.2: Results of the standard and modified Proctor tests performed on a) COXc and b) the grain- and powder-mixtures

Three different aqueous solutions, namely, deionized/ demineralized water (DW), artificial Bure site solution (ABSS) and artificial Portland cement solution (APCS), were employed.

Table 3.3: Compounds and characteristics of solutions being employed

Compound/ Ion species	Artificial Bure Site Solution (ABSS)		Artificial Portland Cement Solution (APCS)	
	c (Compound)	[mmol/l]	c (Compound)	[mmol/l]
Na ⁺		44.8		22.1
K ⁺		0.5		8.0
Ca ²⁺		5.3		19.0
Mg ²⁺		8.5		-
Cl ⁻		35.3		30.1
HCO ₃ ⁻		1.5		-
SO ₄ ²⁻		1.8		-
OH ⁻		-		38.1
I	[mmol/l]	105.0		87.0
pH	[-]	7.8		12.4

c (Compound): Molar concentration of the compound

They varied in their chemical compositions, ionic strengths and pH values. DW represented the reference case, since its chemical composition was expected to not affect the material behavior, while ABSS and APCS were believed to alter the swelling behavior as the site water at a depth of – 490 m and the occurring hyperalkaline solution, respectively. Both solutions were prepared according to information given by ANDRA. The compounds, main ion species and other characteristics of ABSS and APCS are compiled in *Table 3.3*.

3.4 Methods

The materials were prepared following the previously established protocol (Section 3.3). The samples were envisaged to be compacted to maximum dry densities ($\pm 1\%$) at individual optimum water contents ($\pm 1\%$), as determined in modified Proctor tests. Variations in the initial dry density were portrayed by reducing the maximum dry density of samples by 2.5%, 7.5% and 17.5%, while keeping the optimum water content. In the following, coefficients of dry density reduction were indicated by $R_{pd, max}$. Although it must be assumed that values of the initial dry density were shifted to the dry side of the compaction curve by reducing the maximum dry density and keeping the optimum water content, the approach was believed to adequately portray the conditions in situ. The reduction of the initial dry density by 17.5% with respect to the maximum dry density, for instance, corresponds to a loss of compaction energy of approximately 20%. Such a loss of compaction energy is likely to occur, if the materials are compacted close to the drift wall or the drift top. Conversely, the preparation of backfill materials to their optimum water contents and their conservation were less challenging tasks in situ (Gunnarsson et al., 2001).

The samples were compacted statically to target dry densities at a controlled rate of 0.1 mm/s inside the rings. The initial dimensions of each sample were 15 mm in height and 70 mm in diameter. By compacting the samples directly inside the rings, the risk of creating preferential flow paths and, in turn, saturating the samples heterogeneously, was significantly reduced. The ring, which contained the compacted sample being sandwiched between two porous discs, was screwed to the lid and the bottom plate. Then, the assembled cell was positioned in a load frame and the bottom plate was connected to a volume-/ pressure control unit, enabling the saturation of the sample with a given pressure from the bottom of the cell upwards. A graduated flask was

used to collect the outflowing solution. The load frame was equipped with an external load sensor, an internal load sensor, and a linear transducer. The linear transducer monitored the vertical position of the piston. Detecting an upward movement that was triggered by material swelling, the load frame automatically adapted the position of the piston downwards. By these means, the volume was kept constant. The evolving swelling pressure was recorded by two load sensors.

First, the experiment protocol envisaged to subject the samples to a vertical stress equal to 10 kPa. This approach served the purpose of establishing a good contact between the bottom plate, the porous disks, the sample, and the piston. The load frame kept the position of the piston constant afterwards. The bottom plate was flushed before imposing the injection pressure of 15 kPa, corresponding to a hydraulic gradient of 100, considering a sample height of 15 mm. By these means, the residual air in the bottom plate was removed. The swelling pressure experiments were stopped after 10 000 minutes (≈ 7 days). Detailed information about the samples and their major initial characteristics are given in *Table A.1*.

3.5 Results

The constant-volume swelling pressure experiments aimed to investigate the impact of replacing 30% of COX_c with bentonite on the short-term evolution of the swelling pressure of COX_c and the mixtures. The complementing experiments analyzed the response of the swelling pressure to variations in the dry density, as well as the saturating solution chemistry.

The evolutions of the swelling pressure of COX_c and the mixtures are depicted in *Figure 3.3*. Materials being compacted using higher energies generally exhibited higher swelling pressures. The maximum swelling pressures of COX_c and the grain-mixture were comparably low, while the powder-mixture was characterized by slightly elevated pressures, if it was compacted using standard energy. The maximum swelling pressure of the powder-mixture was 990 kPa, corresponding to an increase by 30% and 65%, compared to the maximum values of the grain-mixture and COX_c, respectively.

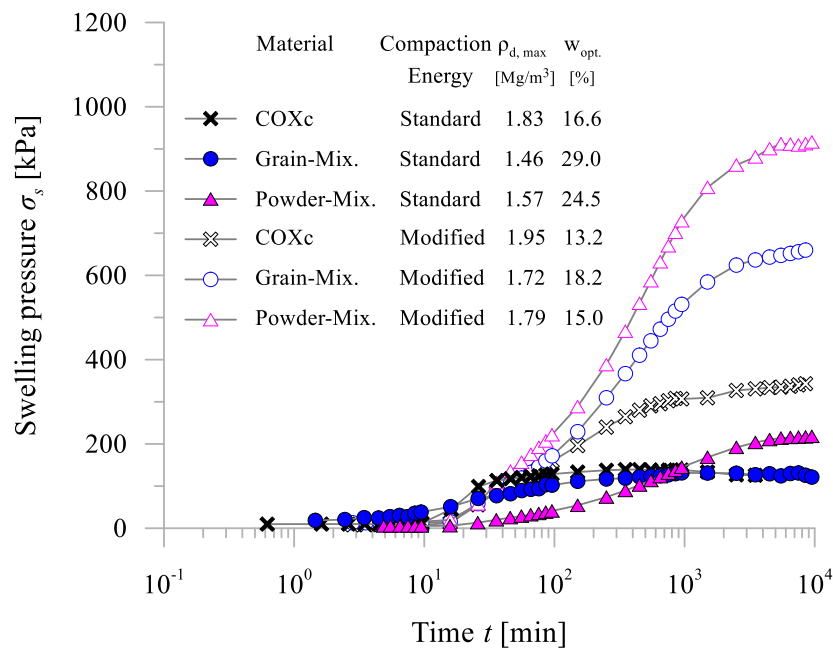


Figure 3.3: Evolution of swelling pressure of COX_c, the grain- and powder-mixture compacted to their individual maximum dry densities at optimum water contents and saturated with demineralized/ deaired water (DW)

Generally identified, the mixtures reacted to variations in solution chemistry less susceptibly than COX_c, when being compacted to maximum dry densities at optimum water contents. The impact of variations in the solution chemistry was thus more pronounced in the case of COX_c. The comparison of the material response is depicted in *Figure 3.4*. It became evident that the alkaline solution impaired the material performance more significantly than ABSS, although it had a lower ionic strength. For instance, the saturation with ABSS reduced the maximum swelling pressure by 6% in the case of the grain mixture and by 44% in case of COX_c. The grain-mixture lost 13% of its maximum swelling pressure, while a loss of 69% was measured upon bringing COX_c in contact with APCS.

The reduction in the dry density caused a significant loss in the swelling pressure in the individual experiments, when compacting the material at optimum water content. The impact of the reduced dry densities in the case of the grain-mixture is presented in *Figure 3.5*. Accordingly, maximum values were determined at the highest dry densities. A reduction of 2.5%, 7.5% and 17.5% decreased the maximum swelling pressure by 20%, 65% and 85%, respectively. Moreover, the material saturation accelerated as the dry density decreased.

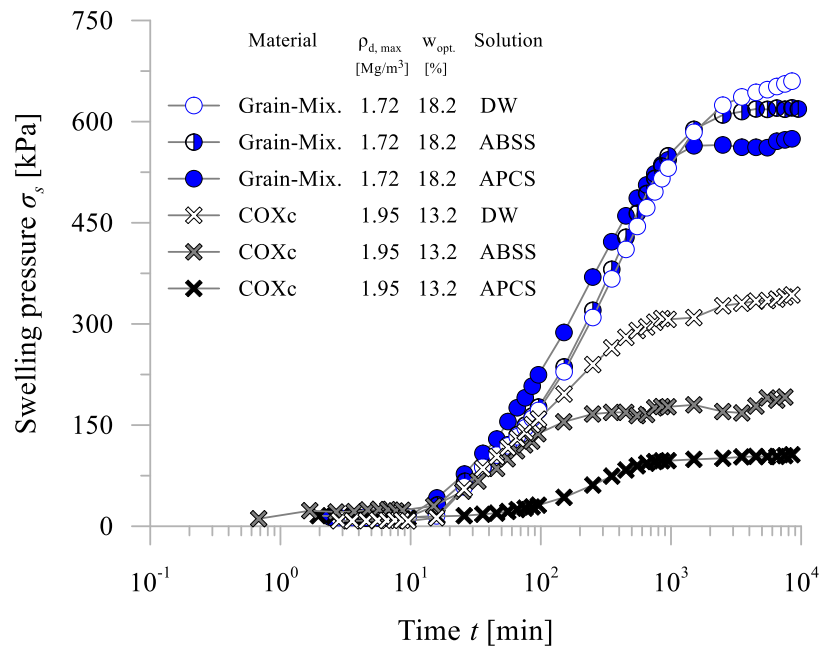


Figure 3.4: Evolution of swelling pressure of COXc, the grain- and powder-mixtures compacted to their individual maximum dry densities at optimum water contents and saturated with demineralized/ deaired water (DW), artificial Bure site solution (ABSS) and artificial Portland cement solution (APCS)

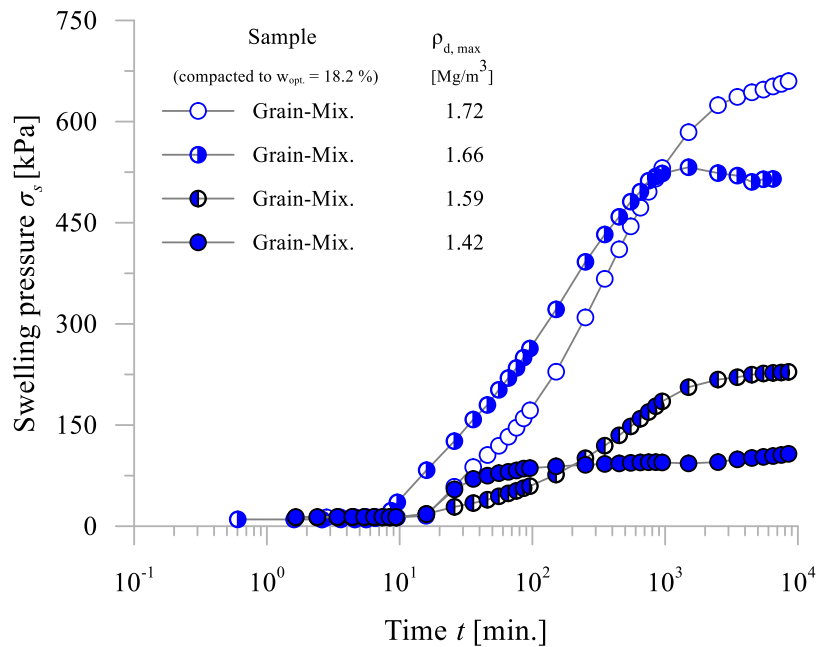


Figure 3.5: Evolution of swelling pressure of the grain-mixture compacted to 1) maximum dry density, 2) maximum dry density reduced by 3.5%, 3) maximum dry density reduced by 7.5%, and 4) maximum dry density reduced by 17.5% at optimum water content and saturated with deaired/ demineralized water (DW)

The reduction in the maximum dry density and the maximum swelling pressure of both mixtures were exponentially related (*Figure 3.6*) The corresponding regression line is given by the equation:

$$\sigma_s = \sigma_{s,max} \exp(-\beta R_{\rho_{d,max}}) \quad (3.1)$$

where $\sigma_{s,max}$ is the highest expectable swelling pressure and β is the slope indicating the swelling pressure decrease with the dry density reduction.

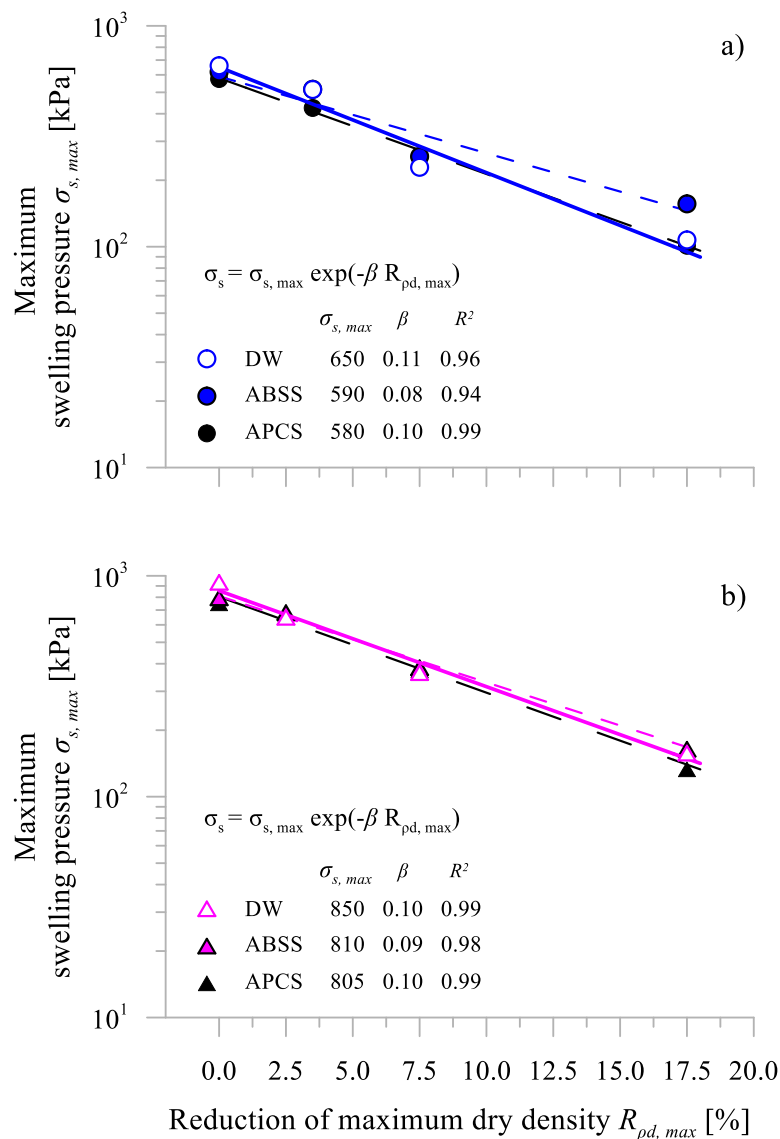


Figure 3.6: Depiction of the exponential relation between the reduction of initial dry density and the maximum swelling pressure, including the impact of the saturated solution chemistry: a) Relation of grain-mixture, b) Relation of powder-mixture

The major results of the performed swelling pressure experiments are compiled in *Table A.2*. Information about the major final characteristics of samples are added. The expansive mineral dry density (EDD) will be introduced in section 3.6.

3.6 Discussion

Most of obtained results are neither comparable nor interpretable with relations that are presented in the literature, since the reduction in the maximum dry density $R_{pd, \max}$ represents a value being relative to the individual maximum dry density. Thus, replacing the reduction by a generally more applicable variable might be recommended. Section 3.6.1 briefly introduces the expansive material dry density (EDD) and its major purpose, while the following sections discuss the obtained results.

3.6.1 Introduction of expansive mineral dry density (EDD)

COX_c and MX80-bentonite are referred to as expansive materials that are generally composed of expansive and inert mineral phases. Results of constant-volume swelling pressure experiments performed on COX_c suggested a non-negligible contribution of the expansive mineral phases in COX_c to the maximum swelling pressure of mixtures (*Figure 3.3*). It was thus assumed that the total fraction of the expansive mineral phases must account for the swelling characteristics of mixtures. Concepts such as the bentonite dry density attributing the behavior of mixtures of bentonite and non-expansive materials only to the bentonite fraction (Bucher and Jedelhauser, 1985; Villar and Rivas, 1994; Dixon, 2000; Agus and Schanz, 2008; Wang et al., 2012) were hardly applicable in the case of claystone/ bentonite mixtures, as they disregard expansive mineral phases in COX_c on the one hand and inert mineral phases in MX80-bentonite on the other hand. Unlike the approach of Zeng et al. (2019) which considered the contribution of expansive mineral phases in COX_c to material swelling of bentonite/ claystone mixtures by introducing an inhibition factor, the expansive mineral dry density (EDD) was aimed at relating the swelling characteristics of bentonites and their mixtures to their mineralogical composition. Apart from attributing material swelling to the total fraction of the expansive mineral phases in the mixtures, the following assumptions are also considered prior to its employment. The pore water being present is exclusively attached to the expansive mineral phases; the porosity of the fraction of inert mineral phases is so low that expansive mineral phases occupy the entire

macro-pore space when they swell; and material compaction only causes a reduction in the macro-pore space.

In the following, materials containing expansive mineral phases are classified into the expansive and inert mineral phases, as well as the fluid phase and the gas phase. The corresponding phase diagram is depicted in *Figure 3.7*.

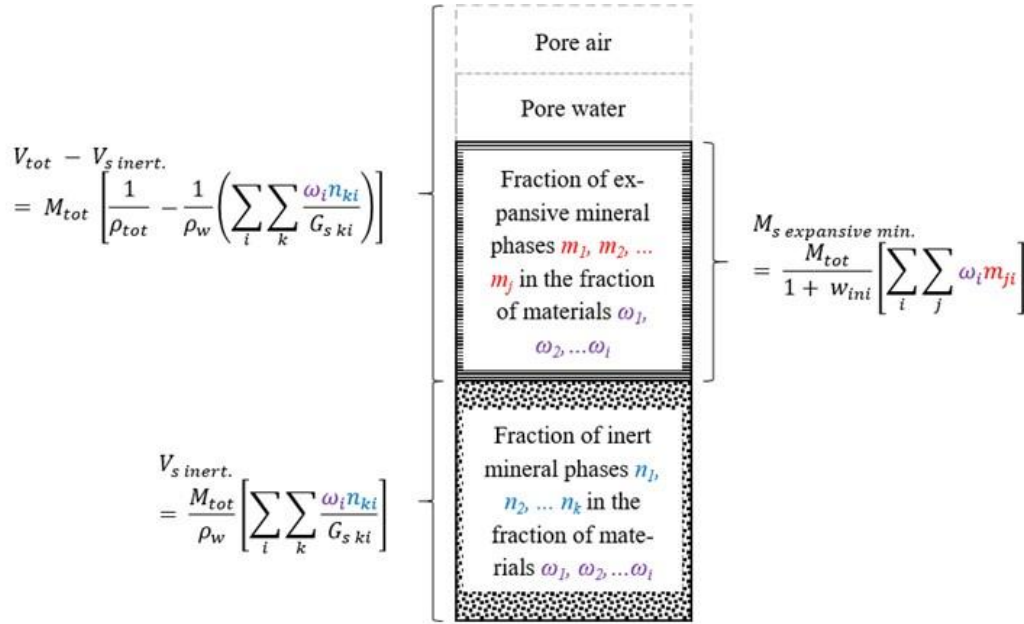


Figure 3.7: Defined four phases of a mixture composed of different expansive soils

The total fraction of expansive mineral phases in the mixtures was calculated by first summing the fraction of expansive mineral phases (x_{ji}) in each material (i) up and then multiplying the obtained sum by the total fraction of the corresponding material in the mixture (f_i). The results of the second step were then summarized to consider all materials in the mixture. The total fraction of inert mineral phases in the mixtures was calculated similarly. For instance, the total fraction of smectite in the mixture was calculated by first multiplying 0.83 (*Table 3.1*) representing the fraction of smectite in MX80-bentonite by 0.3 representing the fraction of MX80-bentonite in the mixture. The fraction of smectite in COX_c was assumed to be equal to 0.15 as COX_c only contains fractions of interstratified illite/smectite. Its multiplication by 0.7 makes the fraction of smectite in COX_c. The final value of the fraction of smectite in the mixture is obtained by summing 0.25 and 0.15 up being equal to 0.35. EDD was defined as the ratio of

the dry mass of the total fraction of expansive mineral phases in the mixture to the combined volume of the total fraction of expansive mineral phases in the mixture and the pore volume. The denominator of the ratio is substitutable by the difference between the total volume of the mixture and the volume of the total fraction of inert mineral phases in the mixture. EDD is given as:

$$EDD = \left[\sum_i \sum_j f_i x_{ji} \right] \left[\frac{1}{\rho_d} - \left(\frac{1 + w_{ini}}{\rho_w} \right) \left[\sum_i \sum_k \frac{f_i y_{ki}}{G_{s\ ki}} \right] \right]^{-1} \quad (3.2)$$

where f_i is the mass fraction of material i in the mixture, x_{ji} is the mass fraction of expansive mineral phase j in material i , y_{ki} is the mass fraction of inert mineral phase k in material i and $G_{s\ ki}$ is the specific gravity of the inert mineral phase k in the material i . For instance, the calculation of the mass fraction of smectite in the investigated mixtures proceeds as follows: The mass fraction of MX80-bentonite in the mixture is initially multiplied by the mass fraction of smectite in MX80-bentonite. Similarly, the mass fraction of smectite in COX_c, which is present in the mixture, is calculated in the next step. The sum of both multiplications eventually gives the mass fraction of smectite in the investigated mixtures.

The equation is complemented by the dry density of the mixture (ρ_d), the density of the water (ρ_w), and the initial water content of the mixture (w_{ini}). Its utilization allowed a comparison of the impact of densification on the maximum swelling pressure of not only the bentonites being predominantly composed of expansive minerals, such as MX80-bentonite, but also mixtures of those bentonites with less- and non-expansive materials, such as COX_c or sand.

3.6.2 Impact of expansive mineral content and grain size distribution

First, the impact of COX_c-replacement by bentonite on the compaction and swelling properties was assessed. Comparing the compaction curves of COX_c and both mixtures, COX_c exhibited a significantly higher compactibility, indicated by the higher dry densities (*Figure 3.2*). The compaction behavior of the mixtures was alike that of pure MX80-bentonite, since varying water contents had a minor impact on the attained dry densities at the dry side of the compaction curve (Dixon et al., 1985). These findings were complemented by Pusch (1995), Keto et al. (2006) and this study. They observed a more pronounced sensitivity of material dry density to

varying water content and compaction energy with a lower amount of expansive material in the mixture. Dixon et al. (1985) related the observed insensitivity of MX80-bentonite to the higher viscosity of adsorbed water on clay particles, which induces an elevated shear strength. This resistance might be higher than the applied compaction energies. Consequently, the shear strength might decrease with an increasing amount of less- or non-expansive material. As described by Komine and Ogata (1999), an increasing fraction of expansive material in these mixtures provokes higher swelling pressures, if compacted to maximum dry density at optimum water content.

Referring to the impact of the amount of fines on the compaction and swelling properties, it became evident that the powder-mixture exhibited a higher compactability than the grain-mixture when compacting it by using the modified compaction energy. The measured swelling pressures of the powder-mixture were higher than those of the grain-mixture due to the higher dry density and the lower optimum water content. Keto et al. (2006) performed modified Proctor experiments on crushed granite rock/ bentonite-mixtures. According to their findings, the highest dry densities can be attained by employing materials having the widest grain size distribution and the highest amount of fines. A wider grain size distribution provokes a denser packing of particles and, in turn, reduces the amount of macro-porosity.

3.6.3 Individual impact of EDD and solution chemistry

The introduction of EDD aimed to compare the impact of densification on any material that contains fractions of expansive minerals. Its applicability was verified by calculating EDD derived from different literature and plotting the values against the reported maximum swelling pressures. The obtained results compared to the literature data are depicted in *Figure 3.8*.

The comparison affirmed the significance of EDD as one key variable governing the maximum swelling pressure of materials containing expansive mineral phases. The grain- and powder-mixture reacted to elevated EDD with increasing swelling pressures as depicted in *Figure 3.8*.

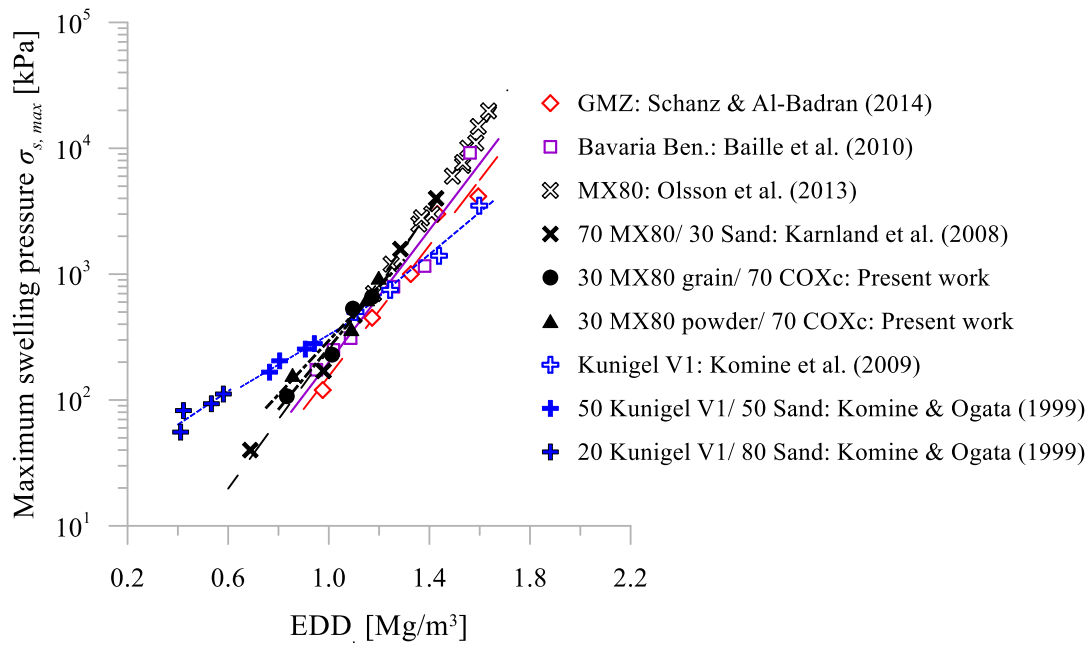


Figure 3.8: Exponential relationship between EDD and the maximum swelling pressure including results of various expansive clays and their mixtures with varying amounts of non-expansive materials taken from literature

According to section 3.2, these results were most likely attributable to the higher probability of double layer repulsion. The exponential relationship of EDD and the maximum swelling pressure of each bentonite, including its mixtures, seemed to be unique although this issue has not been confirmed. This trend was particularly noticeable by comparing the slope of the individual regression lines of the materials composed of MX80-bentonite. The general trend can be approximated by the following generalized equation of the regression curve:

$$\sigma_{s,max} = \sigma_{s,min} \exp(\beta^* EDD) \quad (3.3)$$

where $\sigma_{s,min}$ can be considered to be the minimal swelling pressure that is theoretically evolving, if the material is in a loose state, while β^* identifies the actual impact of varying EDD on the maximum swelling pressure. Apart from the initial dry density and the initial water content, the β^* parameter is predominantly controlled by the mass fraction of expansive minerals in the material. This finding is consistent, as EDD might increase with a higher mass fraction of expansive mineral phases at the same dry density. *Table 3.4* gives information about the different values of $\sigma_{s,min}$ and β^* .

Table 3.4: Material parameters obtained by correlation of experiment and literature data

Reference	Material	$\sum \sum_i x_{ji}$	$\sigma_{s, min}$	β^*	R ²
		[-]	[kPa]	[-]	[-]
Schanz and Al-Badran (2014)	GMZ01 bentonite	0.75	0.39	5.99	0.971
Baille et al. (2010)	Bavaria bentonite	0.78	0.47	6.05	0.947
Olsson et al. (2013)	MX80 bentonite	0.83	0.15	7.59	0.907
Karnland et al. (2007)	70% MX80/ 30% Sand	0.58	0.42	6.78	0.992
Komine et al. (2009)	Kunigel V1 bentonite	0.57	6.60	3.85	0.975
Komine and Ogata (1999)	50% Kunigel/ 50% Sand	0.17	32.00	1.97	0.617
Komine and Ogata (1999)	20% Kunigel/ 80% Sand	0.11	18.68	2.58	0.751
Present work: Grain-mix.	30% MX80 gr./ 70% COX _c	0.35	1.40	5.24	0.962
Present work: Powder-mix.	30% MX80 po./ 70% COX _c	0.35	2.00	4.99	0.963

$\sum \sum_i x_{ji}$: Accumulated mass fraction of expansive minerals (in the mixture)

COX_c, the grain- and powder-mixtures were characterized by initial suctions of 1.5 MPa, 2.9 MPa and 4.3 MPa, respectively, when the samples were compacted to the maximum dry density at their individual water content by using modified compaction energy. These initial suctions suggest that osmotic swelling might more contribute to the development of swelling pressure under constant-volume conditions than crystalline swelling. As the magnitude of osmotic swelling is susceptible to the saturating solution chemistry, particularly the cations in solution and the ionic strength, the swelling pressures of COX_c and the mixtures were expected to be affected by the employed solution. Interestingly, such an impact was observed only in the case of COX_c whereas both mixtures hardly reacted to the different solutions. The higher susceptibility of COX_c cannot be reasonably explained yet, thus demanding more investigations.

3.6.4 Combined impact of solution chemistry and EDD

Comparable to this study, some studies also emphasized the impact of variations in the ionic strength of solutions on the swelling pressure of different bentonites that were compacted to different dry densities (Pusch, 1980; Karnland, 1997; Dixon, 2000; Pusch, 2001a; Castellanos et al., 2008; Komine et al., 2009; Xiang et al., 2019). Generally, the impact of the ion concentration is more pronounced in the case of less compacted bentonites. The observed effect vanishes as the dry density and montmorillonite content increase.

Conversely, the different saturating solutions had a minor impact on the maximum swelling pressure of the grain- and powder-mixtures, even when the samples were compacted to lower values of EDD. This finding can be deduced from $\sigma_{s, min}$ and β^* parameters in *Figure 3.9a* and *Figure 3.9b*, despite the grain-mixture saturated with ABSS exhibited a greater deviation of those parameters.

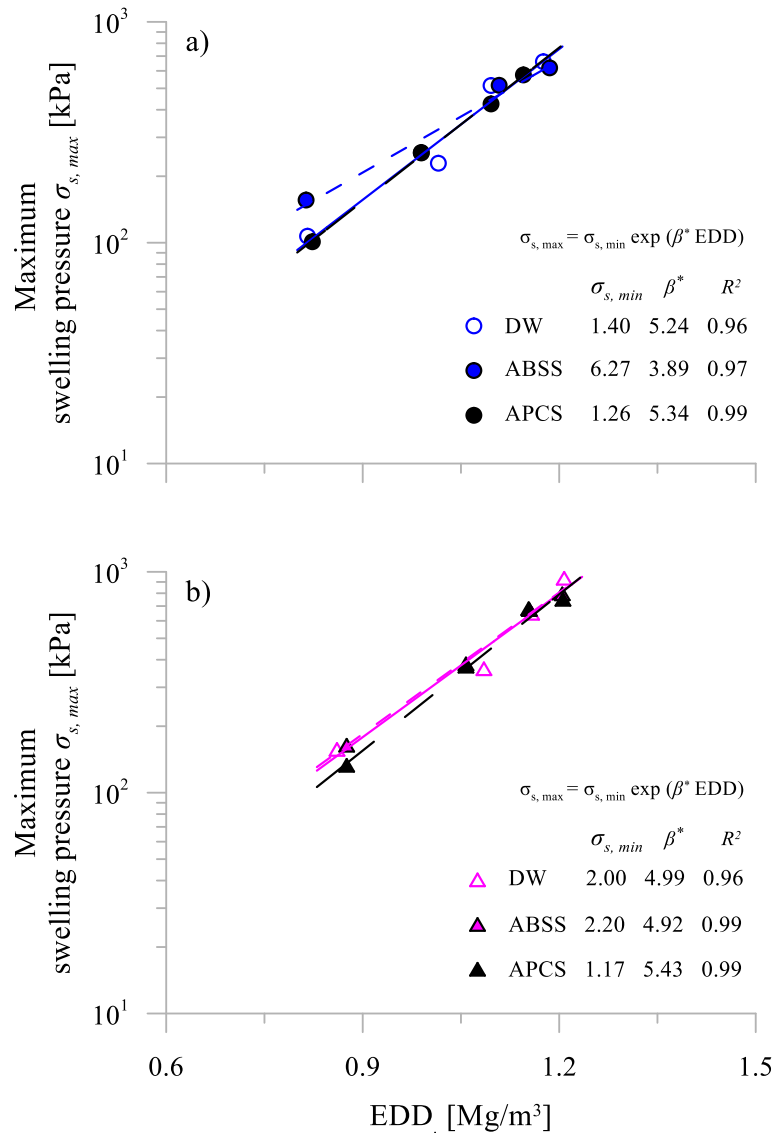


Figure 3.9: Exponential relation of EDD and maximum swelling pressure in the case of the a) grain-mixture and b) the powder-mixture (saturated with deaired/demineralised water (DW), artificial Bure site solution (ABSS) and artificial Portland cement solution (APCS))

Most probably, the low concentration of cations in solution caused an only partial exchange of cations hardly affecting the thickness of diffuse double layers and in turn the maximum swelling pressure of the grain- and powder-mixtures.

3.7 Conclusions

The current laboratory experimental program assessed the impact of partly replacing crushed COX-claystone (COX_c) with MX80-bentonite on the compaction and on the swelling behavior of mixtures that could potentially be employed to backfill drifts and shafts of a future repository for nuclear waste in deep sedimentary rock formations. Complementary experiments investigated the impact of variations in the dry density and saturating solution chemistry on the evolution of the swelling pressure. The reference concept envisages the employment of conventional compaction techniques to install the backfill directly inside the drifts and shafts.

The considered backfill materials are composed of 70 % crushed COX-claystone (COX_c) and 30 % MX80-bentonite grains or powder in wet mass. COX_c served as a reference material to identify the impact of the material replacement. Evolving swelling pressures were determined by means of the constant-volume method. The employed samples were then prepared to maximum and reduced dry densities at optimum water contents, which were obtained in modified Proctor tests. The samples were saturated with three solutions, greatly varying in pH values and ionic strengths. The following conclusions can be drawn from the laboratory experimental program:

3. The replacement of 30% COX_c by either MX80-bentonite grains or powder caused a shift in the maximum dry density to lower values and of the optimum water content to higher values, regardless of the applied compaction energy. Compared to the grain-mixture, the powder-mixture exhibited a higher maximum dry density at a lower initial water content when compacting using the same energy. This finding was attributed to an optimized particle packing caused by a higher amount of fines. The maximum swelling pressure of both mixtures was higher than that of COX_c, despite the lower maximum dry density. Generally, these findings were in accordance with the literature, as the amount of expansive mineral phases in the mixtures was higher.

4. The swelling pressure of the claystone/ bentonite mixtures was identified as being hardly affected by the saturating solution chemistry, when compacting both mixtures to their maximum dry densities at optimum water contents. This might be caused by the low ionic strength of the employed solutions. The swelling pressure of COX_c seemed to be more susceptible to the saturating solution chemistry. More experiments are required to adequately explain this point. Generally applicable, expansive mineral dry density (EDD) improved the comparability of the impact of densification on the swelling pressure of materials that contain fractions of expansive mineral phases. Its introduction was claimed by the considerable contribution of expansive mineral phases in COX_c to material swelling. The exponential relationship of EDD and the maximum swelling pressure was identified as being unique in the cases of every bentonite and its mixtures.
5. In the case of the grain-and powder-mixture, the different saturating solutions had a minor impact on the maximum swelling pressure of the grain- and powder-mixtures, even when the samples were compacted to lower values of EDD. This finding can be predominantly attributed to the low concentration of cations in solution and the low ionic strength of the employed saturating solutions.

It is recommended that MX80-bentonite powder-based mixtures are favored over grain-mixtures if employing conventional compaction techniques to install backfill in drifts and shafts, as higher short-term swelling pressures can be attained. It became evident that varying dry densities affect the material performance of the claystone/ bentonite mixtures more significantly than potential environmental conditions. Thus, high demands must be made on the quality management during backfill installation. Generally, this study improved the knowledge about mixtures of the materials each containing expansive mineral phases in terms of their compaction and swelling behavior. Future studies will assess the long-term evolution of the material behavior of grain- and powder-mixtures, especially the swelling pressure and hydraulic conductivity. It is also of interest to investigate the material behaviors under varying degrees of saturation.

4 Hydraulic conductivity, microstructure and texture of compacted claystone/ bentonite mixtures saturated with different solutions

Based on the submitted manuscript of the following article:

Middelhoff M, Cuisinier O, Gaboreau S, Masroui F, Talandier J and Michau N (2020) Hydraulic conductivity, microstructure and texture of compacted claystone/ bentonite-mixtures saturated with different solutions. *Engineering Geology*, (under review)

Abstract

The French reference concept for the disposal of intermediate- and high-level nuclear waste (ILW/ HLW) in the Callovo-Oxfordian sedimentary rock formation (COX-claystone) considers the employment of crushed COX-claystone and its mixture with MX80-bentonite as potential backfill materials installed in drifts and shafts once the operational phase of the future repository is terminated. The fraction of MX80-bentonite in the mixture is limited to 30% in weight. Over time, the backfill is saturated with solutions that originate in the surrounding host rock formation and percolate through the concrete lining left in place. The major characteristic of the leachate is its high pH-value. In addition to the swelling pressure, the sealing properties of the backfill are mainly determined by the hydraulic conductivity. Unlike previous studies, this laboratory experimental study aimed to understand the hydraulic conductivity evolution of potential backfill materials under realistic conditions in terms of compaction conditions, solution chemistry and temperature, and to relate the results determined at the macroscale to results of

microstructural and textural analysis. Also, the impact of the solution chemistry was envisaged to be evaluated by these means. The constant-head, mercury intrusion porosimetry and nitrogen-gas sorption techniques were employed to determine the hydraulic conductivity, microstructural and textural properties, respectively. In the case of mixture-samples, no stabilization of hydraulic conductivity was detected, despite the duration of the experiments being about one year. There was no detectable impact of the solution chemistry in the course of experiments, which was attributed to the low reaction kinetics under imposed conditions. Subsequent microstructural analysis indicated material swelling probably triggering rearrangements in the micro- and macro-pore space and lowering the fraction of hydraulic conductive voids. Interestingly, neither the saturation nor the solution chemistry had an impact on the specific surface area of materials.

4.1 Introduction and background

The French reference concept considers the disposal of intermediate and high level nuclear waste in the Callovo-Oxfordian sedimentary rock formation located 500 m below ground level (ANDRA, 2005). Henceforth, the sedimentary rock formation is referred to as Callovo-Oxfordian (COX) claystone. The encapsulated nuclear waste is emplaced in horizontal drifts, which are sealed and backfilled once the operational phase of the repository is terminated. Unlike the seals, backfill is envisaged to be installed in situ by means of conventional compaction techniques. It swells upon its saturation and inhibits the flow of fluid phases from the emplacement drifts to accessible biosphere over time. Its installation particularly aims to limit the propagation of the excavation damaged/ disturbed zone (EDZ) and to close the hydraulic conductive pore space. In addition to the swelling pressure evolving under the constant volume conditions, the hydraulic conductivity can be considered as one of the key parameters which govern the sealing properties of backfill and is thus of major interest in this study.

Potential backfill materials are re-employed COX-claystone and its mixture with MX80-bentonite. COX-claystone is obtained during drift excavation and processed afterwards. Henceforth, crushed and sieved COX-claystone is referred to as COX_c. Its re-employment particularly aims to inhibit mineralogical and physico-chemical incompatibilities with the surrounding geological formation (ANDRA, 2005). A mixture composed of COX_c and MX80-bentonite is considered alternatively, since the increased smectite fraction might enhance the hydro-mechanical behavior of backfill. Like other smectite-containing materials, COX_c and its mixture might be affected by variations in the material properties (e.g. physico-chemical characteristics, microstructure, initial dry density etc.), the environmental conditions (e.g. degree of saturation, solution chemistry etc.) and stress history (e.g. preconsolidation pressure etc.) with regard to their hydro-mechanical behavior (Alonso et al., 1987; Chen, 1988). It must be thus evaluated whether the sealing properties of backfill are stable to possible variations over time.

In this regard, numerous laboratory experimental studies addressed the impact of the saturating solution chemistry on the physico-chemical and textural characteristics (e.g. Ramírez et al., 2005; Herbert et al., 2008), the microstructure (e.g. Cuisinier et al., 2008; Fernández et al., 2014) and the hydro-mechanical behavior of smectite-containing materials (e.g. Villar, 2006;

Karnland et al., 2007; Cuisinier et al., 2014; Ye et al., 2014b; Chen et al., 2015). Considering the reference concept, the impact of the pH is of particular relevance, as described below.

Once the closure phase of the repository is terminated, the backfill might be saturated with solutions, which originate in the surrounding geological formation and percolate through the concrete lining left in place. The initial leachate is characterized by a pH above 13.5. This elevated pH is attributable to the release of potassium and sodium hydroxides from the concrete. After their leachate, the solution chemistry is controlled by the dissolution of portlandite at a pH of 12.5 and later by the dissolution of cement phases at a pH ranging from 10.5 to 12.5. The phenomenon is referred to as hyperalkaline plume and might trigger different geochemical reactions while saturating the backfill (e.g. Huertas et al., 2000; Michau, 2005).

Ion exchange at clay mineral surfaces can be expected once the alkaline solution percolates the backfill material. For instance, sodium ions can be replaced by calcium ions from the alkaline solution as their hydration potential is higher (Mitchell and Soga, 2005). Simultaneously, the dissolution of clay minerals can be triggered as they remain relatively stable up to a pH of 9 and start dissolving once the pH exceeds 10. Secondary minerals, such as carbonates, clay minerals, cement phases, silicates, and zeolites, can precipitate or form afterwards. Their reaction kinetics and reaction mechanism are controlled by the pH of solutions and the ambient temperature, among other factors (Krauskopf, 1956). The analysis of concrete-claystone interfaces sampled in situ indicated that the reaction kinetics are very low under real conditions (e.g. Gaboreau et al., 2011; Gaboreau et al., 2012), thus the impact of the saturating solution chemistry on the sealing properties of backfill must be expected to be highly time-dependent.

In order to investigate the impact of the solution chemistry on the backfill materials in a reasonable period of time, most studies considered simplified conditions, instead of realistic conditions. Simplified conditions comprise an increased liquid to solid ratio, an increased ionic strength of solutions, the employment of homoionic solutions and an increased temperature. In the case of hydraulic conductivity experiments, values can be obtained faster by imposing higher hydraulic gradients. However, there are no information about whether the imposed hydraulic gradient has an impact on the reaction kinetics.

The impact of saturating solution chemistry on the physico-chemical and textural characteristics of smectite-containing materials is mainly investigated by conducting batch experiments characterized by a high liquid to solid ratio (e.g. Herbert et al., 2004; Hofmann et al., 2004; Ramírez et al., 2005; Fernández et al., 2014; Elert et al., 2015). However, there are significant inconsistencies, particularly with regard to the cation exchange capacity and specific surface area. Inconsistencies are attributable to the differences in the composition, ionic strength, and pH of solutions and in imposed temperatures. In general, results lack transferability to compacted materials predominantly due to the high liquid to solid ratio.

Micro- and macropores characterize the microstructure of compacted smectite-containing materials in unsaturated state and correspond to pores between clay aggregates and soil aggregates, respectively. Their existence is indicated by a bi-modal pore-size distribution curve commonly obtained by means of mercury intrusion porosimetry (MIP) experiments (Alonso et al., 1987). There are only a few studies addressing the impact of solution chemistry on the microstructure of smectite-containing materials. For instance, the study of Cuisinier et al. (2008) comprised an aging process, in which compacted clayey soil samples were saturated with a portlandite-saturated solution ($\text{pH} > 12$) under elevated temperatures ($> 50^\circ\text{C}$). The aging process lasted longer than 12 months. Subsequent MIP-experiments revealed that the macropores increased significantly, whereas the micropores remained stable. The dissolution of smectite accounted for the increase in the amount of macropores, and might in turn provoke an increase in hydraulic conductivity (e.g. Romero, 2013). In general, the results are less transferable to compacted backfill materials, since the elevated temperatures imposed during the aging process accelerated the reaction kinetics and might have induced different reaction mechanisms.

There is a wealth of studies aiming to analyze the impact of saturating solution chemistry on the hydraulic conductivity behavior of compacted backfill materials under realistic conditions (e.g. Mata, 2003; Villar, 2006; Castellanos et al., 2008; Ye et al., 2014b; Chen et al., 2015; Zhang and Kröhn, 2019). Realistic conditions refer to the initial compaction conditions of samples, the saturating solution chemistry, and the ambient temperature. Their major conclusion was that the impact vanishes upon the ionic strength decreases or the dry density increases. Results were attributed to the modification of the pore size distribution and to the mobility of

the water molecules within the macropores. However, interpretations were mainly based on diffuse double layer (DDL) theories and thus lack experimental evidence.

Only a few studies related changes in the hydraulic conductivity behavior of smectite-containing materials to the impact of the saturating solution chemistry on the physico-chemical and textural characteristics and microstructure (Pusch et al., 2003; Cuevas, 2005; Karnland et al., 2007; Musso et al., 2013; Cuisinier et al., 2014). Indeed, parts of the studies of Pusch et al. (2003) and Cuevas (2005) were conducted under realistic conditions and are thus of special interest. However, both studies lacked completeness as they disregarded the microstructure and attributed changes in the hydraulic conductivity to the impact of the solution chemistry on the physico-chemical and textural characteristics only. Results indicated that the solution chemistry affected neither the hydraulic conductivity of materials nor their cation exchange capacity and specific surface area. Those observations were attributed to the low reaction kinetics. Despite the conclusion, the sealing properties of potential backfill materials were assumed to be long-term stable to the saturating solution chemistry under realistic conditions.

This study aims to determine the hydraulic conductivity of claystone/ bentonite mixtures by means of laboratory experiments, whose conditions are believed to describe the real conditions in terms of the compaction conditions, saturating solution chemistry and ambient temperature. Subsequent N₂-gas sorption and mercury intrusion porosimetry (MIP) experiments serve the purpose of identifying possible changes in the texture and microstructure of samples which might also indicate to the impact of saturation process and saturating solution chemistry. The relation of the hydraulic conductivity to the possible changes in the texture and microstructure of materials then allows to assess whether the hydraulic conductivity determined still evolves in the short- and intermediate-term or reflects a long-term stable state.

4.2 Materials

The materials investigated were COX_c and its mixture with MX80-bentonite (Wyoming, USA). The latter was composed of 70% COX_c and 30% MX80-bentonite in weight. The limitation of MX80-bentonite to 30% based on the reasons mentioned above. COX-claystone muck was obtained during the excavation of drifts of Andra URL in a depth of – 490 m (Bure, Meuse/ Haute-Marne region, France). Conil et al. (2018) highlight that the mineralogical composition, water

content and porosity of intact COX-claystone samples vary with their position in the rock formation. Correspondingly, COX_c was expected to consist of about 46% phyllosilicates (e.g. illite, ordered illite/ smectite mixed layer minerals), 24% tectosilicates (e.g. quartz, feldspars), 27% carbonates (e.g. calcite, dolomite), and minor fractions of associated minerals (e.g. pyrite). The subsequent processing of material comprised the crushing and sieving to a maximum grain size of 2 mm. The processed material was then stored in airtight containers.

The wealth of information about the volume change, transfer, and sorption behavior of MX80-bentonite accounted for its selection to be mixed with COX_c. MX80-bentonite was supplied by Laviosa-MPC SAS (Limay, France) who already processed the material to a maximum grain size of 2 mm before filling it in airtight containers. Its mineralogical composition is dominated by phyllosilicates (e.g. smectites), whose fraction is about 85%. Other minerals are tectosilicates (e.g. quartz, feldspars) and carbonates (e.g. calcite) (Karnland et al., 2007).

Information about the physical and physico-chemical characteristics of COX_c and its mixture with MX80-bentonite are given in *Table 4.1*. Physical characteristics were taken from Middelhoff et al. (2020). The specific surface area (SSA) and the cation exchange capacity (CEC) were determined by means of the BET-method (Gregg and Sing, 1969) and cobalt hexamine method (Orsini and Remy, 1976), respectively. The latter was also employed in order to determine the exchangeable cation species. Values of SSA and CEC of COX_c were in good agreement with previous studies (Gaucher et al., 2004; Yven et al., 2007).

Table 4.1: Physical and physico-chemical characteristics of COX_c and its mixtures with MX80-bentonite

	Initial water content	Liquid limit	Plastic limit	Specific gravity	Cation exchange cap.	Specific surface area
	w_{ini}	LL	PL	G_s	CEC	SSA
	[%]	[%]	[%]	[-]	[meq/100g]	[m ² /g]
COX _c	5.4	37.3	24.9	2.68	22	37
Mixture	6.4	112.5	34.7	2.64	39	32

The dominant exchangeable cation species in COX_c were Ca²⁺, Mg²⁺, Na⁺, K⁺ and Sr²⁺, listed according to their amount encountered. Corresponding amounts were 53%, 21%, 13%, 12% and 1%, respectively. The replacement of COX_c by 30% MX80-bentonite led to a significant increase in the fraction of Na⁺-ions. The exchangeable cations were then dominated by Na⁺-

ions, followed by Ca^{2+} -, Mg^{2+} -, K^+ - and Sr^{2+} -ions with regard to their amount. Corresponding amounts were 43%, 36%, 15%, 6% and 1%, respectively.

The grain size distribution curves of COX_c and the mixture are shown in *Figure 4.1*. The size distribution of grains being smaller than 0.8 mm was measured by means of laser diffractometry, whereas dry sieving was conducted in order to obtain the size distribution of the residual grains. As depicted, the grain size distribution curves of both materials were comparable.

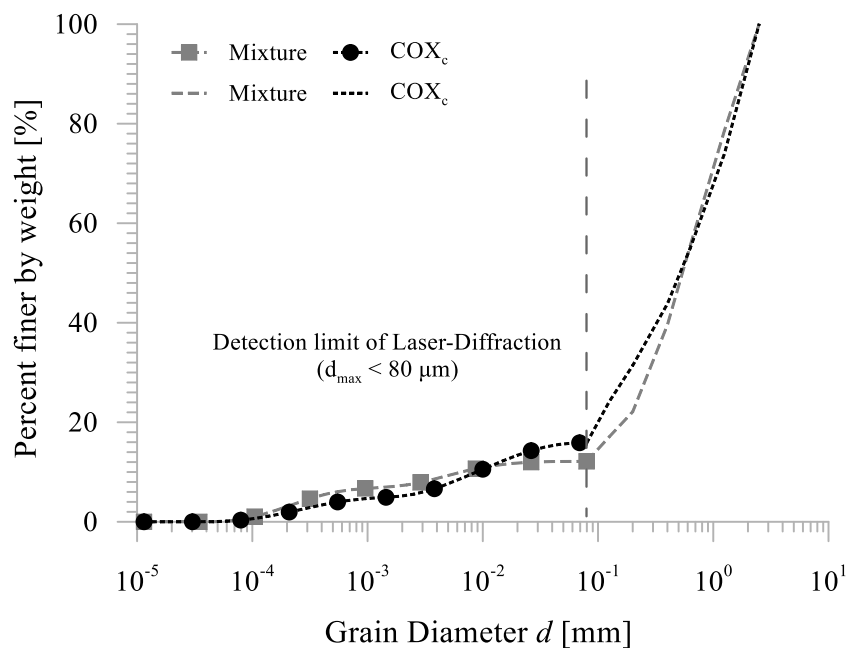


Figure 4.1: Grain size distribution of COX_c and the mixture obtained by dry sieving and laser diffractometry

The compaction behavior of both materials were investigated by means of standard and modified Proctor experiments. Materials were prepared at various water contents and filled in airtight containers afterwards. In order to reach target water contents, deaired/ demineralized water was added. Materials were left in the containers for more than one week, occasionally revolved to guarantee the homogeneous distribution of added water. A detailed description of the results of standard and modified Proctor experiments and their interpretation are given in Middelhoff et al. (2020). As being of interest in this study, modified Proctor experiments revealed that the maximum dry density and optimum water content were 1.95 Mg/m^3 and 13.2%, respectively, in the case of COX_c , and 1.72 Mg/m^3 and 18.2%, respectively, in the case of the mixture. In general, the replacement of COX_c by MX80-bentonite provoked a decrease of the maximum

dry density and a shift of the optimum water content to higher values, regardless of the applied compaction energy.

The laboratory experimental program comprised the saturation of both materials with three solutions differing in their composition and properties. Deaired/ demineralized water served as reference solution. Henceforth, water refers to deaired/ demineralized water, and the subscripts SS and AS indicated the artificial site solution and the artificial alkaline solution, respectively. The compositions of the site and alkaline solution corresponded to the rock formation pore water and as solutions believed to evolve from percolating through the concrete lining, respectively. The compositions of both solutions are given in *Table 4.2*.

Table 4.2: Composition of the site and the alkaline solution (Middelhoff et al., 2020)

Compound	Na ⁺	K ⁺	Ca ²⁺	Mg ²⁺	Cl ⁻	HCO ₃ ⁻	SO ₄ ²⁻	OH ⁻
	[mmol/l]	[mmol/l]	[mmol/l]	[mmol/l]	[mmol/l]	[mmol/l]	[mmol/l]	[mmol/l]
Site solution (SS)	44.8	0.5	5.3	8.5	35.3	1.5	1.8	-
Alkaline solution (AS)	22.1	8.0	19.0	-	30.1	-	-	38.1

The site and the alkaline solutions were comparable in terms of their ionic strength ($I_{SS} = 105$ mmol/l, $I_{AS} = 87$ mmol/l), however the alkaline solution was characterized by an elevated pH ($pH_{SS} = 7.8$, $pH_{AS} = 12.5$). The pH of AS corresponded to the solution chemistry controlled by the dissolution of portlandite.

4.3 Experiments

As already mentioned above, the laboratory experiment program aimed to determine the hydraulic conductivity of COX_c and its mixture with MX80-bentonite by means of constant head experiments, their microstructure by means of mercury intrusion porosimetry (MIP) experiments and their textural characteristics by means of N₂-adsorption experiments. The sample preparation, experiment protocols adopted, and the established program are described below.

4.3.1 Sample preparation

Materials were prepared according to the protocol established in section 4.2. Samples were then compacted to the maximum dry density at the optimum water content by means of the static

compaction method at a controlled deformation rate of 0.1 mm/s. In order to reduce the risk of preferential flow paths alongside the samples, the protocol envisaged the compaction of materials directly inside the mold. Grease is commonly employed to reduce friction at the mold wall during compaction. In this study, its employment was omitted to not impair the subsequent determination of the textural characteristics of materials. The initial height and diameter of all samples were 30 mm and 70 mm, respectively. Information about the initial characteristics of all COX_c and mixture-samples are given in *Table 4.3*.

Table 4.3: Initial characteristics of employed samples

Material	Initial dry density	Initial water content	Initial void ratio	Initial porosity	Initial degree of saturation	Initial suction
	$\rho_{d, ini}$	w_{ini}	e_{ini}	n_{ini}	S	s
	[Mg/m ³]	[%]	[-]	[-]	[%]	[MPa]
COX _c	1.95	13.2	0.37	0.27	0.96	1.5
Mixture	1.72	18.2	0.53	0.35	0.91	2.7

In the case of the mixture-samples, the microstructural and textural analyses were performed shortly after the termination of the hydraulic conductivity experiments. Before they were analyzed, samples were cut perpendicularly to their center axis into discs of same height. The center axis corresponded to the imposed flow direction. The purpose of this preparation step was to determine the possible spatial evolution of the microstructure and texture triggered by the saturation and the solution chemistry. Supplementary COX_c- and mixture-samples were prepared in the same way to evaluate the impact of the partial material replacement and to compare the structure of material before and after saturation.

4.3.2 Hydraulic conductivity

The employed constant-volume hydraulic conductivity cell was composed of its mold, two porous discs, its lid, and its bottom plate each including one joint. The mold containing the sample was sandwiched between the porous discs. This assembly was then placed between the lid and the bottom part, which were finally screwed together. The constant head method was considered to be most adequate to investigate the hydraulic conductivity of both samples (e.g. Dixon et al., 1999; Mata and Ledesma, 2003; Villar, 2006). By means of a constant volume-/ pressure control unit, samples were saturated from the bottom upwards. Solutions that left the cell at its top

and were finally collected in a graduated flask. In order to avoid interaction processes with the atmosphere, the flask was plugged, allowing only solutions to enter. Imposed injection pressures increased stepwise from 15 kPa to 90 kPa in the first weeks of the experiments. Considering a sample height of 70 mm, corresponding hydraulic gradients varied from 50 to 300. Indeed, gradients of 300 do not reflect the conditions encountered in situ and their imposition might involve an overestimation of the in situ hydraulic conductivity (e.g. Dixon et al., 1999; Dixon, 2000). However, there was a need to accelerate the experiments. Experiments were terminated when the volume of solution being equal to two times of the initial pore volume of the samples was injected at least.

4.3.3 Microstructural analysis

Mercury intrusion porosimetry (MIP) experiments were conducted by means of an AutoPore IV 9500 apparatus (Micromeritics, U.S.A.). Prior to the microstructural analysis, samples were dried by heating them up to 80°C under vacuum conditions. The MIP-method bases on the principle of forcing a non-wetting fluid, like mercury, to enter a porous medium by incrementally increasing injection pressures. Detailed information about its principle and procedure are given in Cuisinier and Laloui (2004) and Delage et al. (2006), for instance. Considering cylindrically shaped pores, the diameter of the pores penetrated by mercury can be related to the injection pressure by adopting the capillary pressure equation:

$$d = \frac{4 \gamma \cos \alpha}{p} \quad (4.1)$$

Where d is the entrance pore diameter of the cylindrical pore, γ is the surface tension of mercury, α is the contact angle of fluid interface to solid, and p is the imposed injection pressure. The result of MIP-experiments is the cumulative volume of mercury intruded as a function of the equivalent pore diameter. The pore size distribution (PSD) curve is commonly deduced from those results in order to facilitate their interpretation (Juang and Holtz, 1986). It is defined as the derivative of the total volume of mercury intruded with respect to the common logarithm of the equivalent pore diameter:

$$f(\log(d_i)) = \frac{\Delta V_i}{\Delta(\log(d_i))} \quad (4.2)$$

Where V_i is the volume of mercury intruded at the corresponding diameter. In this study, the approach of PSD-curve determination followed that presented by Juang and Holtz (1986) and used a constant value of $\Delta(\log(d_i))$ being equal to 0.25. The determination of the pore size distribution by means of MIP is limited, in particular regarding to the intrusion of pores, whose diameter are smaller than 7 nm. This diameter usually represents the lower limit of the device. Results might also be impaired through the occurrence of the bottleneck phenomenon or pore entrapment, for instance (e.g. Romero et al., 1999; Delage et al., 2006; Romero, 2013).

4.3.4 Textural analysis

Nitrogen gas (N_2) adsorption-desorption cycles were determined by means of an ASAP 2050 volumetric adsorption analyzer (Micromeritics, U.S.A.) at 77K. Block samples outgassed initially under a residual pressure of 1.6×10^{-6} Pa at 80°C. The outgassing lasted 24 h. The nitrogen gas adsorption method adopts the physical adsorption of non-reactive gas molecules, like nitrogen, on solid external surfaces. Information about its principle and procedure are given in Gregg and Sing (1969), for instance. BET theory and a generalized t-plot method were adopted to describe the texture of solids (Lippens and Boer, 1965; Gregg and Sing, 1969).

4.3.5 Experimental program

The program comprised four samples of COX_c and four samples of the mixture, respectively indicated by the prefix C and M in their sample identification. The suffix I, W, SS and AS referred to samples analyzed in their initial state, and to samples analyzed during/ after the saturation with water, site solution and alkaline solution, respectively. The detailed experiment program is given in *Table 4.4*.

In terms of structural alterations, M-SS and M-AS were expected to react most considerably to the saturation with different solutions due to their elevated smectite fraction and particular solution chemistry. Therefore, they were selected for the subsequent microstructural and textural analysis. This approach provided the basis to evaluate the impact of the saturation process and saturating solution chemistry on the material properties.

Table 4.4: Experimental program including hydraulic conductivity experiments, microstructural and textural analysis

Sample ID.	C-I	C-W	C-SS	C-AS	M-I	M-W	M-SS	M-AS
Material	COX _c	COX _c	COX _c	COX _c	Mixture	Mixture	Mixture	Mixture
Solution		Water	SS	AS		Water	SS	AS
Constant head experiment		✓	✓	✓		✓	✓	✓
Mercury Intrusion Porosimetry (MIP)	✓				✓		✓	✓
N ₂ -adsorption	✓				✓		✓	✓

✓: Experiment performed

4.4 Results

In this section, the results obtained in the hydraulic conductivity experiments are presented first, followed by the results of subsequent microstructural and textural analysis. The presentation reflects the approach of data acquisition.

4.4.1 Hydraulic conductivity experiments

Values of hydraulic conductivity were determined upon the establishment of steady state conditions that were indicated by stabilized rates of inflow and outflow of solutions. Both materials were saturated with water, the site and alkaline solution. The hydraulic conductivity of COX_c and its mixture is plotted against the normalized volume of outflow in *Figure 4.2*. The normalized volume of outflow is the ratio of volume of measured outflow to the initial pore volume and serves the purpose of emphasizing the amount of pore solution exchanged. Data obtained were subsequently processed by means of a moving average method.

Focusing on COX_c, inflow rates increased upon the hydraulic gradient was raised stepwise and stabilized. The volume of injected solution ranged from the threefold to the fivefold of the initial pore volume. The greatest volume of solution was injected into C-AS. In all three experiments, the onset of outflow was determined upon the volume of solution corresponding to one initial pore volume was injected into the samples. Shortly after the onset of outflow was detected,

steady state conditions established at an average flow rate ranging from 2 ml/days to 2.5 ml/day. The former rate refers to C-W. As depicted in *Figure 4.2a*, pore solution was exchanged at least twice within a period of about 60 days. The smallest number of exchanges was exhibited by C-W, which corresponded to the smaller average flow rates. In the course of the experiments, values of hydraulic conductivity calculated decreased initially and stabilized at values between 6×10^{-11} m/s to 9×10^{-11} m/s. Samples C-SS and C-AS exhibited slightly higher hydraulic conductivities than C-W.

The inflow rates exhibited by all mixture-samples stabilized upon imposing the maximum hydraulic gradient. In the course of the experiments, total volumes of solution injected varied from the twofold to the threefold of the initial pore volume and were thus less than that injected into COX_c-samples, despite that the experiments lasted five to six times longer (300 days – 360 days). In the case of M-W and M-SS, outflow was detected after injecting the volume of solution corresponding to one initial pore volume. Interestingly, in the case of M-AS, the volume of solution corresponding to two initial pore volumes were injected prior to the onset of outflow. Indeed, steady state conditions were established shortly after detecting an outflow. However, the inflow and outflow rates decreased steadily in the course of the experiments, starting from 0.4 ml/day at the beginning to 0.2 ml/days in the end. The trend is also identifiable in *Figure 4.2b*. Values of hydraulic conductivity accordingly decreased from 2×10^{-11} m/s to 3×10^{-12} m/s and showed only slight trends to stabilize, in particular M-SS. Comparing the values of hydraulic conductivity at the same normalized outflow of 0.6, M-AS exhibited the smallest values.

The hydraulic conductivity of COX_c was by one order of magnitude higher than that of the mixture. The difference became even more considerable as the values of COX_c stabilized, whereas the values of the mixture progressively decreased in the course of the experiment. Apart from that, the saturation of samples with the site and alkaline solution had no considerable impact on the hydraulic conductivity of both materials. The characterization of the microstructure and texture was of special interest at this stage, in order to evaluate whether the evolution at macroscale was reflected in the material properties at the nano- and microscale.

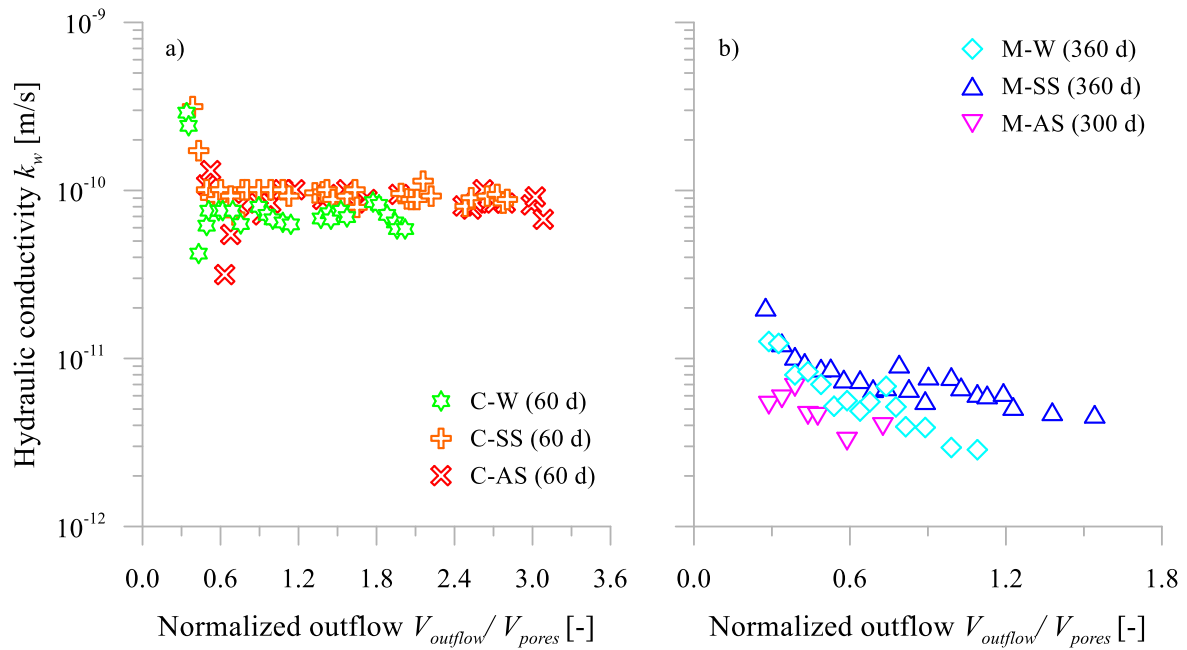


Figure 4.2: Evolution of the hydraulic conductivity of a) COX_c ($\rho_{d, ini} = 1.95 \text{ Mg/m}^3$) and b) the mixture ($\rho_{d, ini} = 1.72 \text{ Mg/m}^3$) as a function of the normalized outflow (saturated with water (-W), site solution (-SS) and alkaline solution(-AS))

4.4.2 Microstructural analysis

Samples were prepared by cutting them perpendicularly to their center axis into two discs of same height in the case of MIP experiments. Henceforth, top part (T) and bottom part (B) referred to the superior and inferior part of the initial sample, respectively. Results of MIP experiments performed on C-I and M-I are depicted in *Figure 4.3*. Pores appeared to be spatially inhomogeneously distributed in the sample since the pore size distribution and cumulative volume curves of the top part were shifted upwards, compared to those of the bottom part. Their shapes were still similar.

A distinct double-peak was revealed by the pore size distribution curves not only in *Figure 4.3a* and *Figure 4.3c*, but also in *Figure 4.4a* and *Figure 4.4c*. It indicated the existence of micro- and macropores. In order to quantify them, PSD curves were split at the pore diameter of their inflection point. Pores with a diameter smaller and greater than that were referred to micro- and macropores, respectively. Their quantities are generally expressed as micro-void ratio (e_m) and macro-void ratio (e_M), respectively (e.g. Romero et al., 1999). The difference between the micro-void ratio and total void ratio (e_{tot}) corresponds to pores whose diameter are too small or

too large to be intruded by mercury. They were henceforth referred to as unaccounted void ratio (e_{un}). The approach was exemplified by M-I (T) and M-I (B) in *Figure 4.3*.

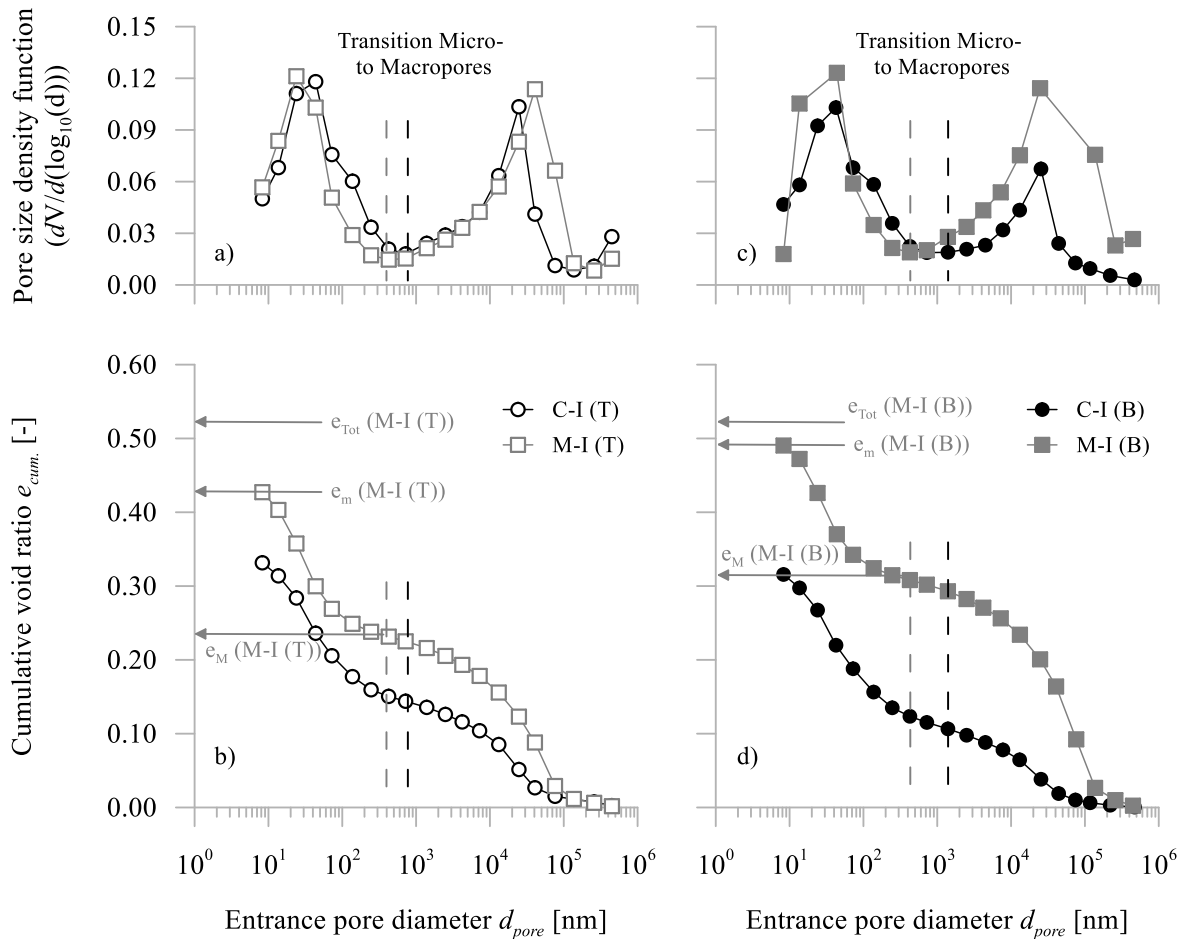


Figure 4.3: Results of mercury intrusion porosimetry (MIP) experiments conducted on the top (T) and bottom (B) parts of C-I and M-I

Microstructural characteristics of samples analyzed by means of MIP-experiments are compiled in *Table 4.5*. Complementing *Figure 4.3* and *Figure 4.4*, it facilitates to evaluate how the replacement of COX_c by MX80-bentonite, saturation and solution chemistry affected the microstructure.

As depicted in *Figure 4.3a* and *Figure 4.3c*, the peaks of micro- and macropores of C-I (T) and C-I (B) occurred at the same pore diameter of about 4×10^1 nm and 2.5×10^4 nm, respectively. The comparison of micro- and macro-void ratios of C-I (T) to those of C-I (B) revealed that ratios increased by about 4% and 21%, respectively, corresponding to the already described

shift of the cumulative volume curve of C-I (T) upwards *Figure 4.3b* and *Figure 4.3d*. M-I (T) was characterized by micro- and macropores at pore diameters of about 3×10^1 nm and 5×10^4 nm, respectively. Like in the case of C-I (B), micro- and macropores occurred at pore diameter of about 4×10^1 nm and 2.5×10^4 nm, respectively, in the case of M-I (B). Compared to those of M-I (T), the micro- and macro-void ratios increased by about 13% and 26%, respectively (*Figure 4.3b*, *Figure 4.3d*).

Table 4.5: Microstructural characteristics of C-I, M-I, M-SS and M-AS obtained by means of MIP-experiments

Sample ID.	Dry density	Total void ratio	Macro-void ratio [^]	Micro-void ratio [^]	Unaccountable void ratio ^{^*}
	ρ_d	$e_{Tot.}$	e_M	e_m	$e_{un.}$
	[-]	[-]	[-]	[-]	[-]
C-I	1.92	0.393	0.146 (0.115)	0.333 (0.319)	0.060 (0.074)
M-I	1.72	0.531	0.229 (0.310)	0.429 (0.494)	0.102 (0.037)
M-SS	1.72	0.531	0.190 (0.188)	0.404 (0.406)	0.127 (0.125)
M-AS	1.72	0.531	0.175 (0.175)	0.383 (0.388)	0.148 (0.143)

[^]: values in parenthesis indicate the bottom part

^{*}: is defined as the difference in $e_{Tot.}$ and e_m

As highlighted in *Table 4.5*, the top part of all mixture samples was characterized by an initial macro-void ratio being lower than that of the bottom part. A particularly considerable spatial difference was determined in the case of M-I. It was about 6%. Conversely, the differences of the other samples ranged only from 0.5% to 2%.

Top parts of M-SS and M-AS were characterized by micropores occurring at a diameter of 2.5×10^1 nm. Micro-void ratios of M-SS (T) and M-AS (T) reduced by about 11% and 6%, respectively, compared to M-I (T). Macropores were determined at a diameter of 4×10^4 nm in the cases of M-I (T) and M-AS (T), and at a diameter of 2×10^4 nm in the case of M-SS (T). The comparison of the macro-void ratio of M-I (T) to those of M-SS (T) and M-AS (T) revealed reductions of about 17% and 23%, respectively. As depicted in *Figure 4.4c* and *Figure 4.4d*, the micropore diameter of M-AS (B) was shifted to a lower value, compared to those of M-I (B) and M-SS (B). The former sample was characterized by a micropore diameter of 2×10^1 nm, whereas the micropores of the latter occurred at 4×10^1 nm. Focusing on the cumulative void ratio curves (*Figure 4.4d*), micro-void ratios of both M-SS (B) and M-AS (B) were reduced by about 20% when they are compared to the reference case. Bottom parts of mixture samples

were characterized by macropores occurring at a diameter of 2×10^4 nm. Interestingly, an additional macropore population was determined at diameters of 8×10^4 nm in the case of M-SS (B). Macro-void ratios of M-SS (B) and M-AS (B) reduced by about 39% and 44%, respectively, compared to M-I (B).

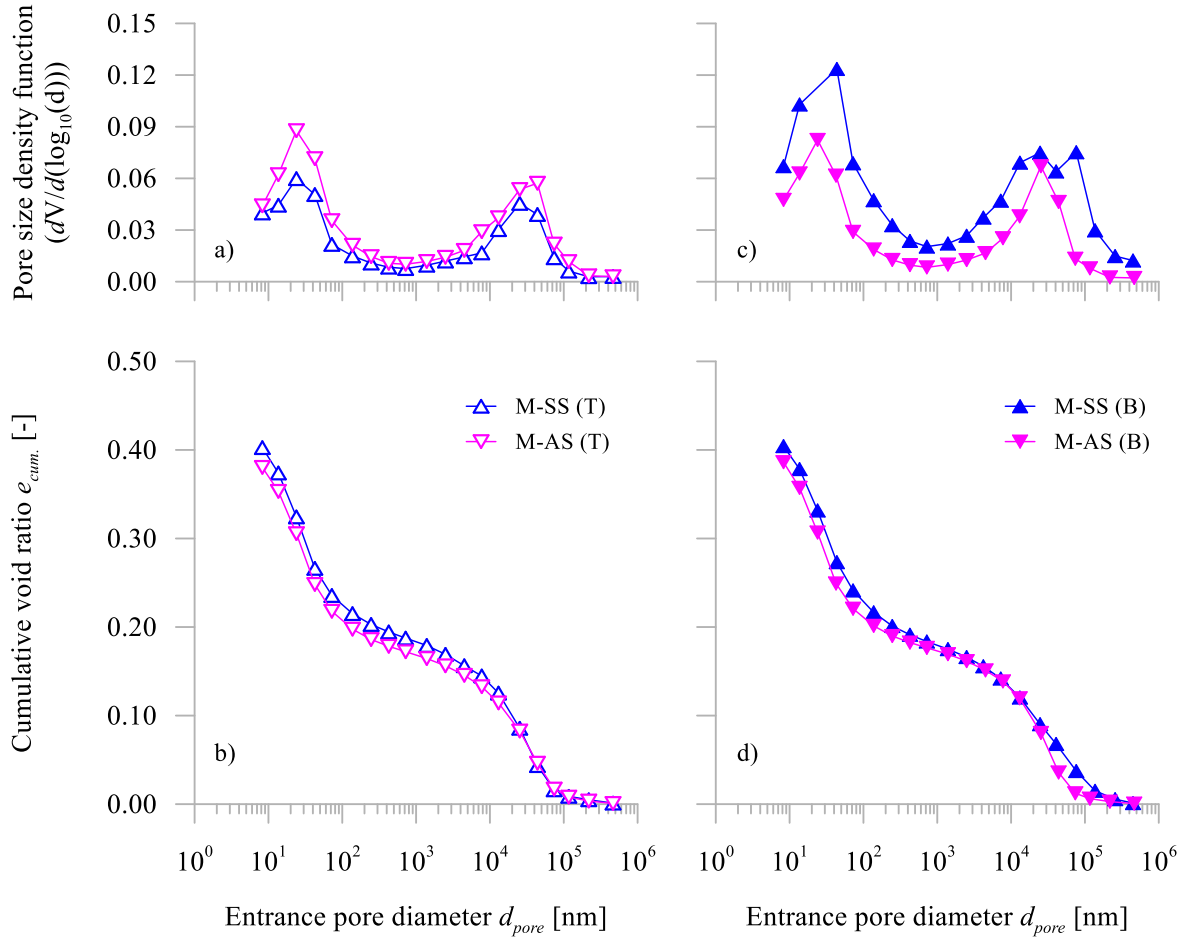


Figure 4.4: Results of mercury intrusion porosimetry (MIP) experiments performed on the top (T) and bottom (B) parts of M-SS and M-AS

An increase in the amount of micropores generally ensued as COX_c was partially replaced by MX80-bentonite. Spatial heterogeneities were small. Unlike the solution chemistry, the saturation had a significant impact on the microstructure of samples since the amount of micro- and macropores reduced, and the amount of unaccounted pores increased homogeneously.

4.4.3 Textural analysis

In the case of textural analysis, sample preparation involved to cut samples perpendicularly to their center axis into three discs of same height in order to identify possible spatial variations in the specific surface area (SSA) along the flow direction. According to IUPAC classification (Thommes et al., 2015), pores, whose diameter either exceeds 5×10^1 nm, or ranges between 2×10^0 nm and 5×10^1 nm, or does not exceed 2×10^0 nm, were referred to as macropores, mesopores and micropores, respectively in the case of N_2 -adsorption.

Isotherms displayed a Type II behavior and a H3 hysteresis loop. The reversible Type II isotherm is the normal form of isotherm obtained with a macroporous adsorbent. The Type II represents unrestricted multilayer adsorption build up and the occurrence of mesopores. The Type H3 loop not exhibiting any limited adsorption at high P/P_0 -ratios was coherent with aggregates of plate-like particles. It gave rise to slit-shaped pores and proved that the samples were mesoporous. Isotherms gave linear BET plots from 0.03 to 0.3 P/P_0 for all tested samples. SSA-values obtained by means of BET- and t-plot-method are compiled in *Table 4.6*.

Table 4.6: SSA-values of different samples obtained by means of BET and t-plot

Sample	Height h [mm]	BET			t-plot	
		V_m^a [cm ³ /g]	C^b [-]	S_{Tot}^c [m ² /g]	$V_{\mu pores}^d$ [cm ³ /g]	S_{Tot}^c [m ² /g]
C-I	3	8.39	274	37	0.0029	37
	15	8.39	274	37	0.0029	37
	27	8.39	274	37	0.0029	37
M-I	3	7.43	431	32	0.0043	31
	15	7.43	431	32	0.0043	31
	27	7.43	431	32	0.0043	31
M-SS	3	7.44	331	33	0.0032	32
	15	7.37	875	32	0.0032	32
	27	7.00	964	31	0.0052	29
M-AS	3	7.36	435	32	0.0039	31
	15	7.23	697	32	0.0039	31
	27	7.00	762	31	0.0046	29

^a: Associated monolayer volume; ^b: BET energy constant; ^c: Total specific surface area; ^d: Equivalent specific volume of micropores

Calculated BET specific surface areas (S_{BET}) and associated monolayer capacity (V_m) exhibited neither variations in SSA among mixture-samples, nor an evolution of SSA over the length of the individual samples. t-plot results were coherent with the S_{BET} - values.

4.5 Discussion

Since the study aimed to understand the hydraulic conductivity evolution of COX_c and its mixture with MX80-bentonite under realistic conditions by relating the results of hydraulic conductivity experiments to the microstructure and texture of materials possibly affected by the solution chemistry, it was suitable for the discussion to evaluate the results obtained at the microscale first, and then the results obtained at the macroscale.

4.5.1 Textural analysis

The specific surface area (SSA) of materials was determined by means of the BET-method, so the determined value refers to specific external surface of particles. In the case of smectites, it generally comprises the basal planes of particles, as well as the micro- and mesopores, which are formed by the irregular stacking of particles and of aggregates, respectively. Micropores are predominantly located at the particle edges due to the irregular stacking of layers. SSA-values thus depend on the microporosity, the nature of exchangeable cations in the interlayer pores, and the pretreatment of samples (e.g. Bérend et al., 1995; Cases et al., 1997).

Changes in the SSA presumably ensue as saturation triggers crystalline swelling involving the increase in the basal spacing and micropores. Particle rearrangements might be then reflected by an altered mesoporosity. Indeed, the assumption appears to be coherent. However, as mentioned above, trends are highly contradictory. Contradictions are attributable to the sample pretreatment and experimental conditions (e.g. Cuevas, 2005; Fernández et al., 2014).

Results contradicted the assumption that crystalline swelling triggers the increase in the SSA-values since the saturation with solutions of different chemistry had no impact on the SSA-values and their spatial distributions within M-SS and M-AS (*Table 4.6*). The confined conditions might limit detectable changes in the mesoporosity. Conversely, they might be beneficial for the homogenous occupation of the interlayer space of particles by water molecules upon saturation, and promote crystalline swelling (Devineau et al., 2006).

SSA-values generally indicated a lack of material swelling upon saturation and a stability of materials to the saturation chemistry in the course of experiments. However, the lack of swelling appeared to be less probable since the results of Middelhoff et al. (2020) emphasized the reactivity of those materials upon saturation (*Figure 4.6*). This finding also highlighted the inconsistency of trends previously mentioned. Apart from that, the apparent stability of materials might be attributable to the low chemical reaction kinetics under imposed conditions.

4.5.2 Microstructural analysis

The existence of micro- and macropores in COX_c and its mixture with MX80-bentonite was indicated by bi-modal PSD-curves which were obtained by means of MIP-experiments. This finding was consistent with the literature as smectite-containing materials are usually characterized by such a double-structure if they are compacted at the dry side of optimum water content (e.g. Alonso et al., 1987). As it is depicted in *Figure 4.3* and *Figure 4.4* as well, the top part of samples was compacted to a slightly higher initial dry density than their bottom part due to the static compaction method. The spatial difference ensued upon a shear strength evolved at the interface between the material and the mold (e.g. Villar, 2006).

Comparing C-I to M-I in *Table 4.5*, the increase in initial dry density apparently lowered the total pore volume, in particular the macropore volume. This finding was consistent with the literature (e.g. Lloret and Villar, 2007). In order to quantitatively evaluate the impact of the partial replacement of COX_c by MX80-bentonite, cumulative void ratio curves were normalized to the initial total void ratios of the individual samples. By this means, the impact of the different initial dry densities on the microstructure was neglected. Normalized macro-, micro-, and unaccounted void ratios are compiled in *Table 4.7*. For comparison purpose, total void ratios are given as well.

Table 4.7: Macro-, micro-, and unaccounted void ratios normalized to the total void ratio

	Total void ratio [^]	Norm. macro-void ratio [^]	Norm. micro-void ratio [^]	Norm. unaccounted void ratio ^{^*}
	e_{Tot}	e_M / e_{Tot}	e_m / e_{Tot}	e_{um} / e_{Tot}
	[-]	[-]	[-]	[-]
C-I	0.393	0.36 (0.29)	0.84 (0.80)	0.16 (0.20)
M-I	0.531	0.41 (0.55)	0.76 (0.87)	0.24 (0.13)
M-SS	0.531	0.33 (0.33)	0.71 (0.72)	0.29 (0.29)
M-AS	0.531	0.31 (0.31)	0.69 (0.70)	0.31 (0.30)

[^]: values in parenthesis indicate the bottom part

^{*}: is defined as the difference in e_{Tot} and e_m

The comparison of C-I to M-I showed that C-I incorporated significantly less macropores and unaccounted pores, and equivalent micropores, as depicted in *Figure 4.5*. Since the micropores are less sensitive to material densification, they indicate the impact of the partial replacement on the microstructure most representatively. Interestingly, the replacement of COX_c by MX80-bentonite hardly affected the average micropore volume.

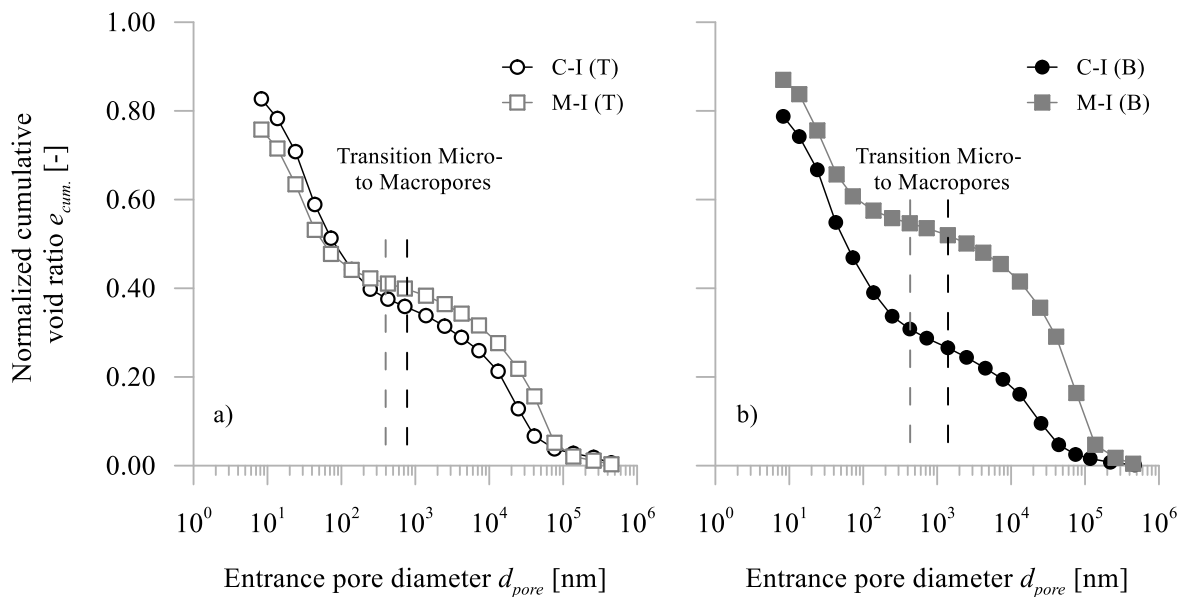


Figure 4.5: Normalized cumulative void ratio curves of the top (T) and bottom (B) parts of C-I ($\rho_{d, ini} = 1.95 \text{ Mg/m}^3$) and M-I ($\rho_{d, ini} = 1.72 \text{ Mg/m}^3$)

The saturation of samples led to a decrease in micro- and macro-void ratios and to an increase in the unaccounted void ratio, regardless of the solution chemistry. The relative extent was

slightly greater in the case of M-AS. It is noteworthy that the small differences along the vertical axis likely indicated a homogeneous saturation of samples. The decrease in the micro- and macropores ensued as materials swelled upon saturation. Indeed, this interpretation contradicted the textural analysis, whose results indicated to a lack of swelling. However, as outlined above, a lack of swelling appeared to be less probable under considered conditions. Further, the approach of pore closure through material swelling upon saturation is usually adopted to interpret structural rearrangements in smectite-containing materials (e.g. Komine, 2004, 2010).

The microstructure of M-SS and M-AS was apparently more affected by the actual saturation rather than by the solution chemistry. Still, as outlined in the introduction, the impact of the solution chemistry must be considered to be highly time-dependent due to the low reaction kinetics under realistic conditions. Considerable microstructural changes likely ensue as, in particular, the alkaline solution percolates the materials over time. The saturation of materials with the alkaline solution provokes the dissolution of clay minerals and, in turn, the increase in macropores (Karnland et al., 2007; Cuisinier et al., 2008; Cuisinier et al., 2014).

The microstructural analysis revealed that the densification of materials led to a decrease in the macropore volume. Interestingly, when focusing on the micropores, which are less sensitive to material densification, their volume was hardly affected by the partial replacement of COX_c by MX80-bentonite. The microstructural analysis also indicated to a significant rearrangement of the pore structure likely triggered by material swelling upon saturation. The interpretation appeared to be consistent with the trends presented in the literature. As outlined above, the low reaction kinetics might involve that geochemical reactions, in particular dissolution and precipitation processes, did not come into effect yet, so the impact of the solution chemistry remained negligible in the course of the experiments.

4.5.3 Hydraulic conductivity experiments

Information about COX_c and its mixtures with MX80-bentonite, in particular their saturated hydraulic conductivity behavior, are scarcely available. Therefore, the recent study of Zhang and Kröhn (2019) was of major interest since it determined the saturated hydraulic conductivity of compacted COX_c and different COX_c/MX80-bentonite-mixtures, among other hydro-mechanical parameters. Prior testing, they compacted all samples to target dry densities of

about 2.0 Mg/m^3 at initial water contents of about 4%. In the case of COX_c , values of hydraulic conductivity were about $5 \times 10^{-13} \text{ m/s}$. Values were assumed to reflect a long-term stable state. Tang et al. (2010) focused on the saturated hydraulic conductivity of COX_c , whose initial water contents ranged between 2% to 8%. Target dry densities were about 2.0 Mg/m^3 . Values of hydraulic conductivity were about $4 \times 10^{-12} \text{ m/s}$. Their results also indicated to a negligible impact of the initial water content on the hydraulic conductivity. In general, probably due to the different initial dry density, the values of hydraulic conductivity recently obtained were higher by one and two orders of magnitude than those described by Tang et al. (2010) and Zhang and Kröhn (2019), respectively.

Saturated hydraulic conductivities of a mixture composed of 80% COX_c and 20% MX80-bentonite ranged from $1 \times 10^{-12} \text{ m/s}$ to $2 \times 10^{-12} \text{ m/s}$ indicating to a good agreement with the values recently obtained (Zhang and Kröhn, 2019). Comparing the performance of all COX_c /MX80-bentonite-mixtures assessed by Zhang and Kröhn (2019), there was no evidence that the hydraulic conductivity decreased as the smectite fraction in the mixture increased. This finding appeared to be inconsistent with the trends usually described in the literature (e.g. Karnland et al., 2008). The results were still remarkable since the hydraulic conductivity of COX_c /MX80-bentonite-mixtures, whose initial compaction conditions (e.g. compaction energy, initial water content) varied significantly, only differed slightly. It highlighted the efficiency of the closure of hydraulic conductive macropores ensuing as the smectite fraction swells upon its saturation. Further, it accounted for the difference in the performance of COX_c and its mixture with MX80-bentonite. As the values of hydraulic conductivity progressively decreased, it might be assumed that the material was still swelling after more than one year, thus the hydraulic conductivity obtained might reflect a short- or intermediate-term state. The swelling pressure evolution in COX_c and mixture-samples under comparable initial and boundary conditions is depicted in *Figure 4.6*. Interestingly, the swelling pressure experiments indicated that the mixture samples likely reach a constant swelling pressure after a period of seven days of saturation. The reasons for the divergence in swelling pressure kinetics cannot be reasonably, yet.

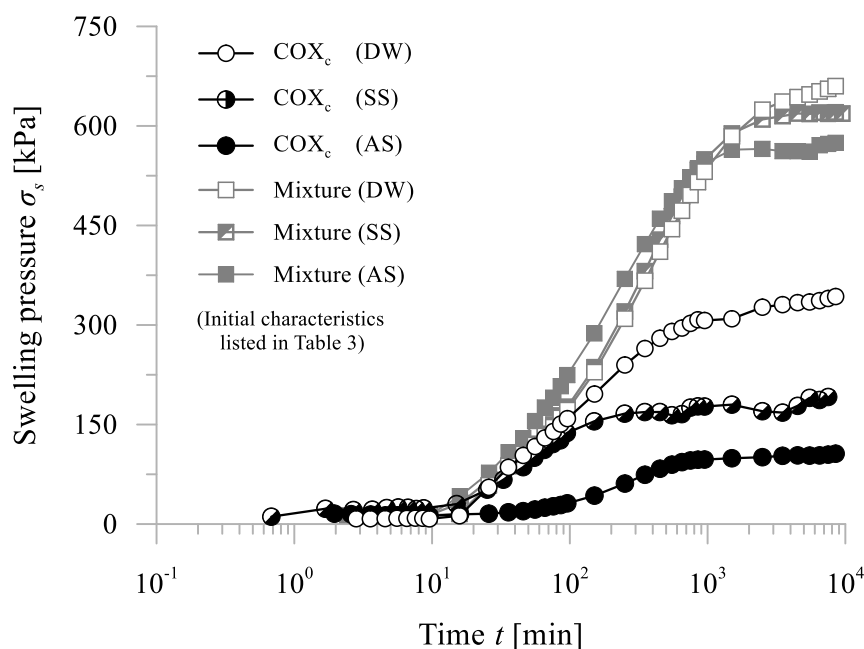


Figure 4.6: Swelling pressure evolution in COXc and mixture-samples under constant-volume conditions taken from Middelhoff et al. (2020) (Initial characteristics of solutions and materials employed coincided the values given in Table 4.2 and Table 4.3, respectively)

The different solution chemistry neither involved variations in the hydraulic conductivity behavior, nor affected it the microstructure or texture of materials. There was no detectable impact of the solution chemistry on the pore closure through material swelling and, in turn, on the hydraulic conductivity behavior. It might be attributed to the low ionic strength of solutions ($I_{SS} = 105 \text{ mmol/l}$, $I_{AS} = 87 \text{ mmol/l}$) and the low volume of exchanged pore solution (e.g. Karnland et al., 2007). According to the theories of diffuse double layers (DDL), the solution chemistry has an impact on the hydraulic conductivity behavior of smectite-based materials, when diffuse double layers evolve in macropores and immobilize water molecules therein. The ion concentration in solution is inversely proportionally related to their layer thickness. An increase in hydraulic conductivity ensues as the ion concentration increases and, in turn, diffuse double layers diminish (e.g. Villar, 2006; Castellanos et al., 2008). Apart from the low reaction kinetics under imposed conditions, the low volume of pore solution exchanged, in particular in the case of M-AS, might account for the apparent stability of materials to the solution chemistry. As shown in Figure 4.2b, the pore solution was exchanged less than once. Geochemical reactions, in particular dissolution and precipitation processes, appeared to not come into effect yet, despite the experiment duration of more than 300 days. The adoption of a different termination

criteria is thus recommended that additionally considers the composition, ionic strength, and electric conductivity of the influent and effluent in order to predict the initiation of geochemical reactions in the course of the experiment more precisely.

In general, values of hydraulic conductivity of the mixture determined were in good agreement with those presented in the literature, despite significantly different initial compaction conditions. This finding highlighted that the microstructural rearrangement through material swelling and the consequent closure of hydraulic conductive macropores was efficient. Further, the process likely accounted for different performance of COX_c and the mixture. In the case of the mixture, progressively decreasing values of hydraulic conductivity might indicate that material was still swelling, so the determined values possibly reflected a short- or intermediate-term state. The low reaction kinetics as well as the low volume of pore solution exchanged were assumed to be the major causes for the apparently negligible impact of the solution chemistry.

4.6 Conclusions

Crushed Callovo-Oxfordian claystone (COX_c) and a mixture composed of 70% COX_c and 30% MX80-bentonite in weight might be employed to backfill drifts and shafts of a future nuclear waste repository located in deep sedimentary rock formations. In addition to the swelling pressure, the hydraulic conductivity is one of the key parameters determining the performance of the backfill. This study aimed to understand the evolution of the hydraulic conductivity by means of laboratory experiments, whose boundary conditions were believed to portray the real conditions in terms of compaction conditions, solution chemistry and temperature. Subsequently conducted microstructural and textural analysis allowed to relate the evolution of the hydraulic conductivity at the macroscale to changes at the microscale possibly affected by the solution chemistry, in particular the pH-value. Following major conclusions can be drawn for COX_c and its mixture with MX80-bentonite:

1. The textural analysis might indicate a lack of material swelling. It was previously assumed that an increase in the specific surface area (SSA) of materials ensues as materials saturate. The saturation involves the increase in the interlayer space of smectite particles which consequently causes material swelling. However, no changes in SSA were ob-

- served, so there apparently was no swelling. The observation cannot be reasonably explained yet. The interpretation approach might be improved by conducting further analysis, such as scanning electron microscopy (SEM) and auto-radiography.
2. The microstructural analysis showed considerable microstructural rearrangements, which were related to closure of macropores triggered by material swelling upon saturation. The interpretation was consistent with the observations and the literature. The negligible impact of the solution chemistry was attributed to the low volume of exchanged pore solution under imposed conditions.
 3. In the case of COX_c and the mixture, values of hydraulic conductivity were in good agreement with the literature. COX_c exhibited stabilized values of hydraulic conductivity soon upon establishing steady state conditions. Conversely, values of hydraulic conductivity of the mixture progressively decreased in the course of the experiment. Considering the results of microstructural analysis, the closure of hydraulic conductive macropores through material swelling upon saturation likely accounted for the evolution of the hydraulic conductivity on the one side and for the difference in the performance of COX_c and the mixture on the other side. The duration of some experiments was longer than one year and highlighted the low kinetics of geochemical reactions under imposed conditions. Hence, the hydraulic conductivity appeared to be little affected by the solution chemistry within one year of experiment duration. In order to study the time-dependent impact of solution chemistry more precisely, it is of interest to conduct experiments which involve the exchange of several volumes of pore solution.

This study revealed that the replacement of COX_c by 30% MX80-bentonite in weight enhanced considerably the performance of compacted backfill materials under realistic conditions in terms of their short- and intermediate-term hydraulic conductivity. The enhancement can be attributed to the more effective clogging of hydraulic conductive voids. However, important questions arose while evaluating the experiments. For instance, it is still unclear how the hydraulic conductivity evolves under imposed conditions in long-term, particularly with regard to the time-dependent impact of the solution chemistry that must not be considered as negligible.

5 Hydro-mechanical path dependency of claystone/ bentonite mixture samples characterized by different initial dry densities

Based on the submitted manuscript of the following article:

Middelhoff M, Cuisinier O, Masrouri F and Talandier J (2020) Hydro-mechanical path dependency of claystone/ bentonite mixture samples characterized by different initial dry densities. *Acta Geotechnica*, (under review)

Abstract

In the context of the French Cigéo-project, a mixture composed of 70% processed Callovo-Oxfordian claystone spoil and 30% MX80-bentonite could be a potential backfill material, whose installation aims to stabilize the surrounding rock formation and to limit the propagation of the excavation damaged zone. The backfill material must sustain the overburden pressure, despite it might be exposed to different hydraulic and mechanical paths. The reference concept considers employing conventional compaction techniques, although their employment involves spatial variations in the dry density after compaction. In general, as the initial dry density has a significant impact on the hydro-mechanical behavior of backfill materials, it is of major importance to relate the variations in the initial dry density to differences in the behavior. This experimental laboratory study aimed to analyze how variations in the initial dry density affects the swelling and compression behavior of the claystone/ bentonite-mixture, in particular in un-

saturated state. Further, it evaluated whether those variations affected possible hydro-mechanical path dependences. The experimental program comprised suction-controlled oedometer and constant-volume swelling pressure experiments, in which samples characterized by different initial dry densities were exposed to different hydro-mechanical paths. The analysis of microstructural and water retention characteristics complemented the program. Major results indicated that the magnitude of swelling pressure at a given suction depends considerably on the initial dry density, but it is independent of the imposed hydro-mechanical path. Interestingly, the dependency of the yield behavior on the hydro-mechanical path appears to be more pronounced as the initial dry density increases.

5.1 Introduction

In the context of the French Cigéo-project, different materials are studied as to whether they could be employed to backfill drifts and shafts of the future repository for radioactive waste located at a depth of approximately 500 m in the clay-rich Callovo-Oxfordian sedimentary rock formation, henceforth referred to as Callovo-Oxfordian (COX) claystone formation (ANDRA, 2005). The installation of backfill aims to stabilize the surrounding rock formation and to limit the propagation of the excavation damaged zone (EDZ) that arises from the excavation of drifts and shafts and lowers the integrity of the repository system. The backfill must thus exhibit such a swelling pressure and compressibility that it sustains the overburden pressure upon terminating the closure phase. As depicted in *Figure 5.1*, the backfill might undergo different combinations of hydraulic and mechanical paths. The path A – C (– D) describes a possible case of (stepwise) backfill material saturation under constant-volume conditions. It might be followed by loading through the overburden pressure, whose onset occurs once convergence processes cause the partial degradation of the concrete lining. Under laboratory conditions, the path A – C corresponds to the path imposed in constant-volume swelling pressure experiments, whereas path A – B – C – D is imposed in oedometer experiments.

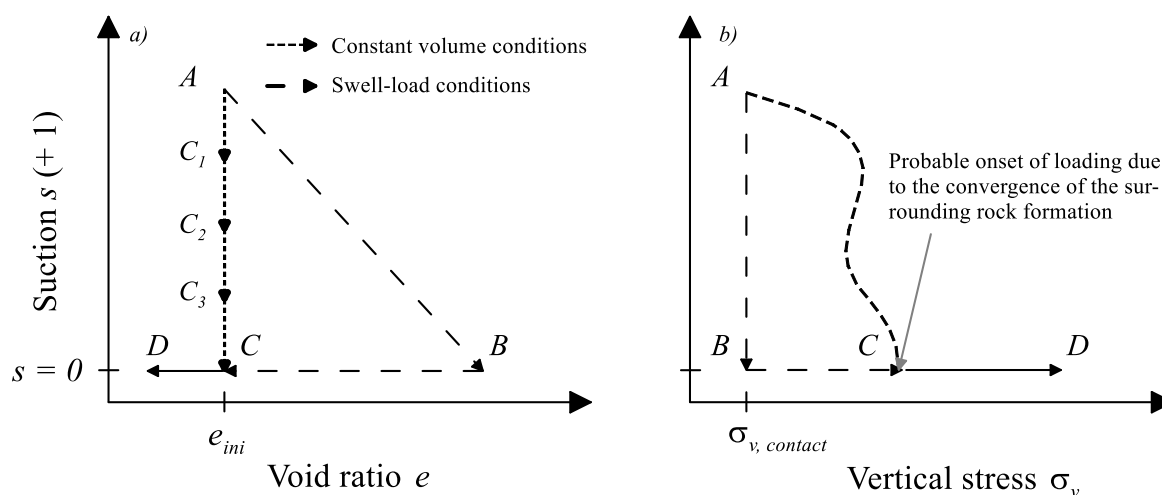


Figure 5.1: Possible combinations of hydraulic and mechanical paths subjected to the backfill upon terminating the installation phase

A potential backfill material is a mixture composed of processed Callovo-Oxfordian claystone spoil and MX80-bentonite, whose dominant mineralogical constituents are phyllosilicates (e.g.

smectites, illite, illite/ smectite mixed layer minerals) (Karnland et al., 2006; Conil et al., 2018). Since conventional compaction techniques are presumably employed to compact it to the maximum dry density at the optimum water content in situ, the material is initially characterized by a degree of saturation greater than 80% and low suctions. The initial dry density determines not only the hydro-mechanical behavior of smectite-containing materials, but also their microstructural and water retention characteristics (e.g. Alonso et al., 1987). It is thus of major interest to analyze how variations in the initial dry density affect the behavior of such materials upon imposing different hydraulic and mechanical paths and their combinations.

In general, there is a wealth of studies aiming to analyze the microstructural and water retention characteristics and volume-change behavior of smectite-containing materials, in particular in unsaturated conditions (e.g. Romero et al., 1999; Lloret et al., 2003; Hoffmann et al., 2007; Monroy et al., 2010; Romero, 2013; Gao and Sun, 2017).

Unsaturated smectite-containing materials are characterized by micro- and macropores, referring to pores between clay aggregates and soil aggregates, respectively. Mechanical and hydraulic loads affect differently those pore populations. Densification reduces only the amount of macropores, whereas the amount of micropores remains stable (e.g. Sivakumar et al., 2006). Hydration affects both pore populations as the amount of micropores increases and the amount of macropores decreases due to the swelling of smectite particles (e.g. Monroy et al., 2010).

The structure determines the water retention characteristics of smectite-containing materials. Densification provokes a shift of the air entry value (AEV) to higher suction values as it reduces the size and shape of macropores. The initial dry density affects those characteristics, only if suction values are lower than few hundred MPa. Below those suction values, dominant capillary phenomena are controlled by macropores (e.g. Gao and Sun, 2017).

Among others, Lloret et al. (2003) studied the volume-change behavior of FEBEX-bentonite in unsaturated conditions. Their experimental program comprised suction-controlled oedometer and constant-volume swelling pressure experiments under different hydro-mechanical paths. Experimental protocols considered the preparation of samples at the hygroscopic water content. Oedometer experiments were conducted on samples, which were characterized by one initial dry density, whereas samples studied in constant-volume swelling pressure experiments were

compacted to different initial dry densities. Oedometer experiments indicated that the material rigidified and the yield stress shifted to higher vertical stresses as the suction was increased. The material response considerably depended on the hydro-mechanical path probably attributable to the differently evolving microstructure. In contrast, there are only a few studies aiming to determine the impact of variations in the initial dry density on the yield behavior of smectite-containing materials upon hydro-mechanical loading. Nowamooz and Masrouri (2009) studied the saturated and unsaturated compression behavior of silt/ bentonite-mixtures by means of suction-controlled oedometer experiments. Sample preparation comprised their compaction to different dry densities at the optimum water content. At a given suction, the yield stress increases as the initial dry density increases, and, at a given initial dry density, the material rigidifies as the suction increases. There is still little understanding about whether variations in the initial dry density alter the yield behavior of smectite-containing materials upon hydro-mechanical loading, and how they affect possible hydro-mechanical path dependencies.

Suction-controlled constant-volume swelling pressure experiments of Lloret et al. (2003) showed that the evolution of swelling pressure was characterized by a double peak pattern upon stepwise decreasing suctions. The characteristic pattern evolved, regardless of the initial dry density. The first maximum value was attributed to the initial swelling of smectite particles, which was followed by the partial collapse of soil aggregates indicating the yield stress. The second maximum value ensued as the swelling of particles prevails over the collapse of soil aggregates. Romero et al. (1999) conducted similar experiments on Boom-clay samples and hypothesized that the yield loci determined in suction-controlled oedometer and constant-volume swelling pressure experiments must coincide. However, only a few studies corroborated the hypothesis (e.g. Alonso et al., 2005b). Further, there are no information about whether variations in the dry density affect the coincidence.

Experiment results are commonly interpreted and reproduced by adopting the constitutive models proposed in Alonso et al. (1990) (*Barcelona Basic Model (BBM)*) and Alonso et al. (1999) (*Barcelona Expansive Model (BExM)*). The latter acknowledges the existence of micro- and macropores and is thus capable to reproduce the characteristic features of smectite-containing materials. As respective experimental studies are scarcely available, only a few constitutive

models allow to consider the impact of variations in the initial dry density on the hydro-mechanical behavior (Sun et al., 2007; Zhou and Sheng, 2015).

In the context of in situ compacted backfill materials, this study aimed to evaluate the impact of variations in the initial dry density on the response of the claystone/ bentonite-mixture to different hydro-mechanical paths. Moreover, it analyzed whether those variations affect the postulated coincidence of yield loci. The evaluation was accomplished by conducting suction-controlled swelling pressure and oedometer experiments on samples which were compacted to different initial dry densities at the optimum water content. Experiments were complemented by analyzing the microstructural and water retention characteristics of the potential backfill material. Obtained results can be useful to improve existing constitutive models regarding the integration of the impact of the initial dry density.

5.2 Material

Following, the section recapitulated the general characteristics of the mixture studied (e.g. physical characteristics, physico-chemical characteristics, compaction characteristics), and described its microstructural and water retention characteristics afterwards.

5.2.1 General characteristics

The mixture studied was composed of 70% processed Callovo-Oxfordian (COX) claystone spoil and 30% MX80-bentonite in weight. The latter was limited to 30% in order to reemploy as much excavated material as possible. Callovo-Oxfordian claystone spoil arose during the excavation of drifts of Andra URL at a depth of – 490 m (Bure, Meuse/ Haute-Marne region, France). The subsequent processing comprised its crushing and sieving to a maximum grain diameter of 2 mm. The processed material was stored in airtight containers afterwards. Henceforth, processed COX-claystone spoil is referred to as COX_c. At that depth, intact COX-claystone contains 27% carbonates (e.g. calcite, dolomite), 46% phyllosilicates (e.g. smectites, illites), 24% tectosilicates (e.g. quartz, feldspars), and minor fraction of other mineral phases (Conil et al., 2018). Likewise, MX80-bentonite (Wyoming, USA) was crushed and sieved to maximum grain diameters of 2 mm and filled into air-tight containers. The dominant mineral

phases are phyllosilicates (e.g. smectites), whose fraction is about 84%. The mineralogical composition is completed by tectosilicates (e.g. quartz) (Karnland et al., 2006).

The mixture was characterized by an initial water content (w_{ini}), liquid limit (LL), plastic limit (PL) and specific gravity (G_s) of 6.4%, 112.5%, 34.7%, and 2.64, respectively (Middelhoff et al., 2020). Its cation exchange capacity (CEC) of 39 meq/100g and specific surface area (SSA) of 32 m²/g were determined by means of the cobalt hexamine method (Orsini and Remy, 1976) and the BET-method (Gregg and Sing, 1969), respectively. The cobalt hexamine method also revealed that the exchangeable cation species were dominated by Na⁺- and Ca²⁺-ions. An elevated compaction energy increased the maximum dry density ($\rho_{d, max}$) and decreased the optimum water content (w_{opt}) of the mixture (Middelhoff et al., 2020). Accordingly, the optimum water content and maximum dry density were 29.0% and 1.45 Mg/m³, respectively, in the case of standard compaction energy employment, and 18.2% and 1.72 Mg/m³, respectively, in the case of modified compaction energy employment. The grain size distribution was determined by means of laser diffractometry and dry sieving and was characterized by 10% - and 60% - passing (D_{10}/D_{60}) values of 0.008 mm and 0.8 mm, respectively.

5.2.2 Microstructural characteristics

Mercury intrusion porosimetry (MIP) experiments were conducted on samples initially compacted to dry densities of 1.72 Mg/m³ and 1.44 Mg/m³ at a water content of 18.2% in order to highlight how possible variations in the initial dry density affect the microstructure. The latter value corresponded to a reduction of the initial dry density by about 17.5% with respect to the maximum dry density. Its consideration facilitated to interpret the results of swelling pressure and oedometer experiments presented later. MIP-experiments were conducted by means of an AutoPore IV 9500 (Micromeritics, U.S.A). The MIP-technique bases on the principle of forcing a non-wetting fluid, e.g. mercury, to enter a porous medium by incrementally increasing the injection pressure. A review of the technique is given in Romero and Simms (2008), for instance. Prior to the analyzes, samples were dried by heating them up to 80°C under vacuum conditions. Apart from that, the experiment protocol followed that established by Cuisinier and Laloui (2004). Approaches for data processing and presentation were adopted from Juang and Holtz (1986).

As depicted in *Figure 5.2a* and *Figure 5.2c*, pore size distribution curves of samples were characterized by two distinct peaks, regardless of the initial dry density. They corresponded to micro- and macropore populations. According to Romero et al. (1999), the inflection point of pore size distribution curves indicated the transition from micro- to macropores. Pores, whose diameters were smaller and greater than the diameter at the inflection point, are referred to as micro- and macropores, respectively. Their quantities are expressed by the micro-void ratio (e_m) and macro-void ratio (e_M), respectively. The unaccountable void ratio (e_{un}) accounts for the pores, whose diameter was too small or too large to be detected.

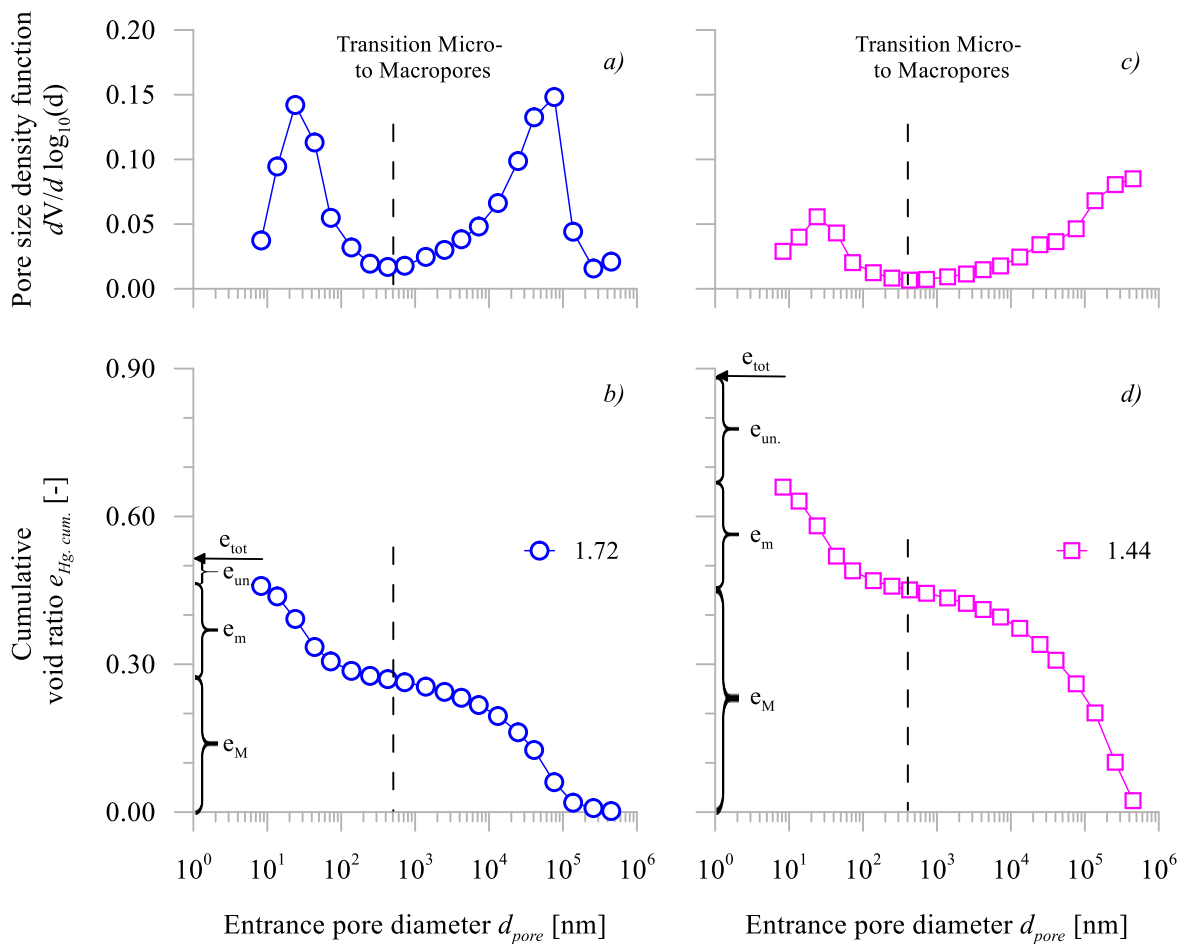


Figure 5.2: Results of mercury intrusion porosimetry (MIP) experiments conducted on samples characterized by initial dry densities of $\rho_{d,ini} = 1.72 \text{ Mg/m}^3$ and $\rho_{d,ini} = 1.44 \text{ Mg/m}^3$

The transition of macro- to micropores occurred at pore diameters of about $5 \times 10^2 \text{ nm}$, regardless of the initial dry density. In all cases, most micropores occurred at a pore diameter of about $2 \times 10^1 \text{ nm}$. In the case of denser samples, the majority of macropores occurred at a pore diameter

of about 8×10^4 nm. Interestingly, in the case of looser samples, the increasing pore size distribution curve indicated that the diameter, at which the majority of macropores occurred, appeared to exceed the limit of the device. Densification reduced the macro- and unaccountable void ratio by about 50%, whereas the micro-void ratio remained stable. The observations were in accordance with the literature as micropores are expected to react sensitively to the hydraulic but not to the mechanical path, such as those imposed by means of the static compaction method (e.g. Romero et al., 1999; Romero and Simms, 2008; Gao et al., 2019). The differences in the unaccountable void ratio might be attributed to pores, whose diameters were in the millimeter range involving the low initial dry density.

In general, the microstructure of mixture samples comprised micro- and macropores, like other smectite-containing materials. As expected, the latter pore population was significantly reduced by densification. It must be thus assumed that the water retention characteristics of denser and looser material differ considerably.

5.2.3 Water retention characteristics

Samples were characterized by initial dry densities of 1.72 Mg/m^3 and 1.44 Mg/m^3 and a water content of 18.2%. A range between few tens of kPa to some hundreds of MPa were imposed by combining the osmotic and vapor equilibrium technique. Their individual ranges overlapped at suctions of about 7 MPa (e.g. Cuisinier and Masrouri, 2005; Nowamooz and Masrouri, 2010). The former technique bases upon the principle that water molecules can go through a semipermeable membrane and move from the pore solution to a macro-molecular (polyethylene glycol (PEG)) solution and vice versa. The migration and its direction is driven by a concentration gradient. Suction is functionally related to the concentration of PEG-molecules in solution as their concentration determines the magnitude of the gradient. A review of the technique is given in Delage et al. (2008). The vapor equilibrium technique adopts Kelvin's equation relating suction to the relative humidity in a closed system. The closed system comprises a gas phase and a liquid phase, whose specific solutes control the relative humidity in the adjacent gas phase. In general, saturated salt solutions are employed as a liquid phase. A review of the technique is given in Delage et al. (1998) and Delage et al. (2008).

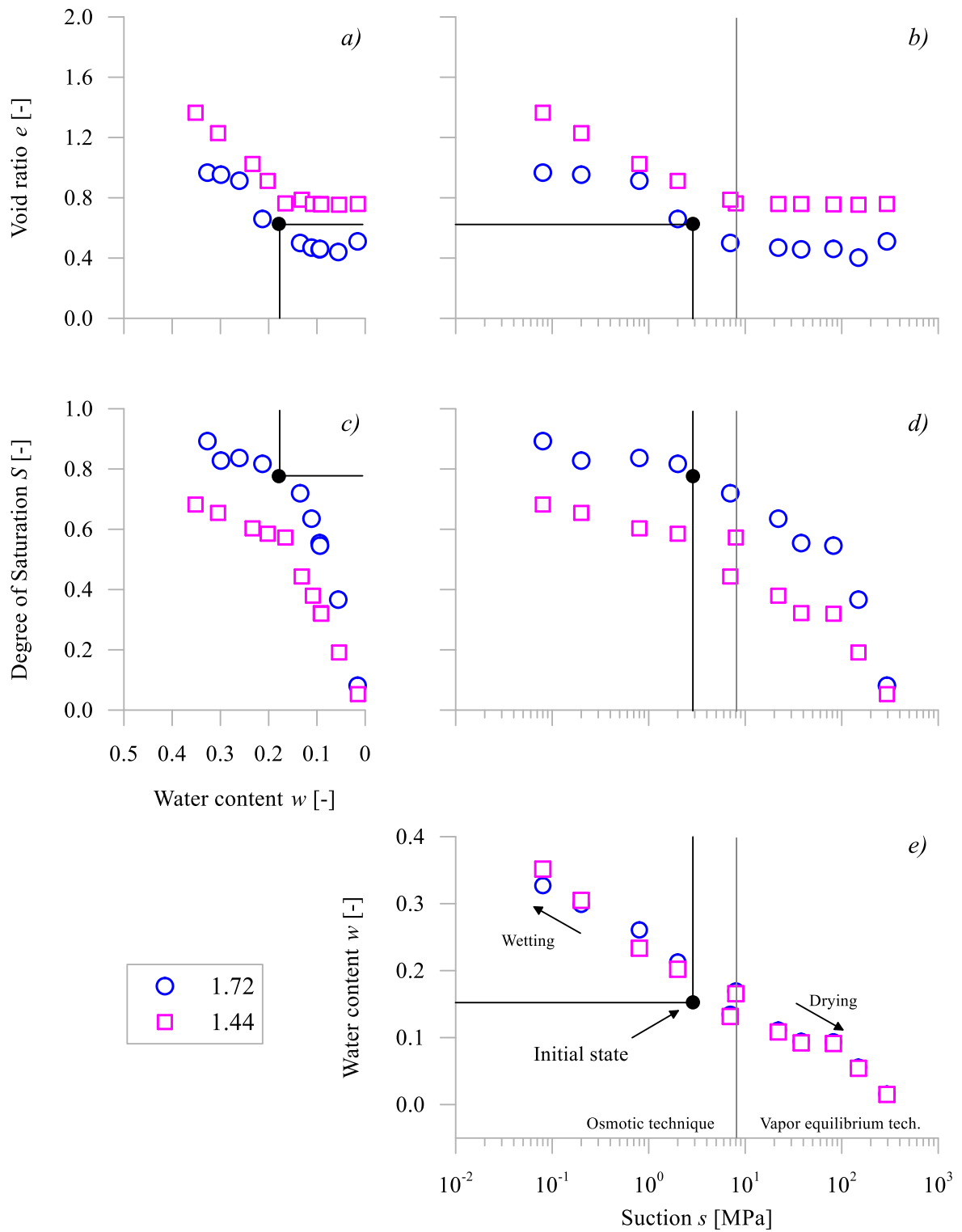


Figure 5.3: Water retention characteristics of mixture samples characterized by initial dry densities of $\rho_{d,ini} = 1.72 \text{ Mg/m}^3$ and $\rho_{d,ini} = 1.44 \text{ Mg/m}^3$

As depicted in *Figure 5.3*, denser samples were initially characterized by lower void ratios and higher degrees of saturation due to the higher initial dry density. Upon hydration, the void ratio and degree of saturation of looser and denser samples increased comparably. Drying had no considerable consequences on both sample types with regard to their void ratios. It affected the degree of saturation of denser samples more significantly than that of looser samples.

The impact of variations in the initial dry density appeared to vanish when imposed suction exceeded values of 200 MPa. This observation was in accordance with the results of microstructural analysis as the vanishing impact of initial dry density indicated the existence of micro- and macropores (*Figure 5.2*). The impact vanished once capillary phenomena were controlled by the water immobilized in the micropores. According to the different diffuse double layer theories, electrostatic interactions between the water molecules and the clay mineral surfaces account for the immobilization (e.g. Romero, 2013).

In general, the water retention characteristics of differently dense mixture samples confirmed the results of microstructural analysis as the vanishing impact of initial dry density at high suctions indicated the existence of micro-and macropores.

5.3 Oedometer and constant-volume swelling pressure experiments

The unsaturated compression and swelling behavior were studied by conducting oedometer and constant-volume swelling pressure experiments, in which the suction was controlled by means of the osmotic technique. Further, different hydro-mechanical paths were imposed to analyze the impact of variations in the dry density on possible path dependencies. The experiment approach considering variations in the initial dry density, the sample preparation, the experiment protocols, and the experiment program are described below.

5.3.1 Approach

Full-scale experiments conducted in situ (e.g. the “*Backfill and Plug Test*” (Gunnarsson et al., 2001), the “*Prototype repository*” (Börgesson et al., 2002)) highlighted the issues involving the employment of conventional compaction techniques to install smectite-containing backfill materials in situ. Their experiment protocols envisaged compacting backfill materials to the max-

imum dry density at the optimum water content in a layer-wise manner. Highest swelling pressure and lowest compressibility were expected to be reached by this means (e.g. Mitchell and Soga, 2005). Unlike the initial water content, whose value remained stable in the cross section of the drift, the initial dry density decreased by up to 20% with respect to the maximum dry density. They attributed this finding to a loss of compaction energy ensuing as the handling of the compactor became difficult, in particular close to the drift top and drift walls.

In order to portray spatial variations in the initial dry density, samples were compacted to the maximum dry density of 1.72 Mg/m^3 at the optimum water content of 18.2%, which was obtained by means of modified Proctor experiments. They were complemented by samples characterized by dry densities of 1.66 Mg/m^3 , 1.59 Mg/m^3 , and 1.44 Mg/m^3 and a water content of 18.2%. The values corresponded to a reduction of the dry density by 2.5%, 7.5% and 17.5%, respectively, with respect to the maximum dry density.

5.3.2 Sample preparation

The material was prepared at the optimum water content and then filled in an airtight container. Deaired/ demineralized water was added in order to reach the optimum water content (Middelhoff et al., 2020). Samples were compacted to the different dry densities at the optimum water content by means of the static compaction method at a controlled deformation rate of 0.1 mm/s. Samples, whose microstructural and water retention characteristics were previously presented, were similarly prepared. Henceforth, the type indicates the initial dry density of samples. Their initial characteristics are compiled in *Table 5.1*.

Table 5.1: Initial characteristics of samples

Type	Initial dry density	Initial water content	Initial void ratio	Initial porosity	Initial degree of saturation	Initial suction*
	$\rho_{d, ini}$	w_{ini}	e_{ini}	n_{ini}	S_{ini}	S_{ini}
	[Mg/m^3]	[-]	[-]	[-]	[-]	[kPa]
I	1.72	0.182	0.53	0.35	0.90	2700
II	1.66	0.182	0.59	0.37	0.82	
III	1.59	0.182	0.66	0.40	0.73	
IV	1.44	0.182	0.86	0.46	0.56	

*: measured by means of chilled mirror method

5.3.3 Suction-controlled oedometer experiments

The protocol of suction-controlled oedometer experiments considered samples of all types. The cell employed in suction-controlled oedometer experiments was composed of a piston, mold, and base (e.g. Delage et al. (1992) or Nowamooz and Masrouri (2008) for further information about its design). The base was characterized by one inlet, one outlet and a mesh, so solutions could be circulated beneath the mesh. It covered a groove spiraling to the center axis of the cylindrical cell and connecting the inlet and outlet. In combination with a semi-permeable membrane separating the sample from the mesh, the design allowed to adopt the osmotic technique in order to impose suctions. The oedometer allowed to apply vertical stresses of up to 3000 kPa. PEG-reservoirs were placed in temperature-controlled baths in order to minimize temperature effects.

5.3.4 Suction-controlled constant-volume swelling pressure experiments

Samples of all types were considered in order to study the evolution of swelling pressure upon stepwise hydration. The constant-volume swelling pressure cell proposed by Yigzaw et al. (2016) was similarly designed allowing to adopt the osmotic technique. However, a porous disc was employed instead of the mesh, and the piston was substituted for a lid, which contained the load sensor. By eventually screwing the components together, a pre-stress of 50 kPa was imposed.

5.3.5 Hydro-mechanical paths and experimental program

The protocol of suction-controlled swelling pressure and oedometer experiments comprised different hydro-mechanical paths depicted in *Figure 5.4* and *Figure 5.5*, respectively. Their imposition aimed to determine how different paths affect the swelling and compression behavior of the potential backfill material, in particular in unsaturated conditions. Since backfill materials are not expected to undergo drying, hydration referred exclusively to the (stepwise) saturation of the mixture, whose initial suction was about 2700 kPa (*Table 5.1*).

Hydro-mechanical paths A, B, C, and D differed in the magnitude of the initial hydration step followed by stepwise mechanical loading and unloading. Hydro-mechanical loads were changed when strains stabilized at rates lower than 0.5 % (of the initial sample height) per day.

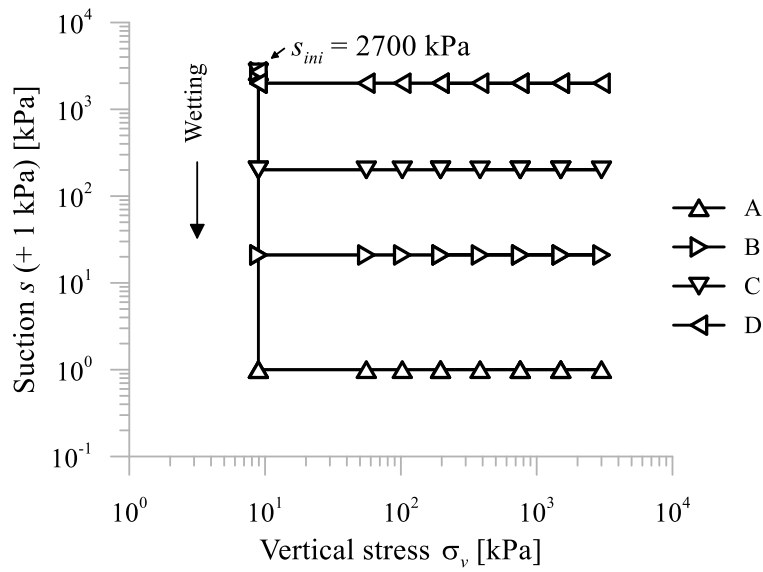


Figure 5.4: Hydro-mechanical paths followed in suction-controlled oedometer experiments

Hydro-mechanical paths E, F, and G differed in the number of stages, in which different suctions were imposed. Imposed suctions were decreased when the swelling pressure stabilized at rates lower than 5 kPa per day.

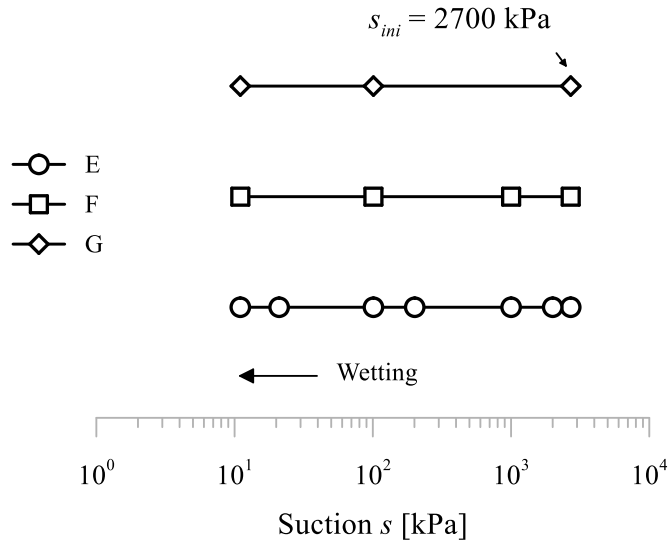


Figure 5.5: Hydration paths followed in suction-controlled constant-volume swelling pressure experiments

Henceforth, samples are identifiable by means of their sample type and imposed hydro-mechanical paths. The prefix refers to the sample type, whereas the imposed hydro-mechanical

path is indicated by the suffix. For instance, sample I - D was characterized by an initial dry density of 1.72 Mg m^{-3} , whose compression behavior was analyzed by adopting hydro-mechanical path D (*Figure 5.4*). The experiment program developed is described in *Table 5.2*.

Table 5.2: Experiment program including microstructural and water retention analysis, suction-controlled constant-volume swelling pressure and oedometer experiments

Sample type ¹	Oedometer experiments ²				Swelling pressure experiments ³		
	A	B	C	D	E	F	G
I	✓	✓	✓	✓	✓	✓	✓
II	✓	✓	✓	✓			
III	✓	✓	✓	✓			
IV	✓	✓	✓	✓			

¹: compare *Table 5.1*

²: Hydro-mechanical paths (compare *Figure 5.4*)

³: Hydro-mechanical paths (compare *Figure 5.5*)

It was believed that this comprehensive experimental program allowed to evaluate how variations in the initial dry density affect the behavior of a potential backfill material under different hydro-mechanical paths.

5.4 Results

Following, the results of suction-controlled oedometer and constant-volume swelling pressure experiments are presented. Since the free-swell potential experiments represented the first stage of oedometer experiments, their results are described in the corresponding section.

5.4.1 Suction-controlled oedometer experiments

Oedometer experiments were conducted on type I- to type IV-samples by imposing hydro-mechanical paths A to D. They were aimed at studying how the one-dimensional compression behavior of the mixture varies as response to the different initial dry densities of samples and imposed hydro-mechanical paths. Additionally, information about the free-swell potential were provided. Their results are depicted in *Figure 5.6a* to *Figure 5.6d*. For clarification purpose, the presentation of the results obtained while unloading is omitted.

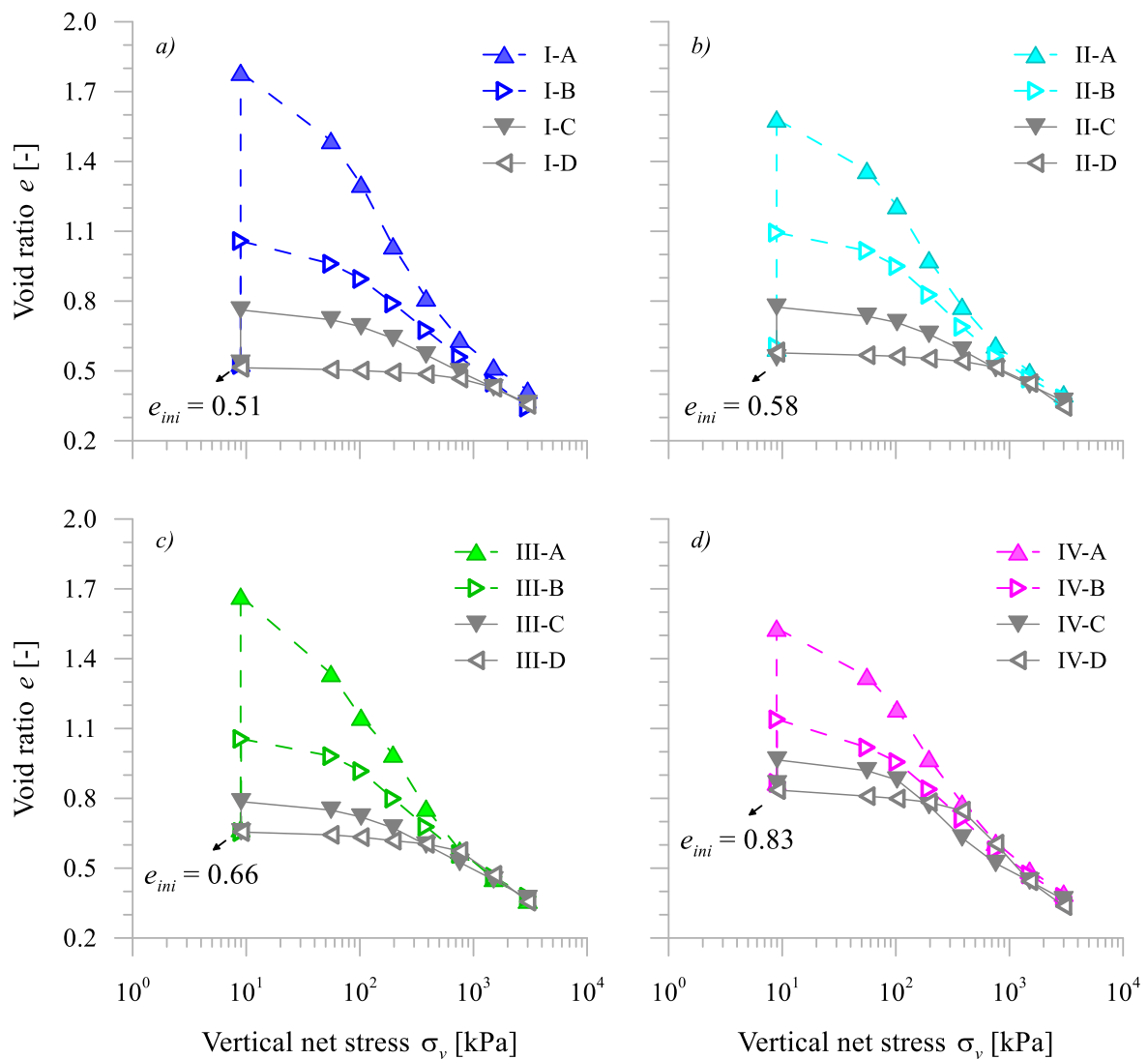


Figure 5.6: Results of oedometer experiments conducted on samples characterized by different initial dry densities upon imposing different hydro-mechanical paths

Compression curves were characterized by two or three zones, in which the slope of the compression line changed. Hydro-mechanical paths C and D involved two zones, whereas the imposition of hydro-mechanical paths A and B implied the development of three zones constituting s-shaped compression curves. Compression lines converged as net vertical stresses were increased beyond about 1000 kPa. Those characteristics were observed, regardless of the initial dry density of samples. In elastoplastic frameworks (e.g. Alonso et al., 1990), the first and second zones are referred to as the elastic and plastic domains, which are separated by the yield stress. Among the different sample types, yield stresses appeared to converge as initially imposed suctions were reduced.

Oedometer experiments also indicated that the free-swell potential increased as the initial dry density was increased, in particular upon imposing lower initial suctions.

In general, the initial dry density affected the one-dimensional compression behavior of mixture samples more considerably when higher suctions were imposed. In saturated state, compression curves appeared to be comparable with regard to their characteristics and shape. The free-swell potential was considerably affected by the initial dry density, in particular in ranges of lower suctions.

5.4.2 Suction-controlled constant-volume swelling pressure experiments

Constant-volume swelling pressure cells controlling suction by means of the osmotic technique were employed in order to study the swelling pressure evolution of the mixture under different hydro-mechanical paths. Evolution of swelling pressure recorded are depicted in *Figure 5.7a* and *Figure 5.7b*.

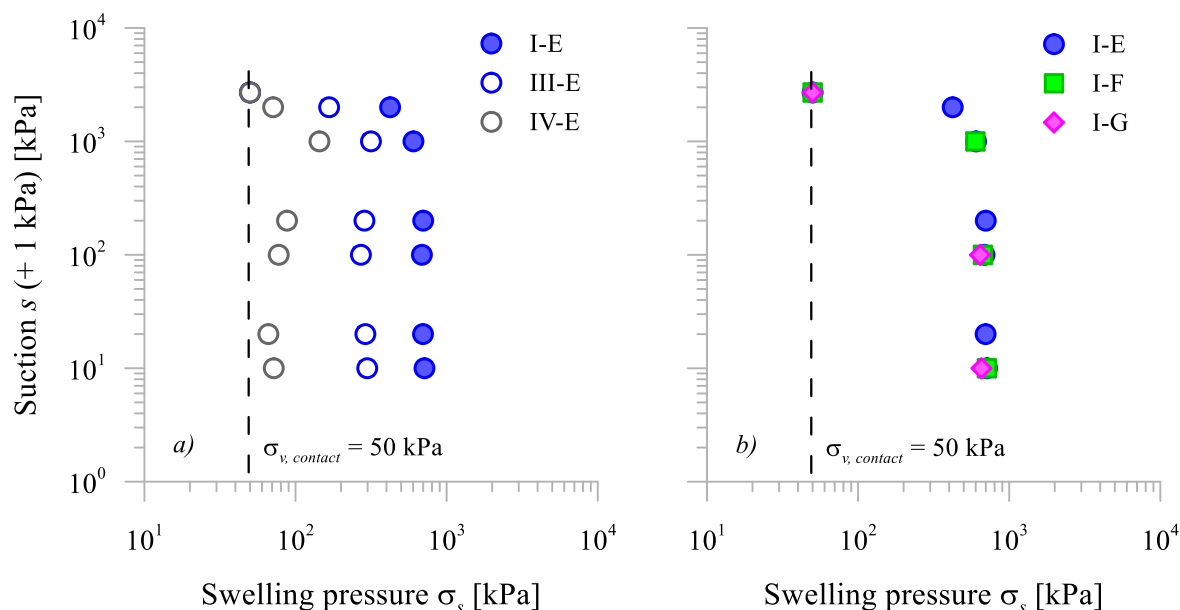


Figure 5.7: Swelling pressure evolution of a) samples characterized by different initial dry densities upon imposing hydration path E and b) samples characterized by the same initial dry density upon imposing hydration paths E, F, and G

In the case of sample II-E, the evolution was not measured due to a malfunction of the load sensor. It still became evident in *Figure 5.7a* that the stabilized swelling pressure at each suction

stage increased as the initial dry density increased. The pattern of the curves was generally characterized by a post-peak stabilization at lower or comparable stresses. In the cases of type III- and IV-samples, the decrease of swelling pressure occurred upon imposing a suction smaller than 1000 kPa, whereas, in the case of the type I-sample, there was only a slight reduction and ensued when suctions were smaller than 100 kPa. As highlighted in *Figure 5.7b*, the mixture reacted to the imposition of different hydration paths identically, since the stabilized swelling pressures at the corresponding suction stages differed negligibly.

In general, suction-controlled constant-volume swelling pressure experiments revealed that the unsaturated swelling pressure of the mixture depended on the initial dry density rather than on the hydraulic path. Further, the results depicted in *Figure 5.7b* indicated a good repeatability of swelling pressure experiments.

5.5 Discussion

The discussion adopted the elastoplastic frameworks proposed in Alonso et al. (1990) and Alonso et al. (1999). It analyzed how variations in the initial dry density affect the compression and swelling behavior of mixture samples. The first and second sections are followed by a comparison which evaluated how those variations alter the response of materials to the different hydro-mechanical paths, in particular the yield behavior. Although representing the first stage of the suction-controlled oedometer experiments, it appears to be more suitable to discuss the results of free-swell potential experiments in conjunction with those of the swelling pressure experiments.

5.5.1 Compression behavior

Suction-controlled oedometer experiments indicated that the shape of compression curves depended on the hydro-mechanical path, in particular on the initially imposed wetting. The dependency was observed, regardless of the initial dry density. The imposition of hydro-mechanical paths C and D led to compression curves characterized by the elastic and plastic domain. In contrast, s-shaped compression curves ensued through the imposition of hydro-mechanical paths A and B. Their nonlinear compression behavior in the plastic domain disagreed with the

formulation of the virgin compression line, whose slope is described by the parameter $\lambda(s)$ (e.g. Alonso et al., 1990). The applicability of the framework thus appeared to be limited.

In general, at a given suction, loading induces the collapse of macropores, and in turn, increases the degree of saturation. In other words, unsaturated samples could saturate through compaction (e.g. Nagaraj et al., 1990). The nonlinear behavior might be related to the fact that the compressibility varied as the degree of saturation increased (e.g. Zhou et al., 2012). Models proposed in Gallipoli et al. (2003) and Zhou et al. (2012) relate the compressibility to the degree of saturation, instead of suction. By this means, they allow to describe the transition of the compressibility in unsaturated state to that in saturated state through compaction. This prediction was consistent as compression curves converged at high vertical stresses ($\sigma_v \geq 1000$ kPa), regardless of the imposed suction. In the context of in situ compacted backfill materials, the prediction implied a negligible impact of the saturation state on the compression behavior when the overburden pressure fully affects the backfill material.

In the frameworks proposed in Alonso et al. (1990) and Alonso et al. (1999), the loading-collapse (LC) curve gives the functional relation between the yield stress and imposed suction. Corresponding yield loci were derived from suction-controlled oedometer experiments. As depicted in *Figure 5.8a*, the variation of yield stress with imposed suction was almost identical, in the cases of type I-, II-, and III-samples. LC-curves thus coincided. Yield stresses of type IV-samples were lower, in particular when hydro-mechanical paths C ($s = 200$ kPa) and D ($s = 2000$ kPa) were imposed. In ranges of lower suctions, the two LC-curves converged.

Two conclusions can be drawn from *Figure 5.8*. At higher suctions, slight variations in the initial dry density had no impact on the yield behavior. There was an apparent threshold, below which the initial dry density came into effect. At lower suctions, the impact of variations in the initial dry density vanished. It was manifested by the convergence of LC-curves.

At lower suctions, crystalline swelling and partial particle breakup ensued as the hydration front propagated entirely through the sample under free conditions. Collapse of macropores was less probable due to the small vertical stress ($\sigma_v \approx 10$ kPa). The processes involved an increase in micropores and a decrease in macropores as swelling particles penetrated the macro-pores. Not only did pore merging turn the bimodal pore size distribution function into a unimodal one, it

also increased the total porosity, regardless of the initial dry density (e.g. Yuan et al., 2016; Yuan et al., 2019). In general, a unimodal pore size distribution function implies that mechanical loading affects the overall structure. At lower suctions, loading in the elastic domain adapted the amount of pores in all samples, as indicated by the coinciding void ratios in *Figure 5.8b*. The pores collapsed under comparable stresses, thus the stiffness of the overall structure and in turn, the yield stresses appeared to converge.

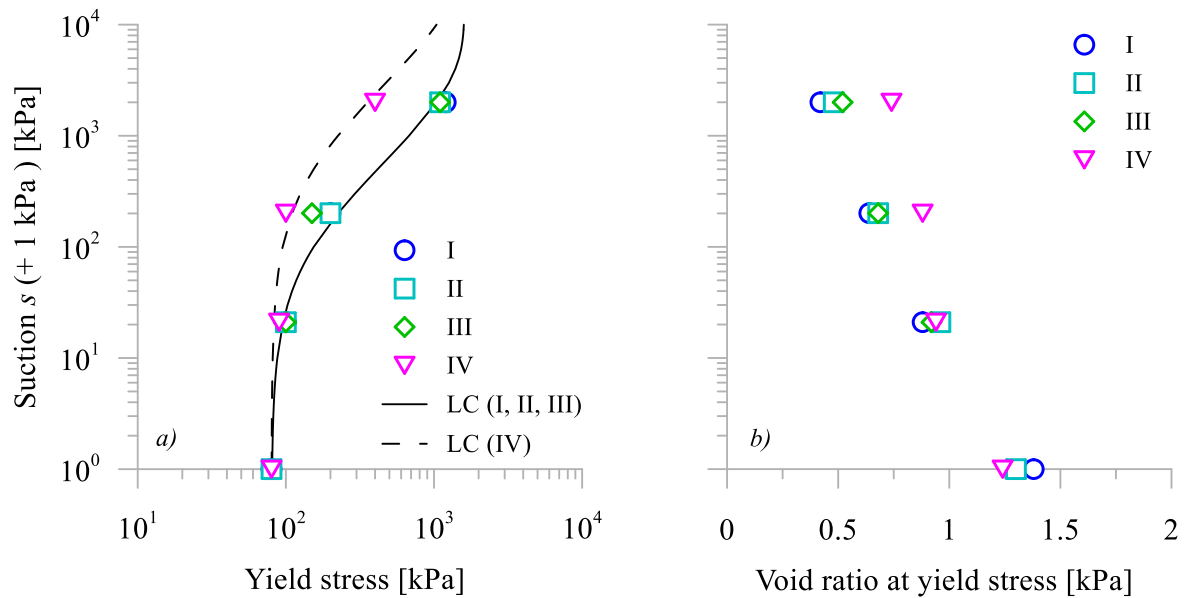


Figure 5.8: Loading-collapse (LC) curves derived from suction-controlled oedometer experiments

In contrast, at higher suctions, the structure of mixture samples was characterized by micro- and macropores, and mechanical loading affected only the aggregates surrounding the latter pore population. LC-curves of type I-, II-, and III-samples might coincide due to a still comparable amount of macropores and, in turn, a similar stiffness of soil aggregates. Accordingly, the elevated macroporosity in type IV-samples accounted for the lower yield stresses. It might be of interest to corroborate the hypothesis of comparable structures after free swelling by means of microstructural investigations (e.g. MIP-experiments).

In the context of in situ compacted backfill materials, the results of suction-controlled oedometer experiments highlighted that the initial dry density has an impact of the compression behavior of the mixture, in particular on the yield behavior, only if lower vertical stresses and

higher suctions are imposed. If samples saturate under free-swell conditions, an adaption of the total porosity appears to involve a comparable stiffness of the overall structure.

5.5.2 Swelling behavior

Suction-controlled constant-volume swelling pressure experiments indicated that the evolution of swelling pressure was characterized by a post-peak stabilization at lower or comparable stresses. Although the increase in initial dry density accompanied an increase in swelling pressure at a given suction (*Figure 5.7a*), there was no functional relation between initial dry density and swelling pressure.

As implied in the introduction, Lloret et al. (2003) adopted parts of the elastoplastic framework proposed in Alonso et al. (1999) in order to interpret the double peak pattern. The initial reduction of suction caused homogeneous swelling of particles. Increasing vertical stresses compensated for the swelling of particles as the stiffness of soil aggregates was high. Decreasing vertical stresses followed the first maximum value and indicated that the yield stress was reached. The partial collapse of macropores lowered the stiffness of soil aggregates and progressing swelling of particles cannot compensate for the collapse of macropores. As the reduction of suction reduction, swelling of particles prevailed over collapse of macropores, and increasing vertical stresses compensated for the swelling of particles again. The phenomenological interpretations proposed in Massat et al. (2016) and Yigzaw et al. (2016) were similar to that of Lloret et al. (2003). Yet, they specified that macrostructural rearrangements accounted for an increase in material stiffness and a consequent dominance of swelling of particles. In this study, the evolution of swelling pressure was characterized by a post-peak stabilization at lower or comparable stresses. In the cases of type I-samples, vertical stresses stabilized at comparable values after reaching the peak. Their lower initial macroporosity apparently limited the structural rearrangement, in particular the collapse of macropores. Conversely, in the cases of type III- and IV-samples, the swelling of particles appeared to be less pronounced than the collapse of macropores, thus the vertical stresses stabilized at lower stresses.

Wang et al. (2012) described a potential functional relation between the imposed suction and swelling pressure which implied a monotonous increase in swelling pressure. Since they attributed this finding to the homogeneous swelling of particles and the high stability of soil aggregates, the question was raised why aggregates might be differently stable.

Middelhoff et al. (2020) conducted constant-volume swelling pressure experiments on mixture samples prepared to the same initial conditions. Their experiment protocol comprised the direct saturation of samples with deaired/ deionized water. The results complemented those recently obtained and highlighted the hydraulic path independency of the material, as depicted in *Figure 5.9a* and *Figure 5.9b*. The independence appeared to be valid, regardless of the initial dry density of the material. Wang et al. (2012) conducted similar swelling pressure experiments on compacted bentonite/ claystone-mixture samples, whose mineralogical composition was dominated by smectites. They also reported on a hydraulic path independency. According to their interpretation, the direct and stepwise saturation triggered sequentially comparable structural rearrangements and led eventually to a similar microstructure.

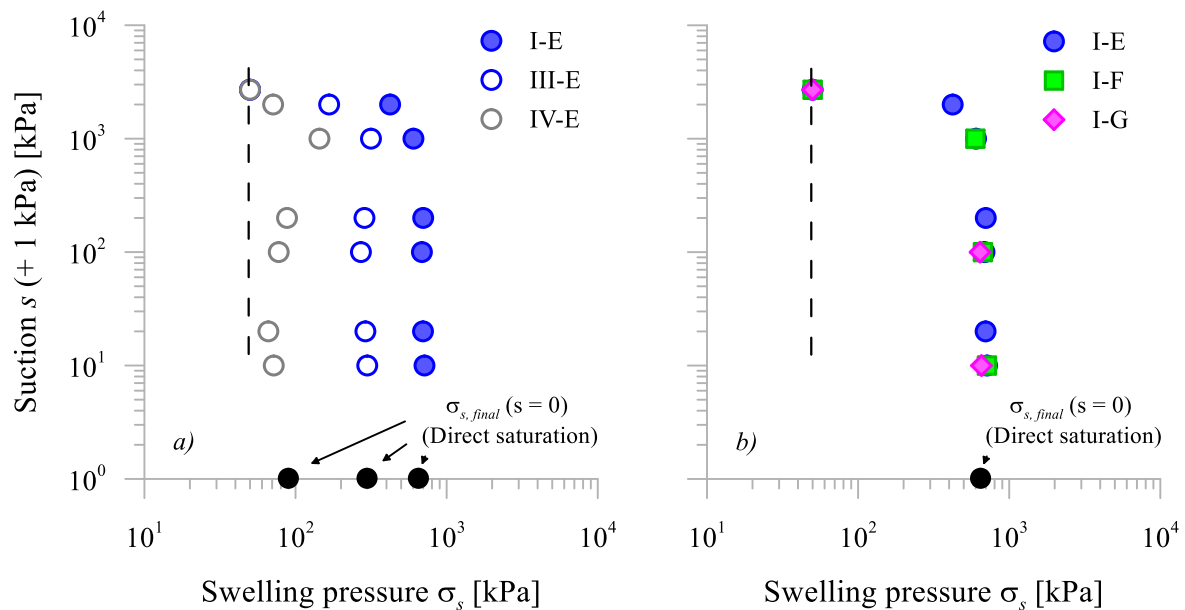


Figure 5.9: Comparison between the swelling pressure evolution of a) samples characterized by the same initial dry density upon saturating directly and imposing hydration paths E and b) samples upon saturating directly and imposing hydration paths E, F, and G

The protocol of suction-controlled oedometer experiments comprised the determination of the free-swell potential of mixture samples at their initial stage. The relationship between the initial dry density and free-swell potential of samples can be described by a linear function, whose slope increased logarithmically as the suction decreases. In the case of suctions being equal to 2000 kPa, no swelling was observed. Presumably, the increasing smectite mass in denser samples caused the linear relation since each particle can undergo crystalline swelling and particle breakup under the availability of water molecules (e.g. Likos and Wayllace, 2010). Major macrostructural rearrangements were less probable due to the low initial vertical load.

In general, suction-controlled constant-volume swelling pressure experiments indicated that stepwise wetting involved a non-monotonic increase in swelling pressure, regardless of the initial dry density. The post-peak stabilization at lower or comparable stresses was attributed to structural rearrangements, in particular particle swelling and partial macropore collapse. In the case of denser samples, the latter aspect might account for the stabilization at comparable stresses. Accordingly, the partial collapse was less significant due to the smaller amount of macropores therein. The evolution of swelling pressure was hydraulic path independent potentially attributable to a similar final microstructure. The free-swell potential experiments indicated a functional relation between the initial dry density and final free-swell potential at a given suction. It was attributed to the availability of water molecules and the larger amount of smectite particles in denser samples.

5.5.3 Comparison of yield behavior

As described above, the (suction-controlled) propagation of the hydration front through the sample under constant-volume conditions involved the initial swelling of particles, followed by the collapse of aggregates and the final dominance of particle swelling over aggregate collapse. The swelling pressure evolved in conjunction with those structural rearrangements. In contrast, under oedometric conditions, structural rearrangements were terminated before loading. The differently rearranging structure might account for the fact that the yield loci of denser samples differed significantly, whereas those of looser samples coincided, as depicted in Figure 5.10.

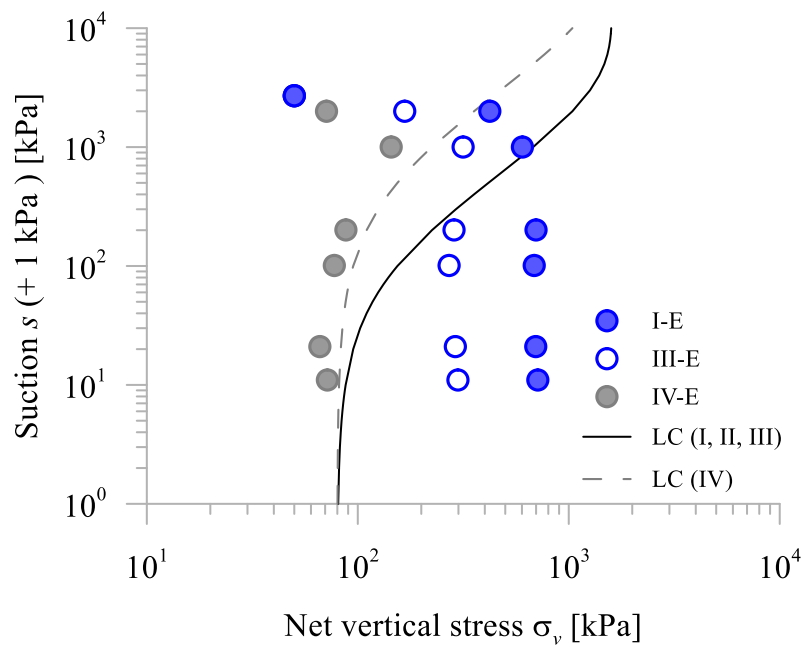


Figure 5.10: Comparison between LC-curves derived from suction-controlled oedometer experiments and swelling pressure evolution under constant-volume conditions

In the case of type I- and III-samples, the partial collapse of aggregates and the subsequent swelling of particles appeared to increase the density of the material and, in turn, the stiffness of the overall structure (Massat et al., 2016). Their yield stress increased as a consequence. Type IV-samples were characterized by an elevated fraction of macropores, and their partial collapse cannot be compensated by the swelling of particles. The densification was less effective, and the stiffness of the overall structure measured under constant-volume conditions became comparable to that determined under oedometric conditions. Indeed, the findings partially corroborated the hypothesis suggested by Romero (1999) as the yield loci of looser samples coincided. However, the yield behavior of denser samples appeared to considerably depend on the hydro-mechanical path.

5.6 Conclusions

The French reference considers a mixture composed of 70% processed Callovo-Oxfordian claystone spoil and 30% MX80-bentonite to be a material, which could be potentially employed to backfill drifts and shafts of the future repository for intermediate- and high-level radioactive

waste in the clay-rich Callovo-Oxfordian sedimentary rock formation. Regardless of the saturation state, the convergence of the surrounding rock formation likely induces mechanical loading. Thus, the occurrence of different hydro-mechanical paths is possible. Installed by means of conventional compaction methods, the backfill material is likely characterized by spatial variations in its initial dry density. Since the initial dry density is one of the factors controlling the water retention characteristics and hydro-mechanical behavior of smectite-containing material, it is of major relevance to analyze the impact of its variations on the performance of claystone/ bentonite-mixtures, in particular in unsaturated state.

At its initial stage, this laboratory experimental program analyzed the mixture with regard to its microstructural and water retention characteristics. Subsequent suction-controlled oedometer and constant-volume swelling pressure experiments aimed to evaluate how variations in the initial dry density affect the compression and swelling behavior. The final comparison of experiment results revealed whether the hydro-mechanical behavior of the mixture depends on the hydro-mechanical path, and whether variations in the dry density have an impact on possible dependencies. Following conclusions can be drawn from the experiments conducted:

1. The results of microstructural analysis agreed with the trends generally described in the literature. In contrast to micropores, whose amount remained stable, macropores were considerably affected by densification. A reduction of dry density by about 20% decreased their amount by about 50%.
2. As expected, water retention characteristics highlighted the existence of micro- and macropores since the impact of the initial dry density vanished at higher suctions. The observation was related to the fact that micropores control capillary phenomena at higher suctions.
3. The impact of the initial dry density on the compression behavior of mixture samples vanished when higher vertical stresses or lower suctions were imposed. Although suctions were imposed, the compression curves of unsaturated samples converged into those of saturated samples at higher stresses.

4. At a given suction, the free-swell potential of the mixture was linearly related to the initial dry density. In turn, the slope of this linear function varied logarithmically with the imposed suction. The findings were attributed to the larger amount of smectite particles in denser samples and to the greater availability of water molecules at lower suctions.
5. Suction-controlled hydration of mixture samples under constant-volume conditions involved the evolution of swelling pressure, whose development was characterized by a post-peak stabilization at lower or comparable stresses. The pattern evolved regardless of the initial dry density and was attributed to rearrangements at the micro- and macrostructural level. The swelling pressure increased with increasing initial dry density at a given suction. Apart from those findings, experiments revealed that the evolution of swelling pressure was independent of the hydraulic path potentially attributable to a similar final microstructure.
6. The comparison of results highlighted that the initial dry density of samples had an impact on their hydro-mechanical path dependency. In the case of looser samples, the yield behavior under constant-volume and oedometric conditions was comparable, whereas, in the case of denser samples, the yield stresses were shifted to lower values under oedometric conditions. The difference in yield locus position was attributed to an adaption of the total porosity and a comparable stiffness of the overall structure.

This study confirmed that the microstructural and water retention characteristics of the claystone/ bentonite-mixture considerably changed as a response to variations in their initial dry density. Variations in the initial dry density had a significant impact on the swelling behavior of the mixture, regardless of the saturation state. Regarding the compression behavior, the impact vanished as lower suctions or higher vertical stresses were imposed. In the context of in situ compacted backfill materials, neither the initial dry density nor the saturation state accordingly have an impact on the compression behavior when the material is subjected to the overburden pressure once the concrete lining degrades. The evolution of swelling pressure under constant-volume conditions was hydraulic path independent, whereas the yield behavior was hydro-mechanical path independent only when the initial dry density of the material was lower.

Regarding future laboratory experimental studies, it might be of interest to corroborate the hypothesis of the comparable stiffness of the overall structure by complementing the different stages in oedometer experiments by means of X-ray tomography.

6 Conclusions and perspectives

In the context of the French Cigéo-project, processed excavated material (COX_c) and its mixtures with MX80-bentonite were studied as to whether those materials can be potentially used to backfill drifts and shafts of a future disposal site of intermediate and high-level radioactive waste located in a clay-rich sedimentary rock formation. The fraction of MX80-bentonite in mixtures studied was limited to 30% in weight in order to reemploy as much excavated material as possible. In this regard, it was of major importance to understand and analyze the hydro-mechanical behavior of potential COX_c-based backfill materials. Considering the fact that the hydro-mechanical behavior of smectite-containing materials depends on the geo-environmental conditions comprising the material properties, environmental conditions and stress history, it was also of great interest to evaluate qualitatively and quantitatively the impact of relevant geo-environmental conditions on the materials. In general, the study of those aspects aimed to improve the confidence in potential COX_c-based backfill materials.

At its initial stage, this laboratory experimental study analyzed COX_c and its mixture with MX80-bentonite with regard to their general, microstructural and water retention characteristics. It was followed by the analysis of the hydro-mechanical behavior in saturated and unsaturated conditions. In addition to the actual analysis, the latter two stages evaluated the individual and combined impact of different geo-environmental conditions on the hydro-mechanical behavior.

6.1 Approaches

The following paragraph recapitulates the relevant geo-environmental conditions and describes the approaches adopted to portray them at laboratory scale:

- The reference concept considers adopting the in-situ compaction method. The method implies the employment of conventional compaction techniques and thus relies on the results of Proctor experiments, in which the compaction energy is limited. Accordingly, backfill materials are prepared to their optimum water content offsite and compacted to their maximum dry density in situ in order to yield the required performance. However, literature data indicated that the as-compacted dry density varies in the cross section of the drifts by about 20% with respect to the maximum dry density attributable to a loss in compaction energy. In this study, spatial variations in the initial dry density were portrayed by compacting samples to the maximum dry density at the optimum water content. For comparison purpose, samples were considered whose initial water content indeed corresponded to the optimum water content, but whose initial dry density was reduced by 2.5%, 7.5% or 17.5% with respect to the maximum dry density.
- Installed by means of the in-situ compaction method, backfill materials are initially characterized by a degree of saturation higher than 80% and low suctions. Solutions coming from the rock formation then penetrate the outer section of the backfill material and trigger a wetting front to propagate towards the center. As a consequence, the backfill material saturates over time. In this study, spatial variations in the saturation state were portrayed by imposing suctions, whose values corresponded to 75%, 7.5% or 0.75% of the initial value.
- Indeed, solutions coming from the rock formation penetrate the backfill material. However, those solutions percolate through the concrete lining left in place before they actually penetrate the backfill material. The percolation alters the characteristics of solutions, in particular their chemical compositions and pH. In this study, the impact of the saturating solution chemistry was portrayed by saturating potential backfill materials with different solutions. In terms of their chemistry, the solutions considered corresponded to the formation water at the disposal site or to the leachate arising from concrete degradation.

In the context of in-situ compacted backfill materials, those approaches allowed to consider the most relevant geo-environmental conditions and to evaluate their impact on the hydro-mechanical of potential COX_c-based backfill materials at laboratory scale.

6.2 Synthesizes and conclusions

The following section synthesizes the individual laboratory experimental programs and recapitulates their major conclusions:

- Initially, it was of relevance to characterize the grain size distribution, as well as the physical and compaction properties of COX_c and its mixtures with MX80-bentonite. In order to evaluate how the grain size distribution affects those properties and the hydro-mechanical behavior, MX80-bentonite was processed to maximum grain diameters of 0.28 mm and 2 mm before it was mixed with COX_c. Later, the mixtures were referred to as powder- and grain-mixture, respectively. Indeed, the physical characteristics were considerably increased by means of the partial replacement. However, the elevated smectite content caused an increase in the optimum water contents and a decrease in the maximum dry densities, regardless of the compaction energy. The laboratory experimental study principally aimed to quantify the individual and combined impact of variations in the initial dry density and saturation solution chemistry on the swelling pressure of COX_c, the grain- and powder-mixture by means of the constant-volume method. As expected, maximum swelling pressures of mixture-samples were higher than those of COX_c-samples due to the elevated smectite content. In addition, the maximum swelling pressure of mixture-samples was exponentially related to their initial dry density. Powder-mixture-samples exhibited higher maximum swelling pressures than grain-mixtures-samples due to their slightly higher maximum dry density. Compacted to their maximum dry density at the optimum water content, mixture-samples were hardly affected by the saturating solution chemistry, regardless of the initial dry density. This was attributed to the low ionic strength of solutions and limited experiment duration. In contrast, COX_c was more susceptible to the saturating solution chemistry, in particular to the saturation with alkaline solution. This finding cannot be explained yet.

- The second part of the laboratory experimental program initially analyzed COX_c and its mixture with MX80-bentonite ($d_{max, MX80} \leq 2$ mm) with regard to their physico-chemical and microstructural characteristics. The partial replacement of COX_c by MX80-bentonite increased the cation exchange capacity and decreased the specific surface area. In addition, the exchangeable cations were dominated by Na⁺-ions instead of Ca²⁺-ions. Both materials were characterized by micro- and macropores, but mixture-samples incorporated more macro- and unaccountable pores than COX_c-samples. This part of the laboratory experimental program principally aimed to relate the evolution of the hydraulic conductivity of materials to changes in the textural and structural characteristics possibly affected by the saturating solution chemistry, in particular by the pH-value. Imposed conditions were believed to portray realistic conditions in terms of compaction conditions, saturating solution chemistry and temperature. Samples were compacted to the maximum dry density at the optimum water content and saturated with different solutions under constant-volume conditions. The saturation hardly affected the specific surface area of samples which might be interpretable as a lack of particle swelling. However, the microstructural analysis indicated that there were considerable microstructural rearrangements. Those rearrangements were related to the closure of macropores triggered by material swelling upon saturation. The hydraulic conductivity of COX_c was greater than that of its mixture by one order of magnitude at least most probably attributable to the progressive closure of macropores. In addition, the finding that the saturating solution chemistry appeared to hardly affect the hydraulic conductivity of materials highlights the low kinetic of geochemical reactions, in particular of dissolution processes, under imposed conditions.
- The third part of the laboratory experimental study aimed to analyze how variations in the initial dry density affects the swelling and compression behavior of mixture-samples, in particular in unsaturated conditions. It was also of great interest to evaluate whether the volume-change behavior depends on the imposed hydro-mechanical load path and whether a possible hydro-mechanical load path dependency might be affected by the initial dry density. The water retention curves of loose and dense samples confirmed the results of microstructural analysis. The existence of micro- and macropores was indicated by the vanishing impact of the initial dry density upon imposing suctions higher than 200 MPa.

The swelling and compression behavior were analyzed by means of suction-controlled constant-volume swelling pressure and oedometer experiments. The relation between the initial dry density and free-swell potential of mixture samples could be described by a linear function, whose slope varied logarithmically with the imposed suction. Upon suction-controlled hydration, the evolution of swelling pressure was characterized by a double peak. At a given suction, an increase in swelling pressure ensued as the initial dry density was increased. The imposition of different hydraulic load paths revealed that the evolution of swelling pressure was independent of the hydraulic load path, which was attributed to a similar final microstructure. The impact of variations in the initial dry density on the compressibility of mixture samples vanished when higher vertical stresses or lower suctions were imposed. The comparison of the yield behavior determined under constant-volume and oedometric conditions revealed how the initial dry density of samples affects the hydro-mechanical load path dependency. The yield behavior of looser samples was comparable under both conditions, whereas a shift of the yield curves to higher vertical net stresses ensued as the samples were saturated under constant-volume conditions. It might be related to an adaption of the total porosity and a comparable stiffness of the overall structure.

6.3 Perspectives

The laboratory experimental study highlighted the complex hydro-mechanical behavior of potential COX_c-based backfill materials, in particular under relevant geo-environmental conditions. Greatest challenges encountered were related to the study of how the performance of potential COX_c-based backfill materials might alter under realistic conditions over time. Considering this aspect, the following paragraph gives suggestions for future laboratory experimental studies, whose future realization can provide confidence in the time-dependent performance of smectite-containing backfill and sealing materials.

The low hydraulic conductivity and high retention capacity of smectite-containing materials lead to a low exchange rate of solution under realistic thermo-hydro-chemical conditions. In particular, as the low exchange rate is accompanied by low kinetics of geochemical reactions (e.g. dissolution, precipitation, modification) under those conditions, it is difficult to evaluate

how the solution chemistry affects the hydro-mechanical behavior over time. In order to distinguish between the short- and long-term behavior, it is thus recommendable to adopt criteria, which rely on hydro-chemical aspects rather than on the experiment duration. The equilibrium of pH and electric conductivity in the influent and effluent represents such a criterion. Such criteria can be complemented by nondestructive microstructural analysis at different experiment stages. Generally, it might be advantageous to perform numerical simulations prior to the experiments. They can help to quantify the kinetics of geochemical reactions and to estimate the time, beyond which the solution chemistry might affect the hydro-mechanical behavior. Those approaches might be promising in order to improve the understanding about the coupling of chemo-hydro-mechanical processes in potential backfill and sealing materials.

The impact of temperature on the backfill was described to be negligible in the introduction. Indeed, the description is valid in the cases of shafts and ramps. However, the decay heat likely increases the temperature in the geological formation surrounding the disposal cells and adjacent access drifts. Consequently, the increase in temperature must not be assumed to be negligible. The impact of increasing temperatures on the hydro-mechanical behavior of smectite-containing materials was analyzed in several studies. In general, elevated ambient temperatures impair the performance of such materials as they provoke not only a decrease in the free-swell potential and swelling pressure, but also an increase in the compressibility and hydraulic conductivity. In addition to those aspects, an acceleration of the kinetics of geochemical reactions ensues as the ambient temperature increases potentially leading to a greater impact of the solution chemistry. It is thus of interest to assess the impact of the temperature on potential backfill and sealing materials under realistic thermo-chemo-hydro-mechanical conditions.

In this study, COX_c-based materials were analyzed with regard to their solution transfer behavior in saturated state. However, as different processes in the repository might generate gas, it must also be of relevance to analyze the gas transfer behavior. Previous studies showed that the initial dry density and degree of saturation control the gas transfer behavior of smectite-containing materials as they determine the quantity of gas-conductive pores. Like the solution transfer behavior, the gas transfer behavior evolves as the material saturates and material swelling occurs.

Further, this study highlighted the significant impact of the initial dry density on the hydro-mechanical behavior of smectite-containing materials, and the consequent importance of its consideration for the development of future constitutive models. The importance is reflected in the exponential relation between initial dry density and maximum swelling pressure, for instance. It can be thus of interest to conduct more suction-controlled oedometer experiments on differently dense samples in order to relate the shift of yield loci to the varying dry densities. Those results might also provide useful information regarding the improvement of micro- and macrostructural coupling functions. Nevertheless, a greater base of consistent experimental data is required in order to improve and advance existing constitutive models in those aspects.

A Supplementary material

Table A.1: Details of COXc, grain- and mixture samples employed in swelling pressure experiments

Sample ID	Solution	Initial material parameters						
		Max. grain size of bentonite $d_{max, ben.}$ [mm]	Reduction* R [%]	Initial dry density ^x $\rho d. ini.$ [Mg/m ³]	Initial water content ^x w_{ini} [%]	Initial void ratio ⁺ e_{ini} [-]	Initial degree of saturation ⁺ S_{ini} [%]	
1	COX – 1111 – 2	DW	-	-	1.83 (1.78)	16.6 (16.5)	0.54	83.0
2	COX – 2121 – 1	DW	-	-	1.95 (1.96)	13.2 (12.8)	0.36	94.0
3	COX – 1221 – 2	ABSS	-	-	1.95 (1.92)	13.2 (13.1)	0.39	89.0
4	COX – 2321 – 1	APCS	-	-	1.95 (1.92)	13.2 (13.1)	0.39	89.0
5	CMX – 1111 – 1	DW	2.00	-	1.46 (1.40)	29.0 (28.7)	0.91	85.0
6	CMX – 2121 – 1	DW	2.00	-	1.72 (1.72)	18.2 (18.6)	0.54	92.0
7	CMX – 1131 – 3	DW	2.00	3.5	1.66 (1.66)	18.2 (18.2)	0.58	82.0
8	CMX – 2141 – 1	DW	2.00	7.5	1.59 (1.59)	18.2 (18.6)	0.65	75.0
9	CMX – 2151 – 1	DW	2.00	17.5	1.42 (1.40)	18.2 (18.6)	0.88	56.0
10	CMX – 2221 – 2	ABSS	2.00	-	1.72 (1.73)	18.2 (18.2)	0.52	91.0
11	CMX – 1231 – 3	ABSS	2.00	3.0	1.67 (1.67)	18.2 (18.2)	0.58	83.0
12	CMX – 2241 – 1	ABSS	2.00	7.5	1.59 (1.57)	18.2 (18.1)	0.68	70.0
13	CMX – 2251 – 1	ABSS	2.00	17.5	1.42 (1.40)	18.2 (18.1)	0.88	54.0
14	CMX – 2321 – 1	APCS	2.00	-	1.72 (1.70)	18.2 (18.1)	0.56	86.0
15	CMX – 1331 – 3	APCS	2.00	3.5	1.66 (1.66)	18.2 (18.2)	0.58	82.0
16	CMX – 2341 – 1	APCS	2.00	7.5	1.59 (1.57)	18.2 (18.1)	0.68	70.0
17	CMX – 2351 – 1	APCS	2.00	17.5	1.42 (1.41)	18.2 (18.1)	0.87	55.0
18	CMX – 2112 – 1	DW	0.28	-	1.57 (1.56)	24.5 (24.5)	0.69	94.0
19	CMX – 2122 – 1	DW	0.28	-	1.79 (1.77)	15.0 (15.0)	0.49	80.0
20	CMX – 2132 – 1	DW	0.28	2.5	1.75 (1.74)	15.0 (13.8)	0.52	70.0
21	CMX – 2142 – 1	DW	0.28	7.5	1.66 (1.68)	15.0 (13.8)	0.56	65.0
22	CMX – 2152 – 1	DW	0.28	17.5	1.48 (1.47)	15.0 (13.8)	0.80	46.0
23	CMX – 2222 – 1	ABSS	0.28	-	1.79 (1.77)	15.0 (14.7)	0.49	79.0
24	CMX – 2232 – 1	ABSS	0.28	2.5	1.75 (1.73)	15.0 (14.7)	0.53	71.0
25	CMX – 2242 – 1	ABSS	0.28	7.5	1.66 (1.65)	15.0 (14.8)	0.60	65.0
26	CMX – 2252 – 1	ABSS	0.28	17.5	1.48 (1.48)	15.0 (14.8)	0.79	50.0
27	CMX – 2322 – 1	APCS	0.28	-	1.79 (1.77)	15.0 (14.8)	0.50	79.0
28	CMX – 2332 – 1	APCS	0.28	2.5	1.75 (1.73)	15.0 (14.8)	0.53	73.0
29	CMX – 2342 – 1	APCS	0.28	7.5	1.66 (1.65)	15.0 (14.8)	0.60	65.0
30	CMX – 2352 – 1	APCS	0.28	17.5	1.48 (1.48)	15.0 (14.8)	0.79	50.0

* : Consideration of dry densities reduced by the indicated value with respect to the maximum dry density

^x : Values in brackets correspond to the values attained after (sample) preparation

⁺ : Calculated from values in brackets

Table A.2: Compilation of results obtained in swelling pressure experiments (comprising COXc, grain- and powder mixture)

Sample ID		Final material parameters						Experi- ment dura- tion
		Exp. Min- eral Dry density*	Final wa- ter content	Final void ratio [#]	Final de- gree of satura- tion ⁺	Maximum swelling pressure	Final swelling pressure	
		<i>EDD</i>	<i>w_{fin}</i>	<i>e_{fin}</i>	<i>S_{fin}</i>	$\sigma_{s, max.}$	$\sigma_{s, fin.}$	
		[Mg/m ³]	[%]	[-]	[%]	[kPa]	[kPa]	
1	COX – 1111 – 2	0.81 (0.75)	-	-	-	139	125	3480
2	COX – 2121 – 1	0.92 (0.93)	17.7	0.46	102.0	343	343	9950
3	COX – 1221 – 2	0.92 (0.88)	17.4	0.49	95.0	192	192	8550
4	COX – 2321 – 1	0.92 (0.88)	19.2	0.47	103.0	106	106	9005
5	CMX – 1111 – 1	0.93 (0.86)	-	-	-	131	122	11500
6	CMX – 2121 – 1	1.17 (1.18)	24.4	0.64	101.0	660	660	9950
7	CMX – 1131 – 3	1.10 (1.10)	23.7	0.63	99.0	532	515	7350
8	CMX – 2141 – 1	1.01 (1.02)	30.7	0.79	103.0	229	229	9850
9	CMX – 2151 – 1	0.83 (0.82)	37.2	0.96	103.0	107	107	9850
10	CMX – 2221 – 2	1.17 (1.19)	23.6	0.62	101.0	620	619	10250
11	CMX – 1231 – 3	1.10 (1.11)	23.4	0.67	93.0	516	516	8550
12	CMX – 2241 – 1	1.01 (0.99)	28.8	0.75	102.0	290	256	10250
13	CMX – 2251 – 1	0.83 (0.81)	37.5	0.98	101.0	182	156	9950
14	CMX – 2321 – 1	1.17 (1.15)	24.6	0.65	101.0	575	575	9000
15	CMX – 1331 – 3	1.10 (1.10)	25.5	0.69	98.0	431	425	20050
16	CMX – 2341 – 1	1.01 (0.99)	28.9	0.76	100.0	279	255	9450
17	CMX – 2351 – 1	0.83 (0.82)	36.3	0.97	99.0	108	101	9450
18	CMX – 2112 – 1	1.03 (1.02)	-	-	-	219	219	11700
19	CMX – 2122 – 1	1.23 (1.21)	31.8	0.80	105.0	935	935	11700
20	CMX – 2132 – 1	1.18 (1.16)	25.0	0.64	103.0	649	647	9700
21	CMX – 2142 – 1	1.07 (1.09)	28.0	0.71	104.0	364	364	27300
22	CMX – 2152 – 1	0.88 (0.86)	36.1	0.91	105.0	157	157	27300
23	CMX – 2222 – 1	1.23 (1.20)	23.0	0.60	102.0	795	795	9480
24	CMX – 2232 – 1	1.18 (1.15)	24.0	0.63	100.0	681	681	9480
25	CMX – 2242 – 1	1.07 (1.06)	25.6	0.68	100.0	383	380	10015
26	CMX – 2252 – 1	0.88 (0.88)	33.4	0.88	100.0	164	145	10015
27	CMX – 2322 – 1	1.23 (1.21)	22.7	0.60	100.0	750	750	10250
28	CMX – 2332 – 1	1.18 (1.15)	24.1	0.68	93.0	674	674	10250
29	CMX – 2342 – 1	1.07 (1.06)	26.3	0.71	98.0	374	374	9800
30	CMX – 2352 – 1	0.88 (0.88)	33.9	0.88	101.0	133	129	9800

* : Values in brackets correspond to the values attained during sample preparation

: The difference between the initial and final void ratio was attributed to the imbibition of water from the bottom plate into the samples instantaneously ensuing when the swelling pressure cells were dismantled.

+ : Values greater than 100 % might be associated with the higher density of interlayer water in the smectitic fraction (Villar et al. (2012)); this phenomenon was not considered in this calculations, so the degree of saturation was computed taking the density of water as 1.0 Mg/m³.

References

- Adamson AW and Gast AP (1997) *Physical chemistry of surfaces*, 6th edn. Wiley, New York, Chichester.
- Agus SS, Arifin YF, Tripathy S and Schanz T (2013) Swelling pressure–suction relationship of heavily compacted bentonite–sand mixtures. *Acta Geotechnica* **8(2)**: 155–165, 10.1007/s11440-012-0189-0.
- Agus SS and Schanz T (2008) A method for predicting swelling pressure of compacted bentonites. *Acta Geotechnica* **3(2)**: 125–137, 10.1007/s11440-008-0057-0.
- Ahn H-S and Jo HY (2009) Influence of exchangeable cations on hydraulic conductivity of compacted bentonite. *Applied Clay Science* **44(1-2)**: 144–150, 10.1016/j.clay.2008.12.018.
- Aitchison GD (1965) *Moisture equilibria and moisture changes in soils beneath covered areas: A symposium in print*. Butterworths, Sydney.
- Al-Mukhtar M, Qi Y, Alcover J-F and Bergaya F (1999) Oedometric and water-retention behaviour of highly compacted unsaturated smectites. *Canadian Geotechnical Journal* **36(4)**: 675–684, 10.1139/t99-035.
- Alonso EE, Alcoverro J, Coste F et al. (2005a) The FEBEX benchmark test: case definition and comparison of modelling approaches. *International Journal of Rock Mechanics and Mining Sciences* **42(5-6)**: 611–638, 10.1016/j.ijrmms.2005.03.004.
- Alonso EE, Gens A and Josa A (1990) A constitutive model for partially saturated soils. *Géotechnique* **40(3)**: 405–430, 10.1680/geot.1990.40.3.405.

- Alonso EE, Gens A and Whight D (1987) General report. In *Groundwater Effects in Geotechnical Engineering* (Hanrahan ET, Orr TLL and Widdis TF (eds)). A. A. Balkema, Rotterdam, Brookfield, pp. 1087–1146.
- Alonso EE, Romero E, Hoffmann C and García-Escudero E (2005b) Expansive bentonite–sand mixtures in cyclic controlled-suction drying and wetting. *Engineering Geology* **81(3)**: 213–226, 10.1016/j.enggeo.2005.06.009.
- Alonso EE, Vaunat J and Gens A (1999) Modelling the mechanical behaviour of expansive clays. *Engineering Geology* **54(1-2)**: 173–183, 10.1016/S0013-7952(99)00079-4.
- ANDRA (2005) *Dossier 2005 Argile Synthesis: Evaluation of the feasibility of a geological repository in an argillaceous formation*. Meuse/ Haute-Marne site, Châtenay-Malabry.
- Armand G, Conil N, Talandier J and Seyedi DM (2017) Fundamental aspects of the hydromechanical behaviour of Callovo-Oxfordian claystone: From experimental studies to model calibration and validation. *Computers and Geotechnics* **85**: 277–286, 10.1016/j.compgeo.2016.06.003.
- Association Francaise de Normalisation (1991) *Soils: Investigation and testing*. Association Francaise de Normalisation (AFNOR).
- Association Francaise de Normalisation (1993) *Soils: Investigation and testing*. Association Francaise de Normalisation (AFNOR).
- Association Francaise de Normalisation (1995) *Sols: Reconnaissance et essais - Essai de gonflement à l'oedomètre - Détermination des déformations par chargement de plusieurs éprouvettes*. Association Francaise de Normalisation (AFNOR), La Plaine Saint-Denis CEDEX.
- Association Francaise de Normalisation (2014a) *Soils: Investigation and testing*. Association Francaise de Normalisation (AFNOR).
- Association Francaise de Normalisation (2014b) *Sols: Reconnaissance et essais - Détermination des références de compactage d'un matériau - Essai Proctor Normal - Essai Proctor modifié*. Association Francaise de Normalisation (AFNOR), La Plaine Saint-Denis CEDEX.
- Association Francaise de Normalisation (2017) *Reconnaissance et essais géotechniques - Essais de laboratoire sur les sols - Partie 5: Essai de chargement par parlier l'oedomètre*, 5th edn. Association Francaise de Normalisation (AFNOR), La Plaine Saint-Denis CEDEX.

- Association Francaise de Normalisation (2019) Reconnaissance et essais géotechniques - Essais de laboratoire sur les sols - Partie 11: Essais de perméabilité, 11th edn. Association Francaise de Normalisation (AFNOR), La Plaine Saint-Denis CEDEX.
- Baille W (2014) *Hydro-mechanical behaviour of clays - Significance of mineralogy*. PhD, Bochum.
- Baille W, Tripathy S and Schanz T (2010) Swelling pressures and one-dimensional compressibility behaviour of bentonite at large pressures. *Applied Clay Science* **48(3)**: 324–333, 10.1016/j.clay.2010.01.002.
- Benson CH and Trast JM (1995) Hydraulic conductivity of thirteen compacted clays. *Clays and Clay Minerals* **43(6)**: 669–681.
- Benson CH, Zhai H and Wang X (1994) Estimating Hydraulic Conductivity of Compacted Clay Liners. *Journal of Geotechnical Engineering* **120(2)**: 366–387, 10.1061/(ASCE)0733-9410(1994)120:2(366).
- Bérend I, Cases J-M, Francois M et al. (1995) Mechanism of adsorption and desorption of water vapor by homoionic montmorillonites: 2. The Li⁺, Na⁺, K⁺, Rb⁺, and Cs⁺-exchanged forms. *Clays and Clay Minerals* **43(3)**: 324–336.
- Bergaya F and Lagaly G (2013) General introduction: Clays, Clay minerals, and clay science. In *Handbook of clay science* (Bergaya F and Lagaly G (eds)). Elsevier, Amsterdam, vol. 5, pp. 2–17.
- Bishop AW and Donald IB (1961) The experimental study of partly saturated soil in triaxial apparatus. In *Proceedings of the 5th international conference on soil mechanics and foundation engineering*. Dunod, Paris, pp. 13–61.
- Bolt GH (1956) Physico-chemical analysis of the compressibility of pure clays. *Géotechnique* **6**: 86–93.
- Börgesson L, Gunnarsson D, Johannesson L-E and Sanden T (2002) *Äspö Hard Rock Laboratory: Prototype Repository - Installation of buffer, canisters, backfill and instruments in section 1*. Technical Report, Stockholm, IPR - 02 - 23.
- Börgesson L, Johannesson L-E and Gunnarsson D (2003) Influence of soil structure heterogeneities on the behaviour of backfill materials based on mixtures of bentonite and crushed rock. *Applied Clay Science* **23(1-4)**: 121–131, 10.1016/S0169-1317(03)00094-2.

- Bradbury MH and Baeyens B (2003) Porewater chemistry in compacted re-saturated MX-80 bentonite. *Journal of Contaminant Hydrology* **61(1-4)**: 329–338, 10.1016/S0169-7722(02)00125-0.
- Brigatti MF, Galan E and Theng BKG (2013) Structure and mineralogy of clay minerals. In *Handbook of clay science* (Bergaya F and Lagaly G (eds)). Elsevier, Amsterdam, vol. 5, pp. 21–68.
- Bucher F and Jedelhauser P (1985) *Verdichtungsversuche an Quarzsand-Bentonit-Gemischen*. Technischer Bericht 85-52, Zuerich.
- Caballero E, Jiménez de Cisneros C and Linares J (2004) Physicochemical properties of bentonite: Effect of the exchangeable cations. In *FEBEX II Project: THG Laboratory Experiments* (Missana T (ed.)), Madrid, pp. 40–51.
- Cases J-M, Bérend I, Francois M et al. (1997) Mechanism of adsorption and desorption of water vapor by homoionic montmorillonite: 3. The Mg²⁺, Ca²⁺, Sr²⁺ and Ba²⁺ exchanged forms. *Clays and Clay Minerals* **45(1)**: 8–22.
- Castellanos E, Villar MV, Romero E, Lloret A and Gens A (2008) Chemical impact on the hydro-mechanical behaviour of high-density FEBEX bentonite. *Physics and Chemistry of the Earth, Parts A/B/C* **33**: S516-S526, 10.1016/j.pce.2008.10.056.
- Chapman DL (1913) LI. A contribution to the theory of electrocapillarity. *The London, Edinburgh, and Dublin Philosophical Magazine and Journal of Science* **25(148)**: 475–481, 10.1080/14786440408634187.
- Chen FH (1988) *Foundations on expansive soils*. Elsevier, Amsterdam, etc.
- Chen YG, Sun Z, Cui YJ, Ye WM and Liu QH (2019) Effect of cement solutions on the swelling pressure of compacted GMZ bentonite at different temperatures. *Construction and Building Materials* **229**: 116872, 10.1016/j.conbuildmat.2019.116872.
- Chen YG, Zhu C, Ye WM, Cui YJ and Chen B (2016) Effects of solution concentration and vertical stress on the swelling behavior of compacted GMZ01 bentonite. *Applied Clay Science* **124-125**: 11–20, 10.1016/j.clay.2016.01.050.
- Chen YG, Zhu C, Ye WM, Cui YJ and Wang Q (2015) Swelling pressure and hydraulic conductivity of compacted GMZ01 bentonite under salinization–desalinization cycle conditions. *Applied Clay Science* **114**: 454–460, 10.1016/j.clay.2015.06.033.

- Chen Z-G, Tang CS, Zhu C, Shi B and Liu Y-M (2017) Compression, swelling and rebound behavior of GMZ bentonite/additive mixture under coupled hydro-mechanical condition. *Engineering Geology* **221**: 50–60, 10.1016/j.enggeo.2017.02.030.
- Chipera SJ, Carey JW and Bish DL (1998) Controlled-Humidity Xrd Analyses: Application to the Study of Smectite Expansion/Contraction. In *Advances in X-Ray Analysis* (Gilfrich JV, Jenkins R, Snyder RL et al. (eds)). Springer US, Boston, MA, pp. 713–722.
- Cho WJ, Lee JO and Chun KS (1999) The temperature effects on the hydraulic conductivity of compacted bentonite. *Applied Clay Science* **14**: 47–58.
- Conil N, Talandier J, Djizanne H et al. (2018) How rock samples can be representative of in situ condition: A case study of Callovo-Oxfordian claystones. *Journal of Rock Mechanics and Geotechnical Engineering* **10(4)**: 613–623, 10.1016/j.jrmge.2018.02.004.
- Cuevas J (2005) Geochemical reactions in FEBEX bentonite. In *ECOCLAY II - Effects of cement on clay barrier performance: Phase II*. Final report (Michau N (ed.)), pp. 105–117.
- Cui S-L, Zhang H-Y and Zhang M (2012) Swelling characteristics of compacted GMZ bentonite–sand mixtures as a buffer/backfill material in China. *Engineering Geology* **141-142**: 65–73, 10.1016/j.enggeo.2012.05.004.
- Cui YJ and Delage P (1996) Yielding and plastic behaviour of an unsaturated compacted silt. *Géotechnique* **46(2)**: 291–311, 10.1680/geot.1996.46.2.291.
- Cui YJ, Tang AM, Loiseau C and Delage P (2008) Determining the unsaturated hydraulic conductivity of a compacted sand–bentonite mixture under constant-volume and free-swell conditions. *Physics and Chemistry of the Earth, Parts A/B/C* **33**: 462–471, 10.1016/j.pce.2008.10.017.
- Cuisinier O, Deneele D and Masrouri F (2009) Shear strength behaviour of compacted clayey soils percolated with an alkaline solution. *Engineering Geology* **108(3-4)**: 177–188, 10.1016/j.enggeo.2009.07.012.
- Cuisinier O, Deneele D, Masrouri F, Abdallah A and Conil N (2014) Impact of high-pH fluid circulation on long term hydromechanical behaviour and microstructure of compacted clay from the laboratory of Meuse-Haute Marne (France). *Applied Clay Science* **88-89**: 1–9, 10.1016/j.clay.2013.12.008.

- Cuisinier O and Laloui L (2004) Fabric evolution during hydromechanical loading of a compacted silt. *International Journal for Numerical and Analytical Methods in Geomechanics* **28(6)**: 483–499, 10.1002/nag.348.
- Cuisinier O and Masrouri F (2005) Hydromechanical behaviour of a compacted swelling soil over a wide suction range. *Engineering Geology* **81(3)**: 204–212, 10.1016/j.enggeo.2005.06.008.
- Cuisinier O, Masrouri F, Pelletier M, Villieras F and Mosser-Ruck R (2008) Microstructure of a compacted soil submitted to an alkaline PLUME. *Applied Clay Science* **40(1-4)**: 159–170, 10.1016/j.clay.2007.07.005.
- Daniel DE (1982) Measurement of Hydraulic Conductivity of Unsaturated Soils with Thermocouple Psychrometers. *Soil Science Society of America Journal* **46(6)**: 1125–1129, 10.2136/sssaj1982.03615995004600060001x.
- Daniel DE and Benson CH (1990) Water Content-Density Criteria for Compacted Soil Liners. *Journal of Geotechnical Engineering* **116(12)**: 1811–1830, 10.1061/(ASCE)0733-9410(1990)116:12(1811).
- Darcy H (1856) *Les fontaines publiques de la ville de Dijon: Exposition et application des principes a suivre et des formules a employer dans les questions de distribution d'eau ; ouvrage terminé par un appendice relatif aux fournitures d'eau de plusieurs villes au filtrage des eaux et a la fabrication des tuyaux de fonte, de plomb, de tole et de bitume*. Victor Dalmont, Paris.
- Darde B, Tang AM, Pereira J-M et al. (2018) Hydro-mechanical behaviour of high-density bentonite pellet on partial hydration. *Géotechnique Letters* **8(4)**: 330–335, 10.1680/jgele.18.00114.
- Delage P, Howat MD and Cui YJ (1998) The relationship between suction and swelling properties in a heavily compacted unsaturated clay. *Engineering Geology* **50(1-2)**: 31–48, 10.1016/S0013-7952(97)00083-5.
- Delage P, Marcial D, Cui YJ and Ruiz X (2006) Ageing effects in compacted bentonite: A microstructure approach. *Géotechnique* **56(5)**: 291–304.
- Delage P, Romero E and Tarantino A (2008) Recent developments in the techniques of controlling and measuring suction in unsaturated soils. In *Unsaturated Soils. Advances in*

- Geo-Engineering* (Toll DG, Augarde CE, Gallipoli D and Wheeler SJ (eds)). CRC Press, pp. 33–52.
- Delage P, Vicol T and Suraj de Silva, G. P. R. (1992) Suction controlled testing of non-saturated soils with an osmotic consolidometer. In *The proceedings of the 7th international conference on expansive soils*. Texas Tech Universtiy Press, Lubbock, pp. 206–211.
- Derjaguin B and Landau L (1941) Theory of the stability of strongly charged lyophobic sols and of the adhesion of strongly charged particles in solutions of electrolytes. *Acta Physicochemica U.R.S.S.* **14**: 633–662, 10.1016/0079-6816(93)90013-L.
- Devineau K, Bihannic I, Michot L et al. (2006) In situ neutron diffraction analysis of the influence of geometric confinement on crystalline swelling of montmorillonite. *Applied Clay Science* **31(1-2)**: 76–84, 10.1016/j.clay.2005.08.006.
- Di Maio C (1996) Exposure of bentonite to salt solution: osmotic and mechanical effects. *Géotechnique* **46(4)**: 695–707, 10.1680/geot.1996.46.4.695.
- Di Maio C, Santoli L and Schiavone P (2004) Volume change behaviour of clays: the influence of mineral composition, pore fluid composition and stress state. *Mechanics of Materials* **36(5-6)**: 435–451, 10.1016/S0167-6636(03)00070-X.
- Diamond S (1971) Microstructure and Pore Structure of Impact-Compacted Clays. *Clays and Clay Minerals* **19(4)**: 239–249, 10.1346/CCMN.1971.0190405.
- Dixon DA (2000) *Porewater salinity and the development of swelling presure in bentonite-based buffer and backfill materials*, Helsinki, 2000-04.
- Dixon DA, Graham J and Gray MN (1999) Hydraulic conductivity of clays in confined tests under low hydraulic gradients. *Canadian Geotechnical Journal* **36(5)**: 815–825, 10.1139/t99-057.
- Dixon DA, Gray MN and Thomas AW (1985) A study of the compaction properties of potential clay—sand buffer mixtures for use in nuclear fuel waste disposal. *Engineering Geology* **21(3-4)**: 247–255, 10.1016/0013-7952(85)90015-8.
- Elert K, Pardo E and Rodriguez-Navarro C (2015) Mineralogical Evolution of Di- and Trioc-tahedral Smectites in Highly Alkaline Environments. *Clays and Clay Minerals* **63(6)**: 414–431, 10.1346/CCMN.2015.0630601.

- Emsley S, Olsson O, Stenberg L, Alheid H-J and Falls S (1997) *ZEDEX: A study of damage and disturbance from tunnel excavation by blasting and tunnel boring*. Technical Report, Stockholm, TR - 97 - 30.
- Fernández R, Ruiz AI and Cuevas J (2014) The role of smectite composition on the hyperalkaline alteration of bentonite. *Applied Clay Science* **95**: 83–94, 10.1016/j.clay.2014.03.015.
- Ferrage E, Lanson B, Sakharov BA and Drits VA (2005) Investigation of smectite hydration properties by modeling experimental X-ray diffraction patterns: Part I. Montmorillonite hydration properties. *American Mineralogist* **90(8-9)**: 1358–1374, 10.2138/am.2005.1776.
- Fredlund DG and Morgenstern NR (1977) Stress state variables for unsaturated soils. *Journal of the Geotechnical Engineering Division* **103(5)**: 447–466.
- Gaboreau S, Lerouge C, Dewonck S et al. (2012) In-situ interaction of cement paste and shotcrete with claystones in a deep disposal context. *American Journal of Science* **312(3)**: 314–356, 10.2475/03.2012.03.
- Gaboreau S, Prêt D, Tinseau E et al. (2011) 15 years of in situ cement–argillite interaction from Tournemire URL: Characterisation of the multi-scale spatial heterogeneities of pore space evolution. *Applied Geochemistry* **26(12)**: 2159–2171, 10.1016/j.apgeochem.2011.07.013.
- Gallipoli D, Gens A, Sharma R and Vaunat J (2003) An elasto-plastic model for unsaturated soil incorporating the effects of suction and degree of saturation on mechanical behavior. *Géotechnique* **53(1)**: 123–135, 10.1680/geot.2003.53.1.123.
- Gao Y and Sun DA (2017) Soil-water retention behavior of compacted soil with different densities over a wide suction range and its prediction. *Computers and Geotechnics* **91**: 17–26, 10.1016/j.compgeo.2017.06.016.
- Gao Y, Sun DA, Zhu Z and Xu Y (2019) Hydromechanical behavior of unsaturated soil with different initial densities over a wide suction range. *Acta Geotechnica* **14(2)**: 417–428, 10.1007/s11440-018-0662-5.
- Garcia-Bengochea I, Altschaeffl AG and Lovell CW (1979) Pore distribution and permeability of silty clays. *Journal of the Geotechnical Engineering Division* **105(7)**: 839–856.
- Gatabin C, Talandier J, Collin F, Charlier R and Dieudonné A-C (2016) Competing effects of volume change and water uptake on the water retention behaviour of a compacted MX-80

- bentonite/sand mixture. *Applied Clay Science* **121-122**: 57–62, 10.1016/j.clay.2015.12.019.
- Gaucher E, Robelin C, Matray JM et al. (2004) ANDRA underground research laboratory: interpretation of the mineralogical and geochemical data acquired in the Callovian–Oxfordian formation by investigative drilling. *Physics and Chemistry of the Earth, Parts A/B/C* **29(1)**: 55–77, 10.1016/j.pce.2003.11.006.
- Gens A and Alonso EE (1992) A framework for the behaviour of unsaturated expansive clays. *Canadian Geotechnical Journal* **29(6)**: 1013–1032, 10.1139/t92-120.
- Gens A, Sánchez M, Guimarães LDN et al. (2009) A full-scale in situ heating test for high-level nuclear waste disposal: observations, analysis and interpretation. *Géotechnique* **59(4)**: 377–399.
- Gens A, Valleján B, Sánchez M et al. (2011) Hydromechanical behavior of a heterogeneous compacted soil: Experimental observations and modelling. *Géotechnique* **61(5)**: 367–386, 10.1680/geot.SIP11.P.015.
- Gens A, Valleján B, Zandarín MT and Sánchez M (2013) Homogenization in clay barriers and seals: Two case studies. *Journal of Rock Mechanics and Geotechnical Engineering* **5(3)**: 191–199, 10.1016/j.jrmge.2013.04.003.
- Goudarzi R (2019) *Prototype Repository: Sensor data report (Period 010917-180101)*. Report No 29, Solna, P - 18 - 22.
- Gouy M (1910) Sur la constitution de la charge électrique à la surface d'un électrolyte. *Journal de Physique Théorique et Appliquée* **9(1)**: 457–468, 10.1051/jphys-tap:019100090045700.
- Graham J, Saadat F, Gray MN, Dixon DA and Zhang Q-Y (1989) Strength and volume change behavior. *Canadian Geotechnical Journal* **26**: 292–305.
- Gregg SJ and Sing KSW (1969) *Adsorption, surface area and porosity*. Academic Press, London.
- Grim RE (1962) *Applied clay mineralogy*. McGraw-Hill, New York.
- Gunnarsson D, Börgesson L, Hökmark H, Johannesson L-E and Sanden T (2001) *Äspö Hard Rock Laboratory: Installation of the Backfill and Plug test*. Technical Report, Stockholm, IPR - 01 - 17.

- Herbert H-J, Kasbohm J, Moog HC and Henning K-H (2004) Long-term behaviour of the Wyoming bentonite MX-80 in high saline solutions. *Applied Clay Science* **26(1-4)**: 275–291, 10.1016/j.clay.2003.12.028.
- Herbert H-J, Kasbohm J, Sprenger H, Fernández AM and Reichelt C (2008) Swelling pressures of MX-80 bentonite in solutions of different ionic strength. *Physics and Chemistry of the Earth, Parts A/B/C* **33**: S327-S342, 10.1016/j.pce.2008.10.005.
- Hoffmann C, Alonso EE and Romero E (2007) Hydro-mechanical behaviour of bentonite pellet mixtures. *Physics and Chemistry of the Earth, Parts A/B/C* **32(8-14)**: 832–849, 10.1016/j.pce.2006.04.037.
- Hofmann H, Bauer A and Warr LN (2004) Behavior of Smectite In Strong Salt Brines Under Conditions Relevant to the Disposal of Low- to Medium-grade Nuclear Waste. *Clays and Clay Minerals* **52(1)**: 14–24, 10.1346/CCMN.2004.0520102.
- Huertas F, Farias J, Griffault L et al. (2000) *ECOCLAY I - Effects of cement on clay barrier performance*. Final report. Off. for Off. Publ. of the Europ. Communities, Luxembourg.
- Imbert C and Villar MV (2006) Hydro-mechanical response of a bentonite pellets/powder mixture upon infiltration. *Applied Clay Science* **32(3-4)**: 197–209, 10.1016/j.clay.2006.01.005.
- International Atomic Energy Agency (2009) *Classification of radioactive waste: General safety guide*. International Atomic Energy Agency, Vienna.
- International Atomic Energy Agency (2011) *Disposal of radioactive waste: Specific safety requirements*. International Atomic Energy Agency, Vienna.
- ISO (2009) Particle size analysis.
- Iyer KKR, Joseph J, Lopes, B. C. F. L., Singh DN and Tarantino A (2018) Water retention characteristics of swelling clays in different compaction states. *Geomechanics and Geoengeering* **13(2)**: 88–103, 10.1080/17486025.2017.1396363.
- Johannesson L-E and Hagman P (2013) *Äspö Hard Rock Laboratory: Prototype Repository - Method for opening and retrieval of the outer section*. Technical Report, Stockholm, P - 13 - 15.
- Juang CH and Holtz RD (1986) A probabilistic permeability model and the pore size density function. *International Journal for Numerical and Analytical Methods in Geomechanics* **10(5)**: 543–553, 10.1002/nag.1610100506.

- Karnland O (1997) *Bentonite swelling pressure in strong NaCl solutions – Correlation between model calculations and experimentally determined data*. Technical Report, Stockholm, TR - 97 - 31.
- Karnland O, Nilsson U, Weber H and Wersin P (2008) Sealing ability of Wyoming bentonite pellets foreseen as buffer material – Laboratory results. *Physics and Chemistry of the Earth, Parts A/B/C* **33**: S472-S475, 10.1016/j.pce.2008.10.024.
- Karnland O, Olsson S and Nilsson U (2006) *Mineralogy and sealing properties of various bentonites and smectite-rich clay materials*. Technical Report, Stockholm, TR - 06 - 30.
- Karnland O, Olsson S, Nilsson U and Sellin P (2007) Experimentally determined swelling pressures and geochemical interactions of compacted Wyoming bentonite with highly alkaline solutions. *Physics and Chemistry of the Earth, Parts A/B/C* **32(1-7)**: 275–286, 10.1016/j.pce.2006.01.012.
- Kassiff G and Ben Shalom A (1971) Experimental Relationship Between Swell Pressure and Suction. *Géotechnique* **21(3)**: 245–255, 10.1680/geot.1971.21.3.245.
- Keto P, Kuula-Vaeisaenen P and Ruuskanen J (2006) *Effect of Material Parameters on the Compactibility of Backfill Materials*. Working Report 2006-34, Olkiluoto.
- Kjellander R, Marcelja S, Pashley RM and Quirk JP (1988) Double-layer ion correlation forces restrict calcium-clay swelling. *The Journal of Physical Chemistry* **92(23)**: 6489–6492, 10.1021/j100334a005.
- Komine H (2004) Simplified evaluation on hydraulic conductivities of sand–bentonite mixture backfill. *Applied Clay Science* **26(1-4)**: 13–19, 10.1016/j.clay.2003.09.006.
- Komine H (2010) Predicting hydraulic conductivity of sand–bentonite mixture backfill before and after swelling deformation for underground disposal of radioactive wastes. *Engineering Geology* **114(3-4)**: 123–134, 10.1016/j.enggeo.2010.04.009.
- Komine H and Ogata N (1999) Experimental study on swelling characteristics of sand-bentonite mixture for nuclear waste disposal. *Soils and Foundation* **39(2)**: 83–97.
- Komine H and Ogata N (2004) Predicting Swelling Characteristics of Bentonites. *Journal of Geotechnical and Geoenvironmental Engineering* **130(8)**: 818–829, 10.1061/(ASCE)1090-0241(2004)130:8(818).
- Komine H, Yasuhara K and Murakami S (2009) Swelling characteristics of bentonites in artificial seawater. *Canadian Geotechnical Journal* **46(2)**: 177–189, 10.1139/T08-120.

- Krauskopf KB (1956) Dissolution and precipitation of silica at low temperatures. *Geochemica et Cosmochemica Acta* **10**: 1–26.
- Lang LZ, Tripathy S, Baille W, Schanz T and Sridharan A (2019) Linkage between swelling pressure, total suction of saturated bentonites and suction of saturating aqueous solutions. *Applied Clay Science* **171**: 82–91, 10.1016/j.clay.2019.02.007.
- Lee J-M and Shackelford CD (2005) Impact of Bentonite Quality on Hydraulic Conductivity of Geosynthetic Clay Liners. *Journal of Geotechnical and Geoenvironmental Engineering* **131**(1): 64–77, 10.1061/(ASCE)1090-0241(2005)131:1(64).
- Leverd PC, Mekki S, Launeau F and Landais P (2017) *Physical protection specificities of a deep geological disposal: The case of the French Project Cigéo*, Vienna.
- Likos WJ and Wayllace A (2010) Porosity evolution of free and confined bentonites during interlayer hydration. *Clays and Clay Minerals* **58**(3): 399–414, 10.1346/CCMN.2010.0580310.
- Lippens BC and Boer JH de (1965) Studies on pore systems in catalysts: V. The t method. *Journal of Catalysis* **4**(3): 319–323.
- Lloret A and Villar MV (2007) Advances on the knowledge of the thermo-hydro-mechanical behaviour of heavily compacted “FEBEX” bentonite. *Physics and Chemistry of the Earth, Parts A/B/C* **32**(8-14): 701–715, 10.1016/j.pce.2006.03.002.
- Lloret A, Villar MV, Sánchez M et al. (2003) Mechanical behaviour of heavily compacted bentonite under high suction changes. *Géotechnique* **53**(1): 27–40, 10.1680/geot.53.1.27.37258.
- Madsen FT (1998) Clay mineralogical investigations related to nuclear waste disposal. *Clay Minerals* **33**(1): 109–129, 10.1180/000985598545318.
- Madsen FT and Müller-Vonmoos M (1989) The swelling behaviour of clays. *Applied Clay Science* **4**(2): 143–156, 10.1016/0169-1317(89)90005-7.
- Marcial D, Delage P and Cui YJ (2002) On the high stress compression of bentonites. *Canadian Geotechnical Journal* **39**(4): 812–820, 10.1139/t02-019.
- Martín PL and Barcala JM (2005) Large scale buffer material test: Mock-up experiment at CIEMAT. *Engineering Geology* **81**(3): 298–316, 10.1016/j.enggeo.2005.06.013.

- Masrouri F, Cuisinier O, Abdallah A, Pelletier M and Ruck Mosser R (2005) *Projet HAVL – Argile: Détermination expérimentale des propriétés hydromécaniques de matériaux de remblais à base d’argilites*. Rapport des tâches 2 et 3, Vandoeuvre-lès-Nancy.
- Massat L, Cuisinier O, Bihannic I et al. (2016) Swelling pressure development and inter-aggregate porosity evolution upon hydration of a compacted swelling clay. *Applied Clay Science* **124-125**: 197–210, 10.1016/j.clay.2016.01.002.
- Mata C (2003) *Hydraulic behavior of bentonite based mixtures in engineered barriers: The backfill and plug test at the Aespoe HRL (Sweden)*. PhD Thesis, Barcelona.
- Mata C and Ledesma A (2003) Permeability of a bentonite-crushed granite rock mixture using different experimental techniques. *Geotechnique* **53(8)**: 747–758.
- Matyas EL and Radhakrishna HS (1968) Volume Change Characteristics of Partially Saturated Soils. *Géotechnique* **18(4)**: 432–448, 10.1680/geot.1968.18.4.432.
- Meerdink JS, Benson CH and Khire MV (1996) Unsaturated Hydraulic Conductivity of Two Compacted Barrier Soils. *Journal of Geotechnical Engineering* **122(7)**: 565–576, 10.1061/(ASCE)0733-9410(1996)122:7(565).
- Meunier A (2010) *Clays*. Springer-Verlag Berlin Heidelberg, New York.
- Michau N (ed.) (2005) *ECOCLAY II - Effects of cement on clay barrier performance: Phase II*. Final report.
- Michot LJ, Bihannic I, Thomas F et al. (2013) Coagulation of Na-montmorillonite by inorganic cations at neutral pH. A combined transmission X-ray microscopy, small angle and wide angle X-ray scattering study. *Langmuir* **29(10)**: 3500–3510, 10.1021/la400245n.
- Michot LJ and Villiéras F (2013) Surface Area and Porosity. In *Handbook of clay science* (Bergaya F and Lagaly G (eds)). Elsevier, Amsterdam, vol. 5, pp. 319–332.
- Middelhoff M, Cuisinier O, Masrouri F, Talandier J and Conil N (2020) Combined impact of selected material properties and environmental conditions on the swelling pressure of compacted claystone/bentonite mixtures. *Applied Clay Science* **184**: 105389, 10.1016/j.clay.2019.105389.
- Mitchell JK and Soga K (2005) *Fundamentals of soil behavior*, 3rd edn. John Wiley & Sons, Hoboken, N.J.

- Molinero Guerra A, Aïmediou P, Bornert M et al. (2018) Analysis of the structural changes of a pellet/powder bentonite mixture upon wetting by X-ray computed microtomography. *Applied Clay Science* **165**: 164–169, 10.1016/j.clay.2018.07.043.
- Monroy R, Zdravkovic L and Ridley A (2010) Evolution of microstructure in compacted London Clay during wetting and loading. *Géotechnique* **60(2)**: 105–119, 10.1680/geot.8.P.125.
- Müller-Vonmoos M and Kahr G (1983) *Mineralogische Untersuchungen von Wyoming Bentonit MX-80 und Montigel*, Zurich, TB -83 - 12.
- Musso G, Romero E and Della Vecchia G (2013) Double-structure effects on the chemo-hydro-mechanical behaviour of a compacted active clay. *Géotechnique* **63(3)**: 206–220, 10.1680/geot.SIP13.P.011.
- Nagaraj HB, Munnas MM and Sridharan A (2009) Critical Evaluation of Determining Swelling Pressure by Swell-Load Method and Constant Volume Method. *Geotechnical Testing Journal* **32(4)**: 1–10, 10.1520/GTJ102051.
- Nagaraj TS, Murthy BRS, Vatsala A and Joshi RC (1990) Analysis of Compressibility of Sensitive Soils. *Journal of Geotechnical Engineering* **116(1)**: 105–118, 10.1061/(ASCE)0733-9410(1990)116:1(105).
- Norrish K (1954) The swelling of montmorillonite. *Discussions of the Faraday Society* **18**: 120, 10.1039/DF9541800120.
- Nowamooz H and Masroufi F (2008) Hydromechanical behaviour of an expansive bentonite/silt mixture in cyclic suction-controlled drying and wetting tests. *Engineering Geology* **101(3-4)**: 154–164, 10.1016/j.enggeo.2008.04.011.
- Nowamooz H and Masroufi F (2009) Density-dependent hydromechanical behaviour of a compacted expansive soil. *Engineering Geology* **106(3-4)**: 105–115, 10.1016/j.enggeo.2009.03.010.
- Nowamooz H and Masroufi F (2010) Relationships between soil fabric and suction cycles in compacted swelling soils. *Engineering Geology* **114(3-4)**: 444–455, 10.1016/j.enggeo.2010.06.005.
- Olsson S, Jensen S, Johannesson L-E et al. (2013) *Prototype Repository: Hydro-mechanical, chemical and mineralogical characterization of the buffer and tunnel backfill material from the outer section of the Prototype Repository*, Stockholm, TR - 13 - 21.

- Orsini L and Remy JC (1976) Utilisation du chlorure de cobaltihexammine pour la détermination simultanée de la capacité d'échange et des bases échangeables des sols. *Bulletin de l'AFES Science du Sol* **4**: 269–275.
- Priyanto DG, Man AG, Blatz JA and Dixon DA (2011) Hydro-mechanical constitutive model for unsaturated compacted bentonite–sand mixture (BSM): Laboratory tests, parameter calibrations, modifications, and applications. *Physics and Chemistry of the Earth, Parts A/B/C* **36(17-18)**: 1770–1782, 10.1016/j.pce.2011.10.007.
- Proctor RR (1933) Design and construction of rolled earth dams. *Engineering News Record* **3**: 245 - 248, 286 - 289, 348 - 351, 372 - 376.
- Pusch R (1980) *Swelling pressure of highly compacted bentonite*. Technical Report, Stockholm, TR - 80 - 13.
- Pusch R (1983) *Use of clay as buffer in radioactive repositories*. Technical Report, Stockholm, 83 - 46.
- Pusch R (1992) Use of bentonite for isolation of radioactive waste products. *Clay Minerals* **27(3)**: 353–361, 10.1180/claymin.1992.027.3.08.
- Pusch R (1995) *Consequences of using crushed crystalline rock as ballast in KBS-3 tunnels instead of rounded quartz particles*. Technical Report, Stockholm, 95 - 14.
- Pusch R (2001a) *Experimental study of the effect of high porewater salinity on the physical properties of a natural smectite clay*. Technical Report, Stockholm, TR - 01 - 07.
- Pusch R (2001b) *The microstructure of MX80 clay with respect to its bulk properties under different environmental conditions*. Technical report, Stockholm, TR - 01 - 08.
- Pusch R and Yong RN (2003) Water saturation and retention of hydrophilic clay buffer—microstructural aspects. *Applied Clay Science* **23(1-4)**: 61–68, 10.1016/S0169-1317(03)00087-5.
- Pusch R, Zwahr H, Gerber R and Schomburg J (2003) Interaction of cement and smectitic clay—theory and practice. *Applied Clay Science* **23(1-4)**: 203–210, 10.1016/S0169-1317(03)00104-2.
- Ramírez S, Vieillard P, Bouchet A et al. (2005) Alteration of the Callovo–Oxfordian clay from Meuse-Haute Marne underground laboratory (France) by alkaline solution. I. A XRD and CEC study. *Applied Geochemistry* **20(1)**: 89–99, 10.1016/j.apgeochem.2004.03.009.

- Rao SM and Thyagaraj T (2007) Swell–compression behaviour of compacted clays under chemical gradients. *Canadian Geotechnical Journal* **44(5)**: 520–532, 10.1139/t07-002.
- Rao SM, Thyagaraj T and Raghuvver Rao P (2013) Crystalline and Osmotic Swelling of an Expansive Clay Inundated with Sodium Chloride Solutions. *Geotechnical and Geological Engineering* **31(4)**: 1399–1404, 10.1007/s10706-013-9629-3.
- Rao SN and Mathew PK (1995) Effects of exchangeable cations on hydraulic conductivity of marine clay. *Clays and Clay Minerals* **43(4)**: 433–437.
- Rawat A, Baille W and Tripathy S (2019) Swelling behavior of compacted bentonite-sand mixture during water infiltration. *Engineering Geology* **257**: 105141, 10.1016/j.enggeo.2019.05.018.
- Richards LA (1941) A pressure - membrane extraction apparatus for soil solution. *Soil science* **51(5)**: 371–386.
- Robinet J-C, Sardini P, Coelho D et al. (2012) Effects of mineral distribution at mesoscopic scale on solute diffusion in a clay-rich rock: Example of the Callovo-Oxfordian mudstone (Bure, France). *Water Resources Research* **48(5)**: 819, 10.1029/2011WR011352.
- Romero E (1999) *Characterisation and thermo-hydro-mechanical behaviour of unsaturated boom clay: An experimental study*. PhD-Thesis. Universitat Politècnica de Catalunya, Barcelona.
- Romero E (2013) A microstructural insight into compacted clayey soils and their hydraulic properties. *Engineering Geology* **165**: 3–19, 10.1016/j.enggeo.2013.05.024.
- Romero E, Gens A and Lloret A (1999) Water permeability, water retention and microstructure of unsaturated compacted Boom clay. *Engineering Geology* **54(1-2)**: 117–127, 10.1016/S0013-7952(99)00067-8.
- Romero E, Gens A and Lloret A (2003) Suction effects on a compacted clay under non-isothermal conditions. *Géotechnique* **53(1)**: 65–81, 10.1680/geot.2003.53.1.65.
- Romero E and Simms PH (2008) Microstructure Investigation in Unsaturated Soils: A Review with Special Attention to Contribution of Mercury Intrusion Porosimetry and Environmental Scanning Electron Microscopy. *Geotechnical and Geological Engineering* **26(6)**: 705–727, 10.1007/s10706-008-9204-5.

- Saba S, Cui YJ, Tang AM and Barnichon J-D (2014) Investigation of the swelling behaviour of compacted bentonite–sand mixture by mock-up tests. *Canadian Geotechnical Journal* **51(12)**: 1399–1412, 10.1139/cgj-2013-0377.
- Saiyouri N, Tessier D and Hicher PY (2004) Experimental study of swelling in unsaturated compacted clays. *Clay Minerals* **39(04)**: 469–479, 10.1180/0009855043940148.
- Sánchez M, Gens A, do Nascimento Guimarães L and Olivella S (2005) A double structure generalized plasticity model for expansive materials. *International Journal for Numerical and Analytical Methods in Geomechanics* **29(8)**: 751–787, 10.1002/nag.434.
- Schanz T and Al-Badran Y (2014) Swelling pressure characteristics of compacted Chinese Gaomiaozhi bentonite GMZ01. *Soils and Foundation* **54(4)**: 748–759, 10.1016/j.sandf.2014.06.026.
- Schanz T and Tripathy S (2009) Swelling pressure of a divalent-rich bentonite: Diffuse double-layer theory revisited. *Water Resources Research* **45(5)**: 1752, 10.1029/2007WR006495.
- Schofield AN and Wroth P (1968) *Critical state soil mechanics*. McGraw-Hill, London, New York.
- Siddiqua S, Blatz J and Siemens G (2011) Evaluation of the impact of pore fluid chemistry on the hydromechanical behaviour of clay-based sealing materials. *Canadian Geotechnical Journal* **48(2)**: 199–213, 10.1139/T10-064.
- Sivakumar V, Tan WC, Murray EJ and McKinley JD (2006) Wetting, drying and compression characteristics of compacted clay. *Géotechnique* **56(1)**: 57–62, 10.1680/geot.2006.56.1.57.
- Sposito G (1992) The diffuse-ion swarm near smectite particles suspended in 1:1 electrolyte solutions (Modified Gouy-Chapman theory and quasicrystal formation). In *CMS Workshop Lectures: Clay Water Interface and its Rheological Implications* (Güven N and Pollastro RM (eds)). The Clay Mineral Society (CMS), Boulder, vol. 4, pp. 128–152.
- Sridharan A and Choudhury D (2002) Swelling pressure of sodium montmorillonites. *Géotechnique* **52(6)**: 459–462, 10.1680/geot.2002.52.6.459.
- Sridharan A, Rao AS and Murthy NS (1986a) Compressibility behavior of homoionized bentonites. *Geotechnique* **36(4)**: 551–564.

- Sridharan A, Rao AS and Sivapullaiah PV (1986b) Swelling Pressure of Clays. *Geotechnical Testing Journal* **9(1)**: 24–33, 10.1520/GTJ10608J.
- Srikanth V and Mishra AK (2016) A Laboratory Study on the Geotechnical Characteristics of Sand–Bentonite Mixtures and the Role of Particle Size of Sand. *International Journal of Geosynthetics and Ground Engineering* **2(1)**: 263, 10.1007/s40891-015-0043-1.
- Sun DA, Sheng DC, Cui HB and Sloan SW (2007) A density-dependent elastoplastic hydro-mechanical model for unsaturated compacted soils. *International Journal for Numerical and Analytical Methods in Geomechanics* **31(11)**: 1257–1279, 10.1002/nag.579.
- Tang CS, Tang AM, Cui YJ et al. (2011a) A study of the hydro-mechanical behaviour of compacted crushed argillite. *Engineering Geology* **118(3-4)**: 93–103, 10.1016/j.enggeo.2011.01.004.
- Tang CS, Tang AM, Cui YJ et al. (2011b) Investigating the swelling pressure of compacted crushed-Callovo-Oxfordian claystone. *Physics and Chemistry of the Earth, Parts A/B/C* **36(17-18)**: 1857–1866, 10.1016/j.pce.2011.10.001.
- Tang CS, Tang AM, Cui YJ, Delage P and Shi B (2010) The coupled hydro-mechanical behaviours of compacted crushed Callovo-Oxfordian argillite. *Journal of Rock Mechanics and Geotechnical Engineering*(**2**): 86–90.
- Tarantino A and Col E de (2008) Compaction behaviour of clay. *Géotechnique* **58(3)**: 199–213, 10.1680/geot.2008.58.3.199.
- Thommes M, Kaneko K, Neimark AV et al. (2015) Physisorption of gases, with special reference to the evaluation of surface area and pore size distribution (IUPAC Technical Report). *Pure and Applied Chemistry* **87(9-10)**: 1051–1069, 10.1515/pac-2014-1117.
- Tombácz E and Szekeres M (2004) Colloidal behavior of aqueous montmorillonite suspensions: the specific role of pH in the presence of indifferent electrolytes. *Applied Clay Science* **27(1-2)**: 75–94, 10.1016/j.clay.2004.01.001.
- Tombácz E and Szekeres M (2006) Surface charge heterogeneity of kaolinite in aqueous suspension in comparison with montmorillonite. *Applied Clay Science* **34(1-4)**: 105–124, 10.1016/j.clay.2006.05.009.
- Tripathy S and Schanz T (2007) Compressibility behaviour of clays at large pressures. *Canadian Geotechnical Journal* **44(3)**: 355–362, 10.1139/t06-123.

- van Geet M, Volckaert G and Roels S (2005) The use of microfocus X-ray computed tomography in characterising the hydration of a clay pellet/powder mixture. *Applied Clay Science* **29(2)**: 73–87, 10.1016/j.clay.2004.12.007.
- van Olphen H (1980) *An introduction to clay colloid chemistry: For clay technologists, geologists and soil scientists*, 2nd edn. Wiley, New York, N.Y., [etc.].
- Verwey EJW and Overbeek JTG (1948) *Theory of the stability of lyophobic colloids: The interaction of sol particles having an electric double layer*. Elsevier, Amsterdam.
- Villar MV (2002) *Thermo-hydro-mechanical characterization of a bentonite from Cabo de Gata: A study applied to the use of bentonite as sealing material in high level radioactive waste repositories*. PhD-Thesis, Madrid.
- Villar MV (2004) *MX80 Bentonite: Thermo-Hydro-Mechanical Characterization performed at CIEMAT in the context of the Prototype project*.
- Villar MV (2006) Infiltration tests on a granite/bentonite mixture: Influence of water salinity. *Applied Clay Science* **31(1-2)**: 96–109, 10.1016/j.clay.2005.07.007.
- Villar MV (2007) Water retention of two natural compacted bentonites. *Clays and Clay Minerals* **55(3)**: 311–322, 10.1346/CCMN.2007.0550307.
- Villar MV, Gómez-Espina R and Gutiérrez-Nebot L (2012) Basal spacings of smectite in compacted bentonite. *Applied Clay Science* **65-66**: 95–105, 10.1016/j.clay.2012.05.010.
- Villar MV and Lloret A (2008) Influence of dry density and water content on the swelling of a compacted bentonite. *Applied Clay Science* **39(1-2)**: 38–49, 10.1016/j.clay.2007.04.007.
- Villar MV, Martín PL, Romero FJ, Iglesias RJ and Gutiérrez-Rodrigo V (2016) Saturation of barrier materials under thermal gradient. *Geomechanics for Energy and the Environment* **8**: 38–51, 10.1016/j.gete.2016.05.004.
- Villar MV and Rivas P (1994) Hydraulic properties of montmorillonite-quartz and saponite-quartz mixtures. *Applied Clay Science* **9(1)**: 1–9, 10.1016/0169-1317(94)90011-6.
- Wang G and Wei X (2015) Modeling swelling–shrinkage behavior of compacted expansive soils during wetting–drying cycles. *Canadian Geotechnical Journal* **52(6)**: 783–794, 10.1139/cgj-2014-0059.
- Wang Q, Cui YJ, Tang AM et al. (2013a) Hydraulic conductivity and microstructure changes of compacted bentonite/sand mixture during hydration. *Engineering Geology* **164**: 67–76, 10.1016/j.enggeo.2013.06.013.

- Wang Q, Cui YJ, Tang AM et al. (2014) Long-term effect of water chemistry on the swelling pressure of a bentonite-based material. *Applied Clay Science* **87**: 157–162, 10.1016/j.clay.2013.10.025.
- Wang Q, Tang AM, Cui YJ, Barnichon J-D and Ye WM (2013b) Investigation of the hydro-mechanical behaviour of compacted bentonite/sand mixture based on the BExM model. *Computers and Geotechnics* **54**: 46–52, 10.1016/j.compgeo.2013.05.011.
- Wang Q, Tang AM, Cui YJ, Delage P and Gatmiri B (2012) Experimental study on the swelling behaviour of bentonite/claystone mixture. *Engineering Geology* **124**: 59–66, 10.1016/j.enggeo.2011.10.003.
- Wind GP (1966) Capillary conductivity data estimated by a simple method. In *Water in the unsaturated zone* (Institute for land and water management research (ed.)), pp. 183–197.
- Xiang G, Xu Y, Yu F, Fang Y and Wang Y (2019) Prediction of swelling characteristics of compacted GMZ bentonite in salt solution incorporating ion-exchange reactions. *Clays and Clay Minerals* **67(2)**: 163–172, 10.1007/s42860-019-00014-3.
- Xu L, Ye WM, Chen B, Chen YG and Cui YJ (2016) Experimental investigations on thermo-hydro-mechanical properties of compacted GMZ01 bentonite-sand mixture using as buffer materials. *Engineering Geology* **213**: 46–54, 10.1016/j.enggeo.2016.08.015.
- Ye WM, Borrell NC, Zhu JY, Chen B and Chen YG (2014a) Advances on the investigation of the hydraulic behavior of compacted GMZ bentonite. *Engineering Geology* **169**: 41–49, 10.1016/j.enggeo.2013.11.003.
- Ye WM, Zheng ZJ, Chen B et al. (2014b) Effects of pH and temperature on the swelling pressure and hydraulic conductivity of compacted GMZ01 bentonite. *Applied Clay Science* **101**: 192–198, 10.1016/j.clay.2014.08.002.
- Yigzaw ZG, Cuisinier O, Massat L and Masrouri F (2016) Role of different suction components on swelling behavior of compacted bentonites. *Applied Clay Science* **120**: 81–90, 10.1016/j.clay.2015.11.022.
- Yong RN (1999) Soil suction and soil-water potentials in swelling clays in engineered clay barriers. *Engineering Geology* **54(1-2)**: 3–13, 10.1016/S0013-7952(99)00056-3.
- Yong RN and Warkentin BP (1975) *Soil properties and behaviour*. Elsevier, Amsterdam.

- Yuan S, Buzzi O, Liu X and Vaunat J (2019) Swelling behaviour of compacted Maryland clay under different boundary conditions. *Géotechnique* **69(6)**: 514–525, 10.1680/jgeot.17.P.140.
- Yuan S, Liu X, Sloan SW and Buzzi O (2016) Multi-scale characterization of swelling behaviour of compacted Maryland clay. *Acta Geotechnica* **11(4)**: 789–804, 10.1007/s11440-016-0457-5.
- Yven B, Sammartino S, Geraud Y and Villieras F (2007) Mineralogy, texture and porosity of Callovo-Oxfordian argillites of the Meuse/ Haute-Marne region eastern Paris Basin). *Bulletin de la Societe Geologique de France*: 73–90.
- Zeng Z, Cui YJ, Zhang F, Conil N and Talandier J (2019) Investigation of swelling pressure of bentonite/claystone mixture in the full range of bentonite fraction. *Applied Clay Science* **178**: 105137, 10.1016/j.clay.2019.105137.
- Zhang C-L and Kröhn K-P (2019) Sealing behaviour of crushed claystone–bentonite mixtures. *Geomechanics for Energy and the Environment* **17**: 90–105, 10.1016/j.gete.2018.09.004.
- Zhou A-N, Sheng D, Sloan SW and Gens A (2012) Interpretation of unsaturated soil behaviour in the stress–saturation space. *Computers and Geotechnics* **43**: 111–123, 10.1016/j.compgeo.2012.02.009.
- Zhou A-N and Sheng DC (2015) An advanced hydro-mechanical constitutive model for unsaturated soils with different initial densities. *Computers and Geotechnics* **63**: 46–66, 10.1016/j.compgeo.2014.07.017.
- Zhu C-M, Ye WM, Chen YG, Chen B and Cui YJ (2013) Influence of salt solutions on the swelling pressure and hydraulic conductivity of compacted GMZ01 bentonite. *Engineering Geology* **166**: 74–80, 10.1016/j.enggeo.2013.09.001.

Résumé détaillé

Contexte

Cette étude se situe dans le cadre du projet français Cigéo de stockage de déchets radioactifs de moyenne et haute activité situés dans une formation rocheuse sédimentaire riche en argile, les argilites du Callovo-Oxfordien. Dans ce contexte, ce travail cherche à étudier les propriétés hydromécaniques des argilites broyées, mélangées ou non avec de la bentonite MX80, l'utilisation de ces matériaux étant envisagée potentiellement utilisés pour remblayer les galeries et les puits d'accès d'un futur site de stockage. La fraction de bentonite MX80 dans les mélanges étudiés a été limitée à 30% en poids afin de réemployer autant de matériaux excavés que possible. À cet égard, il était d'une importance majeure de comprendre et d'analyser le comportement hydromécanique des matériaux de remblai à base de COX_c.

Le comportement hydromécanique des matériaux contenant de la smectite dépend des conditions géoenvironnementales, qui comprennent les propriétés du matériau, les conditions environnementales et de contrainte. Il était donc intéressant d'évaluer qualitativement et quantitativement l'impact des conditions géoenvironnementales pertinentes sur le comportement de ces matériaux.

Organisation globale de l'étude

Dans un premier temps, cette étude expérimentale en laboratoire s'est concentrée sur le COX_c et son mélange avec la bentonite MX80 pour en déterminer les caractéristiques d'identification,

microstructurales et de rétention d'eau. Dans un deuxième temps, l'étude a porté sur l'analyse du comportement hydromécanique dans des conditions saturées et non saturées. En plus de l'analyse proprement dite, les deux dernières étapes ont permis d'évaluer l'impact individuel et combiné de différentes conditions géoenvironnementales sur le comportement hydromécanique.

Le paragraphe suivant récapitule les conditions géoenvironnementales pertinentes et décrit les approches adoptées pour les représenter à l'échelle du laboratoire :

- Le concept de référence envisage la méthode de compactage in situ. La méthode implique l'utilisation de techniques de compactage conventionnelles et s'appuie donc sur les résultats des essais Proctor, dans lesquelles l'énergie de compactage est contrôlée. En conséquence, les matériaux de remblai sont préparés hors site à leur teneur en eau optimale puis compactés en place afin d'obtenir les performances requises. Cependant, les données de la littérature indiquent que la densité sèche dans la section transversale des galeries peut varier de l'ordre de 20% par rapport à la densité sèche maximale. Dans cette étude, on a considéré des échantillons dont les caractéristiques de compactage correspondaient à la densité sèche maximale et à la teneur en eau optimale obtenues dans des essais Proctor modifiés. Les variations spatiales de la densité sèche initiale ont été représentées en compactant les échantillons à des densités sèches, qui ont été réduites de 2.5%, 7.5% ou 17.5% par rapport à la densité sèche maximale, à la teneur en eau optimale.
- Installés au moyen de la méthode de compactage in situ, les matériaux de remblai se caractérisent initialement par un degré de saturation supérieur à 80%. Au cours du stockage, le matériau compacté sera saturé progressivement par les solutions provenant de la formation géologique, depuis la paroi vers le centre de la partie remblayée. Dans cette étude le comportement hydromécanique des matériaux compactés a été étudié à des succions égales à 75%, 7.5% ou 0.75% de la valeur initiale de succion initiale (après la mise en place).
- Les solutions qui vont entrer en contact avec le remblai vont percoler à travers le soutènement en béton laissé en place. La percolation modifie les caractéristiques des solutions, en particulier leur composition chimique et leur pH. Dans cette étude, l'impact de la chimie des solutions saturantes a été décrit en saturant les matériaux de remblai potentiels avec

différentes solutions. En ce qui concerne leur chimie, les solutions considérées correspondaient à l'eau de formation du site ou au lixiviat provenant de la dégradation du béton.

Dans le contexte des matériaux de remblai compactés in situ, ces approches ont permis d'examiner les conditions géoenvironnementales les plus pertinentes et d'évaluer leur impact sur l'hydromécanique des matériaux de remblai potentiels à base de COX_c à l'échelle du laboratoire.

Synthèse de l'étude

La section suivante synthétise les programmes expérimentaux de chaque laboratoire et en rappelle les principales conclusions :

- *Impact des propriétés des matériaux sélectionnés et des conditions environnementales sur la pression de gonflement* : Dans un premier stade, il était pertinent de caractériser la distribution granulométrique, ainsi que les propriétés physiques et de compactage du COX_c et de ses mélanges avec la bentonite MX80. Afin d'évaluer comment la distribution de la taille des grains affecte ces propriétés et le comportement hydromécanique, la bentonite MX80 a été traitée à des diamètres de grains maximum de 0.28 mm et 2 mm avant d'être mélangée avec le COX_c. Par la suite, les mélanges ont été appelés respectivement mélange de poudre et mélange de grains. En effet, les caractéristiques physiques ont été significativement augmentées grâce au remplacement partiel. Cependant, la teneur élevée en smectite a entraîné une augmentation des teneurs en eau optimales et une diminution des densités sèches maximales, indépendamment de l'énergie de compactage. L'étude expérimentale en laboratoire visait principalement à quantifier l'impact individuel et combiné des variations de la densité sèche initiale et de la chimie de la solution de saturation sur la pression de gonflement du COX_c, le mélange de grains et de poudre, au moyen de la méthode du volume constant. Les résultats ont montré que les pressions de gonflement maximales des échantillons du mélange étaient plus élevées que celles des échantillons de COX_c en raison de la teneur élevée en smectite. En outre, la pression de gonflement maximale des échantillons de mélange était liée de manière exponentielle à leur densité sèche initiale. Les échantillons de mélanges de poudres présentaient des pressions de gonflement maximales plus élevées que les échantillons de mélanges de grains en raison de leur densité sèche maximale légèrement plus élevée. Compactés à leur densité sèche maximale à la teneur en eau optimale, les

échantillons de mélange étaient à peine affectés par la chimie de la solution saturante, quelle que soit leur densité sèche initiale. Ceci est dû à la faible force ionique des solutions et à la durée limitée de l'expérience. En revanche, le COX_c était plus sensible à la chimie de la solution saturante, en particulier à la saturation par une solution alcaline.

- *Conductivité hydraulique, microstructure et texture d'échantillons saturés de solutions de chimie différente* : La deuxième partie du programme expérimental en laboratoire a d'abord analysé le COX_c et son mélange avec la bentonite MX80 ($d_{\max, \text{MX80}} < 2 \text{ mm}$) en ce qui concerne leurs caractéristiques physico-chimiques et microstructurales. Le remplacement partiel du COX_c par la bentonite MX80 a augmenté la capacité d'échange cationique et a diminué la surface spécifique. En outre, les cations échangeables étaient dominés par les ions Na⁺ au lieu des ions Ca²⁺. Les deux matériaux étaient caractérisés par des micropores et des macropores, mais les échantillons mélangés comportaient plus de macropores et de pores non comptabilisés que les échantillons de COX_c. Cette partie du programme expérimental en laboratoire visait principalement à relier l'évolution de la conductivité hydraulique des matériaux aux changements des caractéristiques de texture et de structure éventuellement affectés par la chimie de la solution saturante, en particulier par la valeur du pH. Les conditions imposées étaient censées représenter des conditions réalistes en termes de conditions de compactage, de chimie de la solution saturante et de température. Les échantillons ont été compactés à la densité sèche maximale à la teneur en eau optimale et saturés avec différentes solutions dans des conditions de volume constant. La saturation a à peine affecté la surface spécifique des échantillons, ce qui pourrait être interprété comme une absence de gonflement des particules. Cependant, l'analyse microstructurale a indiqué qu'il y avait des réarrangements considérables. Ces réarrangements étaient liés à la fermeture des macropores déclenchée par le gonflement des matériaux à la saturation. La conductivité hydraulique du COX_c était supérieure à celle de son mélange d'un ordre de grandeur au moins, ce qui est probablement attribuable à la fermeture progressive des macropores. En outre, la constatation que la chimie de la solution saturante semblait n'affecter que très peu la conductivité hydraulique des matériaux met en évidence la faible cinétique des réactions géochimiques, en particulier des processus de dissolution, dans des conditions imposées.

- *Dépendance du chemin hydromécanique d'échantillons caractérisés par des densités sèches initiales différentes* : La troisième partie de l'étude expérimentale en laboratoire visait à analyser comment les variations de la densité sèche initiale affectent le comportement de gonflement et de compression des échantillons de mélange, en particulier dans des conditions non saturées. Il était également intéressant d'évaluer si le comportement de changement de volume dépend de la trajectoire de chargement imposée. Un objectif complémentaire était d'évaluer l'influence du chemin de contrainte. Les courbes de rétention d'eau des échantillons lâches et denses ont confirmé les résultats de l'analyse microstructurale. L'existence de micro et macropores a été indiquée par la disparition de l'impact de la densité sèche initiale sur l'imposition de succions supérieures à 200 MPa. Le comportement de gonflement et de compression a été analysé au moyen d'expériences de pression de gonflement à volume constant contrôlé par succion et d'oedomètre. La relation entre la densité sèche initiale et le potentiel de gonflement libre des échantillons de mélange a pu être dépeinte par une fonction linéaire, dont la pente varie de façon logarithmique avec la succion imposée. Lors d'une hydratation contrôlée par succion, l'évolution de la pression de gonflement a été caractérisée par une stabilisation post-pic à des contraintes inférieures ou comparables. À une succion donnée, une augmentation de la pression de gonflement s'ensuivait à mesure que la densité sèche initiale augmentait. Les résultats ont montré que l'évolution de la pression de gonflement était indépendante du chemin d'hydratation. L'impact des variations de la densité sèche initiale sur la compressibilité des échantillons de mélange a disparu lorsque des contraintes verticales plus élevées ou des succions plus faibles ont été imposées. Le comportement de l'élasticité des échantillons plus lâches était comparable dans les deux conditions, tandis qu'un déplacement des courbes d'élasticité vers des contraintes verticales nettes plus élevées s'est produit lorsque les échantillons étaient saturés dans des conditions de volume constant. Cela pourrait être lié à une adaptation de la porosité totale et à une rigidité comparable de la structure globale.

Conclusions générales et perspectives

L'étude expérimentale a mis en évidence le comportement hydromécanique complexe des matériaux de remblai potentiel à base de COX_c, en particulier dans des conditions géoenvironnementales pertinentes. Les plus grands défis rencontrés ont été liés à l'étude de la façon dont

la performance des matériaux de remblai potentiels à base de COX_c pourrait changer dans des conditions réalistes au fil du temps. Il pourrait être intéressant pour de futures études expérimentales en laboratoire d'évaluer de manière plus cohérente l'impact de la chimie des solutions sur le comportement hydromécanique des matériaux à base de COX_c, de déterminer les propriétés de transfert de gaz de ces matériaux, et de générer une base de données cohérente permettant l'adoption ou le développement de modèles constitutifs qui incorporent l'impact de la densité sèche initiale.